THESIS

To obtain

Degree of Doctorate – LMD

In Mechanical Construction

Theme

Modeling and Simulating Boron Diffusion: Machinable Materials Application

Submitted by

Yassine EL GUERRI

Presented on 26 / 09 / 2024 before the Examination Board

El Habib BELARBI	Professor	University of Tiaret	Chairman
Bendaoud MEBAREK	Professor	University of Tiaret	Supervisor
Abdelkader KARAS	Professor	University of Tiaret	Examiner
Said MEKROUSSI	Professor	University of Tiaret	Examiner
Mohamed MOKHTARI	Professor	University of Tissemsilt	Examiner
Abdelkader Djilali HAMMOU	MCA	University of Laghouat	Examiner

Academic Year 2023 – 2024

Statement of Originality

I, Yassine EL GUERRI, in presenting this thesis, Modeling and Simulating Boron Diffusion: Machinable Materials Application, affirm that the work presented herein is my own original product of research. To ensure the integrity of this work, I confirm the following:

- This thesis has not been previously submitted for a degree or any other qualification at this University or any other institution.

- All research and findings presented in this thesis were conducted independently during my candidacy.

- Every citation was individually consulted and attributed after cautious examination with the best of my efforts.

- Any figure, table, or data not my own are appropriately cited.

- Each presented self-work was provided with the doctoral student notebook.

- The contributed work is clearly described as co-authored work and adequately referenced.

"The scholars are the inheritors of the prophets. They inherit neither dinars nor dirhams. Rather, they inherited knowledge. So, whoever took it has taken an abundant fortune."

Prophet Mohamed peace be upon him, from Sunan Ibn Majah, Hadith 223.

Acknowledgments

Contents

List of Figures

List of Tables

General Introduction

Boron diffusion, separating the two terms opens up avenues for intriguing endeavors. Boron, a ubiquitous element not found in its elemental form, with surprising applications. Boron, a maverick metalloid that changes its game depending on the elements paired with it. With these multifarious aspects, its application extends from agriculture as an essential micronutrient for plant growth [1], to electronics, as a doping agent [2], nuclear industries and pharmaceuticals, as an exceptional neutron absorber [3,4], or as an excellent heat resistant in glasses, such as borosilicate glass found in Pyrex cookware [3], and beyond. Hence, the thesis begins by a first chapter incapsulating the element itself, boron.

As for the diffusion part, it concerns boron's interaction with other materials. Principally, the seemingly static nature of materials belies a dynamic reality on the microscopic scale, where individual atoms and molecules are in constant motion, undergoing incessant thermal fluctuations. The fluctuations give rise to naturally occurring compounds such as borax [1], while when forced through diffusion, synthetic boron compounds can be formed, like the nonmetal boron carbide [5], or the metallic borides [2], explaining the metalloid nature of boron.

From an engineering perspective, these forced diffusions are constantly being practiced and researched in material enhancement applications related to this work, where the particularity goes to surface hardening processes, categorized and explained within a second chapter. These processes are triggered by thermal modifications, mechanical alterations, and chemical interactions, which all can be combined in a sequence or simultaneously, and some can have adverse effects on each other [6–8].

That is where the focal point resides, the diffusion of boron through a surface hardening process known as boriding or boronizing. A process that leverages the phenomenon of diffusion to introduce boron atoms into the surface of a material. It was mainly performed on ferrous alloys, and then, further materials that have moderate to high hardness were subjected to it, excluding others like aluminum or copper. Other than that, it is not adept with noble metals nor feasible on nonmetals [9,10].

During boriding, the incessant thermal fluctuations, as previously discussed, provide the driving force for the movement of the atoms, and with the presence of a chemical media source containing boron atoms, diffusion occurs. That is what generates its fundamental basis, a thermochemical diffusion that produces the formation of a boride layer on the surface of the material's surface. This boride layer is a pairing of the diffused boron with the material of the borided substrate. Although, the layer holds numerous borides, some are dominant and constitute the phases of the layer, while others can be distributed as interstitial solutes, discussed within a third chapter.

The nature of the borided materials and the change of process conditions through the boron media source usage or the technique employed influence the composition of the resulting boride layer, generally forming either a bi-phase layer or, in some cases, a mono-phase one. For example, in ferrous alloys, either FeB and Fe_2B phases or a single Fe_2B phase. In addition, other parameters like temperature and time significantly affect the resulting thickness of the layer, affecting the overall properties of the layer. Nonetheless, with its richness in boron, the boride layer possesses superior properties compared to the underlying substrate. These properties often include enhanced hardness, corrosion, and wear resistance, thus improving the properties of the borided material [7,9,11,12].

Briefly, the thesis elaborates in the second chapter on the different surface hardening processes, their possible combination with boriding, and the different boriding techniques. Then, proceeds with a third chapter regarding the intricacies of the boride layers and an inspection of the response of various machinable materials to boriding [13,14].

Conducting experiments helps in obtaining the basis regarding boriding. However, due to the expensiveness of the process, counting as basic as the equipment and the boron media sources, the repetitiveness and exploration of different scenarios quickly become an obstacle. Fortunately, the simulation of these experiments by computational means complements the experiments, allowing insights regarding the changes in the process parameters and leading to a deeper understanding of the diffusion behavior.

Accordingly, as the theme title suggests, the thesis continues with the main focus, modeling and simulating boron diffusion. For this purpose, different models from the literature describing the kinetic growth of boride layers are investigated in a fourth chapter, and their simulations concerning boride layer thicknesses are provided and assessed to optimize the predictions in the fifth and last chapter. This will be done with the aim of having proper selection of the technological boriding parameters that provide the desired thickness, which is tailored to the intended application. Additionally, modeling and simulating the kinetic growth provides valuable visualizations regarding boron diffusion.

CHAPTER   I

BORON EXPLORATION

This opening chapter delves into the multifarious aspects of boron, striving to provide a holistic understanding of this element. It explores its etymology, historical discoveries, and distinctive properties that grant it a particular classification as a metalloid, besides its numerous compounds and application fields.

I.1.   OVERVIEW

Boron is an intriguing chemical element with a multifaceted past. It is not found in an elemental form but observed anywhere in nature, both on the crust and in oceans. In high oxygen environments, boron is always found as borates, a fully oxidized compound form, like boric acid and borax [2]. Life is thought to have evolved in its presence; It, along with other light elements like lithium and beryllium, originates from either astrophysical processes or the big bang nucleosynthesis [15].

Since it is not found naturally, it was used unknowingly in the past as borax by Egyptians, Romans, Babylonians, and others before the common era. It was not until the late 19th century that it was partially discovered, and not until the 20th that its fundamentals were established. Even with that, it is one of the elements still emerging with discoveries in this 21st century [2].

As contemporary as it is, it is also a versatile element that acts neither as a metal nor a nonmetal; specifically, it is a metalloid, acting as both depending on the elements it is paired with. It is found in various compounds, precisely boron compounds, which can act as insulators or superconductors. They can also be advantageous for biological species, including humans, but can be highly toxic if overdosed. Fundamentally, it can be beneficial but also detrimental, contingent on the specific composition, usage, or dosage [2,16].

Earth content-wise, boron is poorly distributed, making it dominant from one supplier to another. Initially, boron ores were exploited by Italy in the thirties of the nineteenth century [16]. Presently, relevant mines are found in the United States, Turkey, Russia, and a few more, Figure 1. The accessible resources exhibit very high concentrations of it. The world's proven boron mineral reserves exceed one billion metric tons, and the annual output is about four million tons [2].
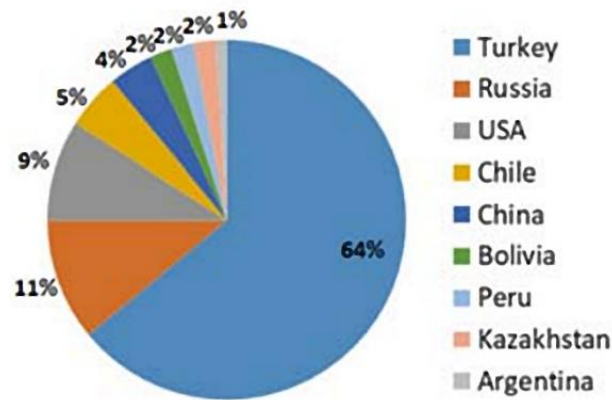
Figure 1. Reserves of boron worldwide [2].

Due to the exhaustion of raw material resources worldwide, boron, as a ubiquitous element found in crust and water, can be synthetically paired with dissimilar elements through several diffusion processes, making it gain increasing prominence in different scientific and industrial applications, and propelling it to the forefront of scientific exploration and technological advancement [3,17].

I.2.   BORON ETYMOLOGY AND HISTORY

The historical roots of boron's name underscore its early significance in alchemical and chemical traditions. Originally, boron was referred to as borax, a boron-containing mineral formerly named in Persian "burah" and Arabic "بورق", spelt "buraq". The English naming resulted from combining two words, borax, the primary boron ore, and carbon, indicating its natural source and resemblance. As for other languages, it is labeled as "bore" in French, "Bor" in German, and "boro" in Italian or Spanish. In nature, boron does not occur in its elemental form. Instead, it is bound to oxygen and found in boron salts: borax, borates, boric acid, colemanite, kernite, ulexite, and the like [3,16].

The usage of boron minerals can be traced back before the common era when the ancient Egyptians, Romans, and Babylonians used borax to produce glass and weld gold. It was not until 1702 that Wilhelm Guillaume Homberg carried out the first chemical processing of boron, and the first synthesized boron compound was produced by reacting natural borax ore with ferrous sulfate, resulting in boric acid [2].

After that, boron had intriguing historical discoveries led by the contribution of many scientists, Figure 2. Initially, it was falsely discovered in 1808 by two French chemists, Joseph-Louis Gay Lussac [18], Louis-Jaques Thénard [19], and Sir Humphry Davy [20], a British, who have all made pivotal contributions in identifying and characterizing boron. Their collective efforts led to the recognition of boron as a distinct element. They lived from the late 18th to the mid-19th century, 1778-12-6 to 1850-9-5, 1777-5-4 to 1857-6-21, and 1778-12-17 to 1829-5-29, respectively. Sir Davy did electrolysis while the Frenchmen, Gay-Lussac and Thénard, combined boric acid with potassium; both processes were done attempting to isolate the element [16].

While these chemists thought that they had discovered pure boron, it was not until a century later, the 20th, in 1909, when a Russian and a United States chemist, born in 1874-7-4, named Ezéchiel Weintraub [21], actually isolated the element boron with ninety-nine percent 99 % purity [22], falsifying the 1808 discoveries that had purities less than half the weight percentage. Nevertheless, pure boron phases were not established until the late fifties of the same century [16].

Figure 2. Boron discoverers: 1808, impure Boron by Joseph-Louis Gay-Lussac, Louis Jacques Thenard, Humphry Davy, and 1909, pure Boron by Ezekiel Weintraub [6-9].

I.3.   BORON PROPERTIES

Elemental boron and boron-rich solids have many applications in research and industry. In particular, boron seems to be a pivotal element in obtaining compounds with high hardness and less sensitivity to oxidation than carbon. As a chemical element, boron has the atomic number 5 and the symbol B. It is the only nonmetal part of Group 13 (formerly Group 3A or IIIA) in the periodic table [23,24], often referred to as the "Boron Group" since it is its first constituent, Figure 3. After Sulphur, Boron has the second most complicated crystalline structure among the elements [25].

Figure 3. *Mendeleev Periodic Table of Chemical Elements* [24].

I.3.1. Atomic Structure

Boron has a relatively simple atomic structure, 5 electrons in its neutral state, distributed in two energy levels, 2 electrons in its first energy level and 3 in its second, constructing the electron configuration of $1s^2 2s^2 2p^1$ along with a state of valence of +4, +3, +2, and +1, with the most common, the oxidation state +3 [16], Figure 4. Its atomic mass is approximately 10.81 amu (g/mol) [2].
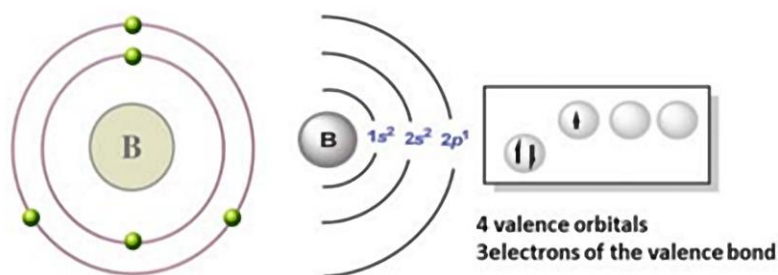
Figure 4. *Boron's nuclear shell model* [2].

A.   Isotopes

It has multiple Isotopes ranging from boron-7 to 17 [16], from which only two are naturally stable isotopes, boron-10 ^{10}B and boron-11 ^{11}B, both as distinct nuclear species of the same element having identical electrons but dissimilar neutrons in their nuclei [26], as illustrated in Figure 5. The latter represents nearly four-fifths (80%) of natural boron [3].
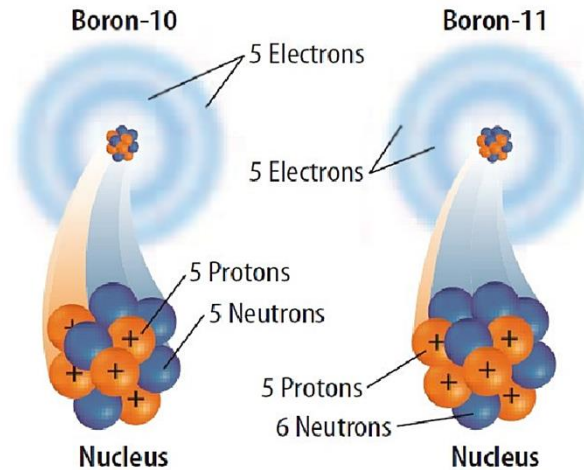
Figure 5. Stable boron isotopes [26].

It is not easy to ascertain an average between both isotopes in land curst as it is the 38th most abundant element [23]. However, in seawater, their aqueous form was determined as the 11th most abundant element [16] or the ninth, according to another recent reference [2]. Boron's existence in a dissolved form in oceans is a matter of pH level [27], where at higher than ten pH, it exists as borate $B(OH)_4^-$, while at under seven pH, as boric acid $B(OH)_3$. Additionally, boron-11 is enriched in boric acids by a fraction of nearly twenty percent relative to the borates due to alterations in molecular geometry and vibrational energy, as given in Figure 6.
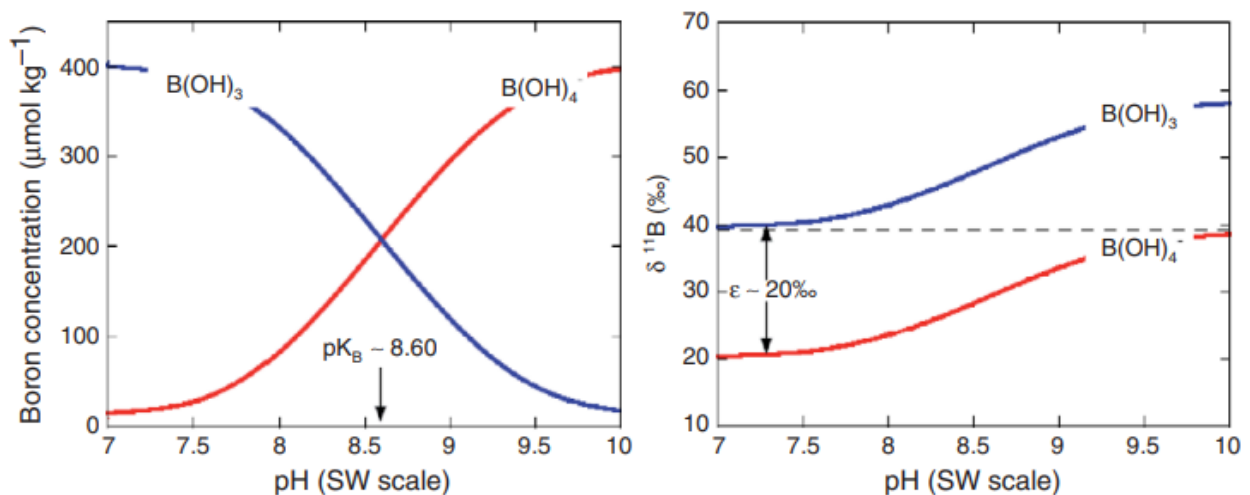
Figure 6. Two of the boron species' distribution in oceans along their isotopic composition [27].

a) Boron-10

This isotope of boron, [10]B, has 5 protons and neutrons in its nucleus. Boron-10 has a unique property: it readily captures neutrons without undergoing significant nuclear reactions [28], and the following reaction describes that:

$$^{10}_{5}B + ^{1}_{0}n \rightarrow (^{11}_{5}B)^{*} \rightarrow ^{7}_{3}Li + ^{4}_{2}\alpha$$
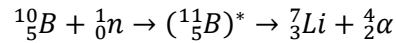
This property makes it valuable in applications where neutron absorption is required because when exposed to neutrons, it undergoes nuclear reactions, emitting charged particles that can be detected and counted. Found in certain use cases as:

- Control rods in nuclear reactors

Control rods absorb neutrons, regulating the rate of nuclear fission and preventing runaway reactions. Boron-10 is used in the form of boron carbide or other compounds in nuclear reactors [3].

- Boron Neutron Capture Therapy

BNCT, as a cancer treatment, boron-10 is selectively delivered to tumor cells, then when exposed to neutrons, the boron-10 in the tumor cells captures neutrons, leading to the release of high-energy particles that damage the cancerous tissue while sparing surrounding healthy tissue [4].

b) Boron-11

This second variant, [11]B, has 5 protons and 6 neutrons in its nucleus. Boron-11 is stable and does not have the same neutron-capturing property as boron-10. Instead, it serves as the predominant form of boron in nature and is used in various industrial applications. A few examples of that are:

- Glass production

Boron is used to produce borosilicate glass, commonly known as Pyrex. This type of glass is known for its high thermal resistance for applications such as laboratory glassware, cookware, and others [3].

- Fluxing agents in ceramics

In cement manufacturing, calcium borates are beneficial fluxing agents because they lower the surface tension of the melt along the viscosity [29]. Also, Boron oxides like borax and ulexite used on clay-based materials demonstrate effective dry route alternatives as fluxing agents [30].
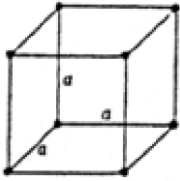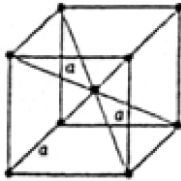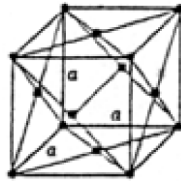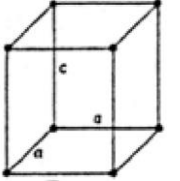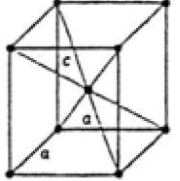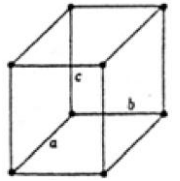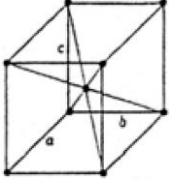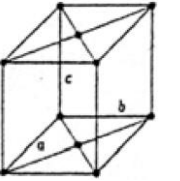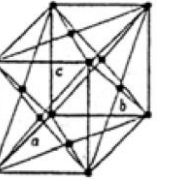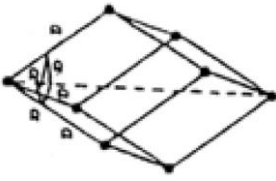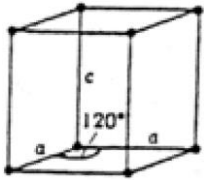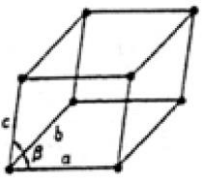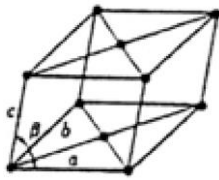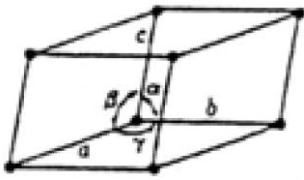
- Semiconductor Industry

In the semiconductor industry, boron-11 is used as a p-type dopant. This atom accepts electrons, creating a hole (positive charge carrier) in silicon wafers to control the electrical properties, which is crucial in producing transistors and other electronic components [31].

B.   Allotropes

Furthermore, elemental boron has nonmetallic properties but can behave as a metal. It exists in different Allotropes, which are different crystalline structures that form the same element, Table 1, depending on its stability at a specified temperature and pressure [32], Figure 8. Its allotropes tend to form structured icosahedral clusters of 12 atoms, equilateral triangles consisting of 20 faces, 30 edges, and 12 vertices. These structures have interstitial sites that are partially occupied, and this occupancy determines the number of atoms in the unit cell [33].

Table 1. *The crystalline structures and their lattices* [34].

System		
Axes and angles		
Lattices		
P - Primitive	F - Face centered	R - Rhombohedral primitive
I - Body centered	C - Base face centered	B - Monoclinic base face centered
Crystalline structure		

Cubic			Tetragonal	
$a = b = c$ $\alpha = \beta = \gamma = 90°$			$a = b \neq c$ $\alpha = \beta = \gamma = 90°$	
P	I	F	P	I

Orthorhombic				Trigonal or Rhombohedral
$a \neq b \neq c$ $\alpha = \beta = \gamma = 90°$				$a = b = c$ $\alpha = \beta = \gamma \neq 90°$
P	I	C	F	R

Hexagonal		Monoclinic		Triclinic
$a=b\neq c$ $\alpha = \beta = 90°$ $\gamma = 120°$		$a \neq b \neq c$ $\alpha = \beta = 90° \neq \gamma$		$a \neq b \neq c$ $\alpha \neq \beta \neq \gamma \neq 90°$
P		P	C or B	P

As many as 16 distinct allotropes were presented as of the late 20th to early 21st century [25,34]. Many were theorized or discovered regularly afterward, as it is an active field. Some allotropes are illustrated in Figure 7, but only those that are thermodynamically stable will be invoked underneath. Additionally, most bulk allotropes are semiconductors at standard conditions, but they can behave with metallic properties when conditioned to high pressures [35].
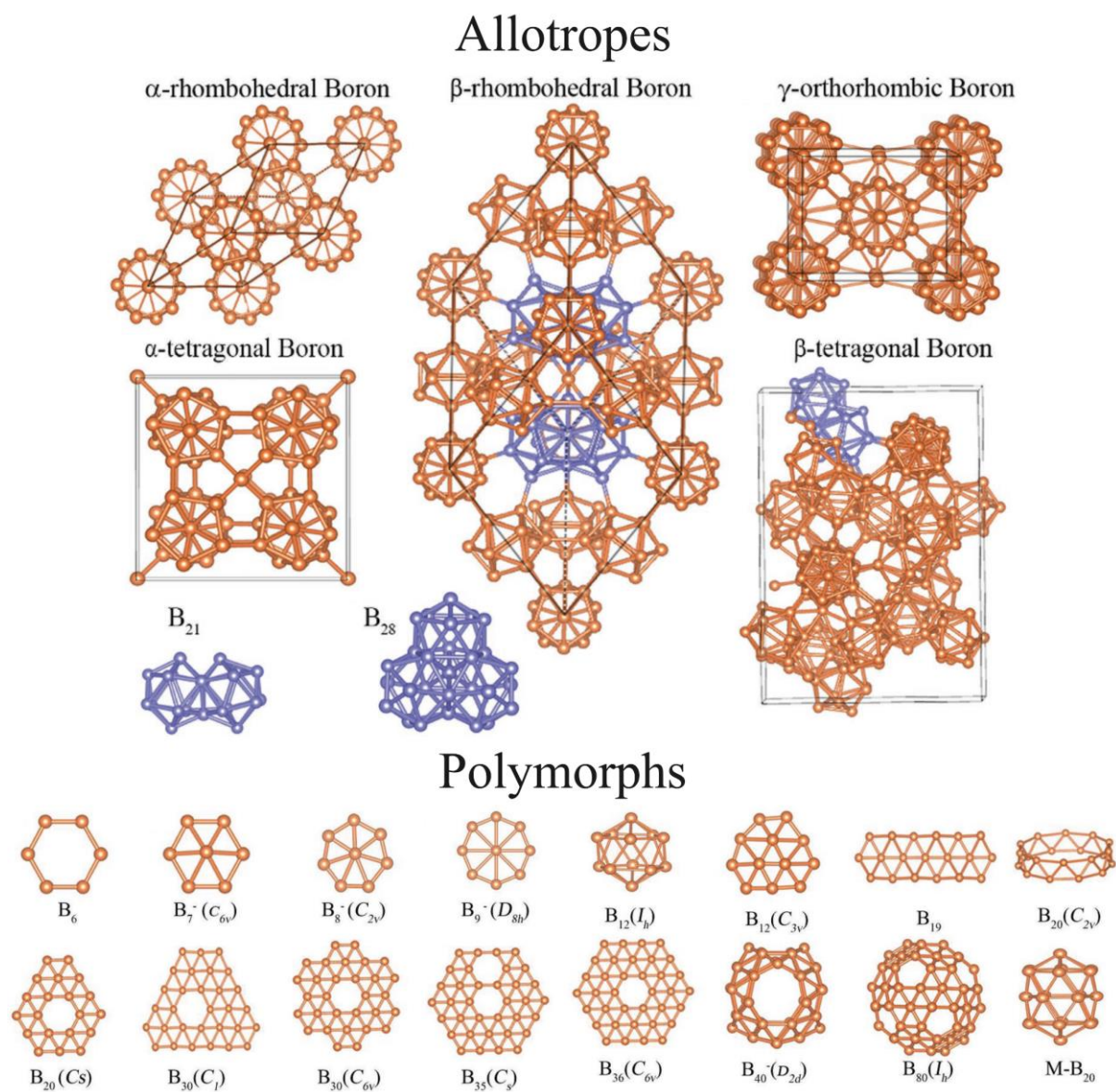
Allotropes

Figure 7. Examples of boron allotropes and polymorphs [36].

a)   α Boron

They are rigid materials and can be found as rhombohedral or tetragonal (α-T-B_{50}) [36], along with other polymorphs, Figure 7, i.e., different compounds, like α-Ga-B, found in extreme pressure conditions [37], or others based on $B_{12}X_2$, with the X atoms in the inter-icosahedra space [25]. However, the most stable one is α-rh-B_{12}, distinguished by its clear red crystals form [38] and a rhombohedral crystalline structure consisting of 12 atoms in its unit cell. This allotrope is more favorable at high pressure and low temperatures and has a Vickers hardness of 42 GPa [39].

b)   **β Boron**

As the hardest stable bulk allotrope, it is dark and shiny and exists as rhombohedral and tetragonal, Figure 7, while the stabler seen is β-rh-B_{105} and B_{106} or others. Conversely to the α-rh, the β-rh with different atoms in its unit cell is more stable in high temperatures and low pressures [25], and it has a slightly higher Vickers hardness of about 45 GPa [39].

c)   **T Boron**

Also seen in α (α-T-B_{50}) or β forms [36], Figure 7, and the most stable of them T-$B_{192.}$ Referred to sometimes as β. It is seen only in extreme conditions, very high temperatures, and high pressures. It has a tetragonal crystalline structure consisting of 192 atoms in its unit cell [39].

d)   **γ Boron**

Limited in its practical applications due to it being unique and unstable unless under extreme conditions [36], known as γ-B_{28}. An orthorhombic crystalline structure with a Vickers hardness exceeding 48 GPa, discovered by Oganov et al. in 2008 [39] as an ionic boron with 28 atoms in its unit cell consisting of pairs of interstitial B_2 and icosahedral B_{12} clusters acting as cations and anions.

e)   **Borophene**

It is a more recent form of allotrope that is either complex or planar as 2D boron sheets [36]. It has metallic characteristics and, in other cases, semi-metallic ones, similar to a highly anisotropic two-dimensional metal [35].

f)   **Amorphous Boron**

Amorphous boron lacks a well-defined crystalline structure because even though it is based on B_{12} icosahedrons resembling those found in β-rh, there is chaos in the connections between its subunits [40].

I.3.2.   Thermodynamic Behavior

Boron has a distinct pressure and thermal resistance, exhibiting an intriguing thermodynamic behavior by having the ability to maintain structural integrity even when undergoing phase transitions to changes in temperature and pressure, Figure 8. That makes it a valuable material in applications where resistance to high temperatures without degradation or structural changes is essential.

a)   **Thermal Stability**

It is a measure that describes the material's ability to maintain its structural integrity and properties when exposed to elevated temperatures. In other words, when subjected to high temperatures, it does not undergo significant chemical or physical changes, such as melting, decomposition, or degradation.

Boron exhibits good thermal stability, especially on certain compounds like Boron nitride (BN) [41], where it emanates in various forms (hexagonal, cubic, and amorphous), found in use as a high-temperature lubricant [42] and as a heat-resistant material as a carborane [2].

b)   Pressure Conditions

Changes in pressure conditions can also impact the boron's thermodynamic behavior. Under high-pressure environments, such as those found in specific industrial processes or during high-pressure research, boron may exhibit altered phase transitions or structural changes. For example, under high-pressure conditions, Figure 8, boron can transform into a unique gamma boron phase γ-B_{28} [39] or even α-Ga-Boron under extreme pressures [37].

c)   Melting and Boiling Points

Boron remains solid at very high temperatures because it has high melting and boiling points, especially compared to many other nonmetals. The melting point T_m of boron is approximately 2,077 °C or higher, Figure 8, and its boiling point T_b is around 4000 °C [3].
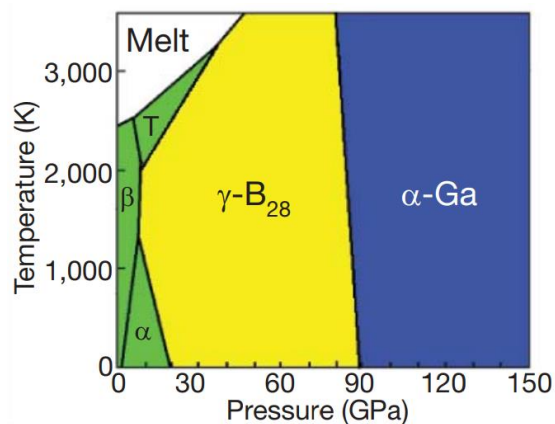
Figure 8. *Stability of boron phases* [32].

d)   Vacuum Environments

In vacuum conditions with minimal or no reactive gases, hydrogen, for example, boron's thermodynamic behavior is often more stable. That makes it valuable in applications involving vacuum environments, such as space technology as α-BN in lubricants [2].

e)   Insulating and Refractory Properties

Pure boron has some intriguing insulation properties, like optical ones, transmitting some infrared portions, and electrical, being a poor conductor of electricity at room temperature contrary to high temperatures [3]. Additionally, boron-based compounds have superior refractory properties to traditional refractory materials, exhibiting good thermal insulation that withstand much higher temperatures. This property makes it useful in specific high-temperature applications, such as thermal shielding [43].

f)   Diffusion behavior

Boron's diffusion unto materials, especially into metals, is invoked in surface hardening processes where it gives rise to boron compounds in a layered form, referred to as boride layers, offering advantageous characteristics and tribological properties that vary based upon the base material that is undergoing the diffusion process. Thus, this creates a wide range of compounds and makes it an active field of interest for industrial applications [1,9].

I.3.3.   Chemical Reactivity

Boron is relatively unreactive at room temperature. It does not react with air, water, or most acids. However, it exhibits unique reactivity due to its electron configuration and bonding behavior, characterized by the following:

a)   Chemical Stability

having a complete first energy level and only three valence electrons in its second energy level drives boron to form compounds where it shares electrons, striving for an octet (eight electrons) to complement its outer energy level and achieve stable electron configurations, forming in most cases covalent bonds with other nonmetals such as carbon, oxygen, or nitrogen, to complete its outer electron shell [3]. Examples of that are Boranes, Boronic Acids, Boroxines, Boron Nitride (BN), Boron Carbide (B_4C), and Boron Trifluoride (BF_3), Figure 9.
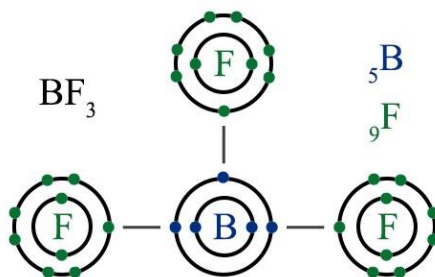
Figure 9. Boron and Fluorine forming covalent bonds in Boron Trifluoride.

b)   Reactivity at Elevated Temperatures

While boron is generally unreactive at room temperature, it becomes more reactive at elevated temperatures, reacting with oxygen and nitrogen. For example, reactions of boron oxides (B_2O_3) release significant amounts of energy. They are exploited in solid rocket propellants to generate thrust as a fuel combustion component [3]. Also, boron, when diffused in nitrides, a high-temperature material is synthesized with applications in lubrication [42] and refractories [43]. In other cases, boron can absorb hydrogen, forming boranes, compounds found in organic synthesis [2], or other applications like medicine, catalysis, storage, and battery applications.

c)   Reactivity with Strong Oxidizing Agents

Boron is used in some pyrotechnic applications as a high burn rate propellant or in mechanisms that are explosive-actuated based, where it can react vigorously with strong oxidizers like potassium nitrate (KNO_3) to produce colored flames [44]. It can also react with halogens like highly reactive fluorine gas (F_2) to form one of the boron halides, boron trifluoride (BF_3) [1], or with concentrated nitric acid (HNO_3) to form various boron oxides and nitrates. Moreover, boron can act as a Lewis acid, accepting pairs of electrons in chemical reactions like in the case of boric acid or boron halides [1]. This property is significant in organic chemistry, where boron compounds are used as reagents in various reactions, including the synthesis of pharmaceuticals and fine chemicals [2].

d)   Electronegativity

A measure of an atom's ability to attract electrons to form chemical bonds. On the Pauling scale, Figure 10, which ranges from 0.7 for Francium to 4.0 for Fluorine, Boron has a relatively moderate electronegativity value of 2.04 eV. Boron's electronegativity is higher than that of metals but lower than that of nonmetals, and because of this intermediate electronegativity, boron does not readily lose electrons to become electropositive, nor does it strongly attract electrons to become highly electronegative. As a result, boron does not typically form ionic bonds, which require a more significant difference in electronegativity to have the potential to form, hence why it tends to form covalent bonds with elements of similar electronegativity [1].
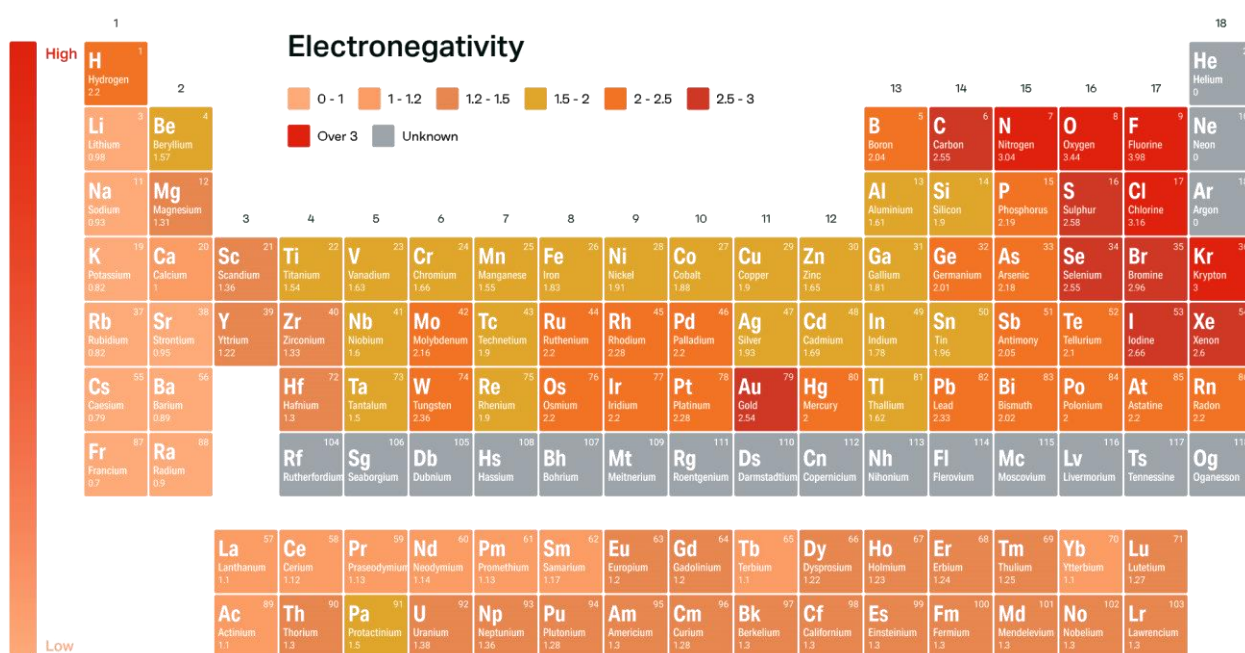
Figure 10. Pauling scale of electronegativity [45].

I.3.4. Electrical Conductivity

Boron has interesting optical characteristics, transmitting portions of the infrared, and is a poor conductor of electricity at room temperature in its pure form, but with a band gap of nearly 1.5 eV, it can be a good conductor at high temperatures, especially when doped in other elements like silicon in electronics industries [3,31]. Additionally, at high pressures or in high temperatures and chemical reactions, boron can form compounds like Boron triiodide, which becomes metallic and acts as a superconductor [1]. Another superconductor boron compound under 230 °C is Magnesium diboride [23].

I.3.5. Appearance

Boron exists in different forms, including bulk amorphous, crystalline, and nanoparticles. Its distinctive appearance is often described as a shiny grey or black for hard crystalline boron, and red crystals for some [38], or brownish-black for amorphous forms [3]. The amorphous form is the most stable, which, at standard temperature and pressure, appears as a dark solid, Figure 11.

Figure 11. Boron's appearance [46]*.*

I.3.6. Density

Boron is one of the lightest solid elements with regard to its mass per unit volume. It possesses a relatively low density ρ compared to most metals but is denser than typical nonmetals. Amorphous and β-rh boron have a 2.34 g/cm^3 density, while the α-rh phase is 2.46 g/cm^3. This value is significantly higher than that of many nonmetals like hydrogen 0.082 g/l, equivalent to 8.2 e-5 g/cm^3, helium 0.164 g/l, and nitrogen 1.145 g/l, which are gaseous while nearing that of carbon as graphite 2.2 g/cm^3 which itself can exhibit both metallic and nonmetallic properties but is considered generally a nonmetal. Compared to typical metals, it is, to an extent, nearing the lower-end ones, iron 7.87 g/cm^3 and copper 8.96 g/cm^3. This intermediate position reflects its unique status as a metalloid, as placed in the periodic table, Figure 3, possessing characteristics that bridge the gap between metals and nonmetals [3,16].

I.3.7.   Hardness and Brittleness

Crystalline boron is a brittle solid with exceptional degrees of hardness that can scratch numerous materials. It is the second hardest material, ranking just below Diamond on the Mohs scale of mineral hardness, Figure 12. Due to its extreme hardness, boron, even though it has some metallic characteristics, does not possess the malleability and ductility commonly associated with metals. Instead, it is characterized by its brittleness, which means it tends to fracture rather than deform when subjected to stress like many nonmetals [46]. Nonetheless, boron fibers' mechanical properties can attain an elastic modulus of 450 GPa compared to steel, which has more or less 200 GPa [1].

Furthermore, boron nitride and boron carbide, as boron compounds, are one of the nonmetallic borides that have remarkable second and third places in hardness. Boron carbide gained the title of black diamond due to this exceptional mechanical property that contributed to its use in diverse industrial applications, including abrasives and cutting tools or demanding uses as in body or tank armors, as well as like a protective material in bullet-proof vests or nuclear reactors [2].

Other hard boron compounds are reached after diffusing boron into a material's surface, forming boride layers constituted from a mono phase or multiple phases, enhancing the material's hardness, wear resistance, and other properties. It is a vital technique in materials science and engineering commonly known as boriding or boronizing, which will be discussed in the next chapter as the main interest of the thesis.

* Kyanite's hardness differs depending on the direction in which it is tested – softer when tested parallel to crystals, and harder when tested perpendicular.
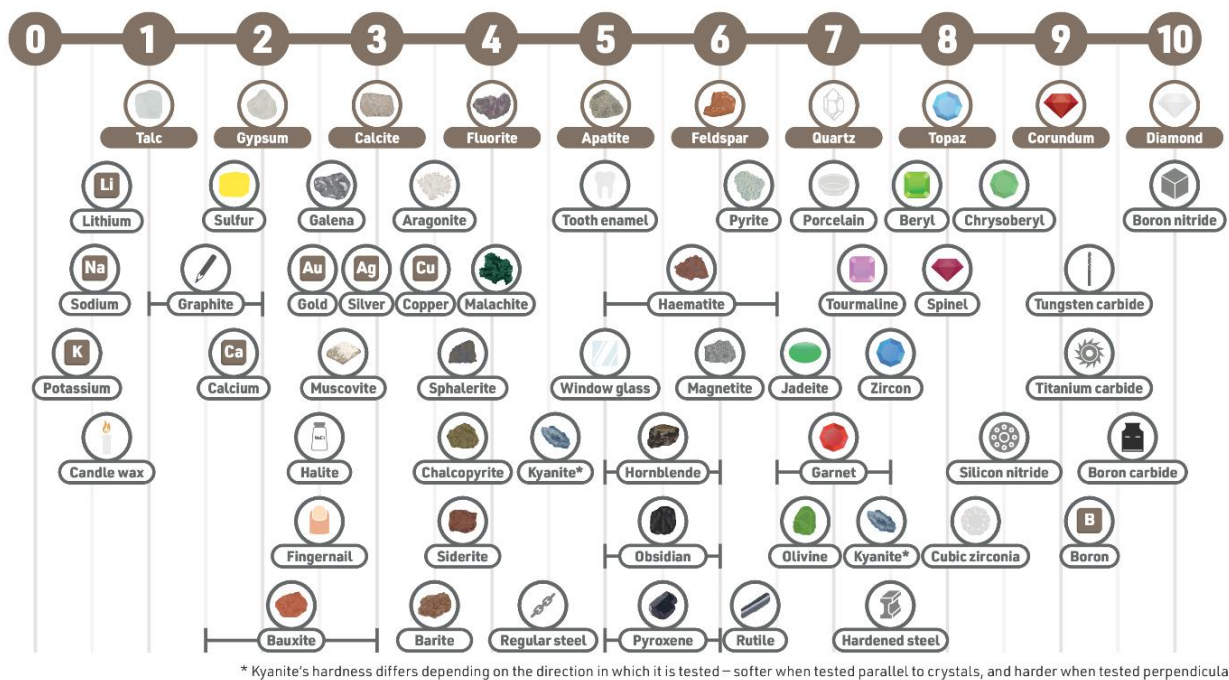
Figure 12. *Friedrich Mohs Mineral Hardness Scale* [47].

I.3.8. Biological Influence

Boron's role in the biological realm is complex and intriguing. While it is not considered essential for biological beings, it holds significance in various aspects, from potential health benefits to human beings to its pivotal role in plant growth.

a)   Health Effects

While boron is not considered an essential element for humans in the same way as in vitamins and minerals, some studies have suggested that it may have potential health benefits for humans when consumed in trace amounts. These potential health benefits may include supporting bone health, wound healing, and hormonal activities, among others [2,48]. However, excessive boron intake can be toxic to humans [16].

b)   Handling Safety

Taking safety precautions and extreme measures is essential when handling boron or its compounds. Proper personal protective equipment, including gloves and goggles, should be worn when working with certain boron substances. For example, some boron compounds can irritate the skin or eyes. Prolonged exposure to boron particles may lead to respiratory irritation and, in extreme cases, death [49].

c)   Environmental Influence

Boron is essential for certain living organisms, particularly plants, as it plays a role in their growth and development [16]. Boric acid added to baits acts as an insecticide, especially for ants and cockroaches [2]. However, Boron compounds can have an impact on the environment; they can accumulate in soil and water, potentially affecting aquatic life and terrestrial ecosystems where they can be considered an environmental contaminant in some regions, having adverse effects on some crops such as kidney beans and lemons [23].

I.4.   BORON CLASSIFICATION

The classification of elements into metals or nonmetals is based on their physical, chemical, and other properties. Boron is classified as a metalloid because it exhibits a spectrum of properties that are intermediate between metals and nonmetals, depending upon the elements that are paired with it. Some characteristics of boron that explain it being a metalloid are:

a)   Atomic Structure

The electron configuration of boron places it on the borderline between metals and nonmetals. It possesses three valence electrons, Figure 4, a characteristic shared with many nonmetals. However, unlike typical metals, it lacks the full complement of valence electrons [2].

Boron's unique position is further highlighted by its intermediate density position and its existence in several distinct allotropes [25,34], some of which exhibit metallic properties, while others are nonmetallic. This diversity of forms, each with varying properties, is a defining feature of metalloids.

b)   Behavioral Variability

Boron forms compounds with both nonmetallic and metallic properties. Depending on the nature of the elements it reacts with, forming compounds that exhibit both metallic and nonmetallic properties. It forms covalent bonds with nonmetals, such as in specific boranes, in boron oxides, or when reacting with halogens like boron trifluoride [3], Figure 9, and can also form ionic bonds when reacting with hydrides (boranes). Nevertheless, it also forms certain compounds called metallic or nonmetallic borides depending on the material it is paired with, magnesium borides as metallic borides, or boron carbides as nonmetallic borides [1]. This dual behavior is a characteristic of metalloids.

c)   Electrical Conductivity

Elemental boron is a poor conductor of electricity at room temperature, a typical property of nonmetals. However, it can act as a semiconductor in other case scenarios or even as a superconductor [31], which is a hallmark of metalloids.

I.5.   BORON COMPOUNDS

Boron compounds are chemical compounds that contain the element boron, which can be the main constituent in some instances, called polymorphs, Figure 7. Boron compounds can take on a wide range of chemical forms and combinations due to the resemblance of boron in electronegativities with other elements, promoting both covalent and ionic bonds, its affinity with elements like oxygen, its small size, which helps in interstitial penetration forming alloys, and so on [1,2].

Moreover, due to their unique properties, they have various applications in industries, science, and everyday life. To distinguish between different types of boron compounds, they are classified distinctively underneath within some broad examples, then into those used in boron diffusions like boriding, a surface hardening process, and found in machinable applications, as they are the interest of this thesis.

I.5.1.   Versatile Boron Compounds

This section presents Boron Compounds that can be used in diverse applications, be they industrial or for specific purposes.

A.   Borates

They are the most significant number of boron-oxygen-based compounds and represent, as mentioned in the introduction, the most abundant mineral resource of boron in nature due to the state of oxidation +3 being the most favored of boron properties [16]. A few examples of borates are:

- **Borax,** with different chemical formulas and names, the main one is sodium borate $Na_2B_4O_7 \cdot 10H_2O$, common in massive or granular aggregates, soluble in water, and has a slightly alkaline taste. It is a salt with a translucent transparency of white or gray and rarely light blue or green [1].

- **Boron oxides,** another borate, and the most known of them is diboron trioxide, also named boric oxide B_2O_3, a white waxy solid that is amorphous and rarely crystalline. It has multiple routes of reactions that result in numerous other boron compounds like boron carbide or boric acid when hydrated. They are used as fluxing agents on clay-based materials [30], fuel combustion components in solid rocket propellants, additives when producing glass fibers, and many more [3].

- **Boric acid,** with a chemical formula of H_3BO_3 or $B(OH)_3$, it is a compound that was recommended for everything, from eye washing to ant poisoning [46], and it is a weak monobasic Lewis acid [1].

B.   Boranes

Boranes, also called boron hydrides or borohydrides, are composed of boron and hydrogen, with a generic formula B_xH_y. Over a hundred of these compounds have been characterized [1], and their physical properties are similar to alkanes C_xH_y. Trihydridoboron BH_3 and borohydride BH_4 are such boranes, but the most known is diborane, formulated as B_2H_6. A colorless gas at room temperature that is easily soluble, volatile, and highly toxic. However, it has excellent affinity with electronegative elements, making it a highly reactive and versatile reagent. It can be used as a propellant for rockets, as a doping agent when producing semiconductors, as a flame accelerator, or in catalyst operations [2].

C.   Carboranes

Carboranes are subunits containing Boron, Carbon, and Hydrogen atoms, which the reaction of boranes with alkynyl reagents can form. It has excellent heat resistance and thermal stability, is used as a flame retardant, and is found in fluorescence imaging and other use cases. Other occurrences are carborane acids found in organic and inorganic synthesis [2].

D.   Boron Halides

Boron halides are multiple; a few are boron trichloride BCl_3, boron trifluoride BF_3, and boron tribromide BBr_3. They are electron-deficient molecules lacking an electron, and because of that, they tend to act as strong Lewis acids. They are used in a multitude of applications, including boriding, where they are sometimes exploited as the primary sources when diffusing boron [2].

E.   Boron Carbide

Boron carbide B_4C is odorless and insoluble in water. It has a dark gray or black solid appearance, called black diamond, due to its extreme hardness, 9.5 to 9.75, third place on the Mohs scale, Figure 12. As a hard ceramic material of density equal to 2.52 g/cm^3, it has excellent structural strength per weight [1,2]. Its utility is enormously versatile, used as a neutron absorber in Boron Neutron Capture Therapy (BNCT) [4] or, as mentioned in the boron-10 isotope section, within control rods in nuclear reactors [3], also used as an engine sabotage solution [46], and many other use cases. Further explanations about how it is obtained are explained in the boride section.

I.5.2.   Boron Compounds Found in diffusion and machinable applications

This section is dedicated to boron compounds found in boron diffusion processes and machinable applications. In doing so, a few versatile compounds are reinvoked to grasp their multi-usage alongside other compounds that are used mostly or specifically in the mentioned applications.

A.   Borax, Boric Acid, and Amorphous Boron

They are all found in diversified applications but are also used as mixes of compounds to create boron-containing pastes or coatings in boriding processes or as additives to improve the cutting tools' performance [1,50]. When added to cutting tool materials, they can enhance their hardness, wear resistance, and overall durability, improving their efficiency and effectiveness in various machinable applications.

B.   Boron Doped Diamond

BDD is a diffusion process consisting of doping boron to diamond, exploited in varied use cases, and valuable as a cutting tool for temperature measurement in the cutting zone for ultra-precision machining purposes [51].

C.   Boron nitrides

Boron nitride BN, the rival of diamond according to the Mohs scale, Figure 12, is a binary boron and nitrogen compound that is not found naturally but rather synthesized into multiple structural forms:

- **Amorphous Boron Nitride,** aBN, even with an amorphous structure, it is a preliminary material for synthesizing other forms of boron nitrides [52].
- **Hexagonal Boron Nitride,** hBN, also known as α-BN or g-BN. It is the most stable and commonly used form of BN with a structure similar to graphite and good thermal stability, making it useful in high-temperature applications or as a lubricant in vacuum conditions within space applications [2] or in machinable applications to reduce friction and wear [42].

- **Cubic Boron Nitride,** cBN, also referred as β-BN or z-BN, is a superhard material rivaling diamond in hardness [3]. However, cBN boasts superior thermal stability, allowing it to withstand high temperatures that would degrade diamond. Unlike diamond, cBN is synthesized through a sintering process where a mixed powder is subjected to extreme pressures (up to 7 GPa) and temperatures (around 1400 °C) below melting points. A small amount of a metal binder, like cobalt or nickel, is often incorporated into the powder mix to enhance toughness. Explicitly used as cBN tools and inserts in hard machining of hard materials like hardened steels, cast irons, and superalloys, making production relatively inexpensive [2,46,53].

- **Wurtzite Boron Nitride,** wBN, a super hard state under high pressure, formed as hexagonal structures with the unique Wurtzite form. It is different from the layered structure in α-BN [2].

- **Boron Nitride Nanotubes,** BNNTs, as one of the most important materials of this century. A polycrystalline material that is similar to Carbon Nanotubes with a nanoscale dimension. It enables precise machining, especially in micro and nano machining applications, which are advanced machining technologies, all while enhancing the performance of cutting tools and abrasive materials with their extraordinary physical properties like its tensile strength about a hundred times stronger than steel and fifty than carbon fibers [2,54].

D. Borides

Lastly, Borides, the boron compounds that are either metallic or nonmetallic depending on the elements that boron is paired with. They are not naturally found but formed through various techniques such as chemical vapor depositing, solid-state reactions, arc melting, direct element pyrolysis [2], and others, including the surface hardening process of boriding.

a) **Nonmetallic borides,** when boron is paired with nonmetallic or metalloids, the resulting material, in some instances, is a nonmetallic boride like the boron nitride or:

- **Silicon Borides,** they are mixtures of two metalloids, silicon, and a set amount of boron from 3 to 6, SiB_x. They put forward a high melting point, good oxidation resistance, and a high radiation-resistant coating [55]. It is not commonly found in machinable applications.

- **Boron Carbide,** B_4C, as a mixture of boron, a metalloid, and carbon, a nonmetal. Due to its extreme wear resistance and hardness, Figure 12, this ceramic and lightweight material with a high melting point cannot go unnoticed on abrasive applications like polishing, cutting, and grinding wheels, which often incorporate it to maintain sharp edges and effectiveness during extended uses in machining. Boron carbide is not a naturally occurring compound. Instead, it is synthesized through various methods, such as the high-temperature reaction between boron oxide B_2O_3 and carbon powder, known as carbothermal reduction, producing a boron carbide powder, or the pyrolysis of boric acid-citric gel material which can be considered a form of carbothermal reduction offering more control over the particle size [5]. Besides its versatile use in machinable applications and other fields, it is also used as a source to diffuse boron in the boriding techniques, upcoming chapter.

b) **Metallic borides,** metallic borides are human-made and used for specific purposes, including machinable applications. They are either synthesized through various processes or diffused onto other materials in boriding, the surface hardening process where a boride layer or coat is formed on the material's surface.

- **Synthesized,** when it comes to their synthesis, they can be produced by chemical vapor deposition, solid-state reactions, arc melting, direct element pyrolysis, or else, forming diborides or higher borides such as rhenium diboride Re_2B, a superhard material of hardness equivalent to diamond [2], Molybdenum diboride MoB_2, Niobium diboride NbB_2, and Zirconium diboride ZrB_2, all of which are synthesized using DC plasma reactors [56]. With other processes, Aluminum diboride AlB_2, Tungsten Diboride WB_2, Tungsten tetraboride WB_4, etc. [57,58].

- **Layered or coated,** found in boriding, a surface hardening process where a material, generally steels or other alloys, is treated, resulting in the formation of a thin metallic boride layer [9]. Examples of that are Iron boride FeB or Iron diboride Fe_2B, Titanium diboride TiB_2, or even those similar to the synthesized mentioned before but diffused on the top of a material's surface rather than found as powders or else. This category will be examined and detailed in the upcoming chapters, as it is the main interest of the thesis.

I.6.   BORON APPLICATION FIELDS

Boron, modestly classified on the periodic table of elements, Figure 3, possesses intricate qualities. Its remarkable characteristics and performances, encompassing elevated hardness, impressive thermal stability, and a tendency to form strong covalent bonds, combined with its ability to adapt to multiple processes, establish it as a significant element among others in the modern industry.

A.   Materials Science

Within the realm of materials science, boron's versatility is particularly pronounced. Its unique properties make it an essential element for enhancing various material characteristics. One of its noteworthy applications lies in the development of materials with augmented hardness, wear resistance, and corrosion resistance. For instance, boron is utilized to create boron carbide, a superhard material that rivals the hardness of diamond as placed in the Mohs Hardness Scale, Figure 12, about 9.5 to 9.75 in Mohs hardness scale [2], or in surface hardening processes, including boriding, the boron diffusion process.

B.   Automotive industry

Boron also contributes to the development of boron steels, which are used in automotive industries to manufacture high-strength and lightweight vehicle structures, enhancing passenger safety and fuel efficiency. For instance, Usibor 1500P and Ductibor 500P are boron steel compounds used to construct safety critical components like door reinforcements and crumple zones [59].

C.   Aerospace Industry

Boron plays a pivotal role in the aerospace industry due to its exceptional properties as a lightweight, high-strength material used in aircraft and spacecraft construction. Boron composites, such as boron-reinforced carbon fiber composites, are extensively demanded and used in these industries [3]. The 787 Boeing Dreamliner, for instance, was the first commercial jet aircraft made primarily of composite materials, incorporating boron-reinforced composites in its airframe [60], enhancing its structural integrity under extreme conditions while reducing the overall weight, thereby improving fuel efficiency, performance, and a reduced environmental footprint.

D.   Electronics Industry

The electronics industry relies on boron doping, a crucial process for controlling electrical conductivity. This application is fundamental in the production of semiconductor devices, which form the backbone of modern electronics. Silicon wafers are doped with boron to create p-type semiconductor materials, essential in components of devices like computer chips. Magnesium diboride, Borophene, and boron nanowires are all boron-based compounds found in electronics, either as superconductors or semiconductors [2].

E.   Nuclear Industry

Boron's importance extends to the nuclear industry, where it functions as a neutron absorber. Control rods and shielding materials contain boron compounds that regulate nuclear reactions and safeguard against radiation. Boron carbide, one of these compounds, when inserted into nuclear reactors, absorbs neutrons, allowing operators to regulate power outputs and prevent overheating by controlling the rate of nuclear reactions to ensure reactor safety [3].

F.   Pharmaceuticals

Boron finds application in pharmaceuticals and medicinal chemistry. Its unique chemical properties enable the synthesis of a wide range of drugs and pharmaceutical compounds, contributing to advancements in the pharmaceutical industry. One notable example is the cancerous treatment with the Boron Neutron Capture Therapy, where boron compounds, boric acid being one of many, are utilized to damage nonhealthy tissue [4]. Furthermore, recent discoveries show that boron compounds were used in antibacterial and antiviral agents along drug delivery assemblies [2].

G.   Sports and Recreation

Boron's utilization extends even to the world of sports and recreation, where its employment is as boron fibers and boron steels, which have excellent tensile strengths, used to increase toughness and durability in composites, procuring power, flexibility, and lightness due to its low density. It is found in sports equipment, such as golf clubs, fishing rods, tennis rackets, and bicycle frames. Mizuno is one of the reputable manufacturers of boron-based sports equipment [61].

H.   Agriculture

Boron is a micronutrient that is essential for plant growth. Its role in agriculture is vital for sustainable food production, and each year, thousands of tons are added to fertilizer [1]. Plants will not pollinate or produce fruit if their soil lacks boron, as they will be stunted. That phenomenon occurred with Greece and Spain's olive groves in old age. They lacked only a fraction of soluble sodium octaborate, which, when applied, eliminates pests like olive flies and moths. Some plants can take up any amount of boron, but for others, the quantities must be carefully envisaged, or else adverse effects can occur, and kidney beans or lemons are one of those [23].

I.   Emerging Applications

Lastly, as an ongoing element researched, boron continues to find applications in emerging fields. It is evolving landscape underscores its relevance in contemporary research and development. For instance, boron nitride nanotubes. Structurally similar to carbon nanotubes, cylinders with submicron diameters and micrometer lengths, but with nitrogen and boron instead of carbon atoms. This difference makes them completely different. While carbon nanotubes can be semiconductors, the boron nitride nanotubes are insulators. They have good tensile strength, are a hundred times stronger than steel, and are fifty times more robust than carbon fibers. They are resistant to high temperatures, good radiation absorbers, and other essential applications in biomedical fields such as gene delivery [2].

I.7.   CHALLENGES AND LIMITATIONS IN BORON USAGE

While boron compounds offer significant benefits in machinable applications and boriding processes, they are not without their specific challenges and limitations:

A.   Microstructure Alteration

When approaching boron compounds in steel components, the diffused layer that includes boron can be observed to have altered properties after the surface hardening process of boriding. In some instances, it is desirable; in others, it can be seen as a limitation. For example, the diiron boride Fe_2B is more favored than the Iron boride FeB. That is because the latter is more rigid and brittle than the first, and additionally, due to the difference between their thermal expansion coefficients, cracks can form and propagate [62].

B.   Surface Finish and Precision

Achieving specific surface finishes and precision in machining with boron-based tools can be challenging. For example, while boron nitrides are highly wear-resistant, they are mainly found in hard machining and may not provide the same level of surface finish. Specifically, high Cubic Boron Nitride tools produce better surface integrity compared to those with low Cubic Boron Nitride, and the surface finish deteriorates with the intensification of the workpiece hardness [53].

C.   Cost

High-purity boron compounds required for precision machining, such as cubic boron nitride cutting tools, can be exceptionally expensive, making the production cost-prohibitive for manufacturers [63]. Not only that, many sources of boron, for boriding specifically or for other purposes, are generally expensive.

D.   Compatibility

Boriding processes, which are boron-based, may not be suitable for all types of materials. For instance, boriding can be challenging when working with certain nonmetallic or low-temperature alloys, limiting its applicability in diverse manufacturing contexts. That will be further developed in the third chapter.

E.   Toxicity and Safety Concerns

While elemental boron and borates are not labeled as toxic, some of the exotic boron hydrogen compounds, like diborane B_2H_6, are highly reactive and toxic gases requiring care usage, and companies must adhere to safety regulations, maintain specialized equipment and ensure compliance [3].

F.   Environmental Impact

Even though certain boron compounds, such as those used in catalyst applications, are predominantly environmentally friendly, the extraction of boron from aluminosilicates, for example, is done by high-temperature hydrolysis, a method that is not that friendly [2]. Additionally, boron diffusion processes, such as boriding, differ in their impact, and some are friendlier than others. An example of that is, plasma paste boriding, an environmentally friendlier technique than plasma gas boriding [64].

I.8.   SUMMARY

Altogether, the miscellaneous applications of boron explored so far underscore its extraordinary adaptability and utility across numerous fields. From fortifying materials in aerospace, regulating nuclear reactions, and enhancing crop yields in agriculture, to basic needs such as in detergents, boron's unique properties, Table 2, have left an indelible mark on a multitude of industries.

Boron's capacity to imbue materials with enhanced hardness, wear resistance, and corrosion resistance makes it an intriguing candidate for surface hardening processes, which are pivotal techniques employed to augment the durability and performance of materials in numerous applications. Whether in industrial machinery, automotive components, or cutting tools, the ability to strengthen only the surface layer of a material while preserving its core properties is of paramount importance.

The boron diffusion, the focus of the thesis, will further be developed by putting forward different boriding techniques. However, former to that, other surface hardening processes are briefly presented to grasp their resemblance to, or compatibility with, boron diffusion processes.

Table 2. Main data of boron

General Information		Miscellaneous Properties	
Atomic symbol	B	**Atomic mass [amu]**	10.81 (10.01, 11.01)
Block	p	**Atomic radius [pm]**	87
Period	2	**Electronic configuration**	$1s^2\ 2s^2\ 2p^1$
Atomic number	5	**Electrons per energy level**	2, 3
Groupe	13	**Oxidation states (Best)**	+4, (+3), +2, +1
Family	Metalloid	**Band gap [eV]**	1.5
Country Producers	Turkey, USA, Chile	**Electronegativity [Pauling scale]**	2.04
Country Reserves	Turkey, Russia, USA	**Specific Heat Capacity [J/g °C]**	1.026
Existence state	Solid, Powder	**Melting point [°C]**	2077
Colors	White, Brown, Black, Grey, Red	**Boiling point [°C]**	4000
Resources (Oxygen bound)	Borax, Boric acid	**Density [g/cm3]**	2.34 - 2.46
Isotopes	^{11}B (80 %), ^{10}B (20 %)	**Hardenability [Mohs scale]**	9.3
Allotropes and Crystalline systems	α-rh, α-t, β-rh, β-t, γ-orthorhombic ...	**Renown Compounds**	Boron Carbide B_4C, Boron Nitrides BN, Borophene ...

BLANK PAGE

CHAPTER II

BORIDING AND SURFACE HARDENING PROCESSES

Subsequent to an exploration of boron's properties and applications, this second chapter delves into surface hardening processes, their variations, as well as their resemblance or compatibility to boriding. Accordingly, boriding is described as a boron diffusion technique that differs in boron source media usages from which, a categorization is made.

II.1. OVERVIEW

The previous understanding of boron's versatility and applications in diverse industries within the previous chapter laid the foundation for a comprehensive exploration of boriding and its role in material enhancement. Table 3 provides different compounds where boron seems from the brittle and high-temperature resistant compounds [8].

Boron, along with boron carbides and nitrides or other synthesized boron compounds, exhibit numerous attractive mechanical and chemical properties, from high melting points and hardness to superior resistance to wear, corrosion, and molten metal attacks, as well as notable electrical conductivity. Consequently, significant opportunities for enhancing the surface properties of metals or ceramics can be envisaged by means of applying coatings constituted from these compounds [14].

Table 3. *Properties of different compounds* [8].

Compounds		Temperature of Melting [°C]	Hardness [HV]	Maximal service temperature [°C]
CrC	Chromium Carbide	1500 - 1900	1700 - 2200	800
WC	Tungsten Carbide	2000	2500	500 - 600
VC	Vanadium Carbide	2200	3000	500 - 600
B₄C	Boron Carbide	2500	3000 - 4000	500 - 600
TiN	Titanium Nitride	3000	3000 - 4000	< 600
TiAlN	Titanium Aluminum Nitride	-	3200	800
CrN	Chromium nitride	1700	2500	700 - 800
TiCN	Titanium Carbo-Nitride	3150	2000 - 3000	< 500
TiBN	Titanium Boron Nitride	-	5500	700
cBN	Cubic Boron Nitride	2700	3000	> 1000
Cr₂O₃	Chromic Oxide	2400	5000	800 - 1000
Al₂O₃	Aluminum Oxide	2050	2000	> 1000
C	Diamond	3800	8000	600
DLC	Diamond-like Carbon	-	1500 - 6000	≤ 400

Surface hardening processes represent a cornerstone in material engineering, offering indispensable techniques to enhance the durability and functionality of components across various industries. This chapter serves as a comprehensive exploration of these processes, beginning with an introduction that underscores their pivotal role in engineering applications and onto meticulous categorization where diverse processes and their characteristics are given.

Moreover, the chapter delves into the intriguing realm of combination possibilities of these surface hardening processes, elucidating combined examples that are synergistically employed to optimize material properties, followed by others that are conflicting, either incompatible or having counter benefits to what proceeded. The section ends with an examination of the concerns associated with combining these processes and a quick comparison between the boron diffusion process and others that are similar to it.

Furthermore, focusing on the focal point in the forthcoming sections, boriding, also known as boronizing, a type of boron diffusion process that exemplifies the utilization of boron's unique attributes in surface hardening processes [6]. The process is explored through Its history and principles, along with the techniques that are applicable within both research and industries, from traditional to modern ones. Accordingly, a categorization of those versatile techniques is provided, differentiating the usage and type of the boron source, along with the power source that allows the boron diffusion.

II.2.   SURFACE HARDENING PROCESSES SHP

Surface hardening processes encompass various techniques, including induction hardening, flame hardening, carburizing, nitriding, boriding, and more. Each method offers distinct advantages and limitations, depending on material compositions, desired surface properties, and application requirements. Common examples of components that undergo surface hardening include gears, camshafts, crankshafts, bearings, cutting tools, and various industrial machine parts.

The surface hardening principle relies on having the ability to strengthen the outer layer of a material through localized or general heating, chemical reactions, or mechanical treatments, all while preserving its core properties, significantly improving wear resistance, fatigue strength, and overall durability, thereby extending the lifespan of the components [6–8].

II.2.1. Categorization

A.   Thermal SHP

This category includes processes that primarily rely on the controlled application of heat to the surface of a material to alter its microstructure and increase hardness, without changing the properties of its core.

a)   Flame Hardening

Employing high-temperature flames via oxyacetylene or oxyhydrogen torch to selectively heat and harden specific areas or general ones of a metal component. That is known as austenitizing the surface of the steel. After that, an immediate quenching in water or other media is followed. With no change in composition, this localized heating and rapid quenching results in a hardened martensite surface layer on top of the ferrite pearlite structure of the core. It's often employed for large and irregularly shaped components, such as gears, machine tool ways, crankshafts, agricultural equipment parts, and machine tools [12,65].

b)   Induction Hardening

Steel parts are placed in an electromagnetic field via an inductor to heat the surface of a metal quickly. After heating, the material is rapidly quenched to achieve a hardened surface layer that is uniform [6]. It has versatile use cases due to faster process, energy efficiency, less distortion, and small footprints.

c)   Laser Hardening

Generally applied to harden localized areas of steel and cast-iron machine components using a high-energy laser beam. The controlled application of laser energy allows for selective and localized hardening with no chemistry changes and produces thin surface zones that become fine martensitic microstructures after quenching, even in steels with relatively low hardenability, procuring high hardness and good wear resistance with less distortion. Found in applications of camshafts and crankshafts due to its flexible use in irregularly shaped components [12].

d)   Vacuum Treatments

Also known as low-pressure treatments, they involve heating the material in an oxygen-free environment to prevent the oxidation of the material for better control of mass transfer rates [7], found in multiple applications, carburizing as given in Table 6, nitriding, or vapor deposition techniques. For instance, in steels, vacuum treatments can remove impurities like hydrogen and nitrogen, and can also be used for decarburization, deoxidation, and desulfurization. In simpler terms, they remove inclusions or contaminants from the material, leading to improved cleanliness and effectiveness.

e)   Tempering

When steel is thermally hardened and quenched, it goes through the transformation from austenite into martensite, creating a brittle structure that is generally capable of offering lots of life. However, in other use cases, the extreme brittleness may become problematic, that is where tempering is needed, changing the unstable nature of the martensite and relieving it from stresses, decreasing hardness but increasing toughness and ductility. It is done by heating the hardened component below the eutectoid temperature and cooling it in a controlled manner [6,65].

f)   Annealing and normalizing

Interchangeable terms to stress relief materials with differences in the cooling method. The first requires slow cooling rates compared to the other, but both in air temperatures. That makes the annealing lengthy, making it unfavored cost-wise but consistent in terms of outcomes [66].

Annealing produces refined grain structures, reducing hardness and improving ductility by softening and stress relieving the material, aiding machinability. Normalizing also produces more uniform, fine-grained microstructures and removes the gummy nature of the metal, making it respond better to the cutting tool action. However, not all steels can be normalized because the technique uses temperatures exceeding critical points. Normalization is used only on low-carbon or some medium alloy steels and can be subsequent to annealing or other heat treatments [65,67].

g)   Cryogenic treatments

After case hardening, components can undergo a cryogenic treatment, which is a post-treatment process that involves subjecting materials to low temperatures, as long as they are chilled to -70 °C, even if with low benefits, there are no reversal effects on the material. Moreover, deep cryogenic treatment DCT is performed at below -170 °C with liquid nitrogen or even to -270 °C with helium and can provide only benefits the lower the temperature gets. It is used to enhance the properties of hardened surfaces by stabilizing and stress-freeing the martensite [12].

These thermal surface hardening processes are used across various industries to improve the surface properties of metal components, making them more resistant to wear, abrasion, and other forms of mechanical stress. They can be used before, during, or after other surface hardening processes depending on the specific end goal and Table 4 presents some of their advantages and disadvantages.

Table 4. Comparison of thermal treatment techniques [12].

Heat source	Advantages	Disadvantages
Induction	Fast process Deep case depth obtainable Lower capital cost than laser High coverage area	Downtime for coil change Quenchant required Part distortion Electromagnetic forces may disturb surface conditions
Flame	Cheap Flexible Mobile	Poor reproducibility Quenchant required Part distortion Environmental problems
Arc	Relatively cheap Flexible	Limited hardening Large thermal penetration Poor control to avoid melting
Laser	Minimal distortion Selective localized hardening Quenchant free Case depth controllable Limited post machining	High capital cost Multiple passes give local tempering

B.   Thermochemical SHP

Also known as a diffusion coating category, it involves altering the surface properties of a material by introducing chemicals in a heated environment. These processes aim to enhance the hardness, wear resistance, and overall durability of the material's surface while maintaining desirable mechanical properties in the core.

a)   Carburizing

Introduces carbon into the surface layer of a ferrous material, usually low-carbon steel, by exposing it to a carbon donor, Figure 13, at various temperatures, from lower than 460 to 930 °C. However, in most cases, it alone isn't sufficient with respect to wear resistance, strength, and cyclic loading. Therefore, it is usually followed with quenching and even tempering sometimes, hence the common naming, case hardening. That is to transform the carbon-enriched surface and the low-carbon core from austenite into martensite [7]. Widely employed in the automotive industry for components like gears and camshafts, where enhanced surface hardness is essential for long-term performance.
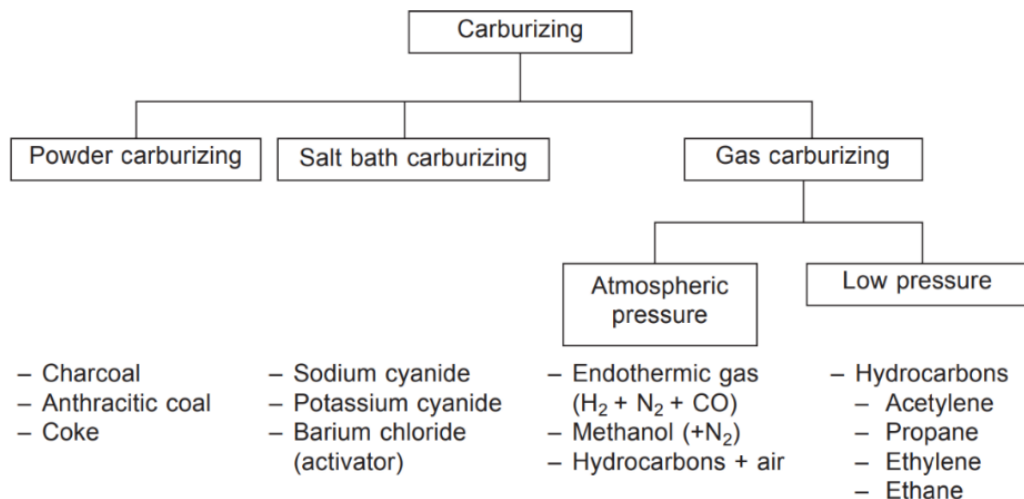
Figure 13. Carburizing technologies by carbon donors [7].

b)   Nitriding

A case hardening process that has been and remains the major thermochemical treatment, it, along with ferritic nitrocarburizing, represent the dominant volume of industrial surface modification technologies. It enriches the surface layer of materials, typically steels, with nitrogen by exposing it to nitrogen-rich gases like ammonia NH_3, alkali salts, or plasmas at diverse temperatures, lower than 470°C and 480 to 600 °C with distinct properties. Multiple applications exist, salt bath nitriding, plasma nitriding, ion nitriding, and others, all ensuing a modified zone that generally deepens up to 300 μm, with a hard, wear-resistant surface layer that has enhanced fatigue and corrosion resistance without requiring additional heat treatments. Figure 14 describes its profile's hardness compared to other treatments [66,68].
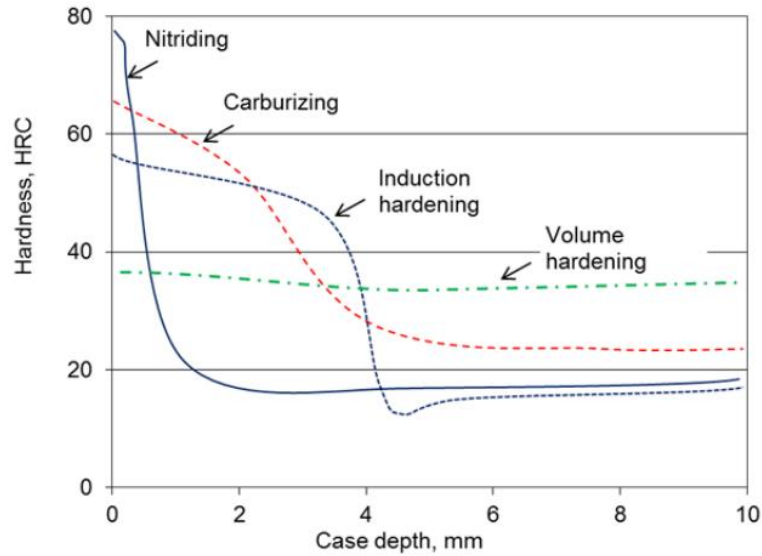
Figure 14. Hardness along the profiles of selected treatments [68].

c)   Boriding

Also referred to as boronizing, and follows the same principles of the previous ones, introducing boron atoms into the surface of a material, typically steel, via a medium donor but mostly with an activator at considerably higher temperatures, effective from 850 to 1100 °C. The process forms a hard boride layer on the surface, as discussed in the previous chapter, enhancing wear and corrosion resistance with extreme hardness up to 2000 HV, way above that of carburizing and nitriding [68], Figure 15. This process will be developed further afterward, as it is the main focus of the thesis.
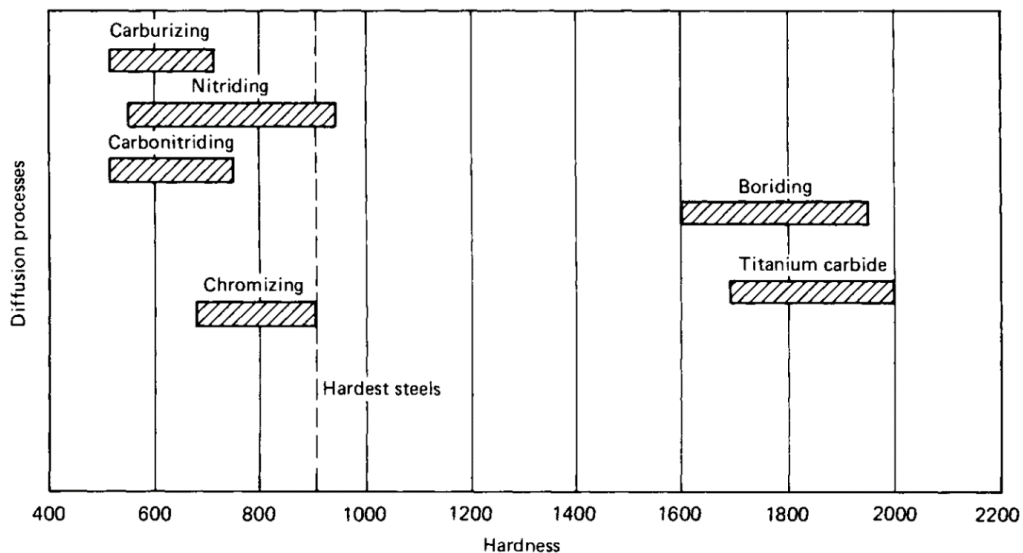
Figure 15. Spectrum of hardness of certain diffusion processes on steels [12].

Even though these thermochemical treatments exist solely, they can also be combined or intertwined with other surface hardening processes, like carbonitriding, or in the case of multicomponent boriding, which is the diffusion of boron with another element like boroaluminizing, borochromizing, borochromtitanizing, etc. [12,14].

C.   Mechanical SHP

Mechanical Surface Hardening Processes Involve altering the surface properties of a material through physical deformation or abrasion, resulting in increased hardness and durability, like:

a)   Peening

Shot peening involves bombarding the surface of a material with small spherical objects, usually steel or ceramic shots, at high velocities to impart compressive residual stresses at the surface, where most fatigue cracks initiate, and work-hardens the surface, improving fatigue resistance and wear characteristics [66]. It is of utmost effectiveness for components that are subject to high-cycle fatigue loading [6]. Similarly, laser shock peening, a high-energy pulsed laser technique, produces the same type of stresses with a higher magnitude and within a deeper depth [8].

b)   Burnishing

A process that involves the use of a hard and smooth tool, usually a ball or roller, to rub solid lubricant powders with pressure, smoothening the surface of a material. Some of those powders are Molybdenum disulfide MoS_2 or Tungsten disulfide WS_2. This can induce work-hardening and improve the tribological properties like surface finishes of roughened substrates [8].

c)   Ultrasonic Impact Treatment

Done by applying high-frequency mechanical vibrations converted over a transducer from High-frequency electrical energy. These vibrations are amplified and transferred to pins that impact repeated strikes to the material surface. Consequently, plastic deformations arise, inducing compressive stresses while reducing harmful tensile stresses to improve fatigue [69].

These mechanical surface hardening processes, including work-hardening processes, can't be carried on all kinds of materials and are often preceded; otherwise, problems arise. For example, if a metal part has residual stresses induced by such techniques prior to heat treatment, unpredictable shape changes or new systems of residual stresses can occur [66].

D.   Coating SHP

Coatings involve applying a protective layer to the material to enhance hardness, wear resistance, or corrosion resistance. Deposition coatings, as opposed to diffusion coatings, are more independent from the substrates and offer chemical composition flexibility. Some of them:

a)   Thermal spraying

A process reliant on partially or totally melted materials that include metals, ceramics, or polymers to coat the base material. Through preparation of the substrate's surface rugosity for optimum adhesion and propelling the melted particles, thin platelets or lamellae called splats conform to the substrate's shape, creating a durable, wear-resistant layer that can improve hardness and protect against corrosion [8].

b)   Plating

A thin coating by deposition of dissimilar materials, mainly on steels, and can encompass diverse applications. Electroplating through electrodeposition, such as tin plating through tin salts decomposed in an electrolytic bath or hard chromium plating, via a chromic acid CrO_3 solution and a catalytic anion. Nickel coating can be done by an electroless plating where the deposition is through an autocatalytic chemical reduction of nickel ions by various compounds. This or other plating coatings provide build-up, decorative aspects, protection against corrosion and carburization, and for brazing operations. The main elements found in its applications are chromium, nickel, zinc, copper, cadmium, and even silver and gold [6,65].

c)   Vapor deposition

This is mainly caused by chemical and physical vapor deposition processes, referred to as CVD and PVD, two distinct approaches used to deposit thin coatings that provide improvements in life service and wear resistance. PVD physically generates and deposits atoms or molecules on substrates in high-vacuum environments. The atom flux encroaching on the substrate is generated by numerous techniques, such as sputtering, ion plating, or evaporation, the latter being less efficient than the others. Conversely, CVD, rather than being mechanical, exposes substrates to gaseous reactants, promoting chemical reactions at atmospheric pressures, therefore having more throwing power, hence the ability to uniformly coat complex shapes, better than the PVD processes [67].

d)   Galvanizing

Commonly known as hot dip galvanizing, it involves immersing steel or iron in molten zinc, creating a coat of zinc and zinc-iron alloy layer, enhancing hardness and mainly excellent corrosion protection, making the ferrous material rust-proof. Another type of galvanizing is sherardizing, but it involves diffusion at elevated temperatures, also referred to as dry galvanizing or vapor galvanizing [7].

Table 5. Comparison of certain coatings [7].

	Sherardizing	Hot dip galvanizing	Electro-plating	Protective paint	Thermal spraying
Hydrogen embrittlement	No	Possible	Possible	No	No
Surface hardness	Hard	Soft	Soft	Soft	-
Process temperature °C	320 - 500	> 440	< 100	< 200	-
Paintable	Yes	Yes *	Yes *	-	Yes *
Uniformity	Good	Good	Good	Good	-
Layer thickness μm	10 - 120	> 30	< 30	< 15	> 70
* Pretreatment needed					

Coating surface hardening processes play a crucial role in extending the service life of components in industries such as aerospace, automotive, manufacturing, and more. The choice of the coating method depends on the specific material, application, and desired properties, Table 5.

II.2.2. Surface Hardening Combinations

The aforementioned surface hardening processes can also be utilized in combinations, either concurrently or as pre- or post-treatments to one another. Some combinations complement each other, synergistically enhancing the material's properties, while others conflict, either due to incompatibility or to counteracting each other's benefits.

A.   Combined SHP

Combined surface hardening processes involve the strategic combination of two or more techniques to achieve a synergistic effect that optimizes the tribological properties of the material's surface.

a)   Case hardening with deep cryogenic treatment and tempering

Samples of H13 tool steel, a hardened steel, after deep cryogenic treatment DCT and additional tempering DCTT, wear resistance was observed to improve by 12 and 24 %, respectively. That can be due to the transformation of the retained austenite to martensite, and to a more uniform and homogeneous carbide distribution [70].

b)   Shot peening post plating or carburizing

If shot peening is carried out after nickel or chromium plating, then the fatigue strength is often increased beyond that of the base metal [66]. Or else, if carried after carburizing, it reduces the retained austenite, improving the bending fatigue performances [6].

c)   Nitriding a quenched and tempered steel

In physical metallurgy, oxides are more stable than nitrides, which themselves are more stable than carbides. By that, the alloying elements of carbide particles formed from quenching and tempering can be replaced by nitride particles if nitriding is carried afterward, resulting in an improved and stabler hardened layer [7].

d)   Nitriding with PVD coating

This duplex process combines plasma nitriding, which introduces nitrogen into the material's surface, with physical vapor deposition PVD coating to deposit a thin layer of a hard material like titanium nitride TiN on top. This combination enhances both hardness and wear resistance [71].

e)   Carbonitriding or nitrocarburizing

They combine the principles of carburizing and nitriding and fall into the case hardening category. They are distinct in their diffused mixture of carbon and nitrogen. One has both diffused, while the other has less carbon content, emphasizing nitrogen, respectively. Additionally, they offer good hardness, Figure 16, while the first is performed at 800 to 850 °C, the latter at much lower temperatures, 570 to 600 °C [66].
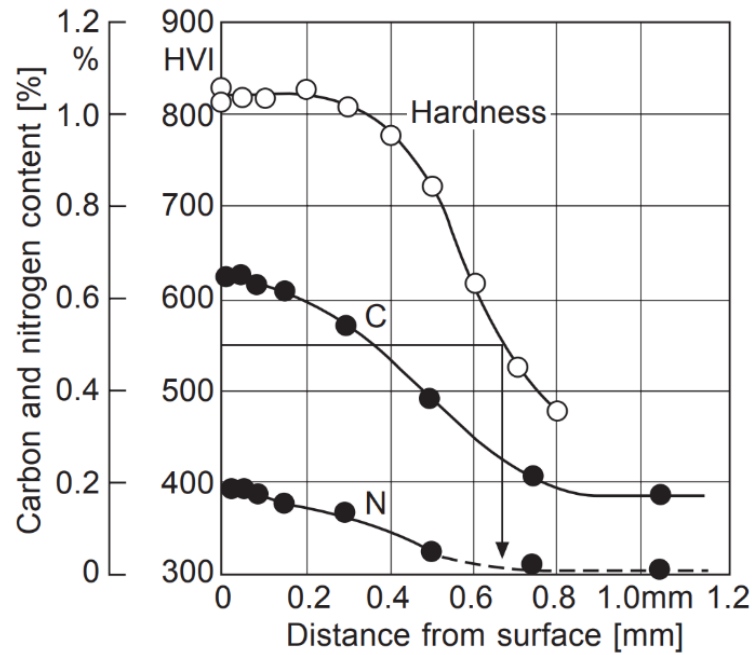
Figure 16. *Hardness profiles in carbonitrided low alloyed steels* [7].

f)   Borocarburizing

Referred to when simultaneous or sequential carburizing and boriding are processed, entailing the diffusion of both carbon and boron and resulting in a borocarburized layer, Figure 17. If it is sequential, a precarbuzing is applied before boriding, resulting in laser-modified borocarburized layers with higher abrasive wear resistance than typical borided and carburized layers [72]. If it is simultaneous, it is due to the utilization of both boron and carbon-rich sources, such as when gas boriding through organic boron compounds like trimethyl borane $(CH_3)_3B$ or triethyl borane $(C_2H_5)_3B$ in order to avoid other toxic gas usages such as boron halides or diborane B_2H_6 [73]. The advantage of such a combined layer lies in the higher frictional resistance compared to a single treatment of either one alone [68].
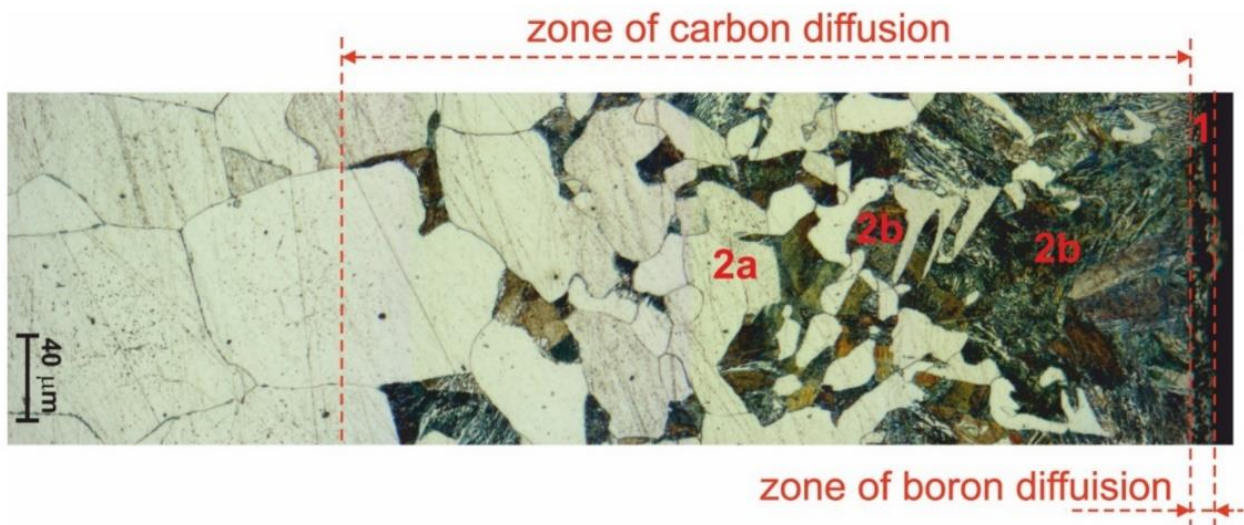
Figure 17. *Optical microscope image of a borocarburized Armco iron showcasing the different diffusion zones (1) iron boride, (2a) pearlite and (2b) ferrite* [73].

g)   Borocarburizing followed by sulfurizing

in a specific study, two surface hardening processes were combined on a 2Cr13 stainless steel substrate, sulfurizing on top of a Borocarburizing process, which itself is a simultaneous combination of boron and carbon diffusion. The sulfurized layer was 18 µm and consisted of Fe_2S and FeS phases, with the latter acting as a solid lubricant, while the borocarburized layer had FeB, Fe_3C, and Fe_2B in a thickness of 120 µm and a maximum hardness nearing 1200 HV. The combination was uniform, dense, and well-joint with the matrix of the 2Cr13 samples, providing excellent wear resistance and antifriction properties. as illustrated in Figure 18 [74].
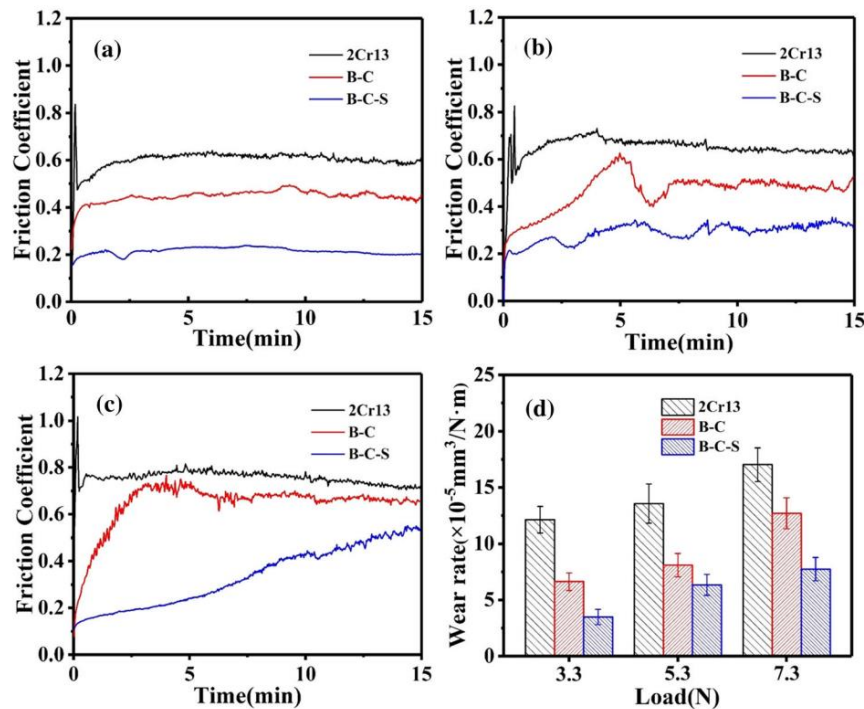
Figure 18. *Friction coefficient as a function of time for different loads (a) 3.3 N (b) 5.5 N (c) 7.3 N on different 2Cr13 samples, untreated, borocarburized, borocarburized and sulfurized, along with (d) their wear rates* [74].

a)   Annealing post boriding

annealing parts after powder pack boriding can allow further diffusion of boron toward the core, reducing the surface concentration of boron. Reallocating the FeB compounds into a single-phase layer of Fe_2B [75]. However, if the FeB content is high, this results in a volume difference between the two iron boride compounds FeB/Fe_2B, which can be problematic, leaving voids in the layer due to volume contraction, so it needs careful processing. Alternatively, sometimes, after boriding, cracks and spalling occur immediately after cooling before proceeding with the annealing [12]. Accordingly, annealing after boriding could either reduce the stresses between the layer phases or transform a particular phase into its adjacent phase, like the case of FeB turning to the Fe_2B phase [75,76].

B.   Conflicted SHP

Examples of surface hardening processes that may not be effective or can lead to undesirable outcomes if combined are:

a)   Copper plating before TRD

TRD, meaning thermo-reactive deposition and diffusion, is a surface hardening process reliant on the precipitation of carbides and nitrides in carbon and nitrogen-containing materials. By the use of reagents known as carbide/nitride forming elements CFE/NFE, carbon and nitrogen atoms in the substrates diffuse to the surface, reacting with these reagents and forming a thick and hardened surface layer [8]. Even though TRD is feasible on nickel or chromium-plated steels, copper-plated steels block carbon and nitrogen from reacting with the CFE/NFE by obstructing their diffusion through the plating, stopping the formation of the carbide and nitride coatings [12].

b)   Nitriding a carburized steel

while carbonitriding or nitrocarburizing are beneficial techniques to steels relying on simultaneous diffusions of carbon and nitrogen, counterintuitively, if one diffusion precedes the other, it does not mean one is as beneficial as it should be. A specific study demonstrated that pre-existing carbon atoms solutioned in steels, like the case of carburized steels, can hinder the growth of nitride layers. That was seen after an air decarburization, which lowered carbon and residual stresses, promoting the increase of the nitrided layer thickness by more than two times if carried directly on a carburized sample, Figure 19 [77].
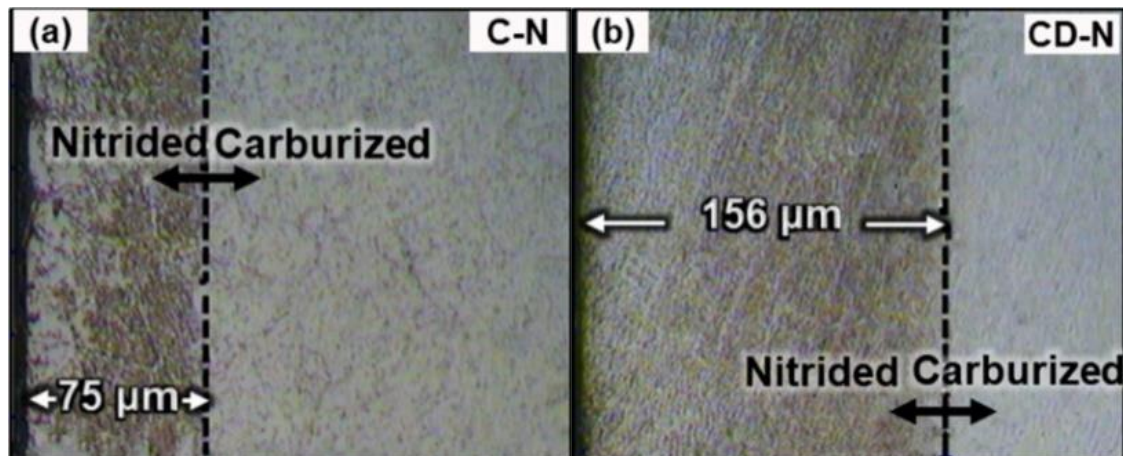
Figure 19. *Cross sectional nitride layers resulted from nitriding a steel that is (a) carburized and (b) carburized then decarburized* [77].

c)   Quenching and tempering after Boriding

Numerous studies report the disadvantages of such practice. One reported that boriding an AISI 5140 steel for four hours at 950 °C gave rise to a boride layer of 90 µm, with an increase in hardness from 265 to 1474 HV and in wear resistance by about four times.

If quenched and tempered, the layer thickness diminished, and its wear resistance weakened to only two times compared to the unborided sample, Figure 20. That was explained and confirmed by X-ray diffraction (XRD) analysis, which showed the disappearance of Fe_2B and its conversion to FeB in quenched and tempered substrates compared to the presence of both phases if not, and the Fe_2B phase has advantageous effects on wear resistance contrary to the FeB phase and its brittle nature [78].
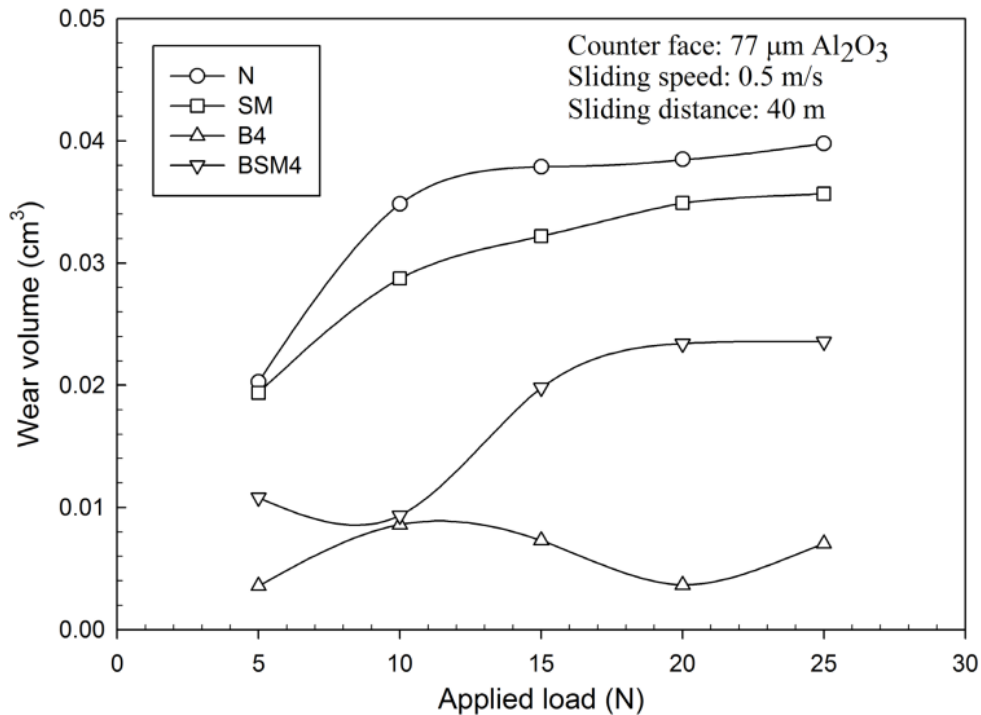
Figure 20. *Wear graph of steels that are (N) unborided, (SM) quenched and tempered, (B4) borided for 4 h at 950 °C, (BSM4) quenched and tempered after boriding* [78].

C.   Combination concerns

Even though combining certain processes may give positive results, some combinations may result in downsides like those mentioned before. Thus, the effectiveness of combining multiple surface hardening processes depends on several factors.

- **Compatibility of Materials**

Some materials may not be compatible with specific surface hardening techniques. Accordingly, combining techniques that have vastly different coefficients of thermal expansion can result in cracking or delamination of the surface layer or even the inability to diffuse, like the mentioned example of applying a thermo-reactive diffusion TRD on a copper-plated substrate [12], or boriding an aluminized steel or steels that contain aluminum where the aluminum produces a softer ferrite zone beneath the layer, reducing its benefits [7].

- **Residual Stresses**

All steel parts have balanced stress systems within them comprising tensile and compressive residual stresses. Compressive stresses are beneficial when it comes to tensile loading, and processes like shot peening are used to increase such stresses at the surface, making these types of residual stresses intentional and part of the design. However, when a metal part has residual stresses prior to heat treatments, random shape changes or new systems of residuals can arise [66].

- **Distortions**

Certain treatments, if combined, may increase the risk of distortion or dimensional changes in the component, which may not be acceptable for precision parts. For example, A-type tool steels are hardened then air cooled, contrary to most other tool steels where water or oil quenching is essential in their processing, and because of that, uneven cooling of surfaces and interiors results in distortions [67]. Boriding can cause thermal distortion in extreme temperatures when it comes to samples of relatively slender sections [14].

- **Surface Finish**

The quality of the surface finish of the steel component prior to surface treatments influences the outcomes. That can be observed in salt bath treatments where enhanced surface polishing before ferritic nitrocarburizing correlates with improved finishing results [66]. Extrapolating that, the starting surface condition, such as variations in the surface's crystallographic orientation, its purity, surface roughness, or contamination, can impact the adhesion and effectiveness of subsequent treatments by hindering the kinetics of the reactions [7].

- **Process Parameters**

Incorrect process parameters, i.e., temperature, time, and pressure, or else, can lead to over-treatment, which can compromise the material's properties or cause distortion, and insufficient treatment may not achieve the desired hardness or wear resistance. So, having processes that have far dissimilar parameters may have counter-impacts.

- **Treatment Sequence**

The order in which surface hardening techniques are applied can significantly impact the outcome. In some cases, applying a certain treatment before another may negate the benefits or lead to undesirable effects, like when quenching and tempering after boriding, which reduced the advantageous wear rates gained to only two compared to four if the boriding alone [78]. On the other hand, annealing post boriding, if properly applied, can provide advantageous properties [12].

- **Cost and Complexity**

Some composite combinations can be costly and complex to implement, making them impractical for specific applications, and that is a challenge still under scrutiny in recent research.

II.2.3. Comparison

If a comparison between surface hardening processes is made, various aspects are of consideration, and the most important ones are, reached hardness, treated base material, and process conditions like what is detailed Table 6. However, focusing on the hardness reached after treatment, which has an essential correlation to wearability, Figure 21 demonstrates that soft steels and ordinary constructional steel or low-carbon steels are below 200 hardness, then high strength low alloy HSLA steels that reach nearly 500, then from which the surface hardening's role appears, beginning by the processes like flame and induction hardening onto carburizing and laser or electron beam for up to 650, onto nitriding and specialized hardenings like that of tool steels approaching 800 and lastly chromium electroplate which reaches the hardness of the hardest steels, 900 to 1000. That is reached and exceeded through coatings like plasma spraying to around 1500. And from that, the hardest traditional thermochemical diffusion treatment, the boriding, or boronizing, ranging from 1600 to nearly 2000. Above it, there are certain cermets, ceramics, titanium compounds coatings, and carbides, boron carbide being the hardest [6].

While invoking miscellaneous surface hardening processes unrelated to boron or boriding may be counterintuitively out of context, a comprehension of their functioning, their purpose, and their compatibility with one another may invoke some insights and questioning in the similarities with the boriding process like carburizing or nitriding [7,66], or the conformity with it, positive or negative, as in the last example where quenching and tempering after some processes has advantageous results contrary to its use after boriding, leading to adverse outcomes, degrading the utility of the boriding process [78].
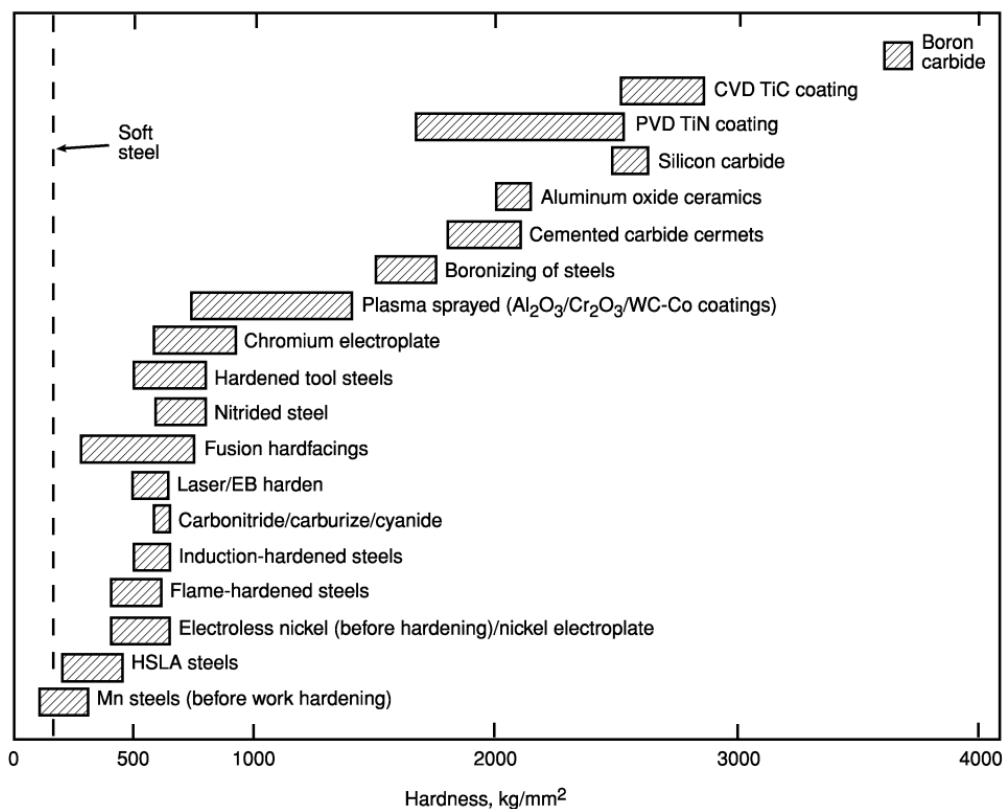
Figure 21. *Range of hardness levels for various materials and surface treatments* [6].

Table 6. Characteristics of certain thermochemical surface hardening treatments [6].

Process	Nature	Temp. °C	Case Depth	HRC	Base Metals	Process characteristics
Carburizing						
Pack	Diffused carbon	815 - 1090	125 μm - 1.5 mm	50 - 63 (a)		Low equipment costs, difficult to control case depth accurately.
Gas	Diffused carbon	815 - 980	75 μm -1.5 mm	50 - 63 (a)	Low-carbon steels,	Good control of case depth, suitable for continuous operation, good gas controls required, can be dangerous.
Liquid	Diffused carbon and possibly nitrogen	815 - 980	50 μm - 1.5 mm	50 - 65 (a)	low-carbon alloy steels	Faster than pack and gas processes, can pose salt disposal problem, salt baths require frequent maintenance.
Vacuum	Diffused carbon	815 - 1090	75 μm - 1.5 mm	50 - 63 (a)		Excellent process control, bright parts, faster than gas carburizing, high equipment costs.
Nitriding						
Ion	Diffused nitrogen	340 - 565	75 μm - 0.75 mm	50 - 70	Alloy steels,	Faster than gas nitriding, no white layer, high equipment costs, close case control.
Gas	Diffused nitrogen	480 - 590	125 μm - 0.75 mm	50 - 70	nitriding steels, stainless steels	Hardest cases from nitriding steels, quenching not required, low distortion, process is slow, is usually a batch process.
Salt	Diffused nitrogen	510 - 565	2.5 μm - 0.75 mm	50 - 70	Most ferrous metals including cast irons	Usually used for thin hard cases <25 μm, no white layer, most are proprietary processes.
Carbonitriding						
Gas	Diffused carbon and nitrogen	760 - 870	75 μm - 0.75 mm	50 - 65 (a)	Low-carbon steels, low-carbon alloy steels,	Lower temperature than carburizing (less distortion), slightly harder case than carburizing, gas control critical.
Liquid (cyaniding)	Diffused carbon and nitrogen	760 - 870	2.5 - 125 μm	50 - 65 (a)	Low-carbon steels	Good for thin cases on noncritical parts, batch process, salt disposal problems.
Ferritic (nitrocarburizing)	Diffused carbon and nitrogen	565 - 675	2.5 - 25 μm	40 - 60 (a)		Low-distortion process for thin case on low- carbon steel, most processes are proprietary.
Other						
Boriding	Diffused boron	400 - 1150	12.5 - 50 μm	40 - >70	Alloy steels, tool steels, cobalt and nickel alloys	Produces a hard compound layer, mostly applied over hardened tool steels, high process temperature can cause distortion.
Thermal diffusion process (TRD)	Diffused carbide via salt bath processing	800 - 1250	2 - 20 μm	>70	Tool steels, alloy steels, medium-carbon steels	Produces a hard compound layer, mostly applied over hardened tool steels, high process temperature can cause distortion.

(a) Requires quench from austenitizing temperature

II.3.   BORIDING PROCESS

II.3.1. History

Within the 19th century, starting from the first trial of boron isolation by different scientists, as seen in the first chapter, Henri Moissan, a French scientist, also had an interest in that. He contributed greatly to applied chemistry through the study of numerous elements, including his discovery of fluorine and designing an electric arc furnace laying the foundation of high-temperature treatments. Afterward, he was able to synthesize numerous high melting compounds, including impure boride phases, and before, he isolated boron by the reduction of boron oxides with magnesium to 95 percent of purity, or to nearly 99 percent with hydrogen in 1891-1892, from 70 percent of purity at that time [79], which was followed in 1909 by Ezekiel Weintraub, as mentioned in the first chapter, who isolated the purest form [22].

Furthermore, Henri Moissan investigated carbides and their diffusion and tried to diffuse boron into steels. He then concluded that it was conceivable to produce surface layers that were hard and wear-resistant through such diffusion in 1895. From which researchers began experimenting in the beginning of the 20th century with the diffusion of boron into metal surfaces [7,10,76], and by the two-thirds of the nineties, the process gained research interest, as illustrated in Figure 22.
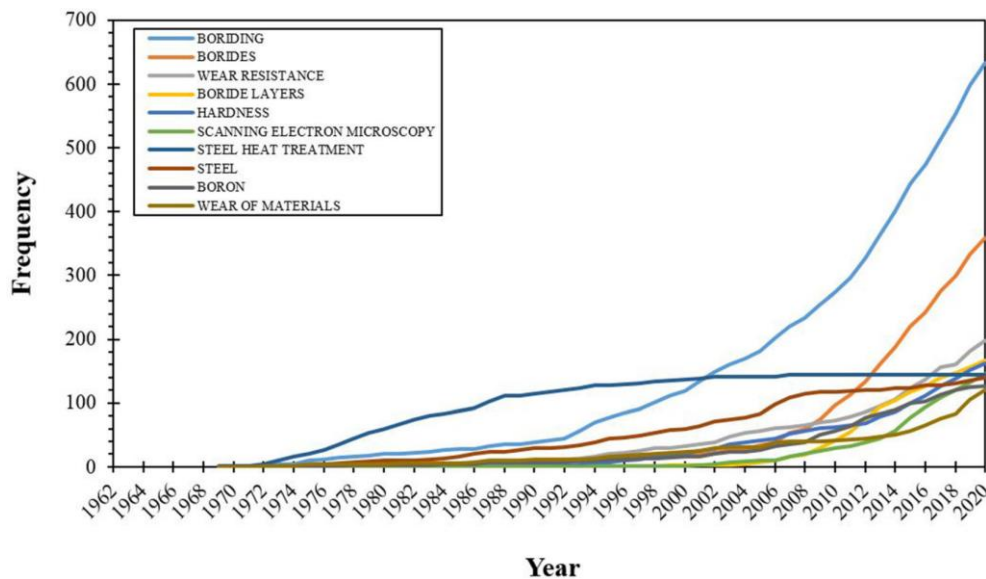
Figure 22. *Evolution of the researched keywords* [80].

II.3.2. Generalities

The boriding or boronizing process is a thermochemical surface hardening treatment, as indicated previously. It is based upon a diffusion process in which boron atoms are introduced into the material's surface, enriching it with boron by forming boron compounds, specifically boride layers, that are corrosion resistant with less wearability to abrasion largely, have an extreme brittleness, that is around a hardness of 2000 HV [68], Figure 21, and a three to ten times service life improvement.
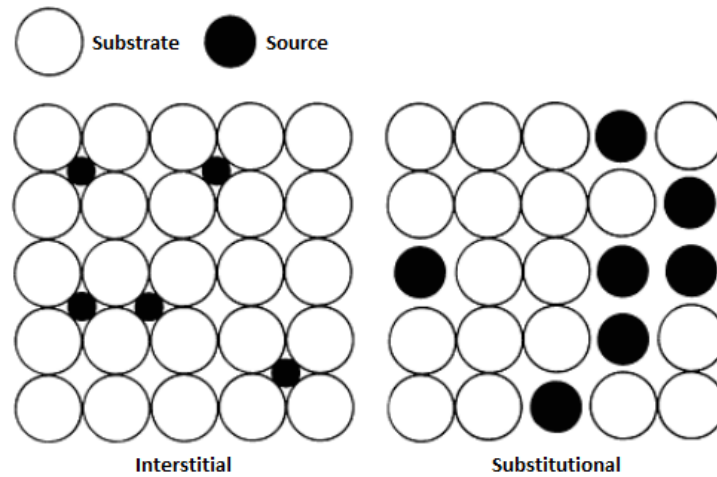
Figure 23. *Diffusion mechanisms* [81].

Traditionally, the process relied on lacunar and interstitial diffusions instead of substitutional ones, Figure 23, by means of a high thermal energy combined with chemical reactions between the substrate and a boron source, which explains each part of the thermochemical naming. By such, the substrate is heated to elevated temperatures, generally around 800 or 1000 °C, for several hours, reaching or exceeding 10 hours [7], in a medium donor from which boron atoms are gained, and with the help of an activator or other means depending on the technique, the boron atoms are induced to diffuse towards the lattice of the surface's parent material, substrate, or workpiece. Moreover, other processes that have a physical aspect were developed afterward, as will be developed in the boriding techniques subsection.

The substrate is generally a metal, predominantly a ferrous and specifically a steel, but can be other than that with varied benefits and challenges, Table 6, which will be discussed in the next segment of the thesis, chapter III. While the mechanical and chemical properties of borided materials are extremely altered than non-borided ones, they themselves differ greatly on certain factors [7]:

- Type of the boriding technique processed.
- Alloying elements' content in the substrate.
- Structuring and composition of the boride layer.
- Thickness of the boride layer obtained.

Cleansing the surfaces of oxides, oil marks, dirt, and other substances that may hinder the diffusion process helps for an efficient treatment. That is done either through degreasing in solvents, such as ether, benzoyl, acetone, spirit, carbon tetrachloride, through chemical and electrolysis etching, or mechanical cleansing, manually, in barrel tumbling or by ultrasound and else [9].

Compared to carburizing and nitriding, boriding has a way better wear strength due to its hardness, which is indicated in the surface hardening processes section above, Figure 21. It gives a hardness reaching 2000 HV instead of under half of that, 1000 HV, for the other two or their combination, carbonitriding and nitrocarburizing.

The process of boriding has a broad spectrum of industrial applications, particularly useful for components subjected to sliding wear and corrosion, and these include extrusion screws, cylinders, textile nozzles, different dies and molds, pressing rollers, mandrels, pharmaceutical parts, heat exchangers, or small drive gears for oil pumps, or more [6,7].

II.4.   BORIDING TECHNIQUES

Boriding or boronizing processes vary from one technique to another and may sometimes be similar or intertwined with other surface hardening processes, making them difficult to classify. Nevertheless, classifications were proposed by different scientists, Minkebich in 1965, Przybyłowicz in 2000 and Krukovich et al. in 2016 [9], and they were based on different criteria:

- Phase compositions, structures, and their properties; single-phase, bi-phase, and else.
- Usage and processing temperatures; from low, medium, to high temperatures, ranging respectively in 550, 900 °C, and above. Used mostly on ferrous alloys.
- Transportation processus of the sub-ions to the surface; in other terms, the characteristics and mechanisms of saturating boron atoms generation.
- Technological specifics; methods and means of boriding and their types, as well as the ways of sealing the mediums.

The most recent classification was by Professor Kulka in 2019, where he took into consideration some of the aspects mentioned above and devised the process into two main categories:

- Chemical techniques; traditional thermochemical boriding in solid, liquid, and gaseous media.
- Physical techniques; more recent and modern approaches.

The categorization was based on the process's characteristics and the formation mechanisms of the free atoms or ions of boron that are adsorbed and diffused on the substrate's surface. Additionally, techniques that are put in boxes with broken lines in Figure 24 represent the most intensively developed techniques, indicating, as his book was titled, the current trends in boriding [10].

Furthermore, the mentioned categorization will be developed underneath, and they all produce different types of boride layers that will be detailed in the next chapter:

- Boride layers; gotten from traditional thermochemical techniques in solid, liquid or gas media and some of the modern physical ones like in glow discharge conditions or surface alloying.
- Superficial layers and coatings; gotten from physical techniques like ion implantation, laser and vapor depositions, painting, enameling, electroplating, hot dip metallization, sol-gel processes, cladding, thermal spraying, and detonation treatments. From which, the high-energy methods, such as the three last mentioned, were mainly the most effective processes of them.
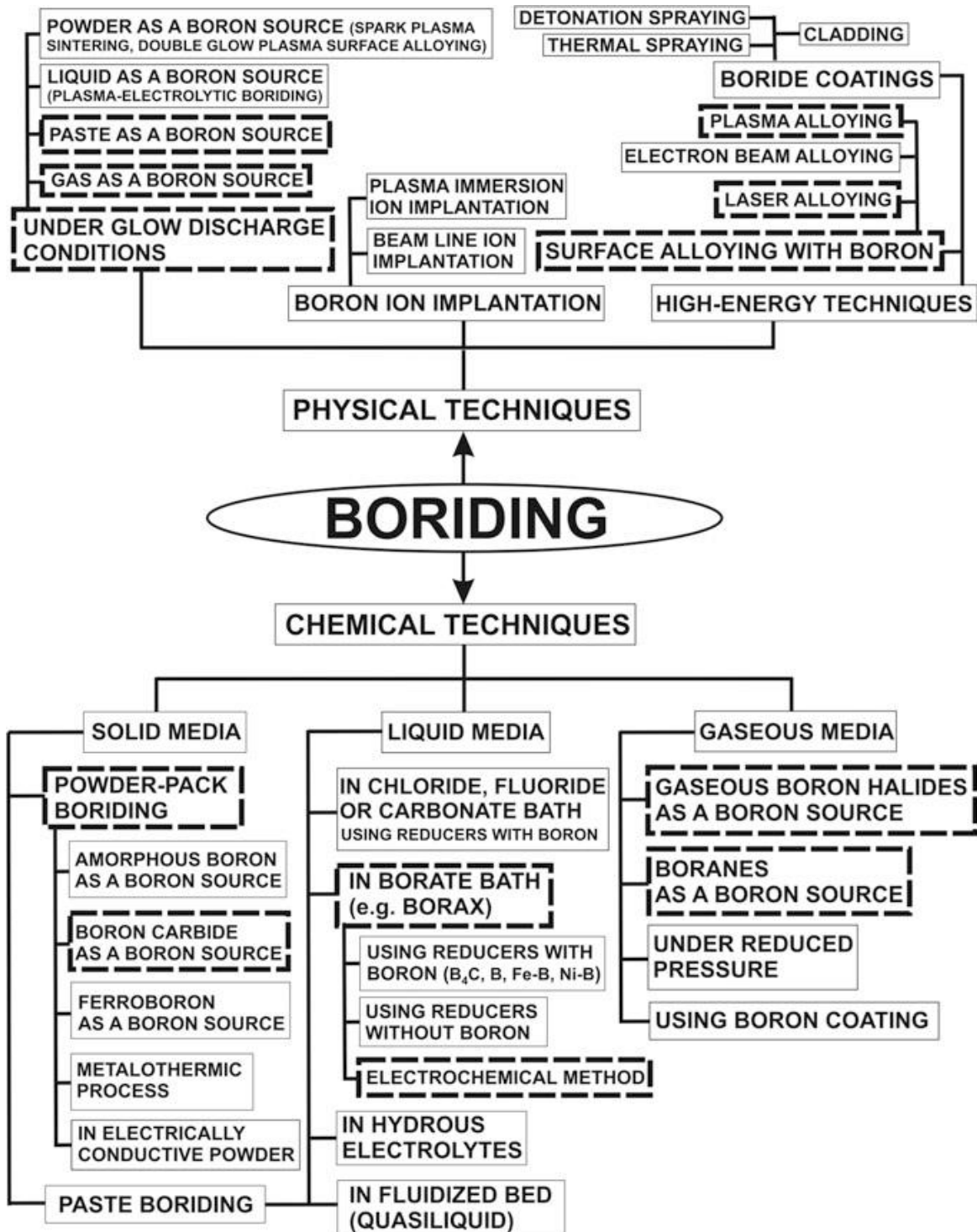
Figure 24. Boriding techniques classification, with the most used ones in broken lines [10].

II.4.1. Traditional techniques

Traditional boriding techniques are based on high thermal energies and chemical reactions between the boron medium and the substrate. They are known as chemical or, more precisely, thermochemical boriding techniques, as classified in the surface hardening processes section. They are done in solid, liquid, and gaseous media.

A.   Solid media boriding

As the naming indicates, the substrate is immersed in a solid medium which is given a high thermal energy to provoke the chemical reaction of diffusion. Two types of media are used in this category, powder and paste mixtures.

a)   Powder boriding

Powder boriding (PB), also known as powder pack boriding (PPB) or Pack cementation boriding, is one of the most widely used process due to its handling ease and safety as first, along with the possibility of different powder composition usages, and limited equipment, making it economic friendly [8,12]. It is a thermochemical treatment where the medium agent is a powder mixture that is composed of a boron source, an activator, and a diluent, all differing depending on the boron compound substance [6,8].

- **Boron sources:** boron carbide B_4C, boron oxide B_2O_3, ferroboron FeB, or amorphous boron.
- **Activators:** Sodium carbonate Na_2CO_3, Barium fluoride BaF_2, Halides like Sodium tetrafluoroborate $NaBF_4$, Potassium tetrafluoroborate KBF_4, ammonium tetrafluoroborate $(NH_4)_3BF_4$, Ammonium chloride NH_4Cl, or Sodium tetraborate $Na_2B_4O_7$ known as Borax. Used to induce and hasten the diffusion of boron to the borided workpiece's surface from the mixture.
- **Diluents:** Silicon Carbide SiC, Aluminum oxides Al_2O_3, or magnesium oxides MgO. As inactive inert fillers to prevent the powder from sintering, i.e. bonding or fusing, and diminish boron's potential, reducing the formation of the brittle FeB phase in borided ferrous alloys, as will be discussed in Chapter III on the boride layers section.

The agents differ in the compositions regarding the constituents and their percentage depending on the brand of commercialization [12].

- 5, 5, 90 % of B_4C, KBF_4, SiC.
- 50, 5, 45 % of B_4C, KBF_4, SiC.
- 85, 15 % of B_4C, Na_2CO_3.
- 95, 5 % of B_4C, Na_2B4O_7.
- 84, 16 % of B_4C, $Na_2B_4O_7$.
- 95 to 97 % purity of amorphous boron.

Some of the renowned commercial powder mixtures are Ekabor and Durboride [8], both based on boron carbide B_4C and were the primary agents during the last decade in the study of powder pack or even other boriding techniques, both in research and industrial applications, with companies like the German BorTec contributing significantly [6]. Ekrit powder was also provided by the same company as a protective outer powder against oxidation, composed of finely grounded SiC [82].

After preparing the powder mixture, the workpieces are enclosed in a container where the powder encompasses them. The container can be found referred to as a box, case, crucible, retort, and else. This container is put in a furnace with selected atmospheric conditions, air, inert gases, or vacuum,

depending on the technique, Figure 25, and heated to the required temperature, generally 800 to 1050 °C, for a treatment of about 1 to 12 hours, or even more in rare cases [7,76,83].

Another setup of powder boriding is given as the last in the same Figure 25 where the powder mixture agent is electrically conductive. Through an activation of the agent by the passage of current, heat is generated. The substances that are added to the mixture to make it conductive can be coke, charcoal, copper, or preferably graphite. However, such a technique is not that common due to the difficulty of temperature control, along with high power and energy consumption [10,84].

During the process, the powder agents form a crust-like deposit on parts that can easily be broken off, and these agents can be reused several times, five or six, in normal operations that last in the neighboring of 6 hours, and after each cycle, fresh powder of up to 50 % is mixed with the recycled material by blending. Their renewal is only required if the treatment is exceptionally long, exceeding 20 hours [6,12].
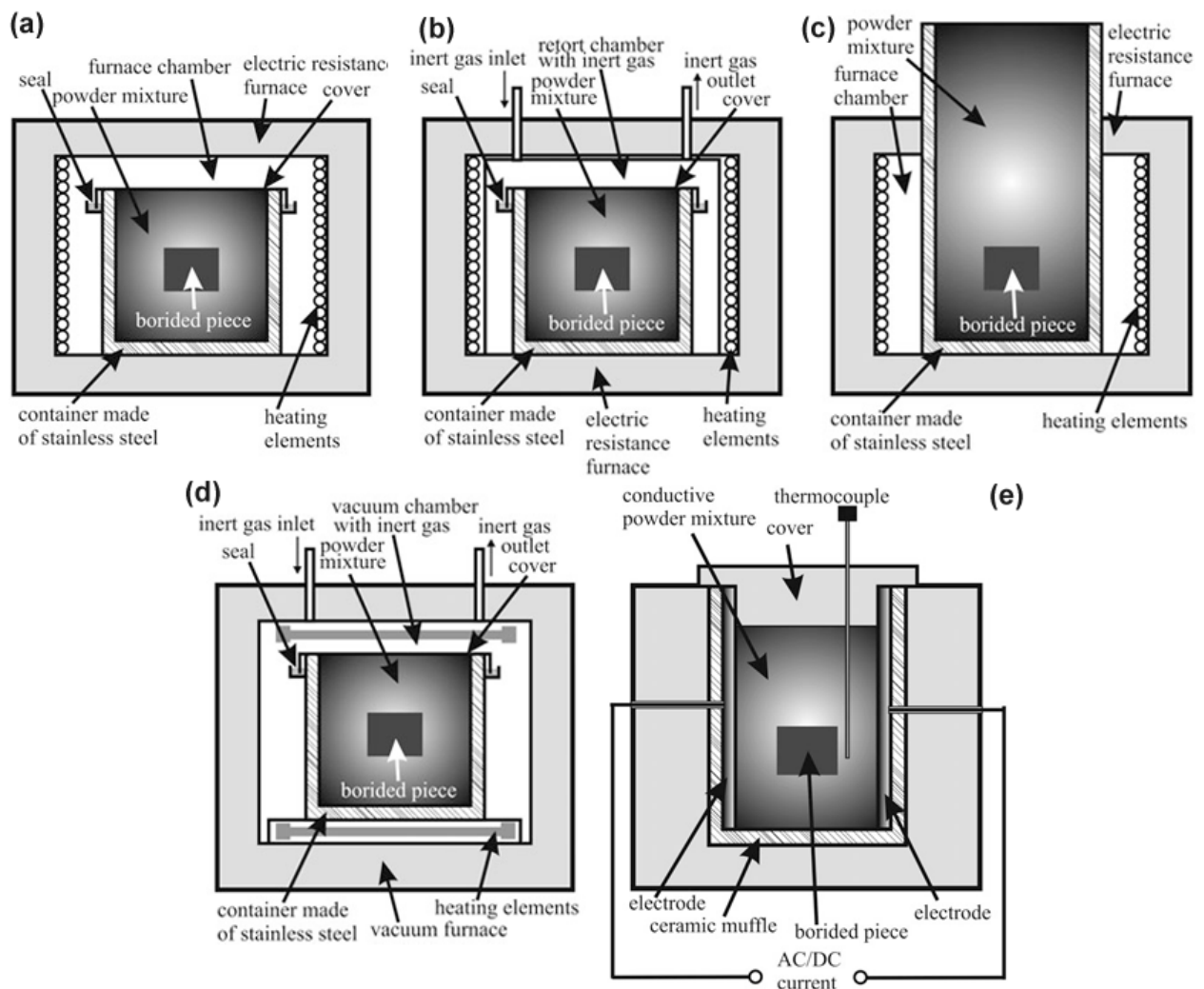
Figure 25. *Schematization of powder pack boriding techniques: (a-c) electric furnace with (a) sealed container in air atmosphere (b) sealed container in inert gases (c) open container, or (d) vacuum furnace with inert gases, or (e) with current passage heating via electrically conductive agents* [10].

b)   Paste boriding

As a follow-up to powder boriding, paste boriding techniques are invoked when certain features of the workpiece are not accessible and challenging to attain through powder, when there are large workpieces or only partial areas to process, or when sealing is costly, laborious, and takes time, minimizing manual work [6,85].
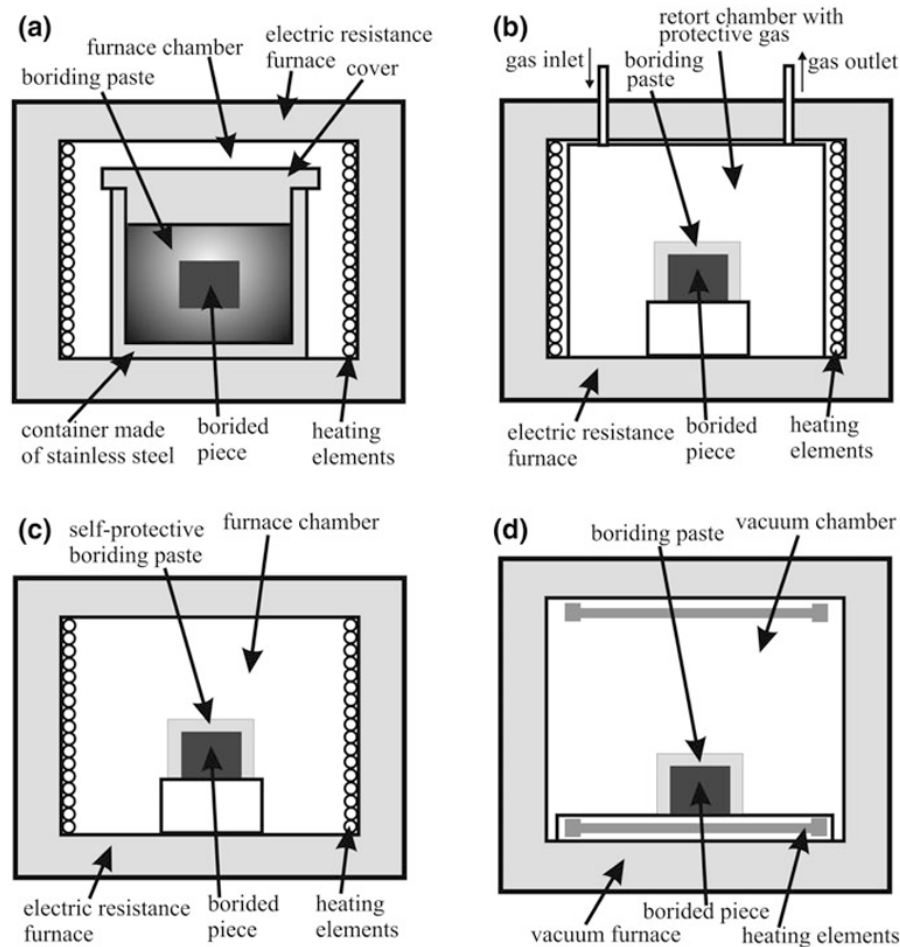
Figure 26. *Schematization of paste boriding techniques: (a-c) electric furnace with (a) closed container in air atmosphere (b) inert protective gases (c) self-protective paste in an air atmosphere, or (d) vacuum furnace* [10].

Commercial pastes are provided in a viscous state that is water soluble to allow diverse consistencies so that the paste can be brushed or sprayed onto the desired surfaces, and they usually contain diverse suspensions of mixed boron compounds with cryolite Na_3AlF_6 or conventional boriding powders of boron carbide B_4C with an organic binder like nitrocellulose $(C_6H_7N_3O_{11})_x$ dissolved in butyl acetate $C_6H_{12}O_2$ or an aqueous solution of methyl cellulose $C_6H_7O_2(OH)_x(OCH_3)_y$ [8].

Before undergoing the thermochemical processing, a series of coatings are applied consisting of an active paste applied multiple times, a binder, and a protective layer.

- **Active paste:** a brushing or spraying of the boron-based paste is applied in the desired areas and left to dry. Then after that, repeated pasting is done until multiple dried layers are formed on top of each other.

- **Binder paste:** if the active paste does not include a binder, an additional one is needed, mixed, or used as a coat, of Sodium Silicate $Na_2O_7Si_3$ or hydrolyzed ethyl silicate $Si(OC_2H_5)_4$.

- **Protective paste:** lastly, a final coating is added as a final protective layer that helps against oxidation depending on the paste boriding technique. It can be of aluminum oxides Al_2O_3 or other antioxidant compounds [86].

Subsequent to the coatings, the thermochemical treatment is processed where the substrate is heated inductively, resistively, or in conventional furnaces depending on the technique, as given in Figure 26.

B.   Liquid media boriding

The sample is dipped into a molten bath that contains borax $Na_2B_4O_7 \cdot 5H_2O$, or boric acid $B(OH)_3$, and ferrosilicon $FeSi_2$. Then, depending on the method, it is heated and held at specific boriding temperatures and times. The lack of need to heat the containers makes this method save some energy, and in some cases, there is no need to seal the container providing the possibility to quench directly afterward.

On the other hand, the clinging of the unreacted boron and bath salt residues to the borided pieces, the need for their removal, and the need for continuous adding of fresh mixtures to the bath can be both expensive and time-consuming. The process is challenging to reproduce due to the careful need to control and monitor the viscosity of the bath, and above all, such a process was not environmentally friendly [76].

a)   Electroless bath boriding

Three different methods are interchanged hither, within the molten bath, only the reducers are boron-based, both the bath and the reducers include boron, and only the bath has boron [10].

- **Boriding in nonboron salt baths using boron reducers**

The bath is composed of chlorides like $BaCl_2$, $CaCl_2$, NaCl, KCl or fluorides like KF, LiF, or NaF, and it could also contain carbonates like Li_2CO_3, K_2CO_3, or Na_2CO_3. Additionally, boron-containing reducers like boron carbide B_4C, potassium tetrafluoroborate KBF_4, ferroboron, or amorphous boron are used as the primary source for diffusion. With that mix, protective atmospheres were not necessary during such technique even though it might be used, represented in (a,b) of Figure 27.

- **Boriding in borate baths using boron reducers**

Carried out in a bath of borax $Na_2B_4O_7$ with the addition of boron carbide B_4C or occasionally $NaBF_4$ as reducers [87]. This method also didn't have the need to use a protective atmosphere, illustrated in (a-d) of Figure 27.

- **Boriding in borate baths using nonboron reducers**

Due to the expensiveness of boron reducers, such technique was thought of where they were replaced by chemically active ferroalloys like ferromanganese FeMn or ferrosilicon FeSi, other metals and their alloys like Al, Be, Ca, Ce, Li, Mg, and Ti, but with high affinity to oxygen than boron, or by silicon carbide SiC, making this method the most popular of the three, (a-c) of Figure 27. Its atmosphere usage wasn't restricted however, a protective atmosphere or other means can be necessary during the addition of the reducers to avoid undesirable reactions [88].
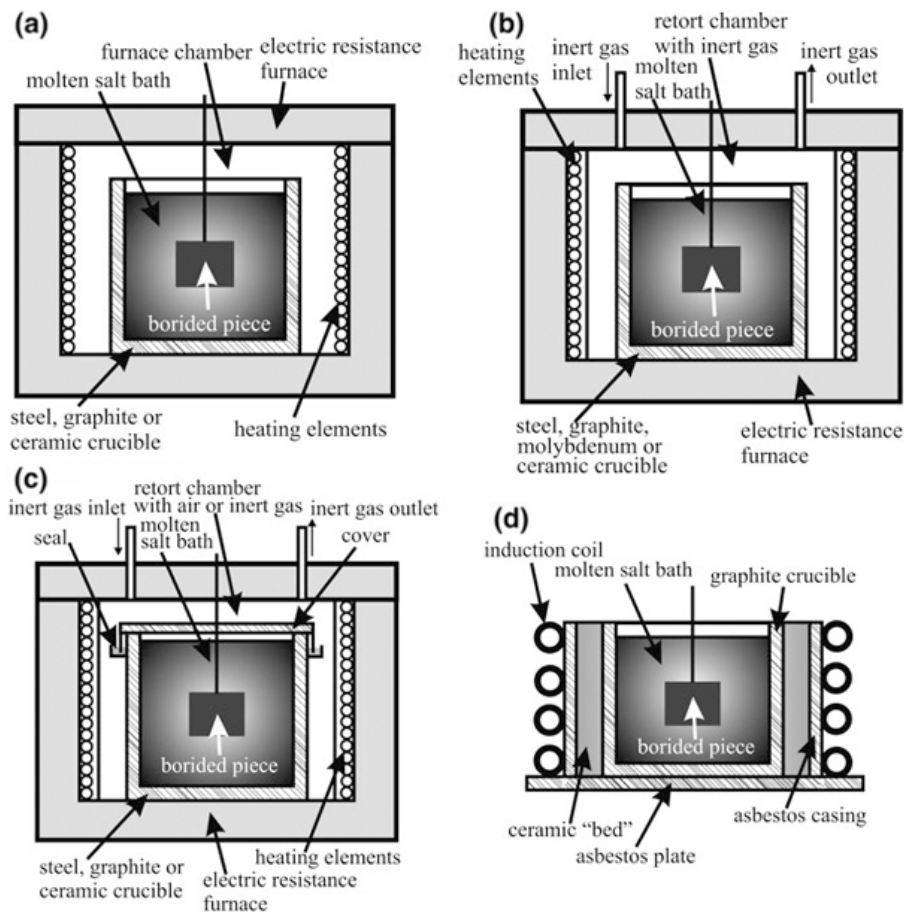
Figure 27. *Schematization of electroless boriding techniques: (a-c) electric furnace with*
(a) unsealed container and air atmosphere (b) unsealed container and inert gases
(c) sealed container, or (d) induction heating of an open container in air atmosphere [10].

b)   Electrolytic bath boriding

Electrolytic boriding is an electrochemical process carried in electrically conductive molten baths, it ended up as the most effective and popular liquid media technique. It provided the possibility to form boride layers with lower temperatures and time intervals compared to many other methods. Its main stages are based on [89,90]:

- Partial thermal dissociation of borax with the formation of boron oxide B_2O_3 and the most stable compound, monoborate $Na_2B_4O_4$.

$$Na_2B_4O_7 \rightleftharpoons Na_2B_4O_4 + B_2O_3$$
$$Na_2B_4O_7 \rightleftharpoons Na_2O + 2B_2O_3$$
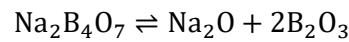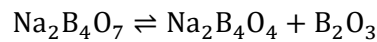
- Electrolytic dissociation and ionization, providing the melt's electrical conductivity.

$$Na_2B_4O_7 \rightarrow 2Na^+ + B_4O_7^{2-}$$
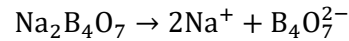
- Deposition of sodium on the cathode.

$$Na^+ + e^- \rightarrow Na$$
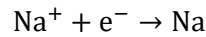
- Anode reaction by discharge of boron-containing anions with formation of boron oxide and evolution of oxygen.

$$2B_4O_4^{2-} \rightarrow 2B_2O_3 + O_2 + 4e^-$$
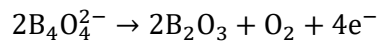
- Reduction of boron with sodium on the cathode surface.

$$6Na + 2B_2O_3 \rightarrow 4B + 3Na_2O_2$$
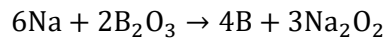
- Oxidation of the carbon anode by atoms of oxygen.

$$C + O_2 \rightarrow CO_2$$
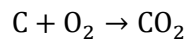
- Diffusion of boron into the substrate (Sub).

$$xSub + yB \rightarrow Sub_xB_y$$
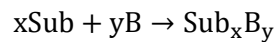
Even though these stages are based on baths that include borax, the technique can also be carried in other boron-based salts like Potassium fluoroborate KBF_4 where reduced temperatures were successful, 600 to 850 or lower instead of more, and even nonboron salt baths with boron reducers [91], or in other mixtures depending on the influence of the elements added [92].

Few compounds that were used in this technique with varied percentages and atmospheres are [12]:

- BF_2 + KF + NaF + LiF mixture in N_2 + H_2 atmosphere at 800 to 900 °C
- KBF_4 + KF + LiF + NaF mixture at 600 to 900 °C
- KBF_4 + KF + LiF mixture under Ar atmosphere
- KBF_4 + KF + LiF mixture at 700 to 850 °C
- KBF_4 + NaCl mixture at 650 °C
- $Na_2B_4O_7$ + NaCl at 800 to 900 °C

In recent years, this technique was intensively developed and had various modifications, like ultrafast boriding, cathodic reduction and thermal diffusion based boriding CRTD-Bor, or phase homogenization electrochemical boriding PHEB [76,93,94].

The equipment used in the technique is shown in Figure 28 and include:

- Direct current source (DC).

- An open container that generally acts as an anode (+).

- The filled bath and the borided pieces as the cathode (-).

- A furnace with a temperature control system and an optional tight retort.
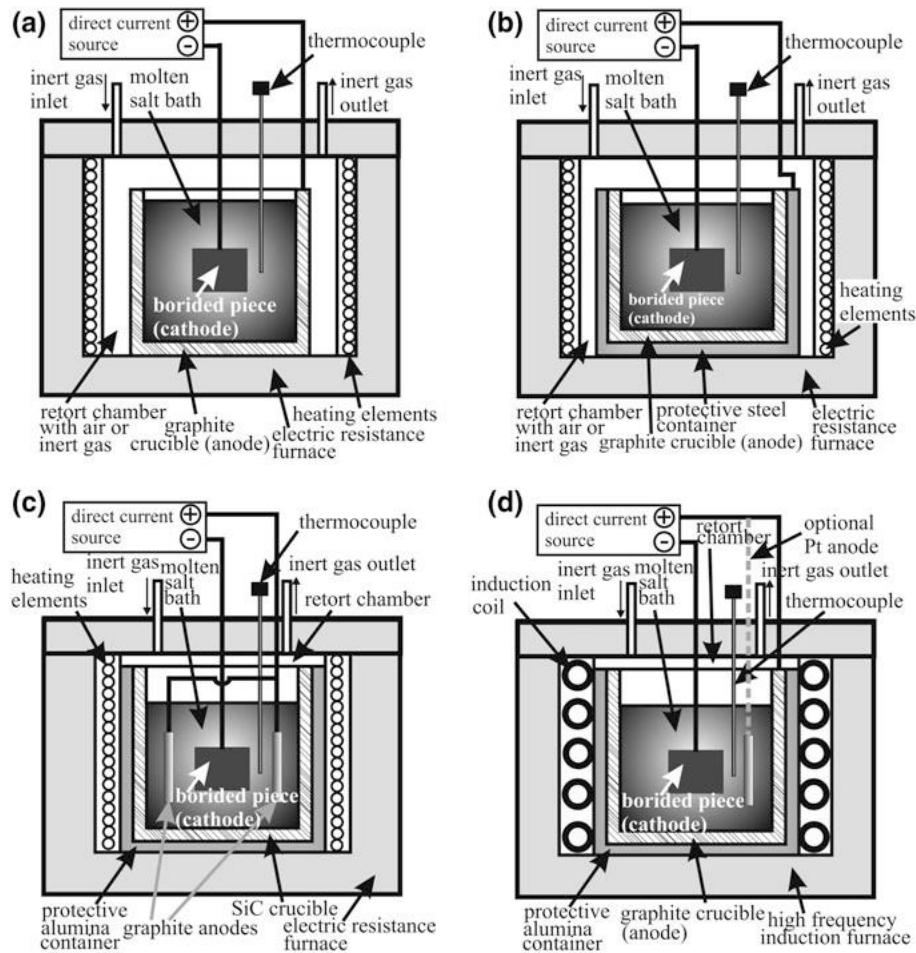
Figure 28. *Schematization of electrolytic boriding techniques: (a-c) electric furnace with various configurations (d) high-frequency induction heating* [10].

c)   **Fluidized bed boriding**

This boriding technique is a quasi-liquid bath having both liquid and solid media relations, with the first as the dominant where the solid bed is constituted of fine particles of powder that are suspended and kept in motion by an upward flow of gas blown underneath it, Figure 29, creating a heterogeneous fluid-like behavior, hence the naming fluidized bed.
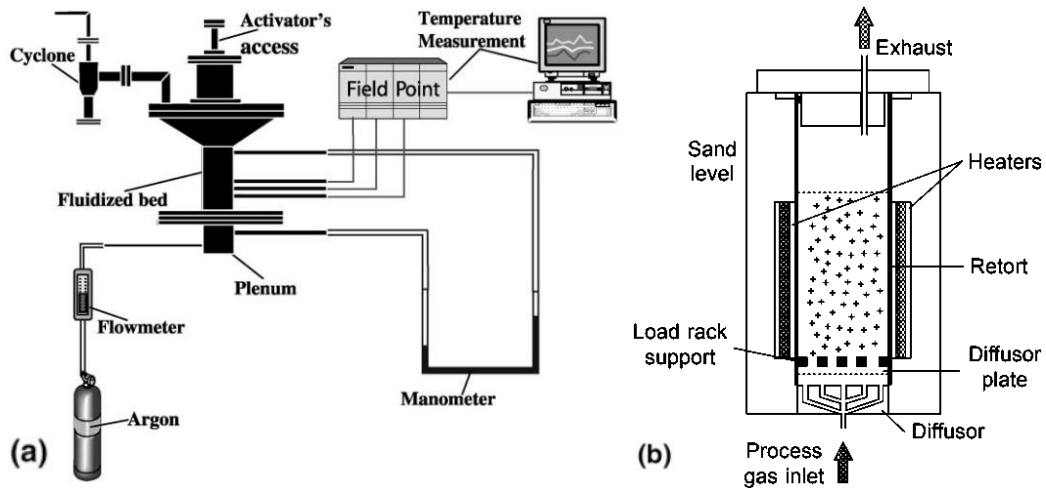
Figure 29. Schematization of fluidized bed boriding techniques, (a) configuration (b) furnace [7,95].

Argon is the main gas blown, and from the behavior of the particles' motion in the bed, an equal distribution of heat and mass is observed with an automatic cleansing of impurities with no contamination of the borided piece. Additionally, the technique had flexible parameter control, safety, efficiency, environmental friendliness, and was less pricey [95].

C.   Gas media boriding

As the naming indicates, this technique uses gas-like boron compounds. It is conducted either by reduction of boron halides, by thermal decomposition of boranes, or by using some organic boron compounds [8].

This particularity of it is that, unlike solid and liquid techniques, which are exhaustible during the process, gas media can be permanently supplemented, providing better control of boron within the chemical composition of the substrate along the depth of the boride layer. However, it comes with environmental and safety concerns [76].

a)   Gas boriding with boron halides

Being the dominant technique in gas boriding, boron trichloride BCl_3, one of the halides that is colorless and toxic, was the most common halide gas medium applied. That was due to its flexibility and to the halide hydrogen reduction, where boron trichloride BCl_3 or other halides are reduced by hydrogen at high temperatures, resulting in a sheet or needle-like structure of boron with up to a thousandths away from perfect purity [2].

$$2BCl_3 + 3H_2 \rightarrow 2B + 6HCl$$
$$2BBr_3 + 3H_2 \rightarrow 2B + 6HBr$$
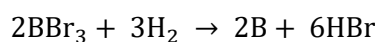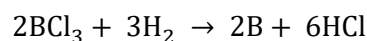
That purity, along with the strong reactivity, helped obtain the optimal diffusion results within the gas media. Hence, the specific categorization of the boron halides gas boriding.

With a similar principle to other techniques, the workpiece is cleaned and put into a furnace and heated for a period of treatment, with the exception that the gas is introduced through a flow subsequently, Figure 30. Formerly, hydrogen was combined alone with the halide, but afterward, it was mixed with argon or nitrogen to minimize corrosion and FeB content in the boride layer, enhancing its performance. Additionally, it was observed that the boron trichloride BCl_3 content needed to be 5 % or lower within the atmosphere for minimal porosity [76].

As for other halides, boron tribromide BBr_3 is pricey and tricky to handle because of its violent reactions with water, while boron trifluoride BF_3 on the other hand, produces hydrogen fluoride HF, a highly reactive and corrosive fume [12].
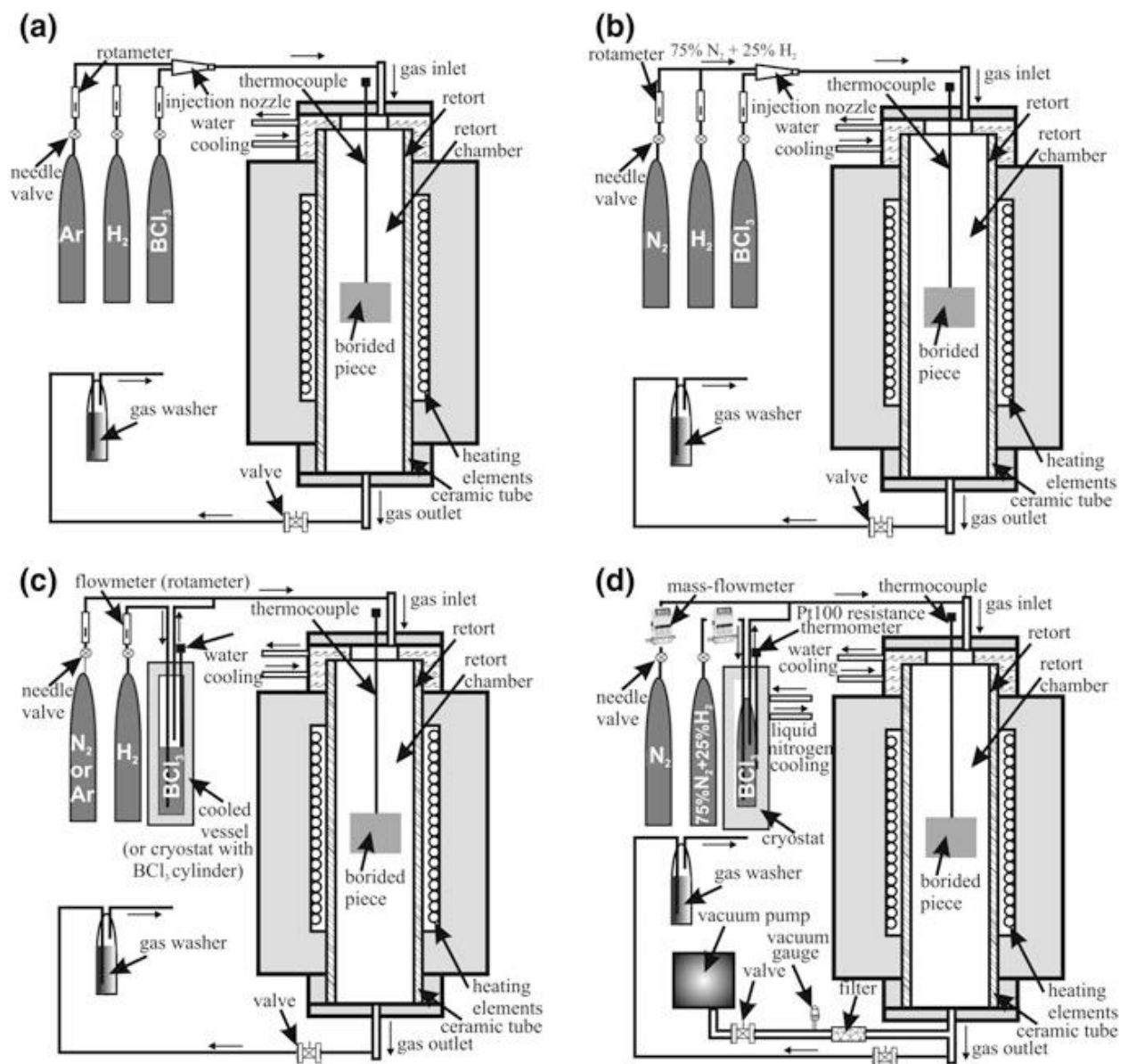
***Figure 30.** Schematization of gas boriding techniques with the most common medium boron tri chloride BCl_3 in different configurations* [10].

b)   Gas boriding with other boron sources

Similarly to the previous but with less popularity, gas boriding is also carried out using other boron sources. Few of them are boranes like diborane B_2H_6 diluted with hydrogen, or organic boron compounds such as trimethyl borane $(CH_3)_3B$ or triethyl borane $(C_2H_5)_3B$ diluted with hydrogen, nitrate, or ammonia. Diborane B_2H_6, being a highly toxic and explosive gas, makes it a less practical option commercially, and organic compounds are rich in carbon, generating boride along with carbide layers concurrently, reducing the performance of the surface [8,9].

Nevertheless, if the goal was simultaneous carburizing and boriding, then the use of organic boron compounds is a viable option renowned as borocarbuziring, which, as mentioned previously, produces an outer layer of iron borides and an inner one being carburized, Figure 17. Additionally, no toxicity is involved in the process, unlike when diborane B_2H_6 or boron halides' are used as media [73].

II.4.2. Moderne techniques

Unlike traditional chemical techniques, these can be categorized into modern techniques that are advanced and intricate in the control of their processing parameters, distinguished by the presence of physical processes along with the chemical reactions where boron is introduced into the substrate, hardening the material.

A.   Glow discharge plasma boriding

This technique utilizes glow discharge to facilitate boriding via plasmas, which are characterized by the presence of charged particles, positive and negative ions, along with free electrons, as well as neutral species [76]. The plasma is formed by the passage of electric current applied with a voltage between two electrodes through a low-pressure gas, consequently helping the diffusion of boron into the surface of the material.

Plasma techniques are adaptable and involve creating a plasma atmosphere by ionizing a medium with an electric field, activating its boron sources, and assisting in the diffusion of boron atoms into the substrate. The extra energy and ionization potential of the plasma increases the surface energy of the material, facilitating a deeper and more uniform diffusion of boron compared to traditional methods. Additionally, the presence of reactive particles along the electric current helps to clean the surface of the workpiece by a sputtering phenomenon [10], in which its particles are ejected outward from its surface by the bombardment of the energy particles.

The adaptability of plasma techniques resides in the medium sources used, which are as seen in the traditional techniques, solid, liquid, or gas, but with the glow discharge conditions.

a)   Plasma gas boriding

This technique uses as the traditional gas techniques do, halides like boron trichloride BCl_3 or boron trifluoride BF_3, boranes like B_2H_6, or organic boron compounds like trimethyl borane $(CH_3)_3B$ or triethyl borane $(C_2H_5)_3B$, in atmospheres of protective gases like hydrogen H_2, argon Ar, or their mixtures [8]. The difference comes with the addition of a direct current (DC) power supply, connecting the walls as positive terminals representing the anode (+), and the borided piece as the negative terminal representing the cathode (-). However, the gas mixtures are in between, introduced after vacuuming the atmosphere and creating the electrical current.

The benefit of plasma over traditional gas boriding resides mainly in the consumption of gas and electricity, which is much lower due to the nature of the interaction between the molecules and the workpiece's surface, where it is a forced attraction provoked by the partial dissociation and ionization of the gas, contrary to the traditional techniques where the interaction is random [96], as illustrated in Figure 31. However, the dominant disadvantage of plasma gas boriding is similar to traditional gas boriding, the extreme toxicity of the gases used makes both techniques out of the commercial adoption [8,76].
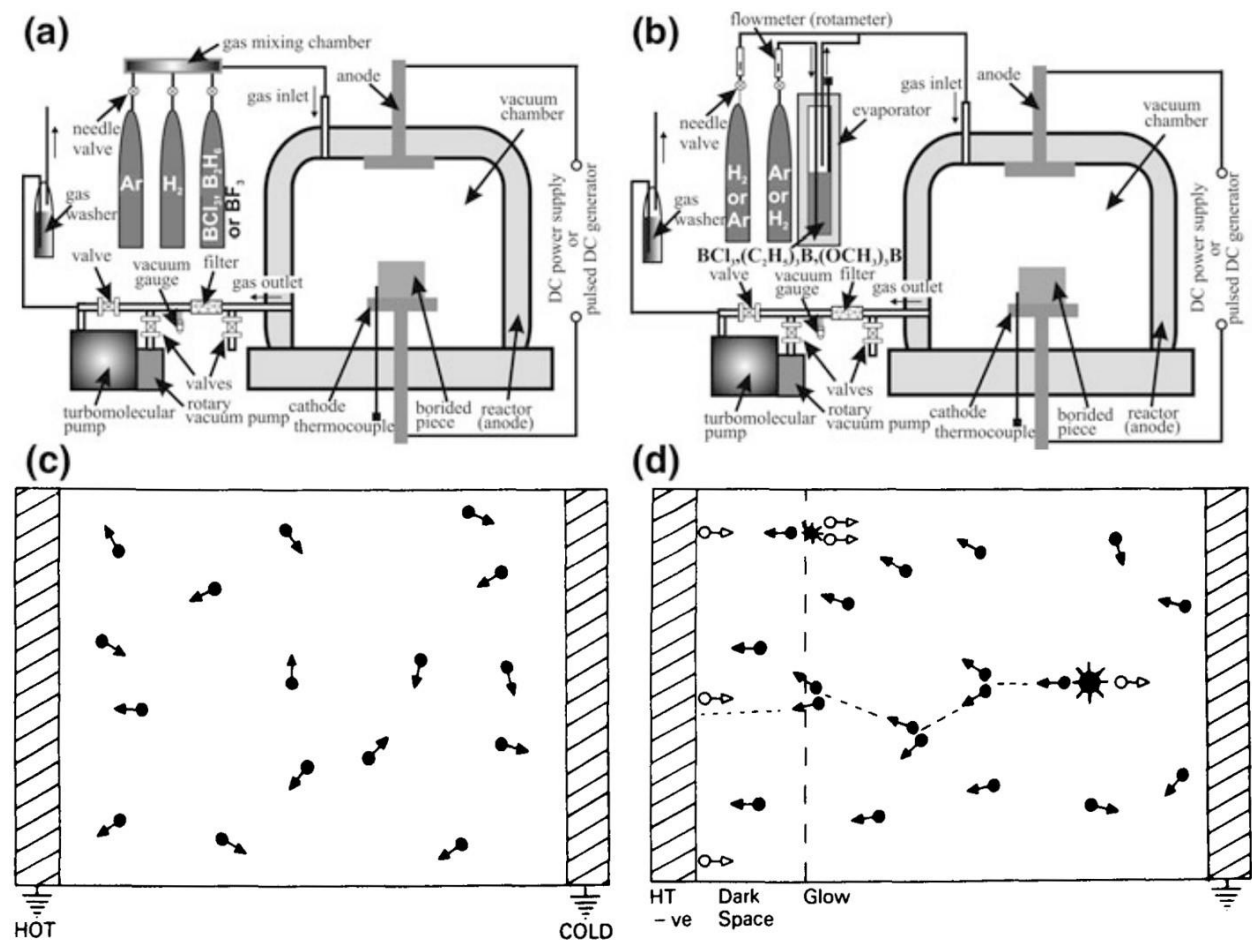
Figure 31. *Schematization of plasma gas boriding techniques (a-b), and representation of molecular motions in (c) traditional gas and (d) plasma gas treatments* [10,96].

b)   Plasma electrolytic boriding

Changing the medium source into a conducive liquid makes it electrolytic, but with the activation through plasma by applying a high-voltage, high-frequency electrical pulse, where boron atoms diffuse into the molten surface layer formed by the plasma discharge and react with the metal to form borides. Figure 32 illustrates two variants of this technique that are used:

- The workpiece acts as a cathode (-) and the container as an anode (+), similar to the previous technique, plasma gas boriding.

- The workpiece acts as an anode (+) and the container as a cathode (-), which is the inverse of the first.

In both variants, the workpiece is immersed in the electrolyte, which is itself poured into a container of either stainless steel or Pyrex. Depending on the boron compounds in the electrolyte, various and sometimes complex surfaces were achieved, borided, borocarburized, and borocarbonitrided workpieces [10].
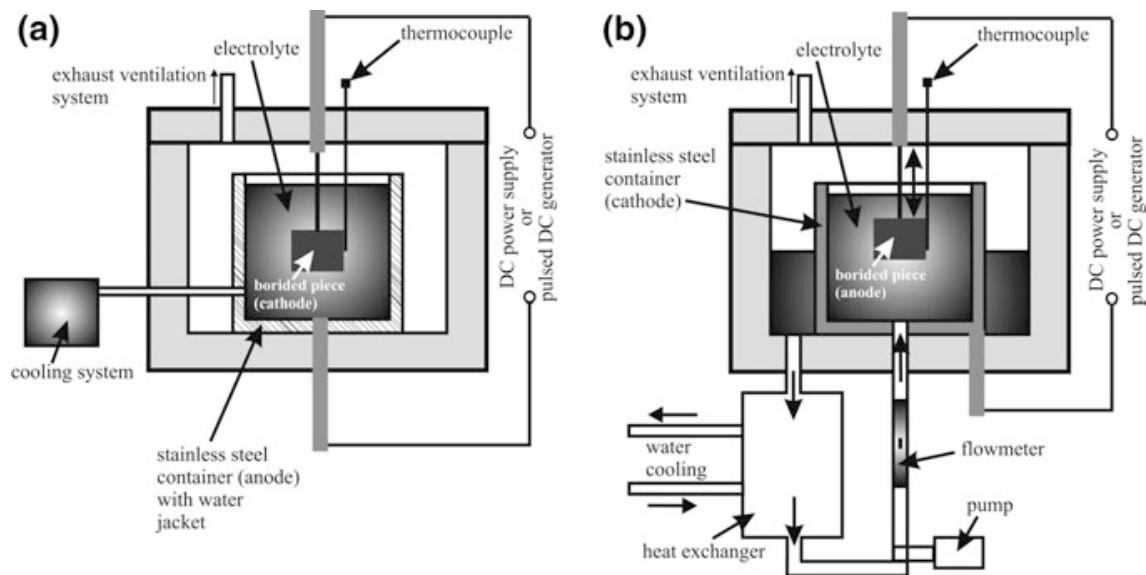
Figure 32. Schematization of plasma electrolytic boriding techniques where the borided piece acts as (a) cathode or (b) anode [10].

c)   Plasma paste boriding

It is a mixing of traditional paste boriding with a similar application of the plasma gas boriding, Figure 33. Nonetheless, the disadvantage of the plasma gas boriding aforementioned is disregarded with the paste application due to the absence of toxic gases and the presence of protective gases alone, hydrogen H_2, argon Ar, nitrogen N_2, or their mixtures. Also, even with the differing pastes, whether in the active, the binder, or the protective paste, and with all of them being environmentally friendly [64,97].
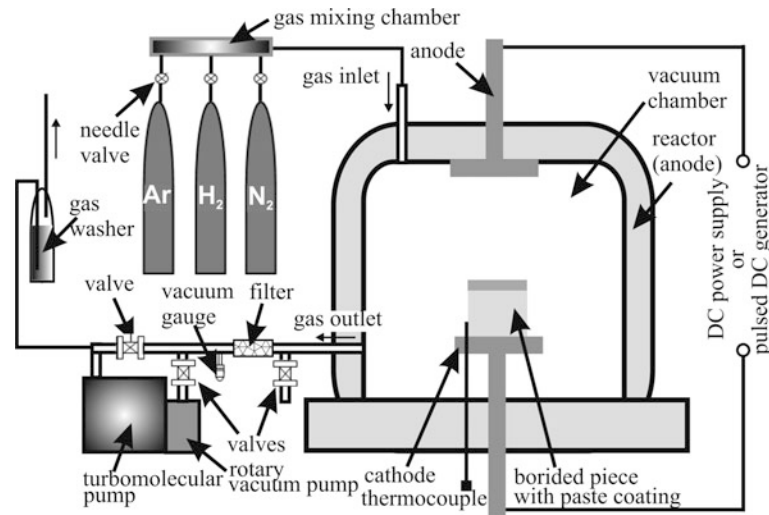
Figure 33. Schematization of plasma paste boriding techniques [10].

d)   **Plasma sintering Boriding**

Done via a high current discharge, i.e. a spark plasma sintering, with a powder mixture media similar to the traditional technique. As illustrated in Figure 34, the workpiece is put into a sintering die and filled with a powder mixture. Then, with an electrical energy of the two upper and lower punch electrodes, the void between the particles is charged and discharged, generating a high-temperature spark discharge or a pulsed plasma. The advantages of such a technique reside in the high activation of boron atoms and their high-speed diffusion due to the fast migrations of ions in the presence of the electrical field [98].
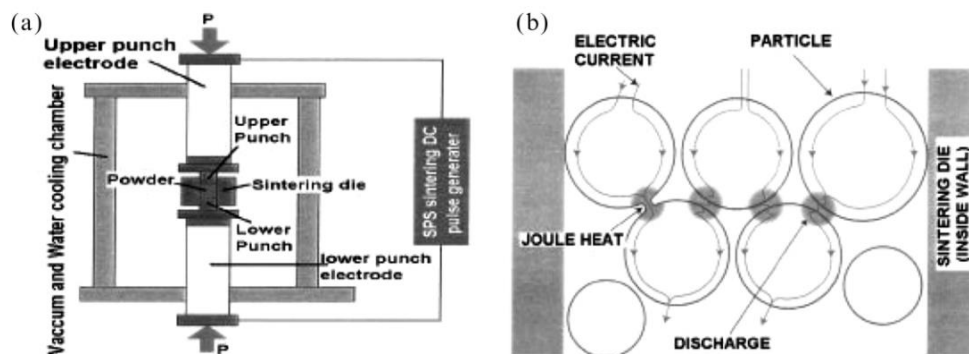
Figure 34. Schematization of plasma sintering boriding techniques (a), and representation of the pulsed current flow through the powder particles (b) [98].

e)   **Double Glow Plasma Surface Alloying**

The process is based on three electrodes, an anode (+) and two negatively charged cathodes (-), to create a double glow discharge in the plasma, Figure 35. This is achieved through the sputtering of alloying element particles from a cathode source (-) by a bombardment of ions, specifically argon ions Ar^+, within the plasma, making the first glow discharge. The activated particles are then transported through the plasma space and diffused into the second cathode (-), which serves as the workpiece. This results in the formation of a second glow discharge within the plasma, which heats the workpiece, enabling the process of alloying [99].
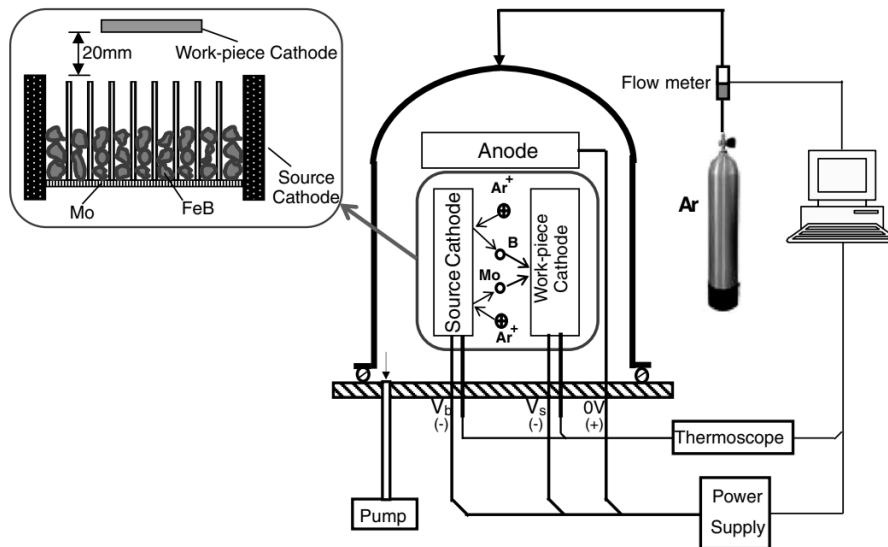
Figure 35. *Schematization of the plasma immersion boron ion implantation techniques* [99].

The cathode source differs in its elemental composition and is made by powder metallurgy. If desired, the argon can be mixed with nitrogen to mix in the layer, which leads to high hardness and excellent wearability [99].

B.   Ion Implantation Boriding

These techniques rely on the implantation of boron ions into the material under specific conditions to induce boron diffusion and reaction with the base material. Compared to other boriding techniques, these techniques form boride compounds at relatively low temperatures. Sometimes, the boron is referred to as a dopant after such processes.

a)   Beam Ion Implantation

This technique is a process where boron ions are accelerated and bombarded toward the surface of a workpiece, penetrating it with a controlled depth and composition at relatively low temperatures. The main elements used when ion implanting are:

- Ion source with a discharge chamber and an ion extractor
- Ion mass analyzer and separator
- Ion focusing and accelerating system
- Ion deflecting system
- Wafer chamber and control systems
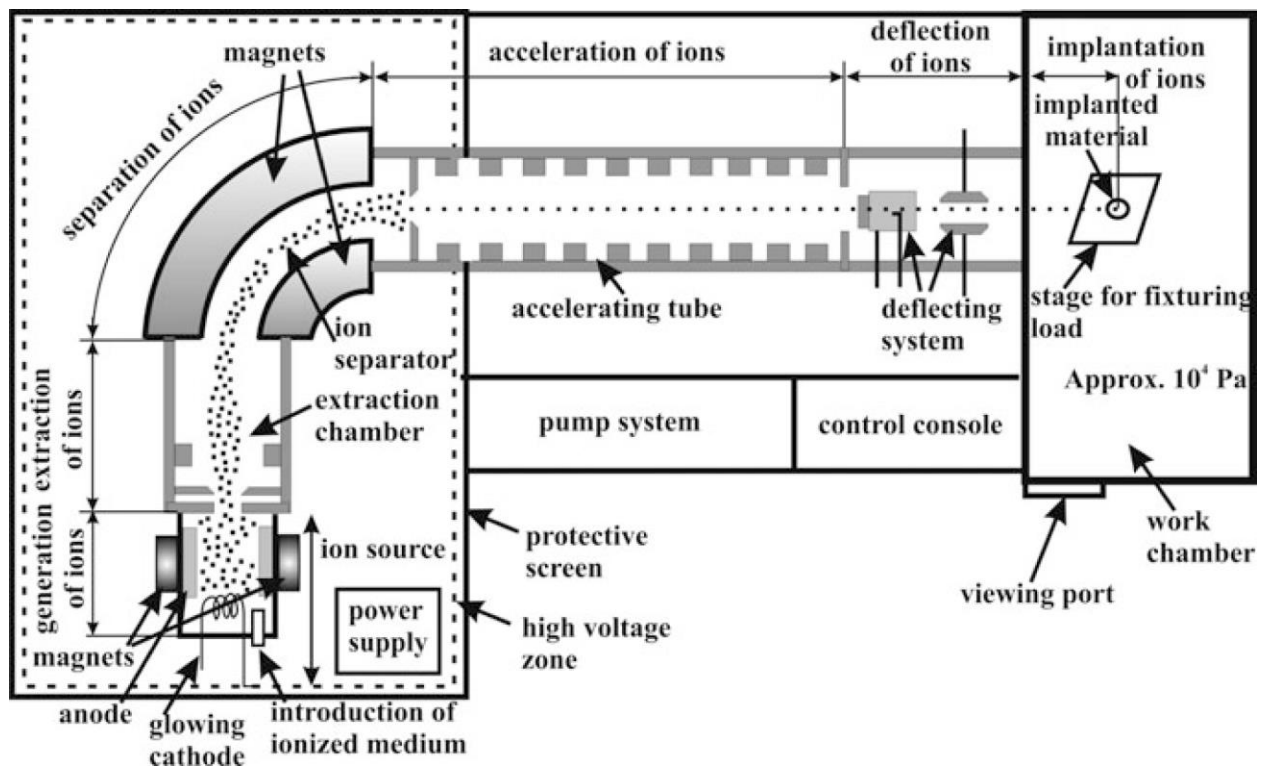
Figure 36. Schematization of the implanter used in beam ion implantation techniques [10].

The design of the machine with the process are given in Figure 36, and depend on the implanter's performance and its doping requirements, along with the characteristics of the implanted flux, beam current, and power density [10,100].

However, the implantation has its downsides where the bombardment that causes the collision of the ions with the workpiece's surface results in crystal damage, or precisely, radiation damage. Additionally, the implanted atoms may not necessarily occupy the crystal lattice sites but rather stay superficially. Fortunately, annealing activates the dopants by allowing them to diffuse into the lattice and removes the damage [100].

b)   Plasma Immersion Ion Implantation

Various terminologies are used for this technique. Regardless, this one describes its essential features, namely ion implantation into a workpiece that is immersed in a plasma as an ion source, Figure 37, conversely to using accelerated ions as a bombarding beam from a remote reservoir of plasma like the beam technique [101].
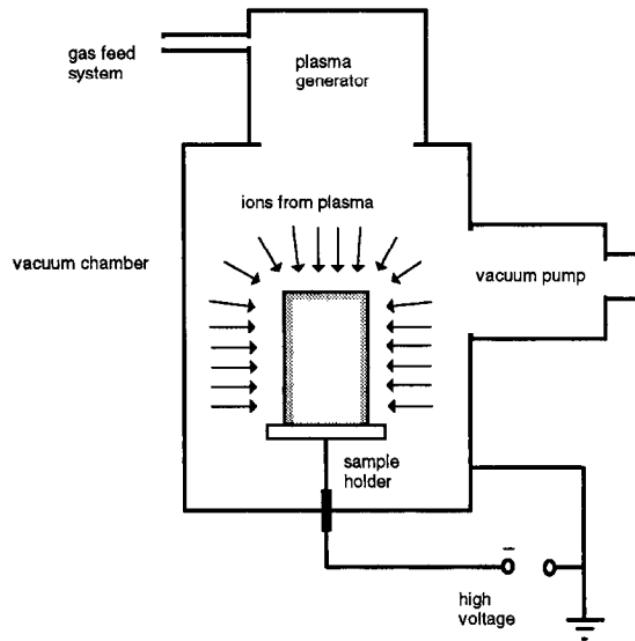
Figure 37. *Schematization of the plasma immersion ion implantation techniques* [101].

C.   Energetic Boriding Techniques

Dissimilar to the previous techniques, where mainly the temperature and time were of concern, these techniques are based on high energy applications, voltage, current, power, and other factors to surface harden the material [10].

a)   Surface Alloying

This technique uses the application of gun-like high-energy heat-generators to mix preexisting alloys with the surface of a material via a melt, either by fusion while injecting the alloys through different boron mediums or by remelting a priorly deposited coat. Those generators produce distinct energy forms:

- **Laser beam,** where a laser beam pressurizes a zone of the workpiece's surface, creating the melt.
- **Electron Beam,** similar to the implantation, where a cathodic source emits electrons that will be accelerated, but without the use of a machine, instead a gun that points to the desired zone and melts it.
- **Plasma,** comparable to welding, a cathodic electrode (-) and an anodic material (+) are momentarily or continuously linked, creating a constricted high-energy plasma arc that produces heat between them providing the melt.

b)   Surface Coating

Coatings involve the deposition of boron-rich layers onto the surface of a workpiece. Such deposition was feasible through thermal spraying, which was explained previously in the surface hardening processes section, or cladding, which encompasses different techniques such as hot dipping, electroplating, or physical vapor deposition.

II.5.   SUMMARY

Summarizing, boriding, or boronizing, as one of the versatile and intricate surface hardening process, introduces boron into the surface of a material through diffusion. It can be combined and synergized with other surface hardening processes, found in multicomponent boriding where the boron is diffused with other elements either simultaneously or in sequence, like Borocarburizing, boroaluminizing, borochromizing, borochromtitanizing, and more, or heat-treated like annealing after boriding [8,12,72,73]. Nevertheless, some combinations have undesirable impacts, like the case of quenching and tempering after boriding, which reduces the hardness and wear resistance of the boride layer [78].

Moreover, the boriding process provides extreme hardness and high properties of corrosion and wear compared to its counterparts like nitriding or carburizing, and can be undergone either through traditional techniques relying mainly on thermochemical parameters that are primarily impacted by time and temperature or through modern techniques which include in addition physical interactions and rely on different parameters that depend on power, current, ampere, and more.

Delineating each of the boriding techniques, as given in Table 7, provides a clearer understanding of their application ranges regarding their parameters, making some techniques demanding where their application takes higher temperatures regardless of time.

An interesting pattern emerges regarding maximum treatment times for different boriding techniques. Gas boriding has the shortest time treatments at approximately 6.5 hours, followed closely by plasma gas boriding at 7.25 hours. On the other hand, liquid and solid boriding techniques require considerably longer times, reaching a maximum of 10 and 12.25 hours, respectively. The same pattern is held true for the minimum temperatures reached as well. Solid, liquid, and gas applications in all boriding techniques require lower temperatures, respectively.

In contrast, traditional thermochemical techniques are applied in extreme temperatures and take longer treating times than modern ones. Within traditional techniques, solid, liquid, and gas have minimal temperatures of 840, 775, and 670 °C, while the modern techniques of plasma stand between liquid and gas with a temperature of 710 °C. On the other hand, while ion implantation and energetic techniques can be used at high temperatures, they are more commonly known for their ability to be performed at low temperatures, even at room temperature.

The applicability of boriding techniques differed in popularity and Figure 24 helps illustrate that. The techniques that were highly practical and intensively developed were [10]:

- Powder pack boriding through boron carbide.
- Electrolytic boriding through borax.
- Gas boriding through boron halides or boranes.
- Glow discharge plasma boriding through gas or paste.
- Surface alloying through plasma or laser.

Furthermore, the borides attained through the boriding technique highlight the intricacies inherent in the process, particularly with respect to the treated base material, raising questions concerning the difficulty of conducting boriding for various materials. Hence comes the subsequent chapter which will delve into the distinct surface layers of borides, shedding light on the complexities of applying boriding across various materials.

Table 7. *Temperature and time ranges in boriding techniques, based on* [10].

Boriding Techniques		Temperature [°C]		Time [h]	
		min	max	min	max
Traditional		**min**	**max**	**min**	**max**
Solid	≈	**840**	**1060**	**1**	**12.25**
Powder boriding (f)		850	1050	30*	12
Powder boriding (nf)		800	1100	1	24
Paste boriding (f)		800	1050	15*	8
Paste boriding (nf)		900	1050	2	5
Liquid	≈	**775**	**1050**	**1**	**10**
Boriding in nonboron salt baths using boron reducers (f)		550	1000	1	18
Boriding in nonboron salt baths using boron reducers (nf)		500	1050	4	24
Boriding in borate baths using boron reducers (f)		850	1050	30*	6
Boriding in borate baths using boron reducers (nf)		950	1000	3	8
Boriding in borate baths using nonboron reducers (f)		800	1030	30*	8
Boriding in borate baths using nonboron reducers (nf)		900	1100	1	4
Electrolytic boriding (f)		700	1000	5*	10
Electrolytic boriding (nf)		800	1200	5*	8
Fluidized bed boriding (f)		800	1050	30*	6
Fluidized bed boriding (nf)		900	1000	1	6
Gas	≈	**670**	**1010**	**1**	**6.5**
Boron trichloride boriding (f)		550	1050	5*	7
Boron trichloride boriding (nf)		910	920	2	3
Boranes or other sources boriding (f)		550	1050	1	10
Modern		**min**	**max**	**min**	**max**
Plasma	≈	**710**	**1040**	**1.25**	**7.25**
Gas boriding (f)		500	1050	10*	10
Gas boriding (nf)		500	1100	1	8
Liquid electrolytic boriding (f)		800	950	3	15
Paste boriding (f)		700	950	2	7
Paste boriding (nf)		700	850	3	7
Powder spark plasma sintering boriding (f)		700	1000	5*	4
Powder spark plasma sintering boriding (nf)		1000	1400	5*	4
Powder double glow plasma surface alloying		800	1000	10*	3
Ion implantation	≈	**< 30**	**950**	**-**	**-**
Beam ion implantation (f)		< 30	950	-	-
Beam ion implantation (nf)		< 30	600	-	-
Plasma immersion ion implantation		-	-	2.5	3.5
Energetic	≈	**< 30**	**1150**	**-**	**-**
Laser or beam or plasma surface alloying		-	-	-	-
Thermal Spraying		< 30	1150	-	-
Cladding		-	-	-	-
(f) ferrous alloys (nf) nonferrous alloys * minutes instead of hours - unspecified					

BLANK PAGE

CHAPTER III

BORIDE LAYERS AND BORIDED MATERIALS

Building on the prior chapters' exploration of boron's properties, its compounds, and surface hardening processes, including boriding, this third chapter focuses on preparation and characterization procedures exploited in boriding. As well as the distinctions and intricacies of the boride layers and the types of materials that can be borided.

III.1. OVERVIEW

Following the exploration of boron and its diffusion techniques within the realm of surface hardening processes, it is deemed fitting to explore the treatment procedures concerning boriding, from how samples are prepared, to the practical techniques used in characterizing the results. The characterization helps in determining the nature of the diffused boride layer and its properties, providing insights about the formation mechanisms and behavior under different treatment conditions.

Therefore, an in-depth analysis of the boride layer is elaborated regarding its composition, the influence of the alloying elements within the substrate, and potential challenges like crack formation and spalling. Additional aspects are also explored, such as wear and corrosion resistance, along with the impact of combining other surface hardening processes with boriding [6]. As a conclusion to the section, brief recommendations regarding the boride layers are given, and their suitable applications [7].

Furthermore, the response of various machinable materials to boriding treatments will be inspected by separating each class and giving its advantages and potential drawbacks. Beginning with ferrous materials due to their relative dominance and the particular interest in the boriding field, a meticulous analysis of the behavior of different ferrous categories to boriding is elaborated, including pure iron, carbon steels, cast irons, and alloy steels [14]. Following that, a brief section on other nonferrous materials regarding the boriding will be explored, including titanium, nickel, and cobalt, in both the pure stat and as alloys [13].

Lastly, boriding encounters varied difficulties and limitations when it comes to certain materials, such as its difficulty to be carried on aluminum due to conflicts of brittleness and softness, copper and silicon due to their premature melting points, the incompatibility of boron to noble metals, or its lesser strong bond to most non-metals.

III.2. TREATMENT PROCEDURES

A comprehensive understanding of the boron diffusion process requires detailed characterization of the material both before and after treatment. This section explores the various techniques employed to prepare and analyze the samples both pre and post boriding.

By studying the pretreatment microstructure and composition, a baseline can be established for the diffusion process. Then, subsequently, post treatment characterization methods reveal the effectiveness of the boriding process by providing crucial insights into the depth, concentration profile, and the resulting microstructure and composition of the diffused boron layer. This combined analysis allows for optimization of the boriding process to achieve desired material properties.

III.2.1. Preparation techniques

The preparation of samples prior to boriding significantly influences the ease of boron diffusion. They are generally machined and cut into small pieces, then further processed by grinding or other suitable techniques to clean or rinse the surface of extra contaminants. Following the treatment process, thorough cleaning of the samples can also be essential prior to characterization to remove any surface contaminants that might interfere with the analysis. These contaminants may include residual materials from the treatments or environmental pollutants. Standard preparation techniques include:

a)   Mechanical Abrasion

Mechanical abrasion is a well-established and efficient method for preparing the sample surface before boriding. Techniques like grinding and sandblasting utilize abrasive forces to remove surface contaminants like oxides or greases. Additionally, they not only clean the surface but also increase its area by roughening it, which improves the adhesion between the substrate and the diffused film. This enhanced adhesion leads to a more durable and long-lasting layer or coating. Grinding can be performed using various methods, such as with emery paper [102].

b)   Polishing

After carrying the boriding, the treated pieces are sectioned to small pieces for cross section analysis. Accordingly, polishing might become particularly important for most characterization techniques that require a smooth surface for analysis. Polishing can be done with silicon carbide SiC papers and diamond paste [102] or other means. In some instances, it can applied before boriding [103].

c)   Chemical cleaning

Cleaning is needed before or after treatment. It is done by degreasing with solvents like acetone C_3H_6O or ethanol C_2H_5OH or CH_3CH_2OH, and/or etching. Etching consists of immersing the sample in a solution that selectively removes surface contaminants, such as oxides, without significantly affecting the material. The choice of etchant depends on the specific contaminant and material being analyzed. If used after boriding, common etchants for iron borides include Nital, which is a nitric acid HNO_3 in ethanol [102] or mixed potassium hydroxide KOH and Potassium Ferricyanide $K_3Fe(CN)_6$ [103].

d)   Ultrasonic rinsing

Also used before or after processing. It is a more gentle approach that uses high-frequency sound waves in a cleaning solution, such as acetone or ethyl alcohol [102], to dislodge and remove loosely attached contaminants like dust or debris particles and residual oxides from the sample surface.

III.2.2. Cutting techniques

Post boriding, the samples are obtained either by machining or cutting from a larger bulk material. This ensures having the desired sample size and geometry for the boriding process. Subsequently, after ending the treatment, to examine the microstructure and composition throughout the produced boride layer, the treated samples need to be sectioned for cross section analysis. Cutting techniques are precise methods used for that purpose, helping to obtain small pieces suitable for various characterization techniques.

Machining rarely comes after the treatment because borided pieces are pretty tricky to machine due to their inherent hard and brittle nature, and machining might potentially damage the boride layer. That is why cutting techniques are used instead. They aim to achieve clean cuts with minimal damage to the microstructure, which is crucial for accurate analysis of the diffused profile and microstructure throughout the material's depth. Embedding the borided samples in a supportive resin can provide additional stability during cutting to prevent chipping or cracking. Additionally, after cutting, the cross section might need polishing to achieve a smooth and defect-free surface for optimal observations. Standard cutting techniques are:

a)   Dicing Saw

Dicing saw is the most widely used form for cutting the borided sample after treatment. It utilizes a thin, diamond-coated blade to achieve clean cuts with minimal damage to the microstructure. The balance between precision, cutting speed, and minimal damage makes it suitable for a range of analyses, including Optical Microscopy OM, Scanning Electron Microscopy SEM, and subsequent analysis like Energy Dispersive Spectroscopy EDS. It is relatively fast and cost-effective but might not achieve the ultra-high resolution required for detailed microstructural analysis.

b)   Laser Cutting

Laser cutting offers the ability to create very smooth sections and intricate patterns in the borided sample. It uses a focused laser beam for cutting, but careful control is crucial to avoid thermal damage to the boride layer, which can potentially alter its properties.

c)   Focused Ion Beam milling

FIB milling is an advanced technique that uses a focused beam of gallium ions to remove material very precisely, enabling the creation of ultra-smooth sections (down to the nanoscale), ideal for advanced characterization with high-resolution transmission electron microscopy TEM analysis. However, FIB milling is expensive, time-consuming, requires specialized training, and may introduce artifacts due to ion beam interaction with the material.

III.2.3. Characterization techniques

Understanding the properties of boride layers requires a comprehensive analysis that delves into various aspects, such as surface roughness, layer thickness, composition, microstructure, hardness, and so on. Depending on the accessibility, diverse techniques exist to achieve this characterization.

The most commonly used technique is microscopy, a technique that creates images of a sample's structure, offering valuable information about morphology, grain size, and potential defects both before and after treatments. Another one is spectroscopy, a technique that analyzes how radiation (light or other forms of energy waves) interacts with a sample to identify the material, providing information about the elemental composition and chemical state. As well as, diffraction analysis, a technique that determines the material's crystallographic structure and phases. These techniques are described in Table 8.

a) Profilometry

Profilometry is a surface metrology technique that measures the overall height variations of a profile, typically to assess the surface roughness. Different types of profilometers exist, each with its own advantages and limitations. Some common types include stylus profilometers, optical profilometers, and white light interferometers.
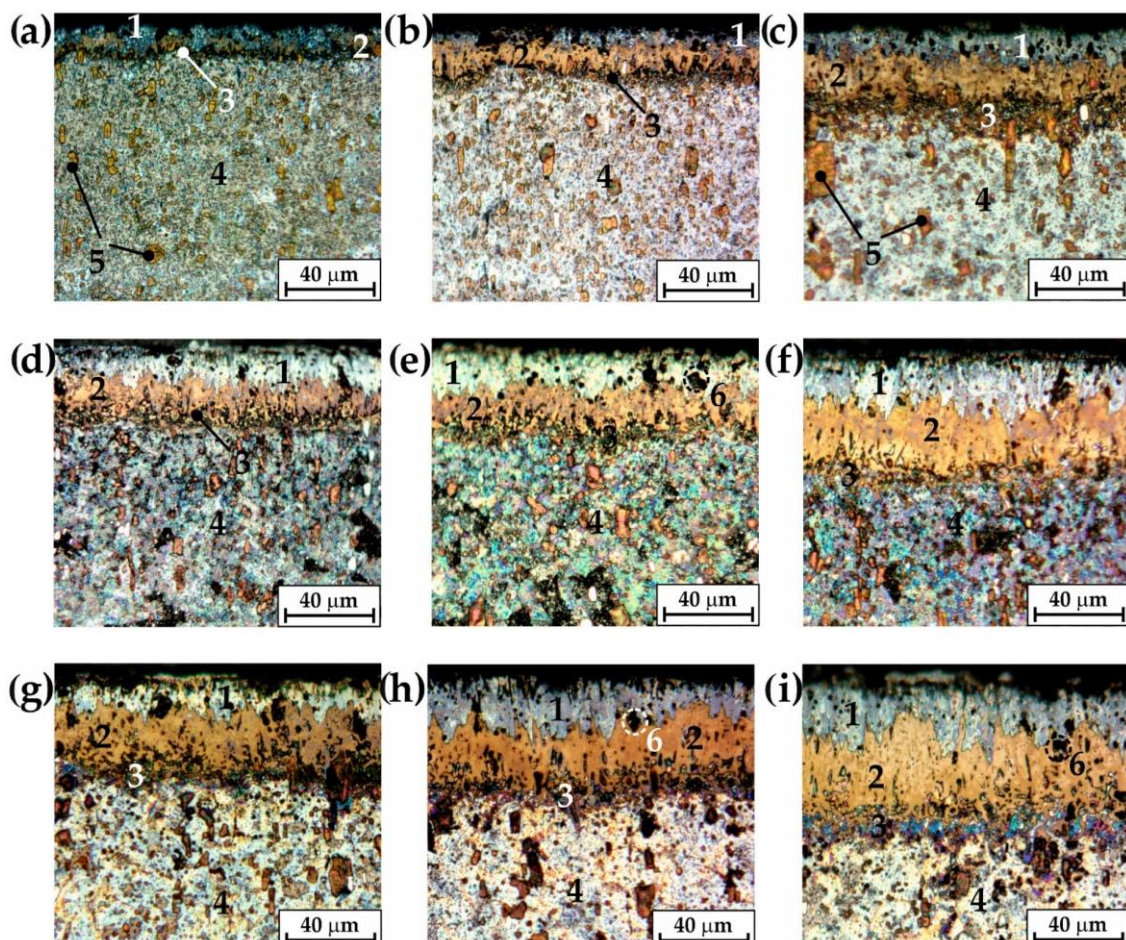
Figure 38. *OM images of X165CrV12 tool steel after powder boriding for 3, 6 and 9h at (a-c) 800, (d-f) 850 and (g-i) 900 °C, with 1-3 FeB, Fe$_2$B and diffusion zone, 4 substrate, 5 carbides and 6 pores* [104].

b)   **Optical Microscopy OM**

OM serves as a cornerstone technique for the initial characterization of boride layers. It offers a magnified view of a substrate, whether from above or from the cross section, allowing visual inspections, Figure 38. Accordingly, the visual inspection reveals features like phase morphologies (shape and texture), grain size distributions, and potential surface defects like cracks or voids. While OM has limitations in resolution compared to advanced techniques, it remains a cost-effective and valuable tool, often paving the way for further analysis with higher-resolution microscopy methods.

c)   **Scanning Electron Microscopy SEM**

SEM offers a much higher resolution view compared to optical microscopy. It works by scanning a focused beam of electrons across the boride layer. The interaction between the electrons and the sample generates various signals that reveal information about the surface topography, composition, and even the crystallographic structure of the layer, Figure 39. While SEM is a more powerful tool than OM, it often requires special sample preparation and can be more expensive.

d)   **Transmission Electron Microscopy TEM**

TEM is a powerful technique that offers significantly higher resolution than SEM. But unlike SEM, TEM utilizes a beam of high energy electrons that are transmitted through an ultra-thin sample. This requires the sample to undergo advanced preparation techniques, such as the FIB milling, to create the necessary thin section. The interaction between the electrons and the sample creates an image of the internal structure of the boride layer at the atomic level.
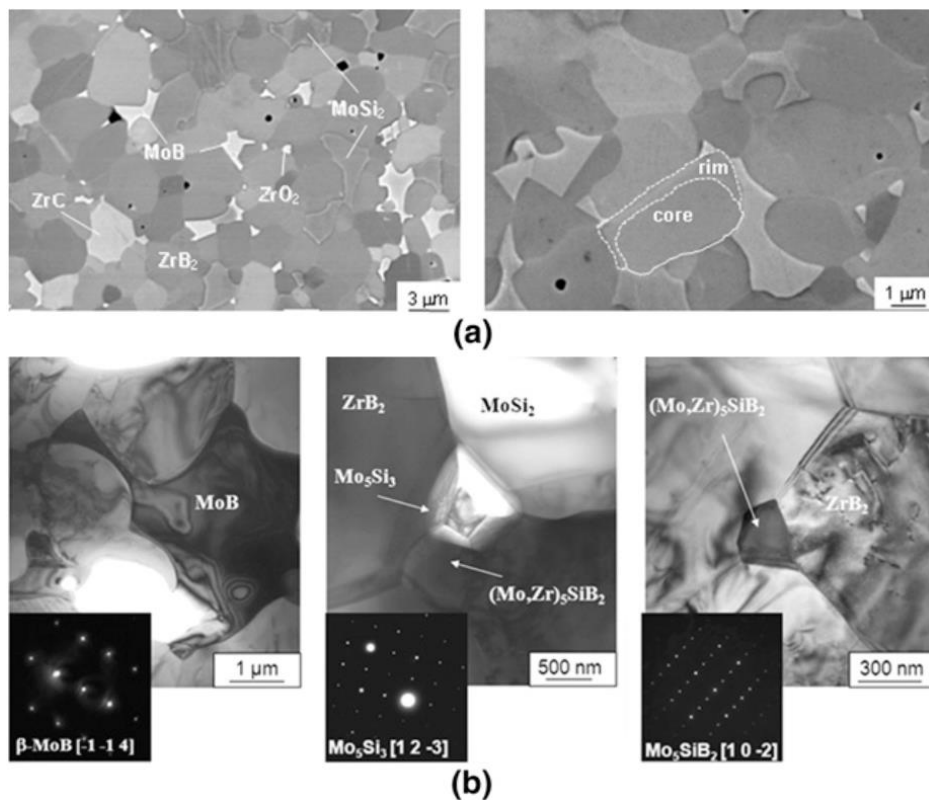
Figure 39. *(a) SEM and (b) TEM images of ZrB$_2$ based compounds in a boride layer* [105].

e)   Energy Dispersive Spectroscopy EDS

EDS, also sometimes referred to as EDX or XEDS, is a microanalytical technique often used in conjunction with SEM. It provides information about the elements present with an estimate of the relative quantity of each element in the composition of the layer, Figure 40. The technique analyzes the X-rays emitted when the sample is bombarded with a focused electron beam, and its accuracy can be affected by factors like surface roughness and the presence of overlapping X-ray peaks.
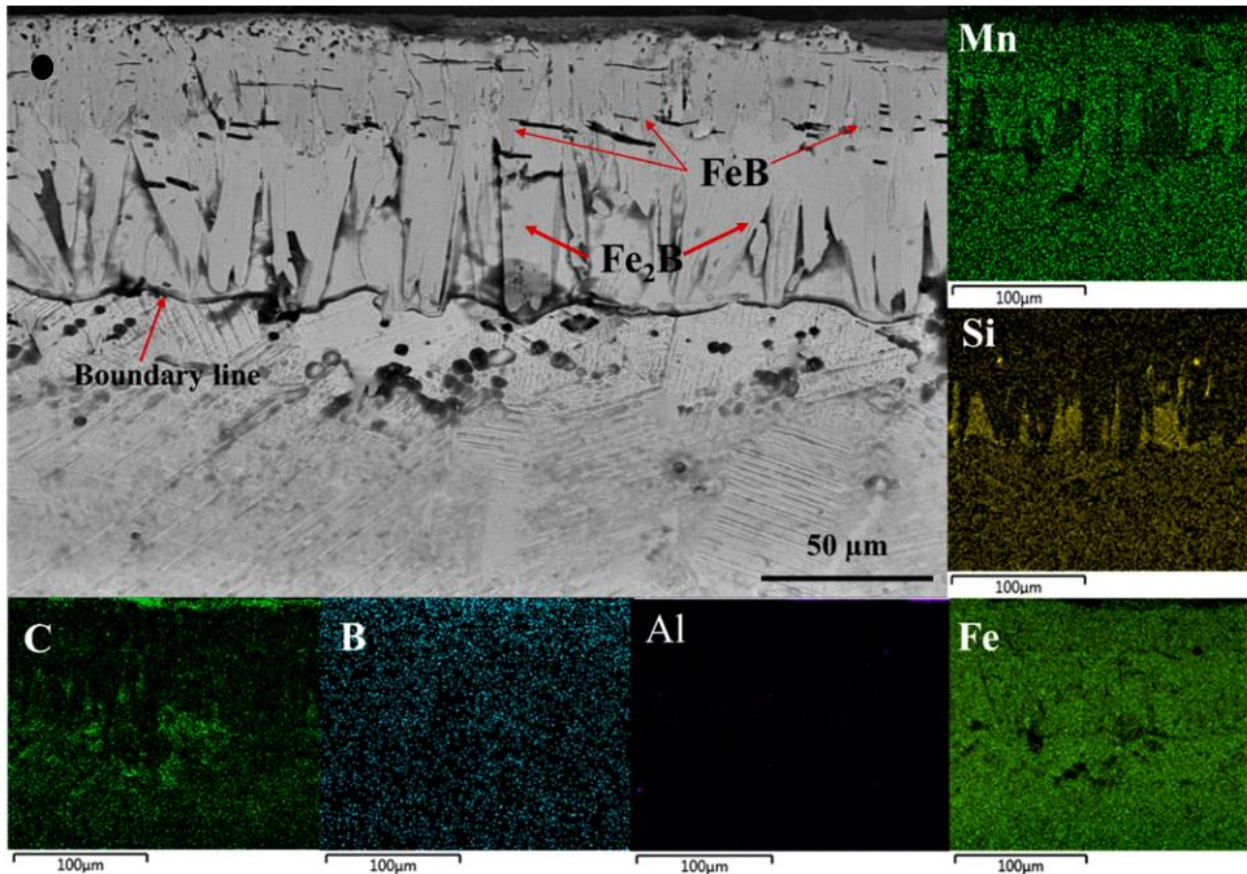
Figure 40. *SEM and EDS elemental mappings of a boride layer formed after boriding high manganese steel for 2h at 950 °C* [106].

f)   X-Ray Diffraction XRD

XRD is a powerful, non-destructive technique, that utilizes X-rays to analyze the crystallographic structure of materials. By directing a beam of X-rays at the sample and measuring the diffracted beam, XRD creates a unique fingerprint that reveals how atoms are arranged within the material. This information allows the identification of the different crystalline phases present, Figure 41, by determining the dimensions and angles of the unit cell, and estimating the average size of the crystallites within the layer. While XRD has limitations for analyzing amorphous materials or performing precise quantification, it remains a cornerstone technique for understanding the fundamental crystallographic structure of boride layers, which plays a crucial role in their properties.
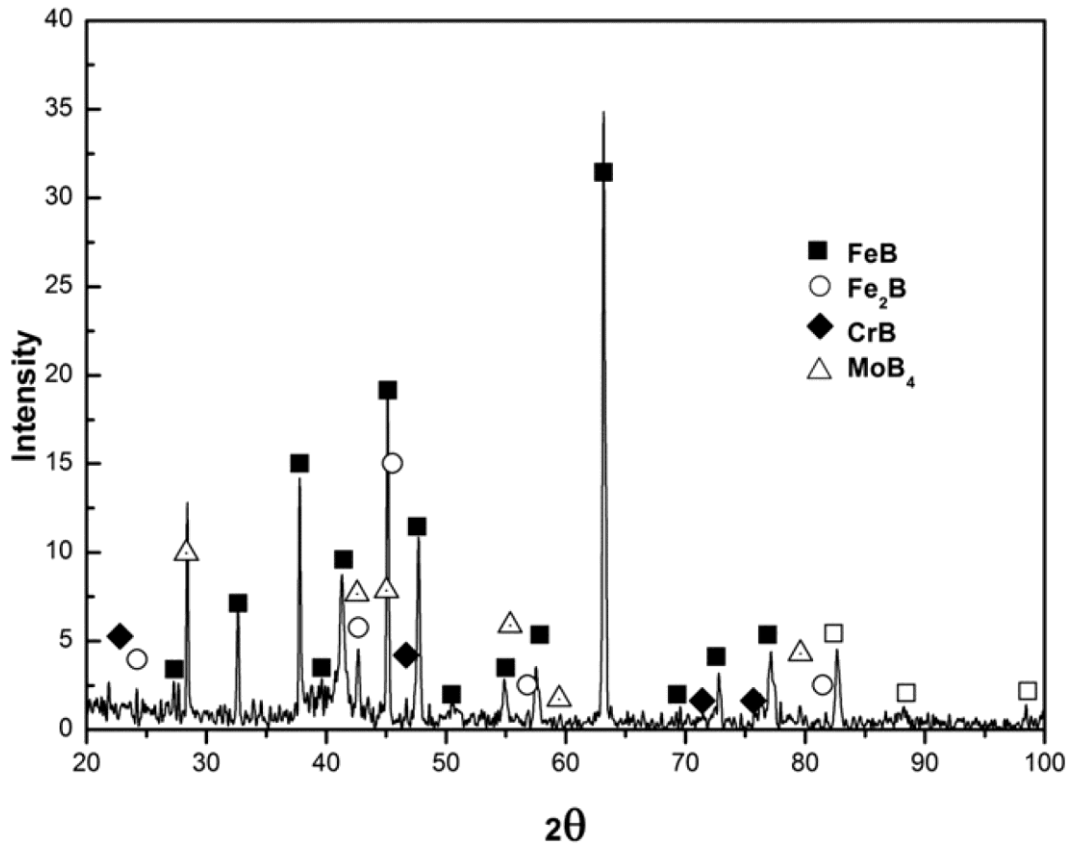
Figure 41. *XRD pattern of borides in AISI M2 steel after boriding for 5h at 1000 °C* [107].

Table 8. *Characterization techniques.*

Technique	Function	Analyzes	Advantages	Limitations
OM Optical Microscopy	Magnifies and visualizes surface features	Morphology (grain size, shape, defects).	Non-destructive. Good initial observations. Large field of view. Cost-effective.	Low resolution compared to SEM/TEM. Limited features.
SEM Scanning Electron Microscopy	Uses a focused electron beam to image surfaces	Surface topography. Composition (elements). Crystal structure (qualitative).	Non-destructive. High resolution. Surface morphology and texture. Good depth of field.	Requires further preparation. Limited information on bulk crystallography and composition. Can be expensive.
TEM Transmission Electron Microscopy	Uses electrons to image thin sections	Internal structure (atomic level). Crystal structure, including defects (quantitative).	Highest-resolution imaging for detailed microstructure analysis.	Can be destructive. Requires advanced preparation (thin sections). Small field of view. Expensive and complex.
EDS Energy Dispersive Spectroscopy	Analyzes X-rays emitted from a sample	Elemental composition of a specific region (quantitative).	Non-destructive. Elemental composition and relative abundance. Often integrated with SEM.	Limited depth information. Influenced by surface roughness. Requires conductive samples. Overlapping X-ray peaks.
XRD X-Ray Diffraction	Analyzes X-ray diffraction patterns	Crystallographic structure (phases, unit cell parameters, crystallite size).	Non-destructive. Identify crystalline phases. Affordable.	Limited to crystalline materials. Limited information on element composition or microstructure. Analysis can be complex.

III.3.   BORIDE LAYERS

As distinguished in the first chapter, borides are synthesized boron compounds that are either metallic or nonmetallic, depending on the element that is paired with the boron. When it comes to the boride layers, also referred as boronized layers, as the naming indicates, they are not synthesized as powders or other forms; instead, they are found on top of a material's surface, layered, after undergoing the surface hardening process of boriding, described in the second chapter. The process allows the diffusion of boron onto surfaces, creating either a superficial layer or a coating, as illustrated in Figure 42.
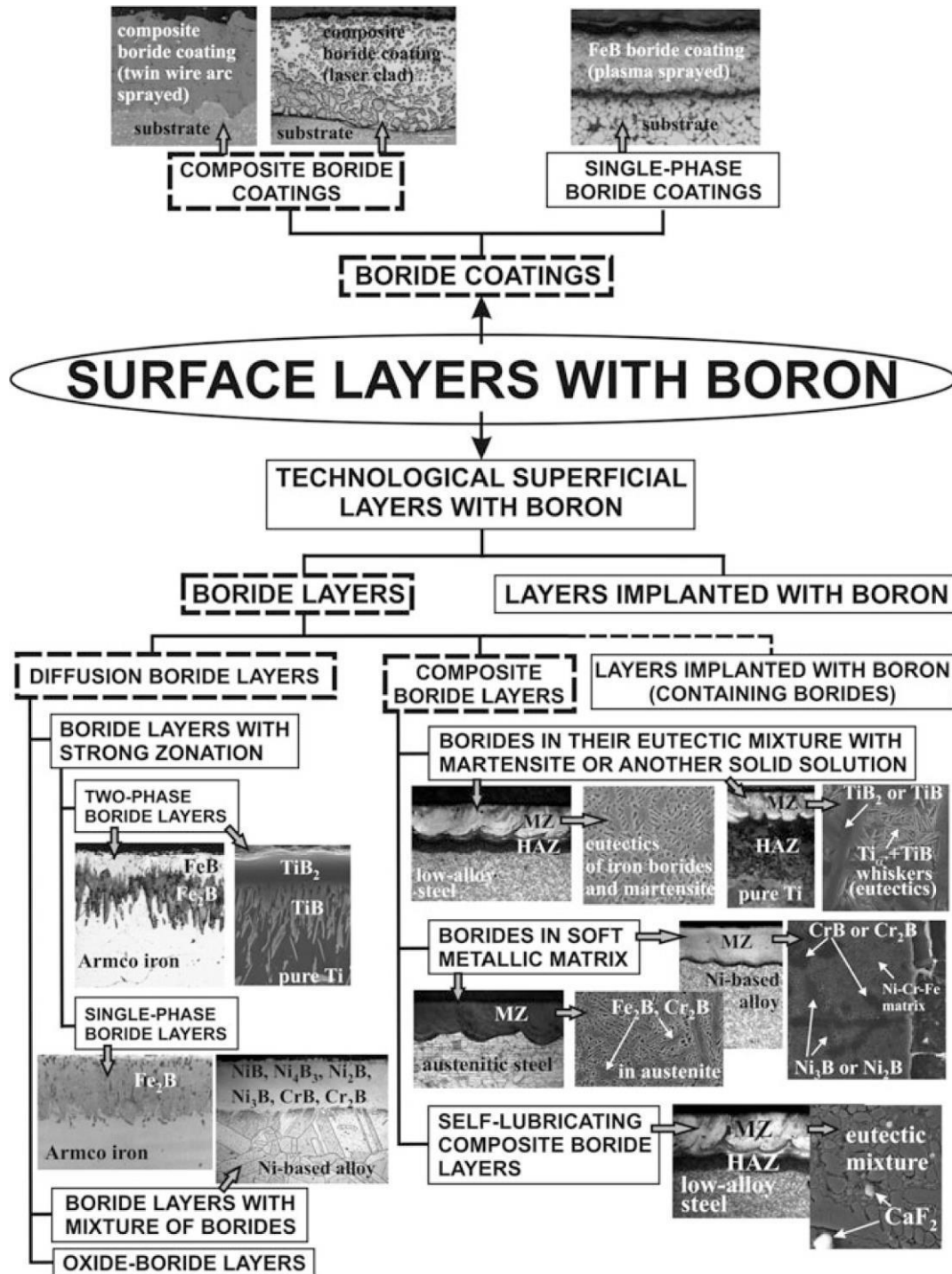
Figure 42. *Microstructural classification of boride layers* [10].

The theories used to estimate the mechanical, chemical, and other properties of boride layers reside on the substrate's bulk, ferrous or nonferrous, the content regarding the alloying elements, the processing technique that diffuses boron into the surface, traditional or modern, all affecting the composition and structure of the processed layer, and lastly the case depth, i.e. thickness, of that layer [7].

Boride layer thicknesses are mainly affected by two decisive parameters, the temperature, and the treatment time exposures. Their effect is seen in Figure 43 where the temperature seems to have a greater impact. Nevertheless, both parameters are crucial prerequisites for careful processing.
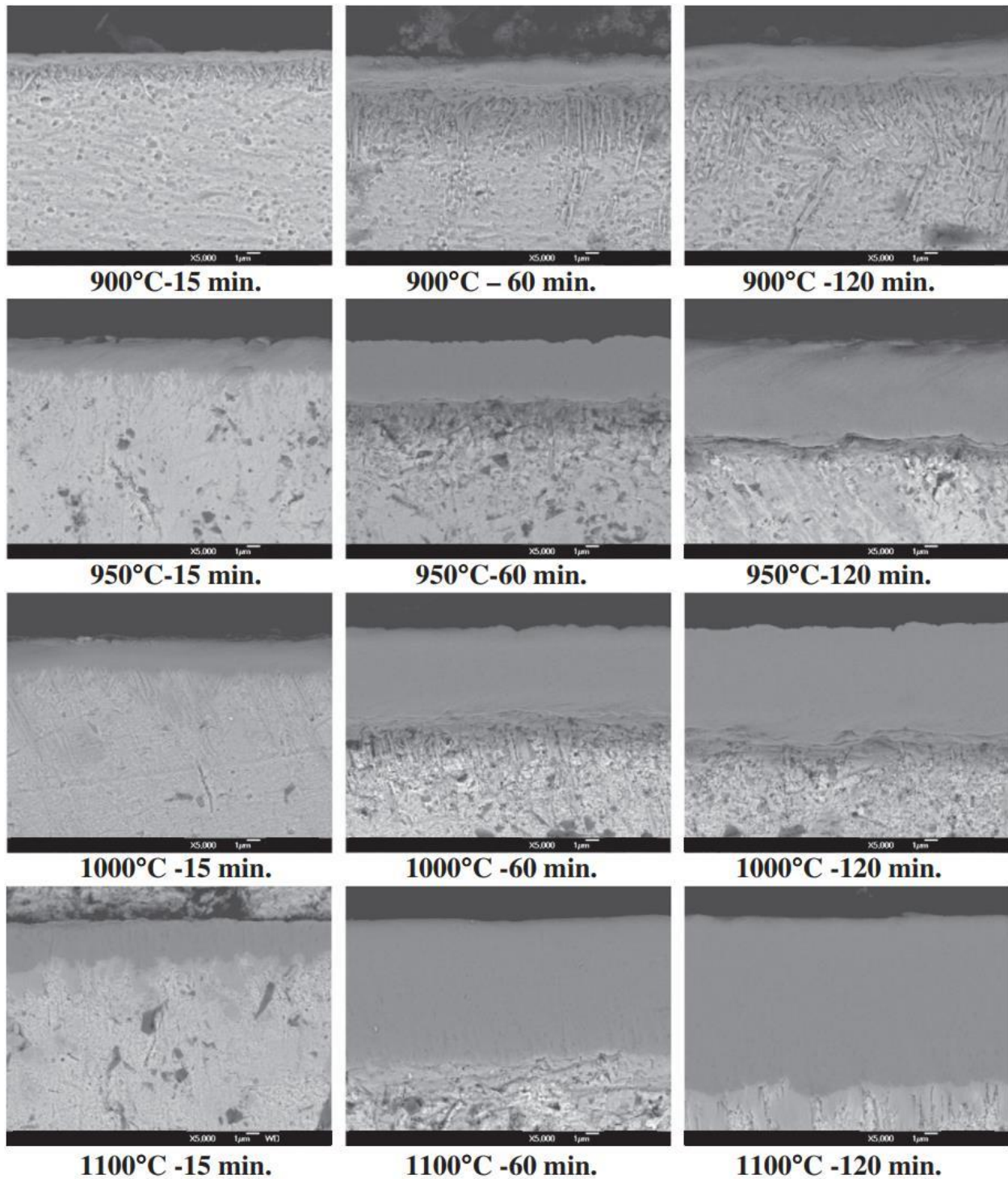
Figure 43. *Cross section micrographs of boride layers formed at different temperatures and times* [90].

A.   Surface layers

Treatment of the surface layers can induce dimensional changes in workpieces, either increasing, decreasing, or leaving them unaltered, as illustrated in Figure 44. Thus, techniques of surface layer treatments are distinguished as [108]:

- **Decremental surface treatments,** referring to techniques that decrease the dimensions of the treated workpiece, like machining or burnishing.

- **Non-decremental surface treatments,** referring to techniques that neither increase nor decrease the dimensions of the treated workpiece, like surface alloying or ion implantation.

- **Incremental surface treatments,** referring to techniques that increase the dimensions of the treated workpiece, like deposition coatings or certain thermochemical treatments.
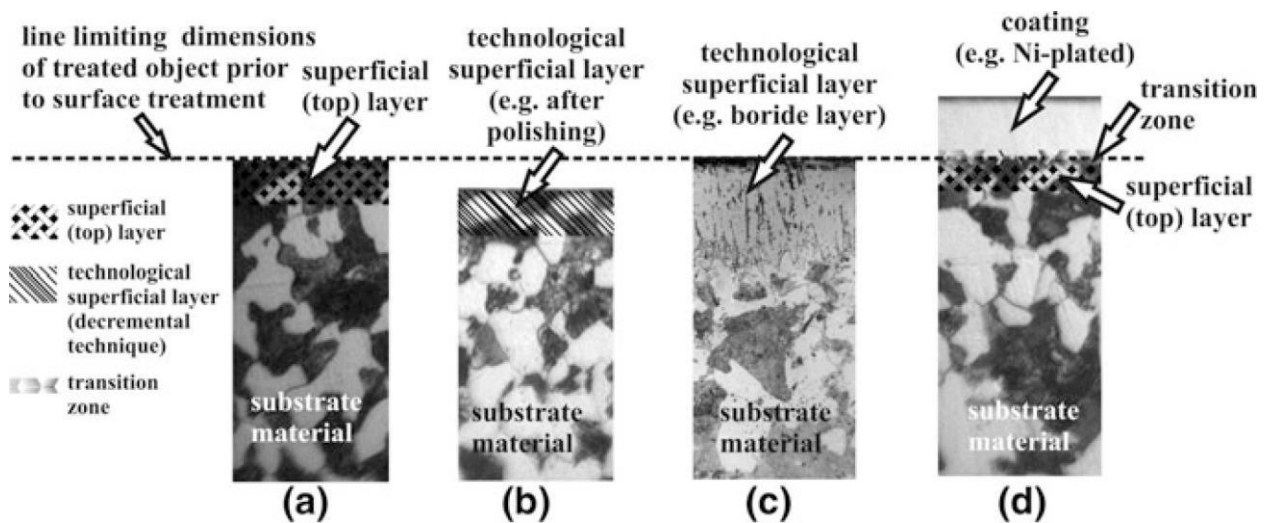
Figure 44. *Representation of different surface layers resulted from, (a) prior to, (b) decremental, (c) non-decremental, (d) incremental, surface treatment techniques* [10].

Whichever the treatment carried, the surface properties get altered, and some of the main advantageous alterations from surface hardening processes, such as diffusing boron, reside in:

- **Corrosion**

An irreversible interfacial reaction of a material with its environment that results in its deterioration. Mostly, it concerns metals and represents their chemical or electrochemical deterioration by either atmosphere, trapped moisture, or other agents such as acids and alkalis [65]. Often, but not necessarily, corrosion results in effects detrimental to the material's usage, like the loss of a material strength and integrity, hazardous functional failures, and others. In the other instances where the corrosion is not necessarily detrimental, an example can be invoked where the formation of a protective oxide layer on some metals itself can help prevent further corrosion.

- **Wear**

A progressive loss of a material from a solid surface due to relative motion against another surface or particles. It can be caused by mechanical actions, such as sliding, rolling, or impact, and also by chemical reactions, like corrosion. The material properties, hardness, toughness, microstructure, and composition can influence directly wear characteristics. Also, the presence of an oxide layer due to corrosion or the treatment of the material's surface itself by creating layers through surface hardening processes can significantly alter these wear characteristics. Additionally, service variables like contact pressure, relative speed, temperature, surface finish, atmosphere, and lubrication all play a role in the wear rate and lifespan of a material. Therefore, wear can manifest in different forms, be it friction, abrasion, adhesion, oxidation, erosion, fatigue, and such [65,108].

- **Hardness**

A material's property that reflects its resistance to permanent deformation from external forces. That is typically manifested through indentation, where if a hard material is subjected to, it resists the creation of a lasting impression. While a stiff material resists elastic deformations by returning to its original state, a hard material resists plastic deformations, retaining a permanent indentation. Hardness is one of the factors influencing the material's toughness (resistance to fracture) and brittleness (ease of fracture).

It is measured by various types of indentation methods: Brinell Hardness, Rockwell Hardness, Vickers Hardness, or else. To relate between certain hardness scales, approximate conversion of hardness values and tensile strengths for steels were common [66]. For example, in the case of unalloyed and low alloyed steels, two formulas were developed to convert from Rockwell C Hardness (HRC) to Vickers Hardness (HV) or inversely [109], equation (1) and (2), then plotted as demonstrated in Figure 45.

$$HV = \frac{223\,HRC + 14500}{100 - HRC} \tag{1}$$

$$HRC = \frac{100\,HV - 14500}{HV + 223} \tag{2}$$
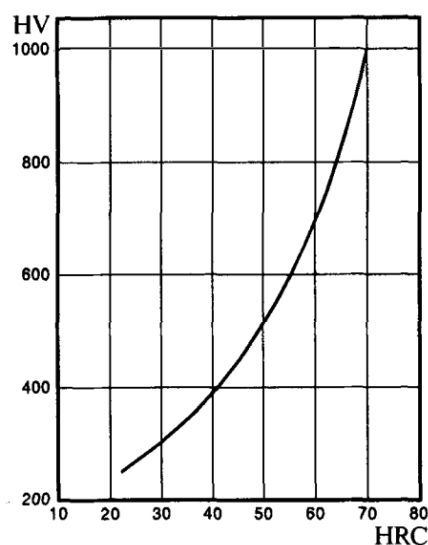
Figure 45. *Vickers hardness as a function of Rockwell C scale* [109].

B.   Layer composition

Boriding can be performed on various materials, though the benefits may differ depending on the substrate, as will be discussed in the borided materials section. However, it finds its most common application with ferrous materials. The boron diffused results in a boride layer that is influenced by the alloying elements Me present in the substrate's chemical composition, and therefore, the layered borides formed take the form of Fe_xB_y or $Fe_xMe_yB_z$ if the substrate is ferrous. Otherwise, If not, its chemical formula becomes Sub_xB_y, and so on [76].
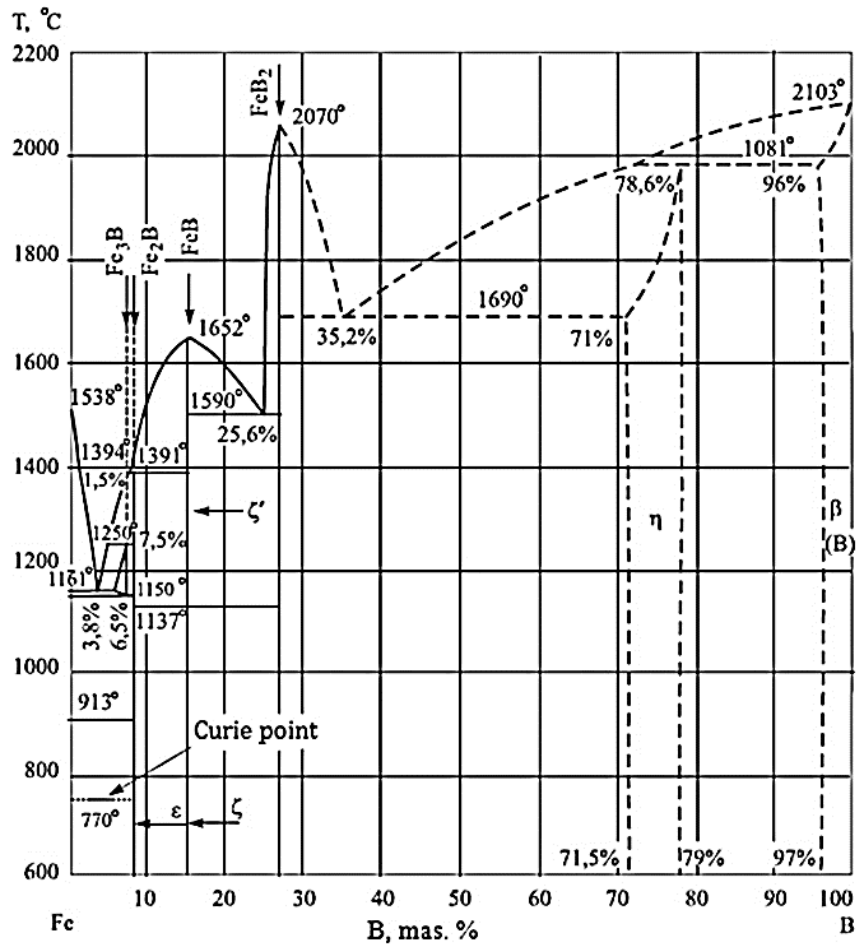
Figure 46. *Fe-B Iron-Boron equilibrium diagram* [7].

According to the Iron-Boron equilibrium diagram, Figure 46, four main iron borides are prominent, rhombic triiron boride Fe_3B, tetragonal diiron boride Fe_2B, rhombic iron boride FeB, and hexagonal iron diboride FeB_2. Their crystal lattice structures are illustrated in Figure 47. The Fe_3B phase is stable only on the thermodynamic equilibrium within a narrow saturation window, Table 10, at temperatures near 1200 °C, therefore it is considered instable.

Additionally, both Fe_3B and FeB_2 phases have difficulties to be distinguished with optical microscopy OM or such means, they are rather detected with advanced means like the nuclear gamma resonance NGR spectroscopy. Thus, the principal phases that are considered in the boride layer, Table 9, due to observation ease, stability, and dominance, are the FeB and Fe_2B phases [7,110].

Table 9. Specters of iron boride phases contents within layer [9].

Analyzed layer's width [μm]	The content of a boronized layer's phases after processing [vol.%]									
	Solid phase boriding					Combined boriding				
	FeB	Fe_2B	Fe_3B	$FeB_{x<0.4}$	$FeB_{x>0.4}$	FeB	Fe_2B	Fe_3B	$FeB_{x<0.4}$	$FeB_{x>0.4}$
0.3	21	14	17	26	22	10	62	2	23	3
20	18	59	4	19	4	15	65	5	13	2
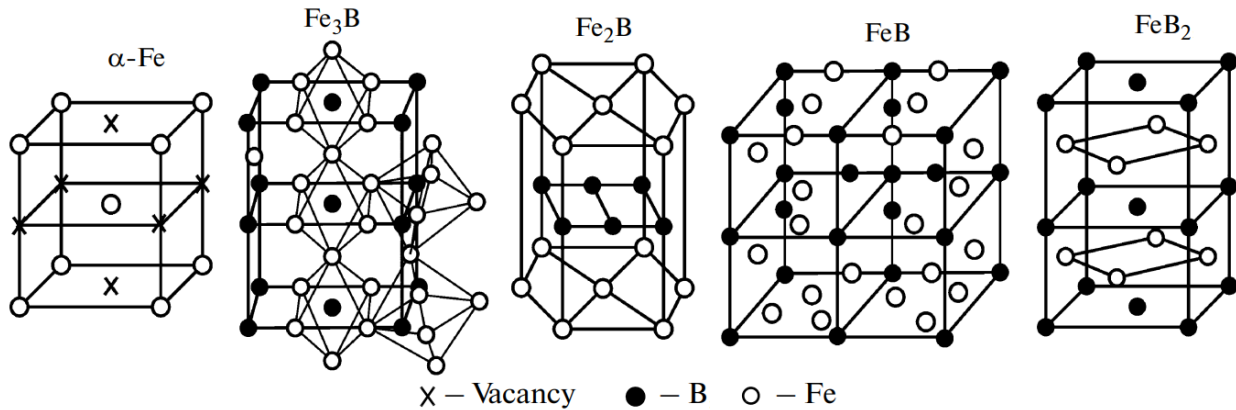
Figure 47. Crystal lattice structures of iron borides [110].

Thereupon, when boriding, either a mono-phase or a bi-phase layer is observed. The first is seen only under specific conditions, mostly in ferrous materials as Fe_2B, while the latter is regularly observed on both ferrous and nonferrous materials under various borides, iron borides FeB/Fe_2B, titanium borides TiB_2/TiB, or chromium borides CrB/Cr_2B, as demonstrated in Figure 42 and Figure 48 [68].

As a side note, nonferrous materials may exhibit similar behavior to ferrous ones regarding boriding, as observed in Figure 48. This boride layer section focuses mainly on ferrous materials due to the literature's abundance and extensive use compared to nonferrous ones. In that, a typical two-phase layer progresses from the surface towards the core as an outer boron-rich phase FeB, followed by a lesser boron-rich phase Fe_2B, onto the ferrous substrate.
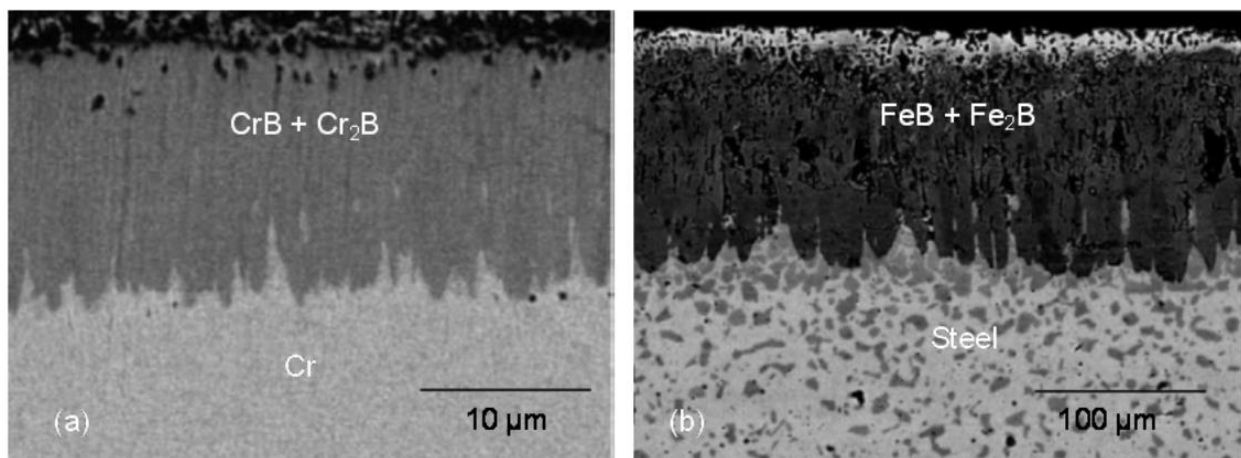
Figure 48. Cross sectional microstructure after boriding (a) pure chromium and (b) steel [68].

C.   Diffusion mechanism

In 1967, H. Kunst and O. Schaaber theorized a diffusion channel theory, describing the formation of boride layers in different stages. Primarily, in stage 1, boron diffuses into the ferrous material's surface, creating a diffusion zone with a velocity dependent on the iron crystalline structure, face or body-centered cubic, and its alloying elements. Upon reaching an appropriate boron concentration in the diffusion zone, at a specific point of stage 2, referred to as incubation time, saturation happens, leading to the nucleation of Fe_2B crystals. An important aspect of nucleation is determined by a specific angle that sits between the crystal's z-axis and an axis perpendicular to the substrate's surface. The decrease of that particular angle determines the ideally oriented growth in which a Fe_2B crystal grain readily diffuses, stage 3. The mechanism was also described by C. Martini, G. Palombarini, and M. Carbucicchio in 2004, where they schematized in Figure 49, the ideal plane (001) of growth to penetrate parallelly along [11].
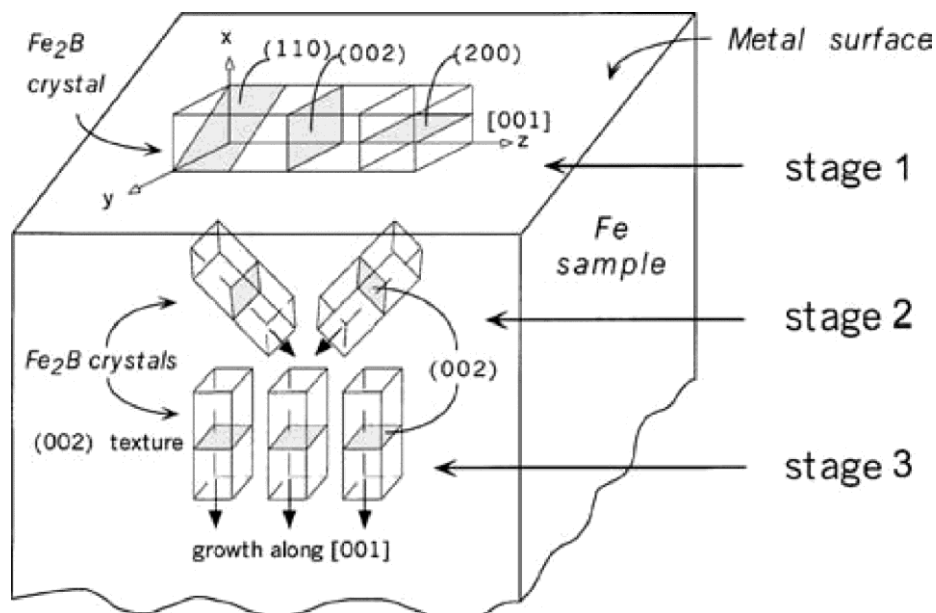
***Figure 49.** Schematization of the Fe₂B crystals' thermochemical growth stages* [11].

Due to the crystal growth being not uniform, well-oriented crystals grow faster along the ideal plane while others get left behind but eventually become part of the larger growing crystals and get incorporated by high temperatures. Meanwhile, the nucleation and growth of the FeB phase on top of the Fe_2B phase is a consequence of both high temperatures and boron potentials in the flux. This phase's growth is similarly affected by the same angle orientation. When high boron content concentrates on the substrate's surface, its fluxing increases, promoting the growth of the FeB phase. Furthermore, when iron borides are massively precipitated without coalescence due to high temperatures, a diffusion zone below these phases can be observed, constituted from small precipitates of the Fe_2B phase in the inner part of the substrate [7].

D.   Alloying elements

Concurrently, regarding the alloying elements, if found in the ferrous materials prior to boriding, after processing, trace amounts of interstitial boron compounds like chromium borides CrB, molybdenum borides MoB, vanadium borides VB, and/or others, may also be observed alongside the primary iron boride phases FeB and Fe_2B. When it comes to the morphology of the boride layer, it is mostly in the form of needles or saw-toothed layers when the alloying elements are low, and tend to flatten with their increase, Figure 67 [14,85]. Their influence on reducing boride layer depths can be categorized by their relative impact. These elements exhibit an increasing influence observed in Figure 50, where the order is nickel, manganese, silicon, copper, chromium, aluminum, tungsten, and molybdenum [111]. Besides, each alloying element also influences the hardness of the phases present in the boride layer, as illustrated in Figure 51.
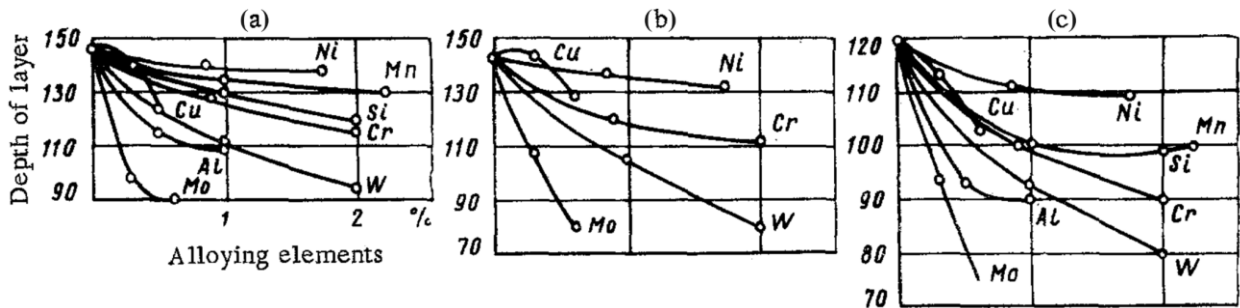
Figure 50. Effect of alloying elements on the boride layer depth in boriding for 6h at 900 °C with powder, (a) ferroboral + 4% NH₄CI (b) ferroboral + B₄C (c) ferroboral [111].
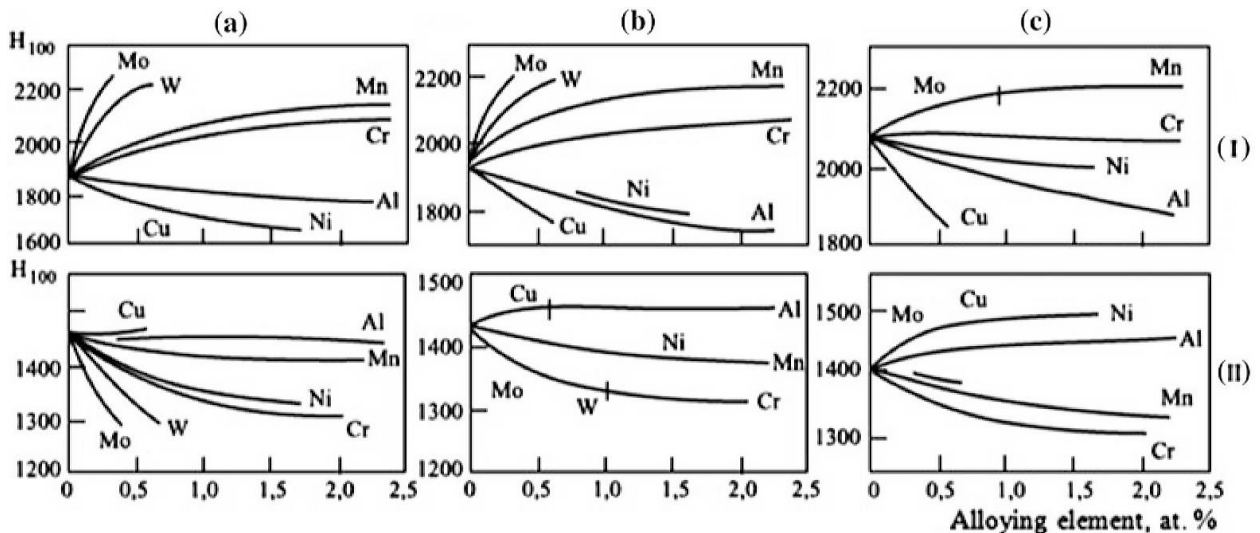
Figure 51. Influence of alloying elements on the hardness of boride phases, (I) FeB and (II) Fe₂B, in different temperatures, (a) 950, (b) 900, and (c) 850 °C [9].

Accordingly, the concentration of alloying elements is a factor that significantly influences the formation of multi-phased layers. Higher alloy contents decrease the diffusivity of boron, hindering its diffusion towards the core of the material. This makes the boron reside and concentrate only on the surface, promoting the formation of the more boron-rich phase at the outer boundary of the layer. Consequently, in ferrous alloys for instance, the formation of FeB is more endorsed than the Fe_2B phase. That can result in shallower total boride layer depths once the outer phase reaches saturation. This factor can be overcome by lowering the boron concentrations in the media while boriding, Figure 52, affecting the flux of boron within the surface without reducing the boron diffusion, therefore, lower potential to form the more spall able boron rich outer phases, such as FeB [12].
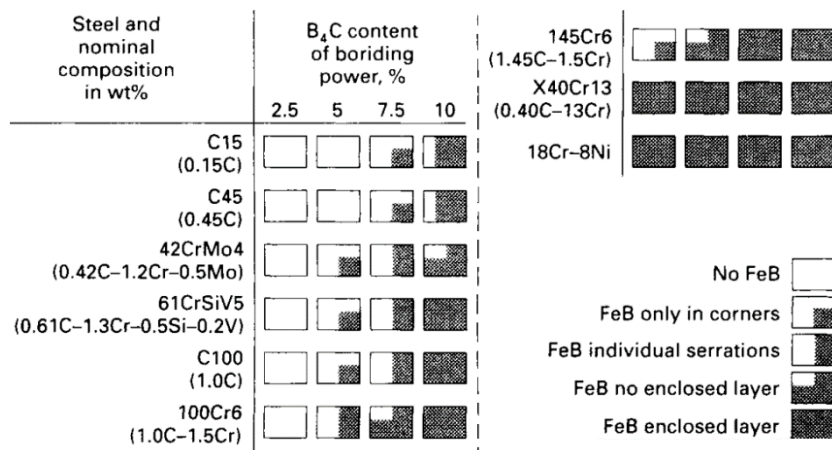
Figure 52. *Influence of B_4C content in the powder mixture on the proportion of FeB phase after powder pack boriding* [6].

E.   Toughness and brittleness

As stated previously, the FeB phase is undesirable because of its mechanical properties, mainly its brittle nature. The toughness of the Fe_2B phase is considerably higher than that of the FeB phase. Thus, increasing boriding temperatures may result in precipitated diffusion, forming a thicker FeB phase, which decreases the toughness of the substrate. That can also be observed in increased boriding durations. Though, annealing and other post treatments help decrease the FeB phase, helping regain good overall toughness, making the substrate more ductile. Figure 53 demonstrates the difference in brittleness within the boride layer regarding its three regions, FeB phase, FeB/Fe_2B interface, and the Fe_2B phase [112].

(a)   (b)   (c)
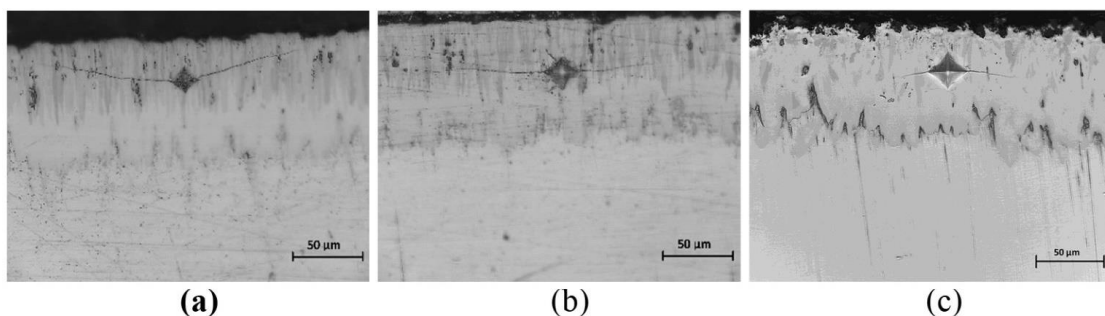
Figure 53. *Crack formations from indentations on (a) FeB, (b) FeB/Fe_2B interface, and (c) Fe_2B* [112].

Additionally, bending forces, inducing transverse loads and shear stresses, can be of concern to borided components, which might act as composites. The resistance of these composite structures to such forces depends on factors like case depth, composition, and mechanical properties. A single Fe$_2$B layer is thereby superior in this matter due to its toughness compared to the brittle nature of the FeB phase. Studies have shown that single phase layers with case depths of 150-200 µm, achieve elongations of up to 4% without crack formations, thus, indicating the superiority of single phased layers to withstand a limited degree of post-treatment straightening without compromising their integrity [6].

F.   Crack formation

A case study investigating a borided AISI D2 tool steel exemplifies the concept where the two-phase layer is found. The thermal expansion coefficients TEC of the FeB, Fe$_2$B, and Fe were 9.3, 6.9, and 12.8, all in 10^{-6} °C^{-1} at temperatures of 100 and 300 °C, respectively. Their Young's modulus was approximately 580, 290, and 200 GPa, respectively. Utilizing those properties, along with the temperature and depth variations within the layer, thermal residual stresses were calculated using equation (3), proposed by Lyakhovich et al. [113].

$$\sigma_{th} = \hat{E}\left(\frac{\int_{h_1}^{h_2} \alpha_i\, \Delta T\, E_i\, dh_i}{\int_0^{hT} \tilde{E}\, dh_i} - \alpha_{ii}\Delta T\right) \tag{3}$$

Where:

- σ_{th} thermal residual stress.
- ΔT interval of the cooling temperatures.
- h_i thickness of the i-th layer where the Berkovich indentation was performed.
- α_i and α_{ii} thermal expansion coefficients at T=566-846 K.
- $\hat{E}$ theoretical Young's modulus in the i-th phase (Fe or Fe$_2$B).
- $\tilde{E}$ theoretical Young's modulus in the preceding phase (Fe$_2$B or FeB).
- E_i experimental Young's modulus obtained by Berkovich nanoindentation at each distance.
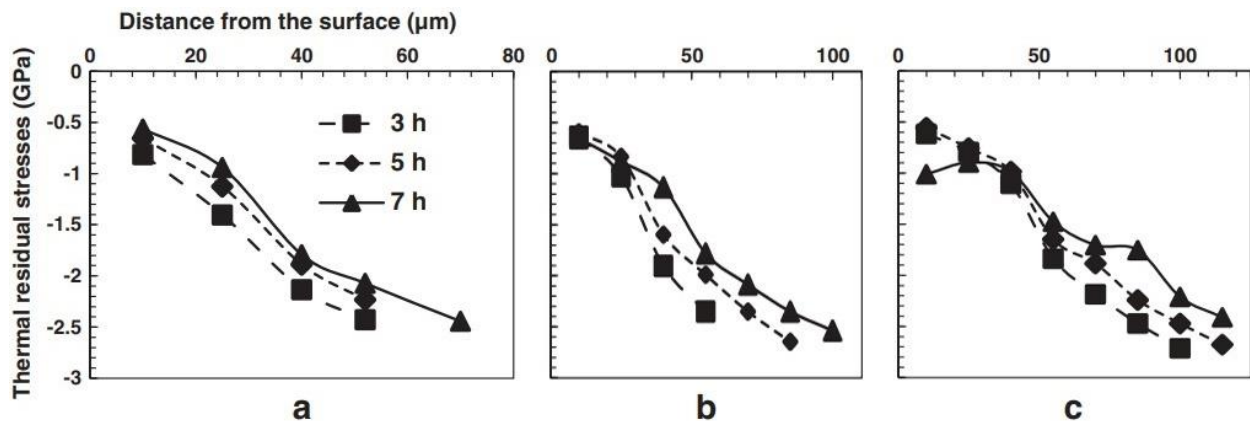
Figure 54. *Thermal residual stresses obtained throughout the boride layer of an AISI D2 tool steel borided at temperatures of (a) 950, (b) 1000, and (c) 1050 °C [114].*

The analysis revealed that the compressive stresses in the FeB phase ranged from 0.6 to 1.3 GPa, and sharply increased reaching a maximum of 2.7 GPa in the Fe_2B phase, illustrated in Figure 54. The presence of these compressive stresses in the boride layer can be advantageous as it enhances the material's capacity to withstand static tensile loads. Furthermore, the hardness of the FeB and Fe_2B phases were reported as 19 and 16.3 GPa, respectively [114].

Another case study specified that the coefficient of expansion of Fe_2B was found to be 2.9 10^{-8} C^{-1}, which is less than that of Fe 5.7 10^{-8} C^{-1}, making the Fe_2B phase remain in compression after cooling. However, that of FeB was 8.7 10^{-8} C^{-1}, which is greater than both that of the Fe and Fe_2B, making the FeB phase in tension. This disparity in residual stresses was then concluded to result in the formation of cracks amid both phases, particularly if exposed to thermal and/or mechanical shocks [8].

G.   Spalling

Even though the presence of a multiphase layer can be beneficial, in several situations, it is regarded as problematic due to the phases having significant property differences. Notably, differences in specific properties, Table 10, such as in thermal expansions, make the phases contract at different rates during cooling after the boriding is completed, leading to tensile stresses in the FeB and compressive stresses in the Fe_2B. Also, significant variances in mechanical properties, make them react to external forces differently, especially when the percentage of FeB content in the total layer thickness is remarkable [7].

Table 10. Typical properties of iron borides and their elements [9,110,115].

Phase	Crystal lattice structure [Å]	Hardness [HV]	Elastic modulus [GPa]	Density [g/cm³]	Melting point [°C]	Coefficient of expansion [ppm/°C]	Concentration of boron [wt.%]
B	Rhombohedral	>4200	>400	2.34	>2070	~6.4 at 100-800 °C	100
FeB₂	Hexagonal a=3.045 c=3.035	2740-2800	230	-	~2070	-	27.9
FeB	Orthorhombic a=0.4061 b=0.5506 c=0.2952 or a=4.053 b=5.495 c=2.946	1850-2100	590	6.75	~1650	23 at 200-600 °C	16-16.4
Fe₂B	Body-centered tetragonal a=5.078 c=4.249 or a=0.5109 c=0.4249	1320-2000	290	7.43	~1390	7.65 and 9.2 at 200-600 °C and 100-800 °C	8.83-9
Fe₃B	Rhombic	-	-	-	~1250	-	6-7
Fe	Face or body-centered cubic	70-180	210	7.87	~1540	~12 at 100-800 °C	0

This mismatch of properties between the phases can lead to the formation of cracks that are parallel to the surface at the interface of the phases, potentially leading to spalling or fracturing of the outer phase, FeB in the case of FeB/Fe_2B, Figure 55.

While cracks may not occur during cooling itself, they may be initiated or encouraged to propagate in these regions under subsequent mechanical strain or exposure to thermo-mechanical shocks [12,76]. To prevent that, a further homogenization of the layer is required where the outer FeB phase is diminished or eliminated. That is done through the employment of additional processes like slow tempering or annealing with precisely controlled temperature profiles and extended exposure times [116].
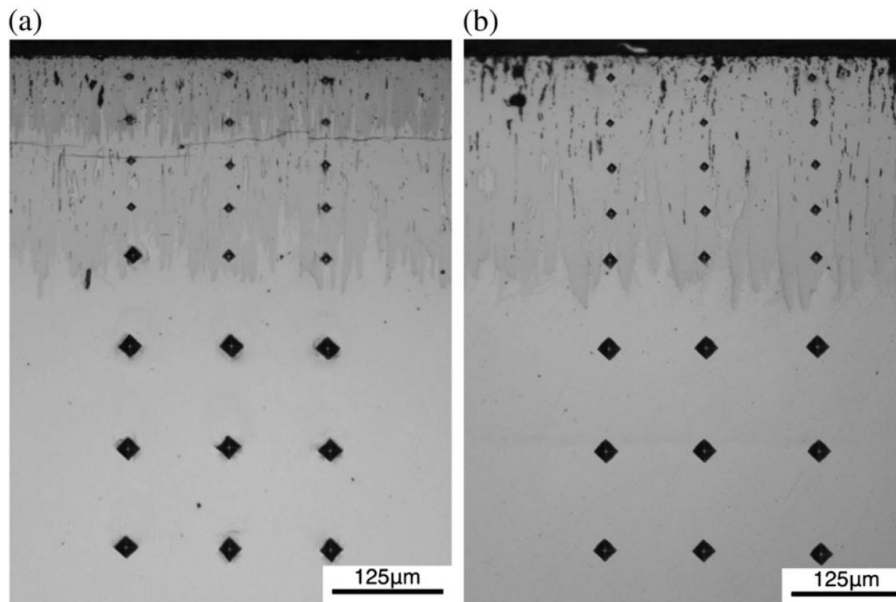
Figure 55. Indentation performed across a boride layer formed after 8h at 950 °C on AISI 1045 with powder pack boriding after (a) no further treatment (b) additional diffusion annealing processing [116].

H.   Geometry

Another factor is observed when intricate parts with localized spots, corners, and sharp edges are borided, their geometry can influence both the formation kinetics and performance of the boride layers. These complex geometries tend to trap higher concentrations of boron due to the multi-directional fluxing, i.e. boron diffusion from multiple directions within a corner, illustrated in Figure 56, promoting the formation of the brittle boron-rich layer and increasing the likelihood of spalling, either simultaneously or under mechanic impacts [12].
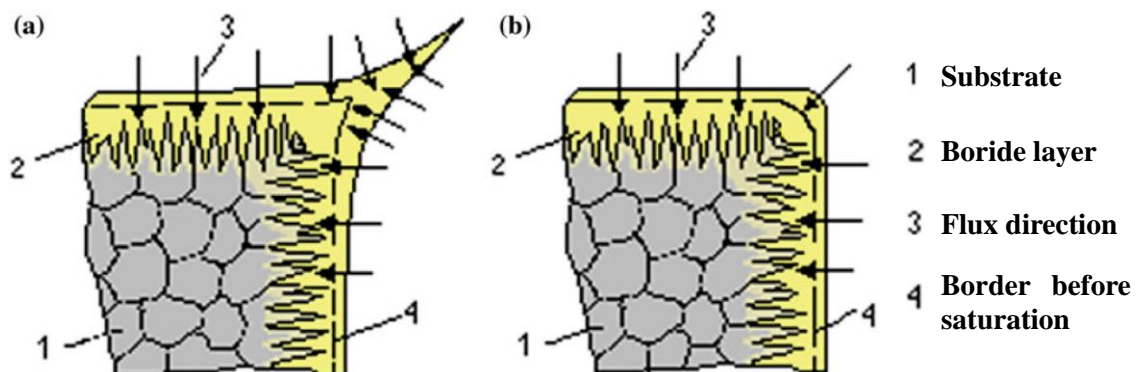
Figure 56. Edges produced after boriding (a) without rounding (b) preliminary rounding [9].

When a corner is borided, its size increases by around 10 % more than one of its sides. To mitigate those effects, features with excessive size complexities should be preliminarily processed through mechanical processes like machining or grinding before boriding. This also minimizes geometry-induced changes during heating.

Additionally, preliminary thermal processing, such as annealing or normalization, may be beneficial before the final polish. The changes in surface roughness (Ra) after boriding are generally either preserved if the initial roughness is around 0.5 µm, decreased if below that value and approaching 0.25 µm, or increased when around 1 µm [9].

I. Combined diffusions

Other practices of combining boriding with other surface hardening processes, either simultaneous or sequential, provide boride layers found below or on top of other nonboron layers, having advantageous outcomes. One of such practices is when borocarburizing [68,72], given in the second chapter, where it is believed that boronizing after carburizing can improve toughness while reducing the brittleness of the boronized layer. This is because the gradient between the iron carbide phases formed during carburizing and the subsequent iron boride phases FeB and Fe_2B becomes shallower. Therefore, residual stresses between the layers may diminish, thereby reducing the likelihood of crack formation, reducing brittleness, and promoting toughness. Moreover, borocarburizing followed by sulfurizing, given in the second chapter, or borocarbonitriding, and other combined processes as those found in Figure 57, are also of such practices which may provide compound layers with advantageous properties [68].

J. Wear resistance

Wear, defined earlier, as a major detriment to many components, can be mitigated to a greater extent through boride layers. Figure 57 demonstrates various practices of surface hardening processes, be they individual or combined, including boriding, carried on a C45 medium carbon steel, then compared to one another by means of two assessments, the Faville test and the grinding disk test. When subjected to abrasive wear, all multi-component boride layers behave excellently and result in a cost-effective treatment that is worthier than the pure iron boride layers [6,117].

The first, the Faville test, showed the importance of the protective boride layer in weight loss when it comes to metal-to-metal wear, which encompasses abrasion, adhesion, fretting, and oxidation wear. Approximately, for the same weight loss of 10 mg, vanadizing outperforms individual treatments with 195, followed by boriding 165, then by far, chromizing 80, and hardening 25 thousand revolutions. Furthermore, when other treatments are carried post boriding, the combined protective layer exceeds even that of vanadizing by not losing less of that weight, even to the extent of not losing at all if combined with vanadizing itself, less than 5mg of weight loss past 200 thousand revolutions.

In the second test, regarding grinding the treated substrates against silicon carbide, one of the hardest common abrasive grains with a 9 to 9.5 hardness on the Mohs scale, the findings suggest that the borided substrates also had excellent advantages against grinding wears which can induce, additionally to the previously mentioned ones, other attritive, thermal, or chemical wears. Vanadizing also presided with an approximate weight loss of 12 mg for more than 10.5 h, followed again by boriding with over 6 h, chromizing 2.4 h, then nitriding and hardening with under 0.5 h. The other combined treatments had less than 5 mg of weight loss, even over 13 h of grinding.
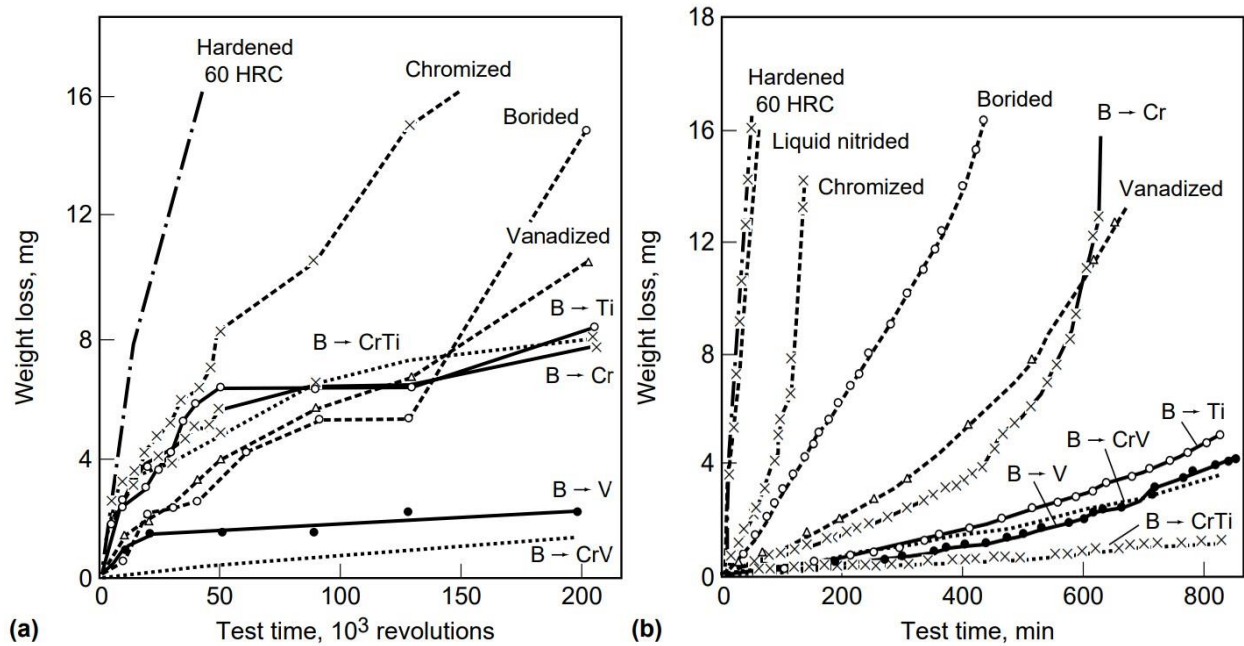
Figure 57. Wear resistance of various individual and combined surface hardening processes applied on C45 substrates with (a) Faville test (Identical metal-to-metal wear), and (b) Grinding disk test (Wear against silicon carbide) [6,117].

K.   Corrosion resistance

Boriding considerably improves the corrosion resistance of boride layers against molten metals such as Zinc or Aluminum melts, where even a tenfold increase in the component's life can be achieved. Also, the layer is resistant to alkalis and certain acids like phosphoric acids H_3PO_4, sulfuric acids H_2SO_4, perchloric acid $HClO_4$, and sodium hydroxide NaOH. However, hydrochloric acids HCl may corrode certain boride layers and not do so for others. On the other hand, nitric acids HNO_3 can corrode boride layers [118].

In a dilute solution of sulfuric acid H_2SO_4 at 56 °C, borided steels has higher corrosion resistance in comparison to steels treated with nitriding, carburizing, and most other surface hardening processes [7]. Then, when it comes to untreated steels, a significant magnitude by which a boride layer can protect steels from corrosion is observed, as in Figure 58.
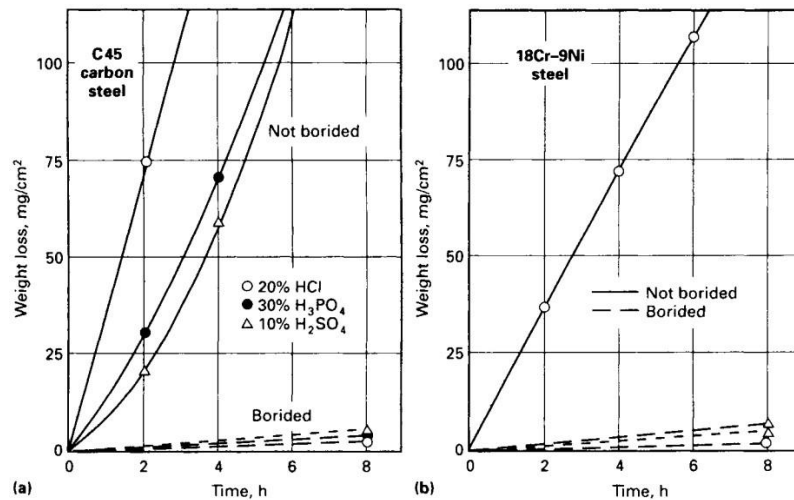
Figure 58. *Corrosive wear of borided and non-borided steels in diluted acids at 55 °C*

for (a) C45 Carbon steel, and (b) CrNi18·9 Austenitic stainless steel [6].

Furthermore, the corrosion resistance of AISI 1020 powder-pack borided steels for 8h at 900 °C, exposed to immersion corrosion testing with naphthenic acids in both liquid and vapor phases at a temperature of 250 °C, showed a substantial increase in corrosion resistance. Naphthenic acids. The estimated weight losses of borided steels compared to non-borided ones were, respectively, 0.04 mg/cm^2 in liquid phase media and 2.4 mg/cm^2 in the vapor phase, vs 25 mg/cm^2 and 52.1 mg/cm^2 [7].

L.   Recommendations

Building on the well-established wear resistance of iron borides, their combination with other titanium or vanadium phases through combined treatments has the potential to create protective layers with substantially more excellent wear resistance and toughness.

However, when it comes to boriding alone, the best practice is to ensure the formation of a single-phase layer, Fe$_2$B in the case of ferrous materials, or at least a bi-phase layer with minor contents of the brittle boron-rich phase, FeB in ferrous materials. That is because thin boride layers have been proven to be very effective in improving the wear and service life of a wide variety of components. Conversely, attempting to produce thicker boride layers can be unnecessary due to the actual possibility of worsening its mechanical and chemical performances because of the inevitable formation of the boron-rich phase. Promoting, as aforementioned, porosities and crack formation, which ultimately lead to flaking and spalling of the layer [12,115].

Eventually, it is recommended that the boride layer thickness should be matched with the base material and the intended application. Layers around and over 150 μm can be formed on steels, but they should be avoided due to their friable nature, except for very light contact loading situations [14]. Thin layers are ideal for applications where preventing initial adhesion and deformation is crucial, such as chipless shaping tools and metal stamping dies. Whereas thick layers are preferred for scenarios with high abrasive wear, where a larger wear volume is necessary for extended service life, such as for extrusion tooling or pressing tools in the ceramic industry [7].

III.4. BORIDED MATERIALS

Borided materials are substances that can readily undergo boriding processes, exhibiting characteristics that allow effective boron diffusion into their surface, resulting in the formation of a protective and durable boride layer that enhances the properties of that surface. Borided materials encompass a wide range of pure or alloyed materials, ranging from metallic, nonmetallic, or metalloid. Figure 59 distinguishes the most common ones and Table 11 provides different boride layer compositions formed on certain of those materials, along with their resulting microhardness.
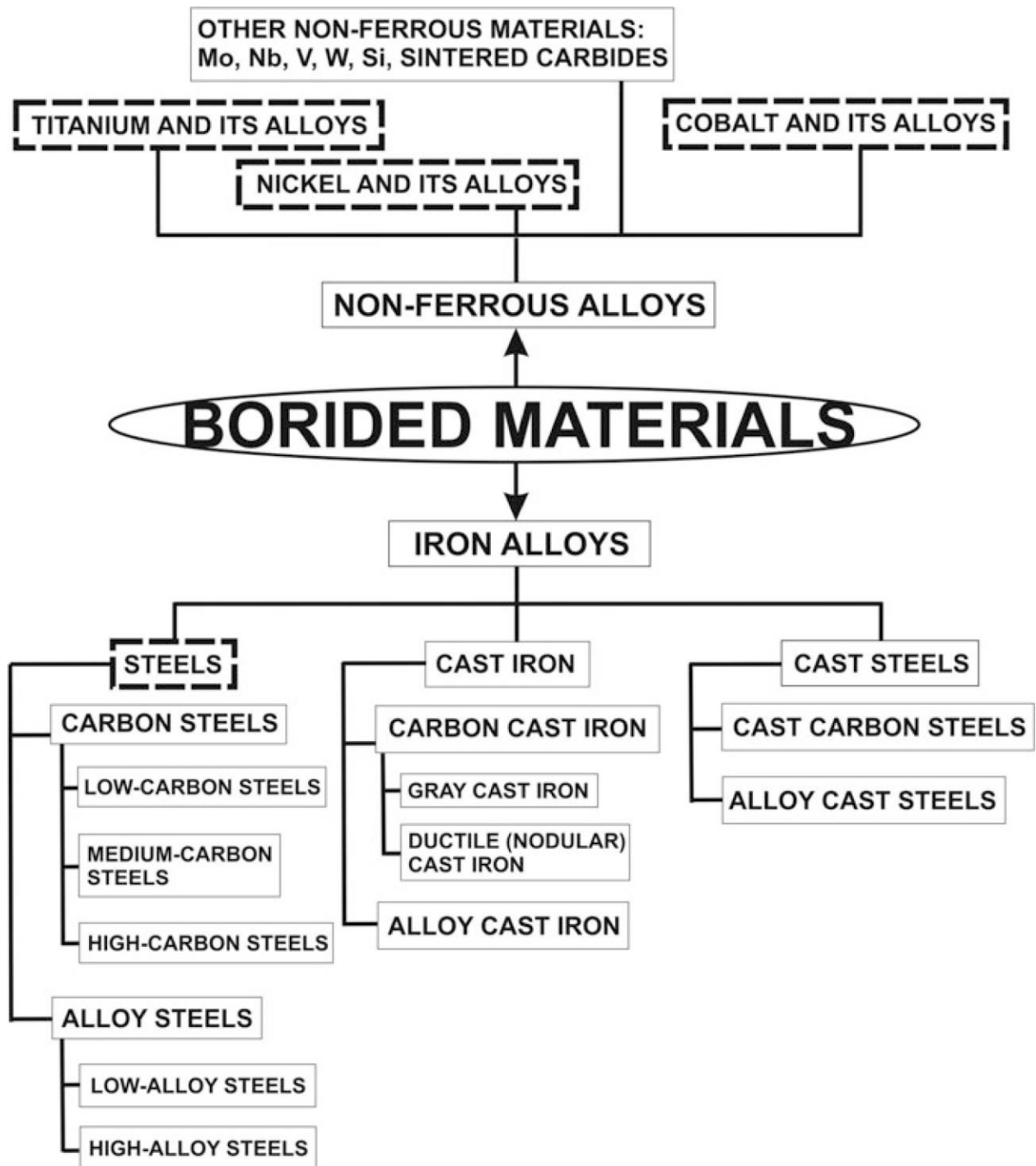
***Figure 59.** Materials that can readily undergo boriding* [10].

Table 11. Composition and microhardness of various boride layers [14].

Substrate	Boride layer Composition	Microhardness of layer [kg mm^2]	Substrate	Boride layer Composition	Microhardness of layer [kg mm^2]
Fe	FeB Fe$_2$B	1900 - 2100 1800 - 2000	**Zr**	Zr$_2$B ZrB$_2$	2300 - 2600 (o)
Co	CoB Co$_2$B	1850 ~ 1550	**Ti**	TiB$_2$ TiB	2500 (o)(g)
Co27·5Cr	CoB Co$_2$B	2200 (g) ~ 1550 (g)	**Ti6Al4V**	TiB$_2$ TiB	3000 (o)(g)
Nb	Nb$_2$B$_4$ NbB$_4$	2600 - 3000 (o)	**Mo**	Mo$_2$B Mo$_2$B$_5$	2400 - 2700 (o)
Ni	Ni$_4$B$_3$ Ni$_2$B Ni$_3$B	1600 1500 900	**W**	(W$_2$B)$_2$ WB$_2$ W$_2$B	~ 2700 (o)
Ta	Ta$_2$B	3200 - 3500	**Re**	ReB	2700 - 2900
(o) overall hardness			(g) 100g load		

Parts focused only on high surface hardness, such as low alloy steels, are more suitable for boriding instead of the more expensive high alloy ones that tend to hinder boron diffusion, which can be convenient cost-wise [14]. Other than steels, nickel Ni and cobalt Co, along with hard metals that contain them, are generally suitable for boriding [13].

As distinguished, materials that can readily undergo boriding seem to be preferably not alloyed for better boron diffusion. The most frequent ones will be listed underneath, with a focus on ferrous materials due to their relevance with the last chapters of the thesis. The other borided materials along with the ones that are not compatible to the process will be briefly mentioned.

III.4.1. Ferrous materials

When it comes to boriding, ferrous materials are the most beneficial of such a process. They can be classified by their microstructure and heat treatment response or by their commercial name and application, Figure 60 [7].

The first classification is based on the phases found in the ferrous materials, generally recognized in the iron-carbon phase diagram, Figure 61. Each phase has different characteristics, which will be elaborated along with their potential regarding boriding. In the end, a summary is given in Table 12. The information provided regarding these phases can be considered accurate in general, but need further investigations with specific studies regarding the boriding part.
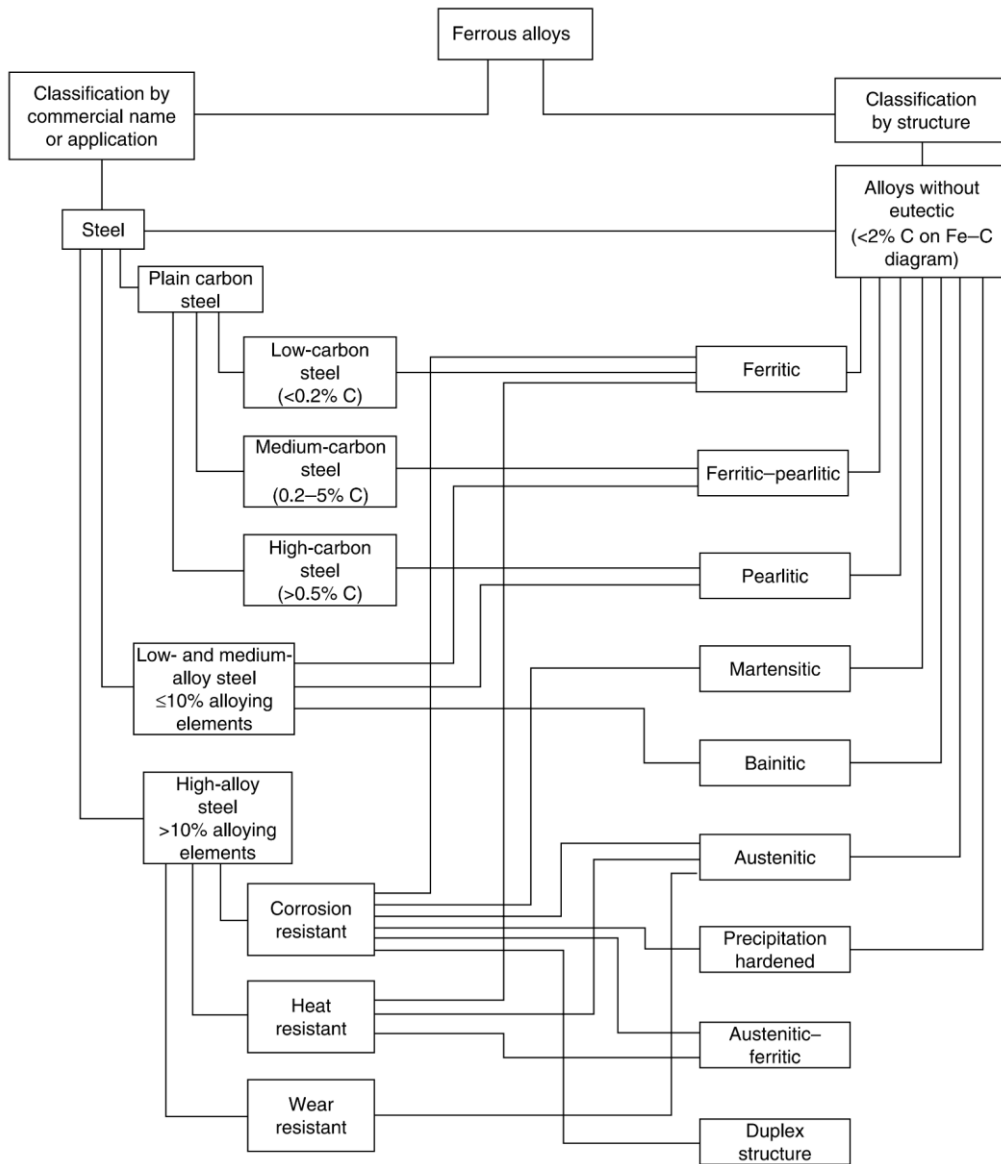
Figure 60. *Classification of ferrous alloy steels* [66].
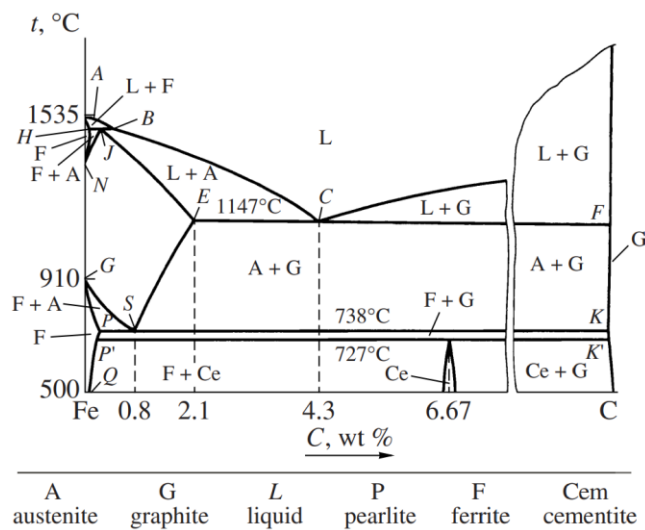
Figure 61. *Iron-Carbon phase diagram* [119].

- **Ferrite**

It is the stable phase of ferrous materials. While different ferrites exist, the most dominant one is α-Fe with a body-centered cubic bcc structure. Ferrite has good corrosion resistance and is the softest and most ductile phase in steel, with a relatively low carbon content. Due to its low carbon content and bcc structure, heat treatments for hardening are generally ineffective, making ferrite nonhardenable. However, some ferritic steels can benefit from boriding if carefully processed due to their soft nature. Factors such as grain size and alloying elements significantly influence boriding.

- **Cementite**

Or iron carbide Fe_3C, has an orthorhombic crystal structure. It is a stable phase in ferrous materials and is hard, strong, and brittle, typically found in high-carbon steels. The presence of alloying elements can alter its chemical composition. Cementite can act as a barrier to boron diffusion during boriding due to the presence of carbon. Boriding steels with high cementite content can further decrease the material's overall toughness.

- **Austenite**

Or γ-Fe, has a face-centered cubic fcc structure with carbon dissolved as a solute, unlike cementite, where carbon is present within the structure. It is malleable with excellent toughness and corrosion resistance. Austenite is a high-temperature phase that serves as a starting point for most steel heat treatments. While not typically present at room temperature in most steels, some alloy steels can retain austenite at room temperature. The presence of carbon only as a solute can may be advantageous for boriding austenite. Boriding can improve austenite's wear resistance and hardness. However, austenite's ductile nature requires careful processing.

- **Pearlite**

Forms during the slow cooling of austenite. It is a metastable lamellar aggregate composed of alternating layers of soft, ductile ferrite and hard, brittle cementite. This structure offers a balance of strength and ductility. The cementite within pearlite can hinder boron diffusion, similar to standalone cementite, but the impact is less severe compared to steels with high cementite content.

- **Bainite**

Similar to pearlite, it is a metastable aggregate but with an acicular microstructure consisting of dispersed carbide particles in soft ferrite. It is formed during intermediate cooling of austenite at temperatures lower than those required for pearlite formation. Bainite offers a good combination of hardness, strength, toughness, and weldability, better than pearlite but less than martensite. The effectiveness of boriding bainite varies depending on the content of carbide particles, which may hinder boron diffusion, though it can be more effective than in pearlite.

- **Martensite**

It is also a metastable phase formed by rapidly cooling austenite by quenching, preventing the transformation to equilibrium phases such as ferrite and cementite found in pearlite or bainite. This rapid cooling traps carbon atoms within the distorted face-centered cubic fcc structure of the parent austenite γ-Fe, resulting in a body-centered tetragonal bct structure that is very hard and brittle. Even with its high hardness, boriding can improve martensite's hardness and wear resistance without significantly decreasing its toughness if carefully processed. Tempering allows some of the trapped carbon atoms to diffuse outward, reducing internal stresses within the martensite structure, resulting in a better balance of properties and potentially improved boriding.

- **Graphite**

Found in cast irons and not steels. It consists of pure carbon in the form of flakes or nodules, depending on the cooling rate and the presence of other elements. The presence of graphite weakens the ferrous matrix but significantly improves machinability. Boriding is not typically applicable to cast irons due to their high carbon content, which can hinder the formation of a uniform boride layer.

Table 12. Metallurgical phases of ferrous materials, their characteristics, and boriding potential.

Phase	Crystal Structure	Characteristics	Boriding
Ferrite α**-Fe**	Body-centered cubic bcc	Stable phase, good corrosion resistance, soft and ductile, low carbon content.	High boriding potential but influenced by grain size and alloying elements. Improves hardness and reduces ductility.
Cementite Fe_3C	Orthorhombic	Hard, strong, and brittle phase, typically found in high-carbon steels.	Low boriding potential because high carbon content hinders boron diffusion. Reduces overall toughness.
Austenite γ**-Fe**	Face centered cubic fcc with carbon as a solute	A high-temperature phase that is malleable and tough with good corrosion resistance.	Moderate to high boriding potential. Improves wear resistance and hardness. Careful processing due to ductile nature.
Pearlite	Lamellar, layered as Cementite and ferrite	Metastable, a balance of strength and ductility. Moderate hardness.	Moderate boriding potential because of cementite.
Bainite	Acicular, precipitates of carbides in ferrite	Metastable, good hardness, strength, toughness, and weldability.	Moderate to high boriding potential, varies with carbide particle content, can be better than pearlite.
Martensite	Body-centered tetragonal bct of iron trapping carbon	Metastable, very hard and brittle Good wear resistance.	Good boriding potential, improves wear resistance without significant toughness reduction, especially if tempered.
Graphite	Hexagonal of carbon as flakes or nodules	Found in cast irons, not steels Brittle, good machinability.	Poor boriding potential due to high carbon content. Ununiform boride layer formation.

The second classification of ferrous materials is based on iron as the base material with varied additional alloying contents, from nearly null to high, differentiating and ranging them as carbon steels, cast irons, or alloy steels, including specialized machinable materials. Table 13 lists practical applications of ferrous materials that have been borided.

Table 13. Borided steels applications [6,13].

Substrate material		Application
AISI	**DIN**	
	St37	Bushes, bolts, nozzles, conveyer tubes, base plates, runners, blades, thread guides.
1020	**C15 (Ck15)**	Gear drives, pump shafts.
1043	**C45**	Pins, guide rings, grinding disks, bolts.
	St50-1	Casting inserts, nozzles, handles.
1138	**45S20**	Shaft protection sleeves, mandrels.
1042	**Ck45**	Swirl elements, nozzles (for oil burners), rollers, bolts, gate plates.
	C45W3	Gate plates.
W1	**C60W3**	Clamping chucks, guide bars.
D3	**X210Cr12**	Bushes, press tools, plates, mandrels, punches, dies.
C2	**115CrV3**	Drawing dies, ejectors, guides, insert pins.
	40CrMnMo7	Gate plates, bending dies.
H11	**X38CrMoV51**	Plungers, injection cylinders, sprue.
H13	**X40CrMoV51**	Orifices, ingot molds, upper and lower dies and matrices for hot forming, disk.
H10	**X32CrMoV33**	Injection molding dies, fillers, upper and lower dies and matrices for hot forming.
D2	**X155CrVMo121**	Threaded rollers, shaping and pressing rollers, pressing dies and matrices.
	105WCr6	Engraving rollers.
D6	**X210CrW12**	Straightening rollers.
S1	**60WCrV7**	Press and drawing matrices, mandrels, liners, dies, necking rings.
D2	**X165CrVMo12**	Drawing dies, rollers for cold mills.
L6	**56NiCrMo12**	Extrusion dies, bolts, casting inserts, forging dies, drop forges
	X45NiCrMo4	Embossing dies, pressure pad and dies.
O2	**90MnCrV8**	Molds, bending dies, press tools, engraving rollers, bushes, drawing dies, guide bars, disks, piercing punches.
E52100	**100Cr6**	Balls, rollers, guide bars, guides.
	Ni36	Parts for nonferrous metal casting equipment.
	X50CrMnNiV229	Parts for unmagnetizable tools (heat treatable).
4140	**42CrMo4**	Press tools and dies, extruder screws, rollers, extruder barrels, non-return valves.
4150	**50CrMo4**	Nozzle base plates.
4317	**17CrNiMo6**	Bevel gears, screw and wheel gears, shafts, chain components.
5115	**16MnCr5**	Helical gear wheels, guide bars, guiding columns.
6152	**50CrV4**	Thrust plates, clamping devices, valve springs, spring contacts.
302	**X12CrNi188**	Screw cases, bushes.
316	**X5CrNiMo1810**	Perforated or slotted hole screens, parts for the textile and rubber industries.
	G-X10CrNiMo189	Valve plugs, parts for the textile and chemical industries.
410	**X10Cr13**	Valve components, fittings.
420	**X40Cr13**	Valve components, plunger rods, fittings, guides, parts for chemical plants.
	X35CrMo17	Shafts, spindles, valves.

A.   Pure iron

The purest ferrous material is pure iron Fe. It can be found as Armco iron, which was first industrialized by the American Rolling Mill Company in 1909. With all natural impurities largely removed and a near absence of alloying elements, the bulk is rendered to over 99 wt.% of purity [7]. Pure iron can benefit greatly from boriding, especially if the boriding is done effectively forming a single phase Fe_2B boride layer. Its hardness can increase from 100 to 150 to more than 1000, 1500 HV, or higher, depending on the boriding technique and treatment conditions.

In a particular case study, borided 99.97 wt.% pure iron reaches a peak hardness of 1700 HV for a layer of about 40 to 45 μm formed with powder boriding for 8 hours at 800 °C. The powder mixture contained B_4C, KBF_4, and SiC, with dosages of 5, 5, and 90 %, industrialized as the Ekabor powder, which controls the boron diffusion flux [120]. Another study used powder mixtures similar to the previously given, but lowering SiC and adding different fractions of ZrB_2 accordingly, 0, 5, 10, 15, and 20 %, to boride pure iron for 4 hours at 800 °C. All mixtures provided a similar average thickness of 140 μm with a slight decrease of hardness with increasing ZrB_2 content due to hindering of boron diffusion into the surface, from 1890 to 1765 HV, approximately [82].

B.   Carbon Steels

Carbon steels are a category of steels that primarily consist of iron and carbon as the major elements. Small amounts of other elements like manganese, silicon, and copper, though these are limited by specific standards. These steels are known for their relatively simple composition and are widely used due to their versatility, cost-effectiveness, and range of mechanical properties, including strength, hardness, and ductility, Figure 62. The naming comes from their carbon content, from nearly 0 to about 2 wt.%, and within this range, three distinct categories are recognized, low, medium, and high carbon steels [121].
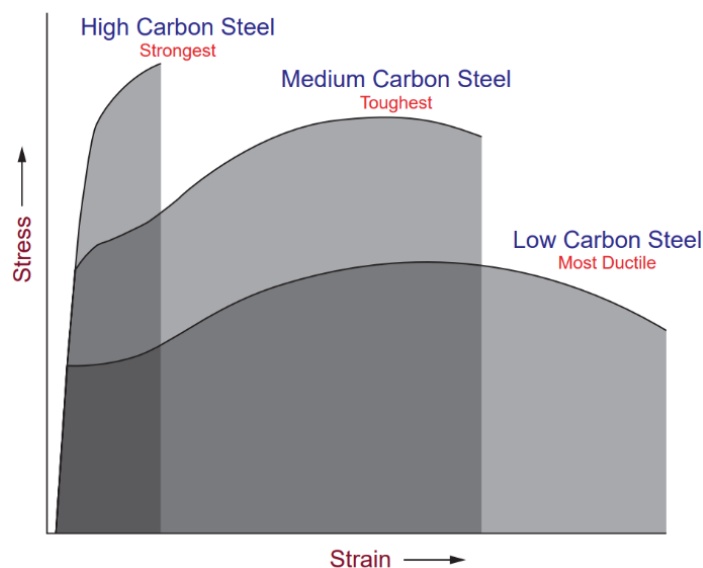
Figure 62. *Properties of carbon steels identified through stress-strain curves* [121].

Lower carbon content generally facilitates the diffusion of boron during the boriding process, Figure 63, and results in thicker boride layers for longer treatment exposures, Figure 65. This improved diffusion leads to a more effective treatment, enhancing the final properties of the steel. However, it is important to note that the specific effects can vary depending on the chosen boriding technique, including the media composition, Figure 52.
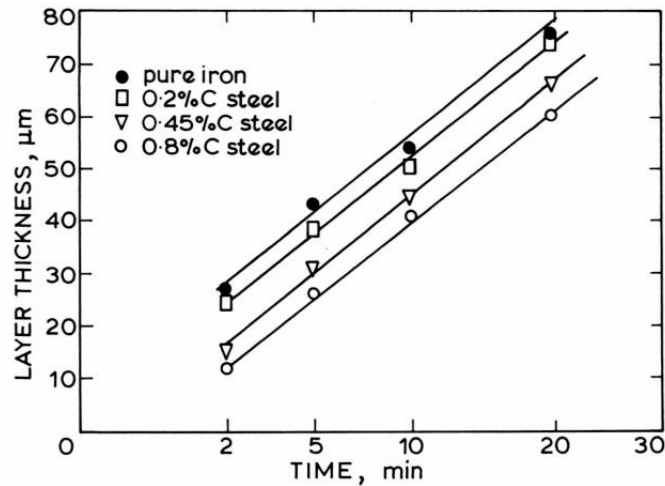
Figure 63. *Boride layer thickness growth over time with the same parameters*
for different carbon contents within iron [14].

- **Low carbon steels**

With carbon contents ranging from 0.05 to 0.25 wt.%, they are the most ductile of carbon steels, Figure 62 [121]. However, boriding decreases their ductility, especially if a bi-phase configuration with a thick FeB phase is formed within the layer, which increases the brittleness. Despite the decrease in ductility, boriding significantly increases the hardness of low-carbon steels, around 10 times or more, second to pure iron when it comes to the effectiveness of the boriding process, especially regarding the boride thickness formed, Figure 65.
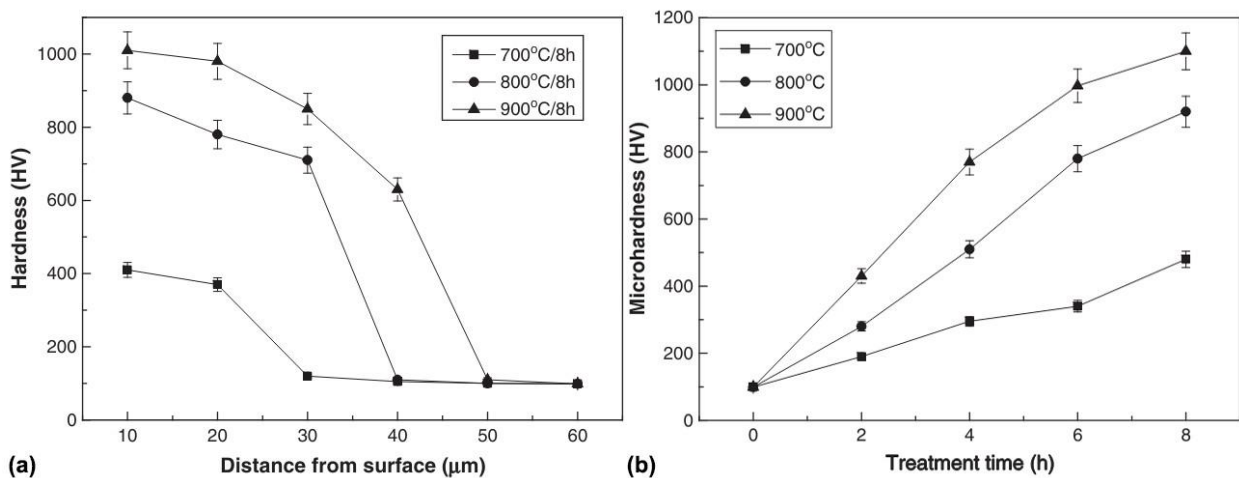
Figure 64. *Variations of the microhardness of borided low carbon steel (a) within the boride layer,*
and (b) for different boriding conditions [122].

In a specific case study, Figure 64, an increase from 99 to around 1100 HV was observed after the formation of a single phase Fe_2B boride layer of about 50 μm by surface alloying boriding for 8 hours at 900 °C [122]. Another study obtained an increase of hardness from 200 ±20 to 1700 ±200 HV, with a bi-phase boride layer thickness of about 250 ±25 μm for around 2 hours of electrochemical boriding [123].

- **Medium carbon steels**

With carbon contents ranging from more than 0.25 to around 0.5 wt.%, they offer a balance between strength and ductility, making them the toughest steels, Figure 62 [121]. They, too, can benefit from boriding, although depending on the increase in carbon content, they might require careful processing to avoid potential issues regarding the formation of a thick FeB phase within the layer, which may result in excessive brittleness. If the same conditions are applied, the overall boride layer thickness formed on them is generally thinner than the one formed on low carbon or non-alloyed steels.

In a specific case study, which used combined carburizing followed by boriding, termed borocarburizing, a bi-phase boride layer was obtained with a thickness of 100 to 125 μm and a microhardness of 1450 to 1900 HV. The boride layer was formed on top of the initially carburized layer, which had a microhardness of 950 HV. The combined processing helped reduce the microhardness gradient to the substrate (350 HV), compared to applying only the boriding, resulting in a wear resistance that is higher than either boriding or carburizing solely [124].

- **High carbon steels**

With carbon contents ranging from 0.5 to 1.25 until around 2 wt.%, they are the strongest, the most hard and wear-resistant steels, Figure 62 [121]. Boriding can contribute to further hardening and improving their wear resistance. However, the lower boron diffusion growth results in thinner boride layers, Figure 63 and Figure 65, and with the increase of carbon, the potential for forming the FeB phase boride layer increases, making them less prone to boriding.
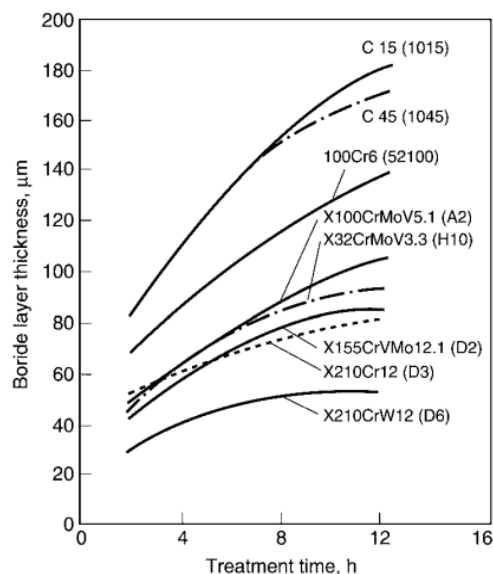
Figure 65. *Influence of the increased alloying elements on the overall boride layer thickness* [6].

Nevertheless, a specific case study compared the effect of boriding on C15 steel, a low carbon steel, C45, a medium carbon steel, and C70W2 a high carbon steel, with diverse treating conditions. A confirmed decrease of maximum boride layer thickness was observed, 240, 210, to 180 μm [125]. In a similar study having similar results, the hardness for the C15 and C70W2 steels was nearly identical, 1443-1645 HV, and 1488-1603 HV, indicating that the case of carbon steels, along with temperature and time conditions, do not affect significantly the final hardness [126]. However, considerable differences are to be investigated.

C.   Cast Irons

Cast irons have carbon contents ranging from around 2 to 6.67 wt.% within the substrate, higher than carbon steels, making them a different and distinct material class due to the formation of the graphite, found in the iron-carbon phase diagram, Figure 61. Other than carbon, they contain silicon as a second major alloying element. They are known for their relatively low melting points, excellent castability, good heat retention, and excellent wear resistance. Cast irons are widely used for their ability to be cast into intricate shapes and for their durability. Commonly used in automotive applications such as camshafts, cylinder and engine blocks, brake drums, and clutch plates for heavy-duty service [127].

Boriding is not generally considered for cast irons. Regardless, a specific case study borided different cast irons, ductile iron, gray iron, and compacted graphite iron, obtaining similar boride layer thicknesses of a bit over 120 μm with extreme hardness values of 2685 from an initial hardness of 347 and 289 HV for the ductile and compacted iron, respectively, and 2465 from 306 HV for the gray iron, Table 14 [128].

Table 14. Cast irons alloying elements and maximum hardness before and after boriding [128].

Material	Alloying elements [wt.%]	Hardness [HV]	
		Boride layer	Substrate
Ductile iron	3.49 C, 2.23 Si, 3.276 other	2685	347
Gray iron	3.22 C, 1.93 Si, 0.812 other	2465	306
Compacted graphite iron	3.80 C, 2.94 Si, 0.964 other	2685	289

D.   Alloy steels

Carbon steels are widely utilized in various industries due to their ease of fabrication, affordability, and range of mechanical properties. However, they may lack certain characteristics like high corrosion resistance or specialized mechanical properties required for specific applications. In such cases, alloying elements are added to modify the properties, Table 15, resulting in different types of alloy steels categorized based on the properties they confer and the alloying elements' content.

- **Low alloy steels,** with alloying content of under 5 wt.%, they tend to exhibit improved strength and toughness, weldability, machinability, and other properties while maintaining broad application usage.

- **Medium alloy steels,** with 5 to 10 wt.% of alloys, they offer a balance of properties but might have limitations in specific applications due to their tailored characteristics.

- **High alloy steels,** with more than 10 wt.% of alloying elements, they possess exceptional but extremely specific properties designed for intended applications, making them unsuitable for general use.

Table 15. *Effects of alloying elements on steel characteristics* [65].

Alloy		Effect on steel
Al	Aluminum	Deoxidizes in the steel-making process. Restricts grain growth and helps produce fine grain structure.
B	Boron	Increases hardenability in low-carbon steels. Reduces shock resistance in low temperature applications.
Ca	Calcium	Imparts better machinability. This non-metallic element from the earth is dirt and does not dissolve in the steel melt. It may form stringers, voids, and inclusions and has a poor effect on the strength and causes a loss of shock resistance.
C	Carbon	Added to iron, it forms steel. 0.06 to 0.25 % allows shallow case hardening. 0.25 to 0.60 % allows easier case hardening. 0.60 to 0.80 % increases hardenability. 0.80 to 2.1 % increases wear up to a point, not hardness.
Cr	Chromium	Forms chromium carbides when iron and carbon are present. Adds wear resistance and toughness and contributes to corrosion resistance.
Co	Cobalt	Forms cobalt carbide in a carbon matrix. Improves heat-resistance properties.
Pb	Lead	Adds machinability. Does not dissolve in metal, and globules of lead can leave voids on the surface of steel during heat treating. Is being used less because of environmental concerns. Should not be heat-treated or welded due to danger to health and pollution from escaping vapors.
Mn	Manganese	Increases deeper hardening abilities. Improves steel transformation phases.
Mo	Molybdenum	Forms molybdenum carbide when carbon is present in correct quantity. Adds heat resistance and hardenability. Improves corrosion and wear resistance. Minimizes temper embrittlement in alloy steels.
Ni	Nickel	Adds toughness, strength, and some wear. Reduces hardenability.
Nb	Niobium	Reduces grain growth and helps produce a finer grain structure. Prevents some creep at high operating temperatures. Reduces hardenability.
P	Phosphorous	Imparts better machinability. This nonmetallic element from the earth is dirt and does not dissolve in the steel melt. It may form stringers, voids, and inclusions and has a poor effect on the strength and causes a loss of shock resistance.
Si	Silicon	Adds strength and toughness but decreases machinability and surface finishes if above 1 %. Is used to deoxidize during steel making.
S	Sulfur	Imparts better machinability. This nonmetallic element from the earth is dirt and does not dissolve in the steel melt. It may form stringers, voids, and inclusions and has a poor effect on the strength and causes a loss of shock resistance.
Ti	Titanium	Forms titanium carbide but does not enhance hardenability. Deoxidizes and reduces grain growth. May increase temper embrittlement and lower shock resistance. Forms carbide but reduces hardness in stainless steels.
W	Tungsten	Adds wear resistance.
V	Vanadium	Forms vanadium carbide with carbon. It refines the steel into a finer grain structure and prevents excess grain growth. Improves hardenability of steel.
Zr	Zirconium	Great deoxidizer. Strong deterrent to grain growth.

The alloying of these types of steels does not come without drawbacks, the same analogy to carbon steels holds, which is, the lower the alloying, the better the boron diffusion, rendering boriding more suitable to low alloy steels rather than high alloy ones. That is appropriate since alloy steels are pricey and often already tailored to specific applications, which might not coincide with the enhancements offered by boriding [14].

For other steels, even if low alloyed, certain alloying elements such as aluminum Al or silicon Si make them unsuitable for boriding due to the resulting structure of the surface layer. These elements tend to settle below the Fe_2B boride layer in the diffusion zone, resulting in a softer ferrite, and with the greater gradient of hardness between the phases, an extremely hard boride phase anchored to a soft ferrite phase, when workpieces undergo strong mechanical loads, the hard phase is pressed into the soft one, and due to its brittle nature, cracks, and spalling occur, resulting in a destroyed layer [13]. Thus, even with the convenience of soft steels for boriding, careful processing is required, tailored to the specific application.

Carbon, silicon, and aluminum are insoluble in the FeB and Fe_2B iron borides during the boron diffusion. Thus, they are displaced underneath them, forming precipitates of iron silicoborides, $FeSi_{0.4}B_{0.6}$ or Fe_5SiB_2, and iron carboborides, $(Fe_{23}(B,C)_6$ or $Fe_3(B,C)$. Moreover, steels containing large quantities of silicon and aluminum are not suited to boriding because both elements can form a soft ferrite region underneath the hard boride layer, which can result in cracks during service. Most alloying elements, except nickel, cobalt, and manganese, Figure 50 and Figure 66, hinder boride layer growth, proportionally increasing the formation of the FeB phase within the layer [14], while also influencing the resulting hardness, Figure 51.
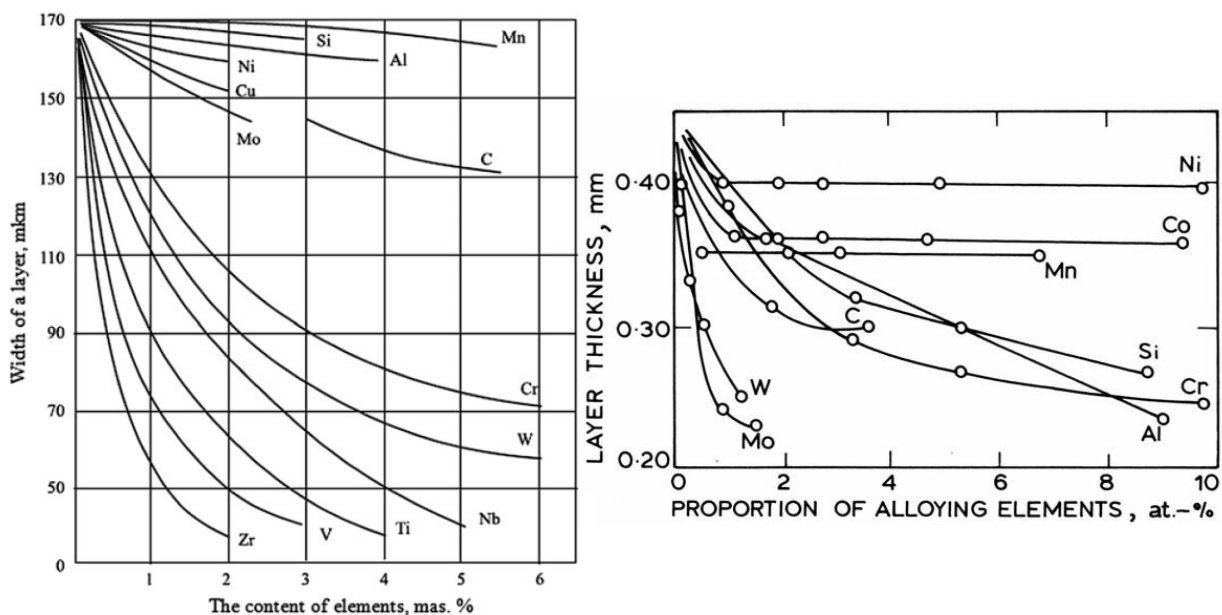
Figure 66. *Influence of the alloying elements on the boride layer thickness* [9,14].

Furthermore, the morphology of the boride layers depends fundamentally on the substrate's chemical composition. In low alloy steels, saw-toothed layers are observed, whereas in high alloyed ones, they tend to be flat [85]. Consequently, the saw-toothed morphology of the boride layer becomes less pronounced with respect to the increase of alloying elements, Figure 67 [14].
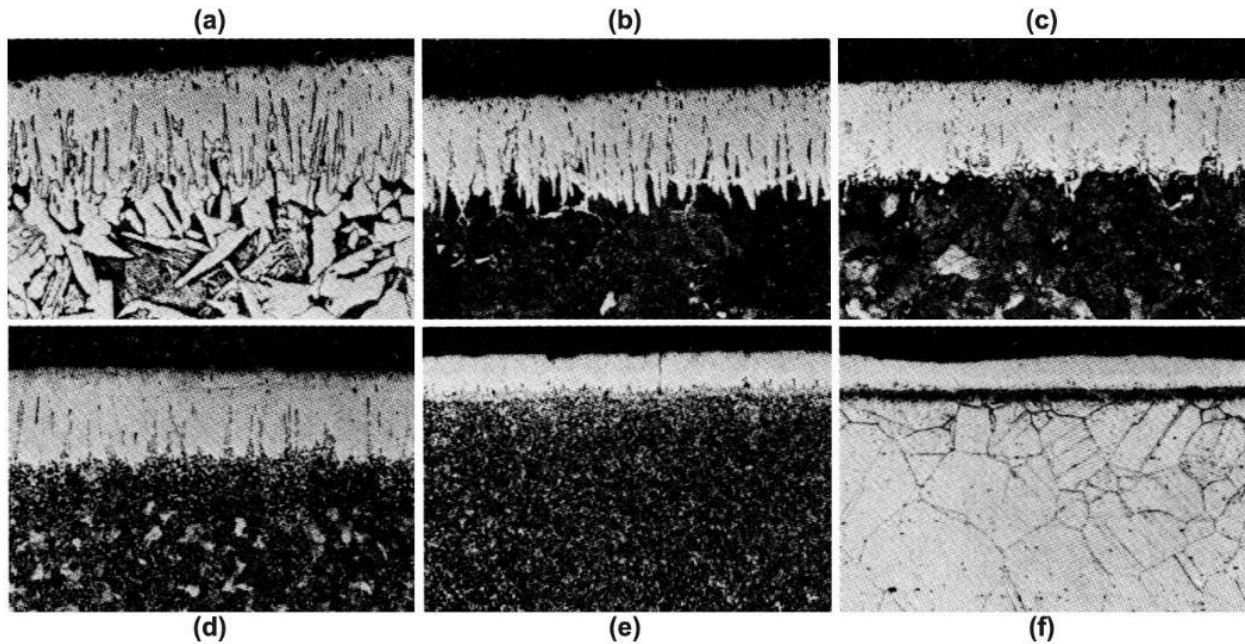
Figure 67. Powder pack boriding for 5 h at 900 °C of (a) C15, (b) C45, (c) C100, (d) 145Cr6, (e) X40Crl3, and (f) X5CrNi18.9 [14].

The boride layer thicknesses observed on low carbon and low alloy steels range from 50 to 250 μm and can be mono or bi-phased, whereas in high-alloy steels, it is significantly lower, from 25 to 76 μm, mostly bi-phased [7]. FeB formation should be avoided, but this is not achievable on high alloy steels such as stainless or high-speed steels. This makes high alloy steels less suited to boriding because the resulting boride layer can be thin and poorly adherent [14].

III.4.1.   Nonferrous materials

Although nonferrous materials can be refined or rarely found pure, in most practical cases, they are used with certain impurities or mostly alloyed. Nickel Ni and cobalt Co, along with any other hard metal containing these elements, are generally successfully borided [13]. So, both of them and Titanium, which is commonly borided, will be mentioned briefly, while others are highlighted in Figure 42 and Figure 59. Different boron concentrations within borides that may be found after boriding such materials are given in Table 11 and Table 16.

Table 16. *Boron concentrations of certain borides* [81].

Phase	wt.%B	Phase	wt.%B	Phase	wt.%B	Phase	wt.%B	Phase	wt.%B
$Pd_{16}B_3$	1.9	W_2B	2.9	Mn_4B	5	Ni_3B	6	YB_2	19.6
Pd_3B	3.4	WB	5.2-5.4	Mn_2B	9	Ni_2B	8.4	YB_4	32.7
Pd_5B_2	3.9	W_2B_5	11.1	MnB	16	Ni_4B_3	11.5-12.5	YB_6	42.2
Boron-Palladium		WB_4	21.1	Mn_3B_4	20.8	NiB	16	YB_{12}	59.3
Co_3B	7.8	**Boron-Tungsten**		MnB_2	28.3	NiB_2	26.9	YB_{66}	85.6
Co_2B	8.4	MoB	9-10.4	MnB_4	44	NiB_{12}	68.8	**Boron-Yttrium**	
CoB	15.5	MoB	16-18	**Boron-Manganese**		**Boron-Nickel**		B_2Nb	73-83
Boron-Cobalt		MoB_2	18.6-20			ScB_2	33	B_4NB_3	86.6
Fe_3B	6	MoB_4	30			ScB_{12}	73	B_6Nb_5	87.8
Fe_2B	8.8	**Boron-Molybdenum**				**Boron-Scandium**		BNb	90
FeB	16-16.2	V_3B_2	12			$B_{12}Zr$	40.9	B_2Nb_3	93
Boron-Iron		VB	18			B_2Zr	80-83.8	**Boron-Niobium**	
Re_3B	2	V_5B_6	20.3	Cr_4B	5	**Boron-Zirconium**		B_2Ta	85.5-91
Re_7B_3	2.4	V_3B_4	22	Cr_2B	9.4	SiB_3	52.7-58.4	B_4Ta_3	92.4-92.9
ReB_2	10-17	V_2B_3	24	Cr_5B_3	11.1	SiB_6	69.8	BTa	94-95
Boron-Rhenium		VB_2	30	CrB	17.2	SiB_n	84.3-93	B_2Ta_3	96.0-96.3
$Ru7B3$	4-6	**Boron-Vanadium**		Cr_3B_4	21.7	**Boron-Silicon**		BTa_2	97.4-97.7
RuB	9-11	TiB	18-18.4	CrB_2	29.4			**Boron-Tantalum**	
Ru_2B_3	14	Ti_3B_4	22.4	CrB_4	45	B_2Pt_3	96	BPt_3	98
RuB_2	17.6	TiB_2	30.1-31.1	CrB_6	55.5	BPt_2	97.3	**Boron-Platinum**	
Boron-Ruthenium		**Boron-Titanium**		**Boron-Chromium**					

A.   Titanium Alloys

Commercially pure titanium cp-Ti offers a remarkable combination of strength, low density, exceptional corrosion resistance, and biocompatibility. These properties can be further enhanced by alloying titanium with various elements to achieve specific performance characteristics. For instance, Ti_6Al_4V is a well-regarded alloy that offers superior strength compared to the pure one.

Boriding titanium generally results in the formation of a dual-phase boride layer containing a continuous hexagonal TiB_2, followed by whiskers of orthorhombic TiB anchored to the substrate, Figure 42 and Figure 43, with hardnesses exceeding 2000 HV, reaching 2867.6 HV [90,129], and 3000 HV for the alloy Ti_6Al_4V, Table 11 [14]. In a specific study, the hardness was observed to increase with boriding time regarding the alloyed one, from 281 ±4 to 1176 ±13 and 1953 ±11 HV after 1 and 3 hours [130].

B.   Nickel Alloys

Whether in pure form or as an alloy, nickel has excellent corrosion resistance, high strength, and good ductility. However, its wear resistance is inferior, making surface hardening treatments beneficial.

The boride layers, produced on pure Ni, were usually composed of only the tetragonal Ni_2B phase and can also be thick. However, some boriding techniques that contain silicon carbide SiC within the media may initiate siliconization, also referred to as silicidation or siliconizing [131], which hinders

boron diffusion, resulting only in the formation of thin layers [132]. As for the nickel alloys, in addition to the tetragonal Ni_2B phase, other phases can be found, such as orthorhombic Ni_3B, orthorhombic Ni_4B_3, and orthorhombic NiB phases, each with varying hardnesses, Table 11.

The boriding's effectiveness on nickel alloys differs with their compositions, and this is because other significant borides are susceptible to form besides the nickel borides. In a specific case study, $Ni_{20}AlB_{14}$ was formed with a hardness of 1100-1250 HV besides the nickel borides that had 850-1000 HV, after boriding nickel aluminide $NiAl_3$, which was about 200 HV [133].

C.   Cobalt Alloys

Cobalt and its alloys excel with superior fatigue strength, abrasion, and corrosion resistance. Regardless, cobalt behaves to being borided just like how nickel does, based on their specific composition, affecting the borides formed in the surface layer. Boride layers formed on cobalt generally consist of an orthorhombic CoB and a tetragonal Co_2B phase, with boron concentrations nearing those of iron borides Table 16.

A particular case study compared the boriding of cobalt and nickel, both alloyed with 7 wt.% of magnesium, CM and NM, having a hardness of 194 and 118 HV, respectively. The process media used contained mixtures of pure Co, Ni, and Mg metal powders. As a result, the thicknesses of the boride layers on the CM alloys were 48-145 μm with Co_2B as the dominant phase, and 67-180 μm for the NM alloys with NiB as the dominant phase. Each having varied hardnesses, 1752-1865 and 1634-1768 HV, respectively, Figure 68.
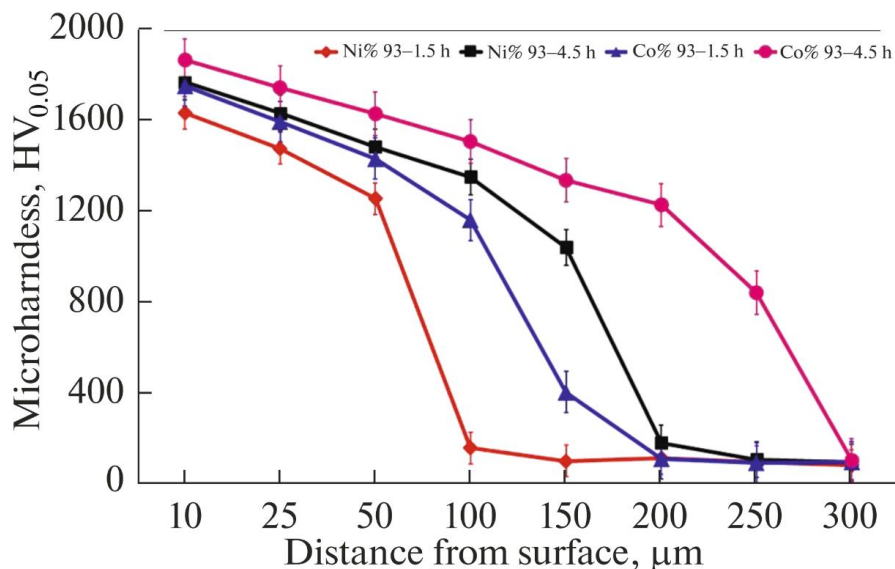
Figure 68. *Hardness profiles of boride layers formed on nickel and cobalt,*
alloyed with magnesium [134].

III.4.2. Unborided materials

Conversely, to the borided materials, there are materials that are difficult to boride or that hardly benefit from boriding. They are materials that exhibit characteristics that go against the boriding process.

A.   Aluminum and Copper

Aluminum Al tends to form stable aluminum oxide layers at relatively moderate temperatures, hindering boron diffusion and preventing the formation of a thick and effective boride layer, making boriding unnecessary. Copper Cu, on the other hand, cannot be borided but is instead used as a masking agent [13].

B.   Silicon

Silicon Si is unsuited for boriding because it forms stable silicide compounds at low temperatures, a premature compound formation impeding traditional boriding's controlled boron diffusion. Yet, silicon is used in numerous media, but as an alloy, silicon carbide SiC.

C.   Noble Metals

Precious metals, including gold Au, silver Ag, and platinum Pt, possess high chemical stability and limited reactivity with boron, making boriding an uncommon practice. Table 16 demonstrates that the concentration of boron within platinum borides is extremely high, suggesting their complex formation.

D.   Nonmetals

Materials like ceramics, glasses, and polymers are fundamentally different from metallic materials in terms of structure and properties. During boriding, boron shares electrons with the metal atoms, creating a strong metallic bond, while nonmetals tend to form covalent bonds, which have lesser strength and stability.

Additionally, metals have a regular arrangement of atoms in their crystal structure facilitating interstitial diffusion, as explained in the previous chapter. Conversely, nonmetals often have more complex or irregular structures making it difficult for boron atoms to diffuse and form a uniform layer.

III.5.   SUMMARY

Surrounding the boriding process, different procedures practiced regarding the preparation and characterization of the samples that undergo the boriding were described. Prior to boriding, samples are machined or cut into small pieces from a larger bulk material, then ground and cleaned to minimize the surface from contaminants. Then, after boriding, the samples are sectioned and cleaned for characterization. However, that must be done carefully because the sectioning must be devoid of potential damage to the resulting boride layer. Furthermore, the cleaning is different from the one used prior to the treatment, it consists of gently removing contaminants that might interfere with the cross-section analysis.

Table 8 summarized the most common techniques for analyzing boride layers, were presented and summarized in. including microscopy, spectroscopy, and crystallography. These techniques provide complementary information about the layer's morphology, elemental composition, and microstructure.

Accordingly, boride layers were observed to be mainly affected by two critical parameters, the treatment time and the temperature exposure, with the temperature having a greater impact. The boride layer progresses from the surface towards the core with different phases, from an outer brittle boron-rich phase to a less brittle and more tough phase with less boron content, anchored to the substrate. Its morphology is mostly in the form of needles or saw tooths if the alloying elements within the substrate are low and tend to flatten with their increase [14,85].

Significant differences in properties, such as thermal expansion and hardness, can lead to substantial gradient differences between the outer phase and the substrate's phase and may subsequently promote the formation of cracks parallel to the surface at the interface of the phases, potentially leading to spalling of the outer phase. These cracks can form either during cooling or under subsequent mechanical strains [12,76]. Annealing can be used to prevent this by diminishing the brittle, boron-rich outer phase and improving overall toughness [116]. Alternatively, combined diffusions approach the problem differently. Borocarburizing, for example, creates a carburized layer beneath the boride layer, reducing residual stresses and the likelihood of crack formation [68,72]. Additionally, multi-component layers exhibit excellent wear resistance, surpassing individual boride layers, especially on ferrous alloys [6,117].

Regarding ferrous materials, the best practice is to ensure the formation of a thin layer constituted from a single and less brittle phase, Fe_2B, avoiding the brittle and boron-rich outer phase, FeB. Attempting to produce thicker boride layers can be counterproductive due to the inevitable formation of the friable FeB phase [12,115]. However, while thin layers are ideal for adhesive applications, thick layers are preferred for scenarios with high abrasive wear [7]. The maximum achievable thickness before FeB formation depends on the steel type where: Carbon steels, up to 0.1 to 0.15 mm. Low to medium alloy steels, about 0.10 mm. Medium to high alloyed ones, like tool steels, to just 0.05 mm. And high alloys, like stainless steel, are tough to boride without FeB. Consequently, the higher the alloying, the more the boron diffusion is hindered, blocking boron near the surface and promoting FeB formation, making the material prone to spalling problems after boriding. Thus, only very shallow boride layers are recommended on highly alloyed materials. That is what makes low carbon and low alloy steels, the most beneficial material classes from boriding, and the convenience of their lower cost comes with it [12,14].

Besides that, boriding generally favors low alloy materials, be they ferrous or nonferrous. While it applies to nonferrous materials such as nickel Ni and cobalt Co and other hard metals like titanium Ti [13], it encounters varied difficulties and limitations when it comes to other ones. For example, its difficulty to be carried on aluminum due to conflicts of brittleness and softness, unsuitability with copper and silicon due to their premature melting points, or the incompatibility of boron with noble metals, and the formation of weak bonds when paired with most non-metals.

BLANK PAGE

CHAPTER IV

MODELS AND SIMULATIONS

Following the investigation of the boride layers and the machinable materials that permit diffusion, this fourth chapter delves into the realm of modeling and simulating the boriding process. It explores the laws governing diffusion mechanisms, allowing the analysis of the process, including the boride layer growth kinetics.

IV.1. OVERVIEW

The success of surface hardening processes, such as boriding, in achieving desired properties like hardness and wear resistance depends critically on the characteristics of the layer formed on top of the substrate, including it being thin or thick. Investigating the kinetics of such a layer by trying to model and simulate its growth is of paramount importance to adequately specifying and predicting its final form according to the demanded application. Based on practical investigations, as stated in previous chapters, thin and thick layers exhibit distinct wear resistance properties, with the former excelling against adhesive wear and the latter against abrasive wear [7].

Modeling, in its simplest form, is the art of creating a simplified version of something real, then trying to approach it to reality as accurately as possible. Within the realm of boriding, it can be as creating a set of equations or other computations simulating and describing how a boride layer forms with respect to time, optimizing boriding processes.

This chapter delves into understanding fundamentals and theoretical concepts underlying boriding, such as the diffusion coefficient [115], then jumps to presenting the theories behind different modeling types and approaches while comparing their functionalities.

While experiments are the cornerstone of scientific discovery, models and simulations offer distinct advantages that can complement them. Experiments can be expensive and time-consuming, while simulations executed on computers significantly reduce their repeatability by allowing for rapid exploration of different scenarios without the need for physical resources. This allows to easily manipulate variables and observe their effects. This enables a more systematic exploration of cause-and-effect relationships within a system, leading to a deeper understanding of its underlying mechanisms.

IV.2. THEORETICAL BACKGROUND

The incorporation of boron atoms into the surface is a critical process for enhancing properties like wear resistance and hardness. To effectively control these properties, it is essential to understand how boron diffuses within the material. This section explores the theoretical foundations of critical aspects regarding modeling the diffusion processes by bringing concepts like point defects, solid-state diffusion, and Fick's Laws, establishing a framework for simulating and predicting boron migration. Understanding this knowledge aids optimize boriding processes and achieving desired surface characteristics for various applications.

A.   Point defects

Solid materials are typically crystalline, with atoms arranged in a regular, ordered structure. Perfect diffusion, where atoms simply swap positions, is improbable at room temperature due to the energy required to break existing bonds. However, imperfections called point defects exist within these crystals. They can be vacancies as empty lattice sites or interstitials as extra atoms occupying positions between regular lattice sites. Increased temperatures intensify atom vibrations, disrupting the structure of crystals and increasing point defects [135]. Accordingly, in boriding, these point defects facilitate the diffusion of boron atoms into the substrate. While vacancy diffusion can occur at very high temperatures, interstitial diffusion is more dominant due to the small atomic radius of boron being 87 pm [136].

B.   Solid state diffusion

The primary driving force for diffusion is a concentration gradient where atoms move from areas of high concentration to areas of low concentration to achieve a more uniform distribution. Solid state diffusion refers to the movement of atoms within a solid material. This movement can occur over long distances or short distances depending on the temperature, time, and diffusion coefficient. The recognized mathematical modeling of such a diffusional flow is described by Fick's laws. Adolf Eugen Fick, 1829-1901, was a German physiologist [135].

C.   Fick's laws

a)   Fick's first law

The first law of Fick relates to the relationship between the concentration gradient and the diffusion by quantifying a diffusive flux that describes the flow rate of atoms across an area per time in a direction characterized as J. It includes the diffusivity or diffusion coefficient D, which is a material property, along with the boron concentration C in a given position x, expressed in equation (4).

$$J = -D \frac{\partial C}{\partial x} \tag{4}$$

The negative sign indicates that diffusion happens down the concentration gradient ($\partial C/\partial x$), with boron atoms moving from areas of high concentration to areas of low concentration.

b)   Fick's second law

The second law of Fick, equation (5), is a second order differential equation that describes how the concentration of boron changes over time due to diffusion, essentially stating that the rate of change in concentration at any point is proportional to the net diffusion flux into or out of that point.

$$\frac{\partial c}{\partial t} = D \frac{\partial^2 c}{\partial x^2} \tag{5}$$

In it, $(\partial C / \partial t)$ gives the rate of change of concentration with time, and $(\partial^2 C / \partial x^2)$ as the second derivative of concentration with respect to the position, describing the curvature of the concentration profile.

D.   Diffusion coefficient

The diffusion coefficient D, also known as diffusivity, is one of the most critical parameters in modeling boron diffusion. It represents the proportionality constant relating the number of elements diffusing across a unit area per unit of time to the concentration gradient driving the diffusion process. In simpler terms, it reflects the ease with which atoms can move within the material. The diffusion coefficient depends on quite a few factors [115]:

- **Temperature:** Diffusion rates increase significantly with temperature due to increased atomic mobility from thermal vibrations, essentially creating more point defects within the material, which facilitates diffusion.
- **Diffusing element:** Each element has a different inherent diffusivity within various materials.
- **Material microstructure:** The microstructure of the substrate material plays a role in facilitating diffusion paths for atoms.
- **Material composition:** The specific alloying elements present in the substrate material can also influence diffusion rates.
- **Material Interactions:** The binding energy between boron and the host material's atoms plays a role. Stronger bonds lead to lower diffusion rates.
- **Activation energy:** The diffusion techniques vary principally on the media, solid, liquid or gas, used to diffuse, influencing a certain activation energy used to differentiate between them.

E.   Activation energy

The activation energy Q reflects the energy required for an atom to overcome a barrier and move from one lattice site to another. It is found in equation (6), which is known as the Arrhenius law and gives the growth rate constant of a chemical reaction within a fixed temperature.

$$k = A \exp\left(-\frac{Q}{RT}\right) \tag{6}$$

The variables in it are the growth rate constant k, Arrhenius constant A, activation energy Q, universal gas constant R, and temperature T.

Alternatively, the diffusion coefficient is, in some cases, formulated as in equation (7), taking the form of the Arrhenius law, equation (6). Either it or the growth rate constant are used after being estimated from experiments, to model the kinetics of boride layer thicknesses.

$$D = D_0 \exp\left(-\frac{Q}{RT}\right) \tag{7}$$

Nonetheless, by modeling and investigating the activation energies, it is possible to understand how sensitive the diffusion is to temperature changes. Still, the activation energy is not affected by such a variant but rather by the substrate's material and the diffusion technique.

IV.3.   MODELING APPROACHES

Various modeling approaches are feasible within the realm of boriding, from studying the kinetics of boride layers to exploring their properties. An example of the latter is modeling the wear behavior of a borided material [137]. However, this section explores modeling approaches for understanding boron diffusion kinetics particularly, specifically concerning the boride layer thickness formation, Figure 69. That is because it is a crucial parameter that underpins the desirable properties of borided materials, including resistance to wear, hardness, and fatigue strength, as highlighted in the former chapter.
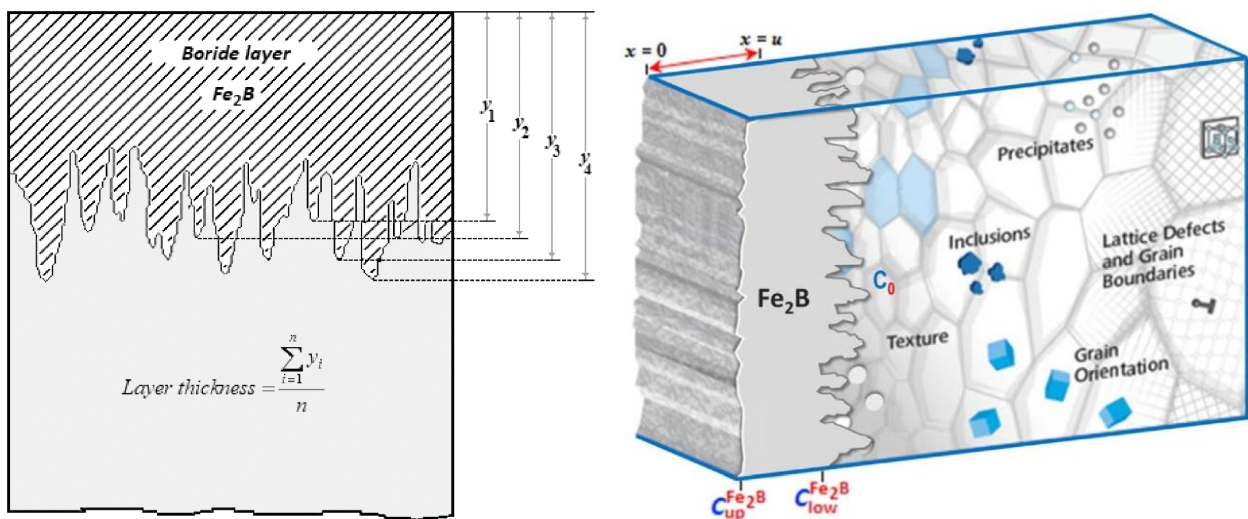
Figure 69. *Boride layer thickness configuration and measurement* [136].

A model is a simplified representation of a system or process. In the context of boron diffusion, a model translates the physical and chemical processes governing the kinetics into a set of mathematical equations or computational simulations. Simulations leverage the power of computers to numerically solve the governing equations and represent the diffusion process virtually. This allows the analysis of complex scenarios and the prediction of boron behavior under a broader range of conditions, providing valuable insights for engineering applications and reducing experimental testing costs.

Specifically, the development of an expression that allows for the estimation, prediction, or determination of the boride layer thickness resulting from a specific boriding process enables the precise selection of technological parameters, thereby guaranteeing the achievement of the desired properties for a particular application [138].

One limitation of current modeling approaches in boron diffusion kinetics is that they may not directly account for certain real-world complexities of boriding processes, such as the influence of surface morphology or interactions with specific alloying elements. Unless these complexities are explicitly considered through reverse engineering, where they are obtained from experiments and used to inform the models, i.e. introduced as independent variables.

IV.4.   MODELS TYPES

Modeling encompasses various types of models, offering a spectrum of complexity and accuracy within their simulations for understanding diffusion phenomena. Focusing on studying the boride layer kinetics, two distinct modeling approaches can be envisaged:

A.   Deterministic Models

These models operate on the assumption of a cause-and-effect relationship. Given a specific set of initial conditions like temperature, concentration, and such, a deterministic model will always simulate the same outcome. Common examples in boron diffusion modeling include models that are based on Fick's Laws, and other regression-based models which may be either linear or nonlinear.

B.   Non-Deterministic Models

Non-deterministic models, unlike deterministic models, can be implemented through computational simulations. These models acknowledge the inherent variability within the system. They may produce different outcomes for identical given information, reflecting probabilistic outcomes. Artificial neural network approaches are examples of non-deterministic models used for boron diffusion analysis.

IV.5.   MODELS EXAMPLES

Different model examples can be unveiled from the literature, ranging from theoretical models focusing on multiple variables to describe boride layer kinetics, including multiple phases, to others that emphasize practicability and provide an engineering-based approach. For preservability, each model will be described according to the data of the paper cited in it, including the symbol usage.

IV.5.1. Artificial neural network models

Artificial neural networks ANNs are one of the most powerful tools used in various scientific and engineering fields, including boron diffusion applications. They are computational programs inspired by the structure and function of the human brain, specifically its foundational unit, the neuron, with its thousands of connections that form networks. The inspiration resulted in the idea of machine learning, where a similar structure is constructed, consisting of interconnected nodes that process information, Figure 70.
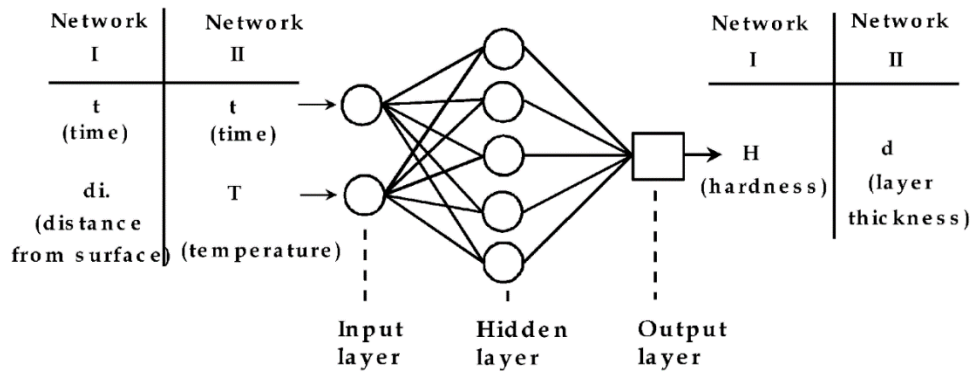
Figure 70. Two artificial neural network structures [139]*.*

Each received information is taken as input and is transferred to multiple nodes with transfer functions that have weights and biases, Figure 71 and Table 17. These weights and biases are like coefficients, which will be adjusted through training to try and predict final outcomes according to the provided data.
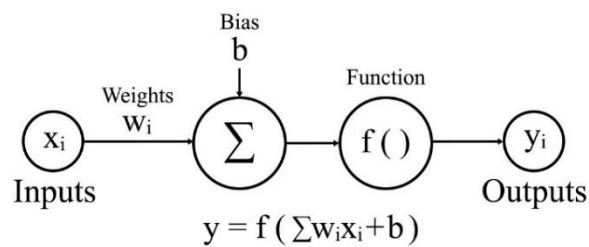
Figure 71. An artificial neuron.

There are several artificial neural network architectures distinguished with regard to the connections between the neurons of each layer and the network structure. Some of the widely used ones are [140–142]:

- **Multilayer perceptron MLP,** a versatile feedforward network with single or multiple hidden layers between the input and output layers that can learn complex relationships.
- **Radial basis function RBF,** a type of network that has a more straightforward hidden layer structure but requires specific basis function choices for optimal performance.
- **Recurrent Neural Network RNN,** designed for sequential data like text or speech, and can learn long term dependencies within sequences.

Simplifying things and concentrating on the first neural network type, the nodes are arranged in multiple layers, essentially, an input layer, a hidden layer, and an output layer, as illustrated in Figure 70.

- **Input layer,** receives variables regarding the raw data that influence the experiments.
- **Hidden layers,** process and extract patterns from the data through training with transfer functions, Table 17, optimization algorithms, and a performance function.
- **An output layer,** estimating the outcomes.

***Table 17.** Artificial neural network transfer functions* [140].

Transfer function f(x)	Input/Output Relation		Plot
Competitive	$f = 1$	neuron with max x	
	$f = 0$	all other neurons	
Positive Linear	$f = 0$	$x < 0$	
	$f = x$	$x \geq 0$	
Log-Sigmoid	$f = \frac{1}{1+e^{-x}}$		
Hyperbolic Tangent Sigmoid	$f = \frac{e^x - e^{-x}}{e^x + e^{-x}}$		
Hard limit	$f = 0$	$x < 0$	
	$f = 1$	$x \geq 0$	
Symmetrical Hard Limit	$f = -1$	$x < 0$	
	$f = +1$	$x \geq 0$	
Linear	$f = x$		
Saturating Linear	$f = 0$	$x < 0$	
	$f = x$	$0 \leq x \leq 1$	
	$f = 1$	$x > 1$	
Symmetric Saturating Linear	$f = -1$	$x < -1$	
	$f = x$	$-1 \leq x \leq 1$	
	$f = +1$	$x > +1$	

Following the architectural and structural choices, the choice of optimization algorithms follows. Several ones exist and the most widely used are:

- **Levenberg-Marquardt,** or LM algorithm, a highly regarded and widely used algorithm that combines the strengths of steepest descent and Gauss-Newton methods, offering fast convergence and good performance on various problems.
- **Adaptive Moment Estimation,** or Adam optimizer, known for its efficiency and effectiveness in handling large datasets and complex network architectures. It adapts the learning rate for each parameter individually, leading to faster convergence.
- **BFGS Quasi-Newton,** or Broyden-Fletcher-Goldfarb-Shanno method, it approximates the Hessian matrix, helping find the optimal solution more efficiently for large-scale problems.

After that, the performance function, with which the neural network evaluates the predictions and keeps training until a threshold is met. It can be set as one of the statistical error metrics, such as the standard error of the estimate SEE, mean squared error MSE, mean absolute error MAE, or others.

With everything established, the ANN model goes through a learning step by having multiple training cycles on a given training data, evaluating itself with the performance function. During training, the network adjusts the connections between nodes with the weights and biases to improve its accuracy in mapping and fitting the inputs to the provided outputs.

ANNs are generally considered non-deterministic models because the initial values assigned to the weights and biases before the training proceeds can have a subtle influence. While these are fixed after training for a specific run, if the network were to be retrained from scratch with different initializations, slightly different final weights and biases could be obtained, potentially leading to minor variations in the output for the same input even after training is complete. Especially regarding data not included in the training set. Even though neural networks trained on small datasets may exhibit seemingly deterministic behavior for repeated inputs, it is more accurate to consider it quasi-deterministic.

In a specific case study [139], two ANNs were trained to simulate the thickness and hardness profile of a boride layer formed on AISI W1 steel after powder pack boriding, Figure 72. Past the training step, the first ANN model was able to predict the hardness of the boride layer at any given distance from the surface of the treated AISI W1 steel, simulating effectively for any given time treatment, the powder pack boriding at a temperature of 950 °C. Parallelly, the second ANN model was able to predict the boride layer thickness at any given temperature and time, successfully simulating the boride layer thickness formed after the powder pack boriding process carried on AISI W1 steel.
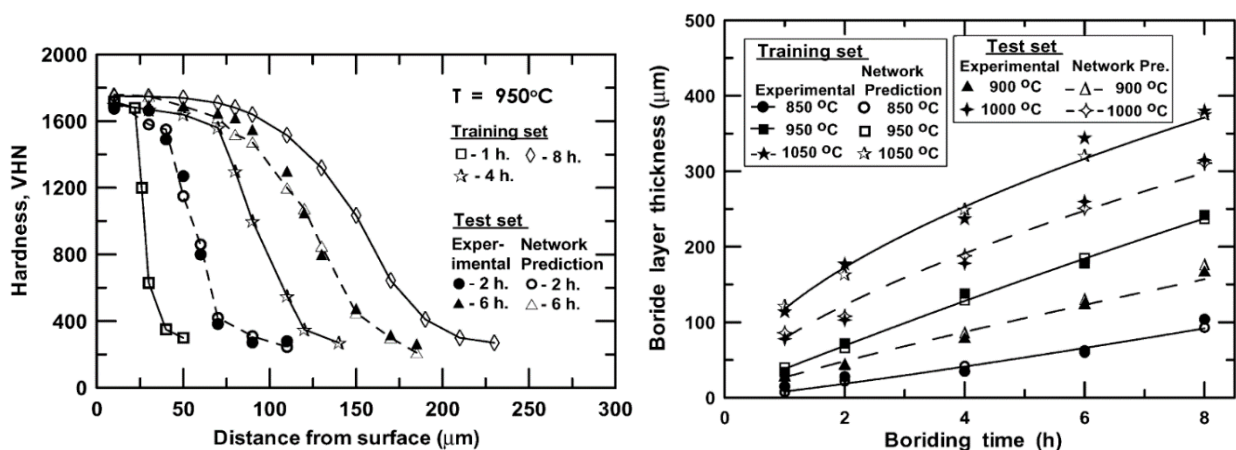
Figure 72. Thicknesses and hardness profiles of boride layers formed after boriding AISI W1 steel established with experimental points and artificial neural network predictions [139].

By successfully and accurately predicting seen data when compared to experimental data, along with unseen data, it can be said that the ANN models are, as stated in the beginning, a powerful tool in modeling, simulating, and optimizing boron diffusion processes. By leveraging their ability to learn from data and capture complex relationships between process parameters, ANNs can aid in achieving precise boron layer characteristics and designing efficient boriding procedures.

IV.5.2. Empirical models

Empirical models are built only on observations and experimental results instead of physical laws. They capture observed patterns but don't necessarily explain the underlying mechanisms. This lack of mechanistic understanding can lead to unpredictable behavior outside the observed data range.

Generally, empirical models are deterministic models, whether they are analytical or numerical regressions. Unless in rare numerical regressions where the optimization algorithms get stuck at a local minimum, then, the globally optimal solution is not reached, providing a non-deterministic nature that depends on the initial or boundary conditions. Though, in most practical applications, numerical regressions are considered deterministic due to the convergence properties of the developed algorithms used.

Empirical models are frequently employed to describe some material engineering processes [137]. When it comes to their application in the kinetic study of boride layers, several mathematical and statistical approaches can be used, from linear or multilinear regressions, to the various non-linear ones, i.e. quadratic, exponential, and so on.

A.   Linear regression models

Linear models are the simplest form of regression. In the context of modeling boron diffusion, a more sophisticated approach of it is applicable, referred to as multilinear regression.

The multilinear regression is a mathematical and statistical technique that employs numerous independent variables to determine the value of a dependent variable by establishing specific coefficients. Its general form is given in equation (8) [143], and it is based on certain assumptions [144,145]:

- Linear relationship between the dependent and independent variables.
- Correlation between the independent variables is minor or absent.
- Constant variance of the residuals.
- Independence of observations.
- Multivariate normality.

$$y = \beta_0 + \beta_1 x_1 + \beta_2 x_2 + \cdots + \beta_p x_p + \varepsilon \tag{8}$$

Where:

- y dependent variable
- $x_1 \ x_2 \ \ldots \ x_p$ independent variables
- $\beta_0 \ \beta_1 \ \beta_2 \ \ldots \ \beta_p$ regression coefficients
- ε residual term

Generally, this model is used to model boride layer thicknesses with two key parameters, temperature and time. Thus, with two independent variables, equation (8) becomes equation (9).

$$y = \beta_0 + \beta_1 x_1 + \beta_2 x_1 + \varepsilon \tag{9}$$

However, these two independent variables have a nonlinear relationship, unsatisfying the earlier assumptions. Consequently, when dealing with complex relationships between such independent variables, a more sophisticated approach is required, overcoming the issue by adding an interaction term to equation (9), which helps adjust the nonlinear relationship, equation (10) [145].

$$y = \beta_0 + \beta_1 x_1 + \beta_2 x_2 + \beta_3 x_1 x_2 + \varepsilon \tag{10}$$

Where the multiplication $x_1 x_2$ represents the interaction term

A case study used such an approach to predict the boride layer thickness as a function of two boriding parameters, temperature T in degrees Celsius and time t in hours. The obtained empirical formula is given in equation (11), and allowed to obtain the simulation of the iso thickness diagram given in Figure 73 [146].

$$u = -223.713 + 0.295 \, T - 113.493 \, t + 0.131 \, Tt \tag{11}$$
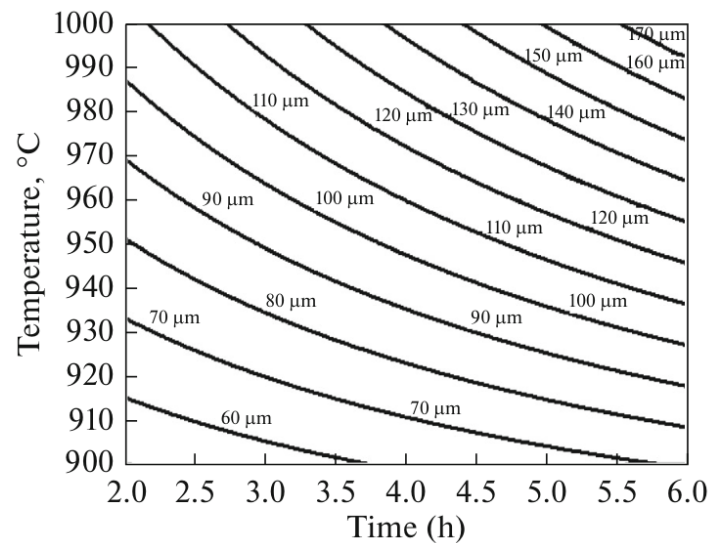
Figure 73. *Iso-thickness diagram of a borided ductile cast iron EN-GJS-400-15* [146].

B.   Nonlinear regression models

Nonlinear regressions vary on the preexisting forms of mathematical expressions selected, Paraboloid, Lorentzian, Gaussian, equation (12) to (14), and so on.

Table 18 provides the usage of such expressions to model a boride layer thickness formed on AISI W1 steel [139], while another used one expression to do the same on AISI H13 and AISI 304 steels, Table 18 and Figure 74 [147].

- **Paraboloid expression** $y = \beta_0 - \beta_1 x_1 + \beta_2 x_2 + \beta_3 x_1^2 - \beta_4 x_2^2$ (12)

- **Lorentzian expression** $y = \dfrac{\beta_0}{\left[1+\left(\frac{x_1-\beta_1}{\beta_2}\right)^2\right]\left[1+\left(\frac{x_2-\beta_3}{\beta_4}\right)^2\right]}$ (13)

- **Gaussian expression** $y = \beta_0 \exp\left[-\beta_1\left[\left(\frac{x_1-\beta_2}{\beta_3}\right)^2 + \left(\frac{x_2-\beta_4}{\beta_5}\right)^2\right]\right]$ (14)

***Table 18.** Empirical nonlinear models for simulating boride layer thicknesses.*

Substrate	Mathematical expression of the model		R^2	Ref.
AISI W1	**Paraboloid**	$d = 550.75 - 2.2T + 37.4t + 0.0017T^2 - 1.08t^2$	0.918	[139]
AISI W1	**Lorentzian**	$d = \dfrac{420.35}{\left[1 + \left(\frac{T - 1034.8}{95.5}\right)^2\right]\left[1 + \left(\frac{t - 7.5}{4.2}\right)^2\right]}$	0.976	[139]
AISI W1	**Gaussian**	$d = 486.3 \exp\left[-0.5\left[\left(\frac{T - 1142.4}{155.3}\right)^2 + \left(\frac{t - 8.4}{4.5}\right)^2\right]\right]$	0.980	[139]
AISI H13	**Gaussian**	$d = 132 \exp\left[-0.5\left[\left(\frac{T - 1399}{148.4}\right)^2 + \left(\frac{t - 10.6}{8.4}\right)^2\right]\right]$	0.9958	[147]
AISI 304	**Gaussian**	$d = 185 \exp\left[-0.5\left[\left(\frac{T - 1285}{110.3}\right)^2 + \left(\frac{t - 32.8}{15.75}\right)^2\right]\right]$	0.996	[147]

d layer thickness [μm], T boriding temperature [°C], t time [h]
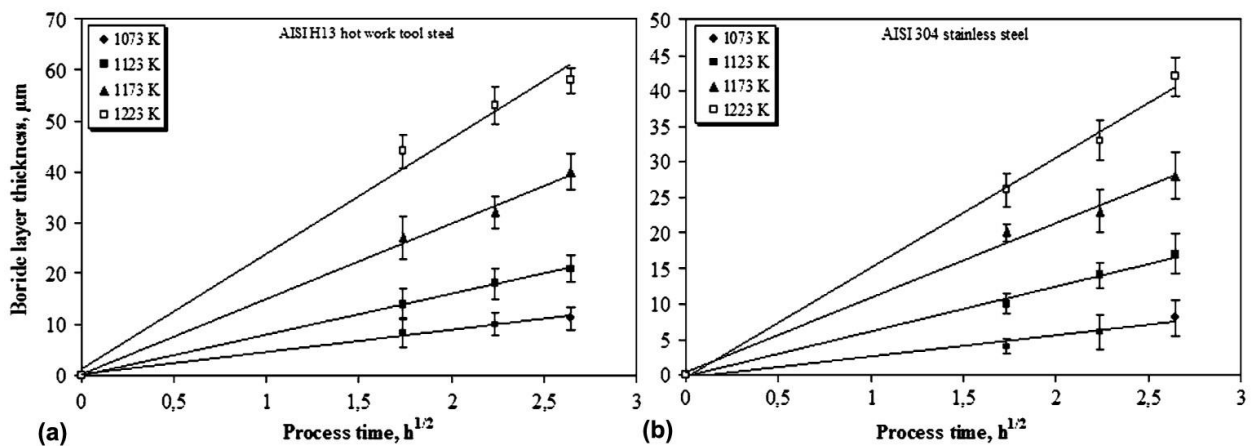
***Figure 74.** Boride layer thickness versus treatment time at various temperatures for (a) AISI H13 steel and (b) AISI 304 steel [147].*

While many mathematical preexisting expressions are available and extensively used in multiple fields, nonlinear regression also allows the customization of an expression depending on the reverse engineering or purpose intended. After all, given the computing power, each expression, preexisting or customized, can undergo numerical regressions to achieve the most accurate fit possible with the given data.

- **Customized expression**

$$u = (k_0 T^\alpha + k_1)\, t^{\eta_0 + \eta_1 N \beta} \tag{15}$$

where k_i, η_i, α, and β are regression coefficients, N is the number of moles.

The given custom expression, equation (15), was proposed in a certain case study [148] as an empirical model that describes the growth of the boride layer through three variables, temperature, time, and substrate size, with the coefficients given in Table 19. The customization was made in a way that permits the determination of the influence of each independent variable on the simulation. Temperature was found to have the greatest influence on the boride layer kinetics, Figure 75, followed by the treatment time and number of moles, respectively.

Table 19. *Coefficients of a custom empirical model describing a boride layer thickness evolution* [148].

Coefficient						
R^2	k_0	k_1	η_0	η_1	α	β
0.97	0.07	–216.71	0.67	–0.77	1.16	0.64
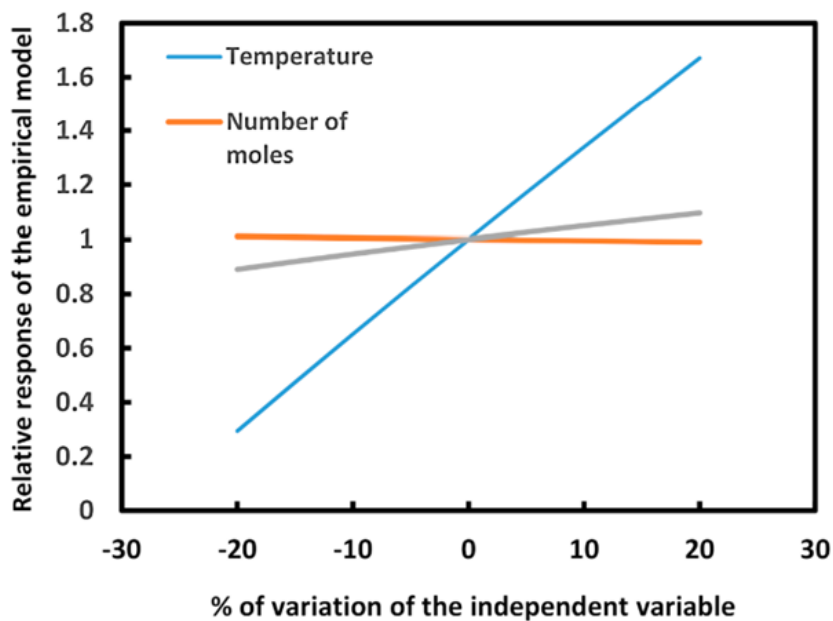
Figure 75. *Variables sensitivity in a custom empirical model* [148].

IV.5.3. Parabolic growth models

Parabolic growth models are a type of deterministic model used to describe boron diffusion. These models employ various parameters, including temperature, time treatment, and concentration profiles within the boride layer, to simulate the kinetics of boride layer formation. They allow for the determination of specific coefficients, such as the growth rate constant, the boron diffusion coefficient, and the activation energy. By doing comparisons of these coefficients with results of other borided materials, certain insights can be gained concerning the relative ease of boron diffusion in different materials.

A.   Simplified model

The simplified parabolic growth model is a type of empirical model that presupposes that the boride layer evolves in a parabolical manner, obeying a physical law, equation (16).

$$u = k\sqrt{t - t_0} \tag{16}$$

Doing so, a form of the Arrhenius law, equation (17), is used to help extract the activation energy Q and a pre-exponential constant k_0 from experimental data, allowing to predict boride layer thicknesses through physical sense due to the presence of the activation energy within the calculations, representing a controlled diffusion [149].

$$k = k_0 \exp(-Q/RT) \tag{17}$$

It is one of the dominant models in modeling and simulating boron diffusion. A specific study used such a model and simulated the boride layer thickness' evolution, along with the growth rate constants of two different steels, AISI H13 tool steel and AISI 304 stainless steel, Figure 76. This allowed the calculation of the activation energy of both steels as 244.37 and 253.35 kJ/mol, respectively, allowing a comparison with other materials, Table 24.
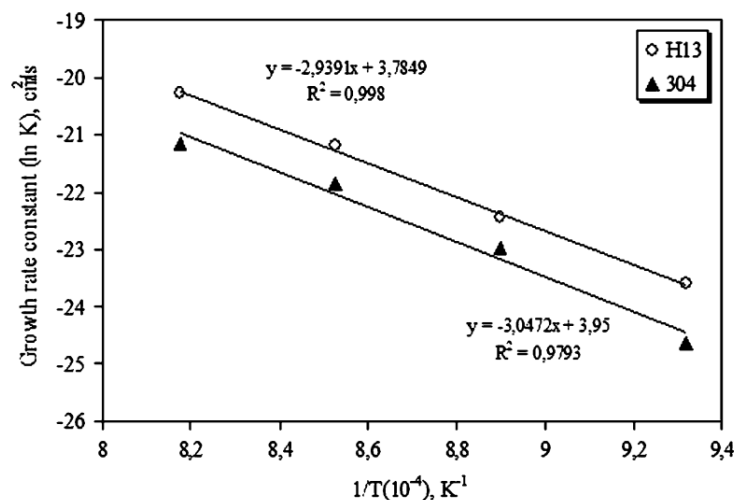
Figure 76. *Growth rate constant versus inverse of temperature for borided AISI H13 tool steel and AISI 304 stainless steel* [147].

B.   Elaborated model

The elaborate model is more detailed [138], and employs more parameters like the boron concentration in its development, and is exploited in different ways. It has the following assumptions concerning the boron diffusion [138,150–152]:

- Growth kinetics are controlled by a diffusion-controlled mechanism.
- Fe_2B boride layer formation is a one-dimensional semi-infinite diffusion problem.
- Fe_2B borides begin to nucleate after a specific incubation time.
- Fe_2B boride layer grows perpendicularly to the surface.
- Local equilibrium occurs at the phase interface
- Planar morphology is assumed for the phase interface.
- Volume changes during the phase transformation are not considered.
- Alloying elements do not influence the growth kinetics.
- The diffused layer is much smaller than the substrate's thickness.
- The substrate has a uniform temperature distribution.

Furthermore, within diffusion kinetics, the diffusion of reactants, such as boron, through the growing layer is generally considered as a rate-determining step, i.e. the speed of the diffusion process ultimately controls the overall rate of boride layer growth. This entails that the layer growth rate, or velocity of the layer, is proportional to the flux, equation (18).

$$\frac{dx}{dt} \propto J(x,t) \tag{18}$$

The flux is given in equation (19) in mol/m^2s.

$$J(x,t) = \frac{dx}{dt} C_{Fe_2B}(x,t) \tag{19}$$

Where: C_{Fe_2B} is the boron concentration profile in mol/m^3 , and dx/dt the velocity of the layer in m/s.

Additionally, the velocity of a particle is proportional to the force on the particle, equation (20).

$$\frac{dx}{dt} = B_{Fe_2B} \, F = -B_{Fe_2B} \, \frac{\partial \mu_{Fe_2B}}{\partial x} \tag{20}$$

Where B_{Fe_2B} is the mobility of the boron atoms, and μ_{Fe_2B} the chemical potential.

Therefore, introducing equation (20) in equation (19) gives equation (21).

$$J_{Fe_2B}(x,t) = -C_{Fe_2B}(x,t) B_{Fe_2B} \frac{\partial \, \mu_{Fe_2B}}{\partial x} \tag{21}$$

The chemical potential takes the entropy form, equation (22).

$$\mu_{Fe_2B} = \mu^0_{Fe_2B} + k_B T \ln(a_{Fe_2B}) \tag{22}$$

Where k_B is the Boltzmann's constant, and a_{Fe_2B} is the activity.

In an ideal system, the concentration is equivalent to the activity. Consequently, after deriving the chemical potential, equation (22), and substituting it into equation (21), a final expression of the flux is obtained, equation (23).

$$J_{Fe_2B}(x,t) = -B_{Fe_2B}k_B T \frac{\partial C_{Fe_2B}(x,t)}{\partial x} \tag{23}$$

Using the final expression of the flux, equation (23), in the equation (18) gives equation (24).

$$\frac{dx}{dt} = (constant)J_{Fe_2B}(x,t) = -(constant)B_{Fe_2B}k_B T \frac{\partial C_{Fe_2B}(x,t)}{\partial x} \tag{24}$$

Assuming that the potential is fixed at the boundaries of the layer, $\partial C_{Fe_2B}(x,t)/\partial x$ can be substituted with the slope $\Delta C_{Fe_2B}/x$ in equation (24). Accordingly, the parabolic growth constant k_{Fe_2B} is introduced in equation (25).

$$k_{Fe_2B} = -(constant)B_{Fe_2B}k_B T\Delta C_{Fe_2B} \tag{25}$$

Combining equation (24) and (25), then rewriting it gives equation (26).

$$xdx = k_{Fe_2B}dt \tag{26}$$

Integrating equation (26) with the boundaries of the layer provides the final expression, equation (27), that models the parabolic growth of the Fe_2B boride layer thickness v.

$$v^2 = 2k_{Fe_2B}\left(t - t_0^{Fe_2B}\right) = 2k_{Fe_2B}t_v \tag{27}$$

Where: $t_0^{Fe_2B}$ represents the incubation time, and t_v represents the effective growth time, Figure 77.
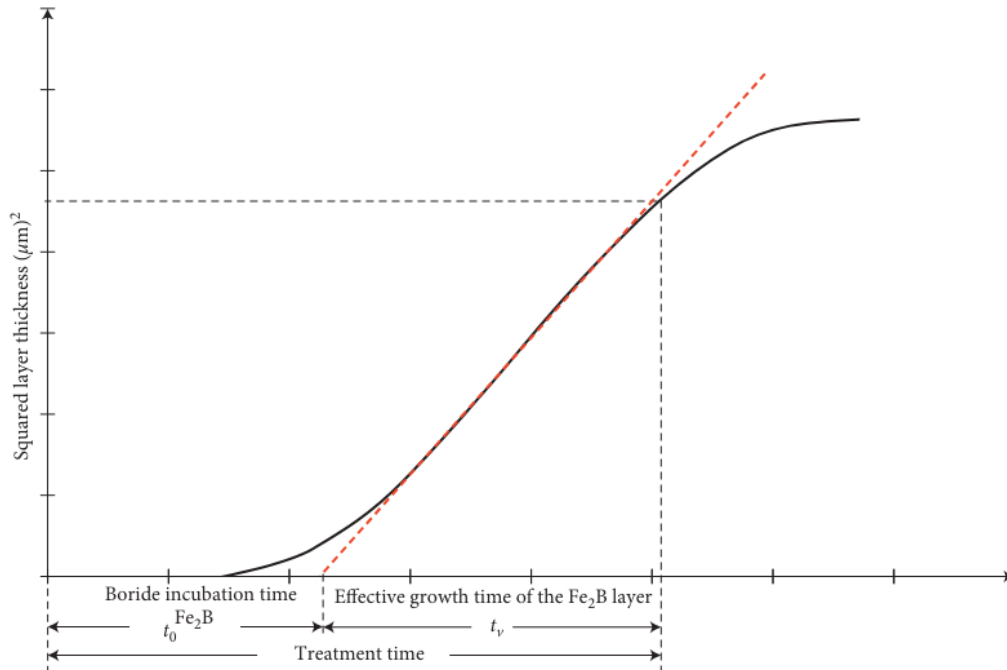
Figure 77. *Schematization of the parabolic growth model of Fe₂B boride layer thickness against boriding time* [138].

When it comes to simulating this boride layer thickness growth with the parabolic growth model, two approaches can be considered. The first is a steady state diffusion, while the second is a non-steady state diffusion or transient diffusion [138,152].

a)   Steady state diffusion approach

Figure 78 describes the growth of the Fe₂B boride layer, which is considered to grow on a substrate having the matrix saturated with boron atoms. The time required for that is the incubation period t_0, and after it, the Fe₂B phase begins to form. v_0 is a thin phase with a thickness of approximately 5 nm that forms during the nucleation stage, negligible compared to the thickness of the Fe₂B boride layer.

The boron distribution in the ferritic matrix before the nucleation of Fe₂B phase is illustrated by the relative function $f(x)$ in Figure 78. $C_{up}^{Fe_2B}$ and $C_{low}^{Fe_2B}$ denote the upper and lower limits of boron content in the Fe₂B phase. x represents the Fe₂B layer thickness at a specific time. C_{ads}^B is the effective adsorbed boron concentration during the process. $a_1 = C_{up}^{Fe_2B} - C_{low}^{Fe_2B}$ defines the homogeneity range of the Fe₂B layer, $a_2 = C_{low}^{Fe_2B} - C_0$ is the miscibility gap with C_0 the boron solubility in the matrix, negligible [138].
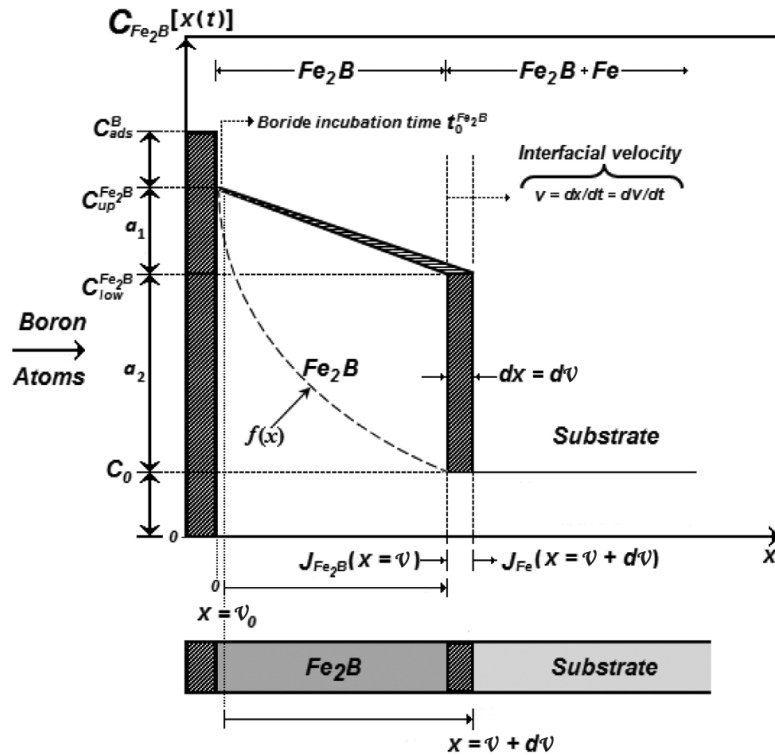
Figure 78. *Boron concentration profile throughout a mono-phased Fe₂B boride layer* [150].

The initial and boundary conditions for the diffusion problem are:

- At $x > 0$ and $t = 0$, $C_0 = 35 \cdot 10^{-4} \approx 0$
- At $x = v_0$ and $t = t_0^{Fe_2B}$, $C_{Fe_2B} = C_{up}^{Fe_2B} = 60 \cdot 10^3 \ mol/m^3$
- At $x = v$ and $t = t$, $C_{Fe_2B} = C_{low}^{Fe_2B} = 59.8 \cdot 10^3 \ mol/m^3$

The mass balance equation at the (Fe₂B/Substrate) interface is given in equation (28).

$$\left(\frac{C_{up}^{Fe_2B}+C_{low}^{Fe_2B}-2C_0}{2}\right)(A\,du) = J_{Fe_2B}(A\,dt) - J_{Fe}(A\,dt) \tag{28}$$

Where: A is the unit area and is equal to one squared.

The fluxes of each phase are given in equation (29) and (30), derived from Fick's first law, equation (4). Since the boron solubility in the matrix is very low, the flux within Fe is negligible

$$J_{Fe_2B}(v,t) = -D_{Fe_2B}\left.\frac{\partial C_{Fe_2B}}{\partial x}\right|_{x=v} \tag{29}$$

$$J_{Fe}(v+dv,t) = -D_{Fe}\left.\frac{\partial C_{Fe}}{\partial x}\right|_{x=v+dv} \tag{30}$$

Afterward, equation (31) is invoked, representing the principle of mass conservation at the interface Fe₂B/substrate, Figure 79.

$$\left(\frac{C_{up}^{Fe_2B}+C_{low}^{Fe_2B}-2C_0}{2}\right)\left.\frac{dx}{dt}\right|_{x=v} = -D_{Fe_2B}\left.\frac{\partial C_{Fe_2B}(x)}{\partial x}\right|_{x=v} \tag{31}$$
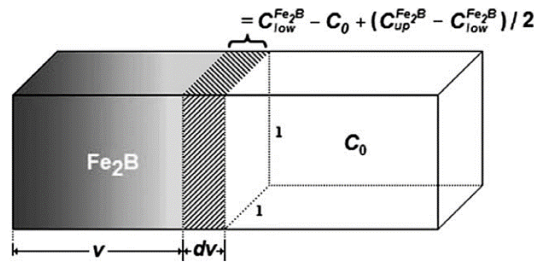
Figure 79. *Representation of the principle of mass conservation at the interface Fe₂B/Substrate* [153].

Assuming a linear boron concentration profile through the Fe₂B boride layer, Fick's Second law, equation (5), is reduced to an ordinary second order differential equation (32), from the solution $\nabla^2 C_{Fe_2B}(x) = 0$ ($\nabla^2 = d^2/dx^2$ is the Laplace operator, or Laplacian, in one dimension).

$$\frac{d^2 C_{Fe_2B}(x)}{dx^2} = 0 \tag{32}$$

Applying the initial and boundary conditions to equation (32), the distribution of boron concentration is attained in Fe₂B, equation (33).

$$C_{Fe_2B}(x) = \frac{C_{low}^{Fe_2B}-C_{up}^{Fe_2B}}{v}x + C_{up}^{Fe_2B} \tag{33}$$

From the equation (33) comes the naming of the approach, stationary or steady state diffusion, indicating that the composition of the boride layer profile does not change with time. Substituting its derivative in equation (32), gives equation (34).

$$\left(\frac{C_{up}^{Fe_2B}+C_{low}^{Fe_2B}-2C_0}{2}\right)\frac{dv}{dt} = D_{Fe_2B}\frac{C_{up}^{Fe_2B}-C_{low}^{Fe_2B}}{v} \tag{34}$$

Finally, by rearranging and integrating equation (34), the diffusion coefficient of boron within the Fe₂B boride layer is attained and expressed in equation (35).

$$D_{Fe_2B} = \frac{1}{2}\left(\frac{C_{up}^{Fe_2B} + C_{low}^{Fe_2B} - 2C_0}{C_{up}^{Fe_2B} - C_{low}^{Fe_2B}}\right) k_{Fe_2B} \tag{35}$$

b) Non-steady state diffusion approach

The second approach [152] also uses the mass balance equation, but describes the evolution of displacement of the growing interface with respect to time. Therefore, the linear boron concentration profile throughout the Fe₂B boride layer is also given by the solution of Fick's second law, but this time with a time dependency, equation (36). Hence, the name transient or non-steady state diffusion is used.

$$C_{Fe_2B}(x,t) = C_{up}^{Fe_2B} + \left(C_{low}^{Fe_2B} - C_{up}^{Fe_2B}\right)\frac{\text{erf}(x/2\sqrt{D_{Fe_2B}\,t})}{\text{erf}(v/2\sqrt{D_{Fe_2B}\,t})} \tag{36}$$

By deriving and substituting equations (36) into (31), the equation (37) is obtained.

$$\left(\frac{C_{up}^{Fe_2B} + C_{low}^{Fe_2B} - 2C_0}{2}\right)\frac{dv}{dt} = \left(C_{up}^{Fe_2B} - C_{low}^{Fe_2B}\right)\sqrt{\frac{D_{Fe_2B}}{\pi\,t}}\,\frac{\exp(-v^2/4D_{Fe_2B}\,t)}{\text{erf}(v/2\sqrt{D_{Fe_2B}\,t})} \tag{37}$$

Substituting the expression of the parabolic growth law obtained from equation (27) into equation (37). A final algebraic equation is attained, equation (38).

$$\left(\frac{C_{up}^{Fe_2B} + C_{low}^{Fe_2B} - 2C_0}{4}\right)\left(2k_{Fe_2B}\right)^{1/2} = \left(C_{up}^{Fe_2B} - C_{low}^{Fe_2B}\right)\sqrt{\frac{D_{Fe_2B}}{\pi}}\,\frac{\exp(-k_{Fe_2B}/2D_{Fe_2B})}{\text{erf}(k_{Fe_2B}/2D_{Fe_2B})} \tag{38}$$

The boron diffusion coefficient within the Fe₂B boride layer D_{Fe_2B} can, therefore, be estimated from equation (38) for a fixed growth rate constant with one of the numerical solvers of algebraic equations, such as the Newton-Raphson method.

c) Simulation

Afterward, for both approaches, equation (27) can be rewritten as equation (39). This same equation may differ in format from one literature to another [150–152].

$$v^2 = 2k_{Fe_2B}\left(t - t_0^{Fe_2B}\right) = 4\varepsilon^2 D_{Fe_2B}\left(t - t_0^{Fe_2B}\right) \tag{39}$$

Where: $\varepsilon^2 = \dfrac{C_{up}^{Fe_2B} - C_{low}^{Fe_2B}}{C_{up}^{Fe_2B} + C_{low}^{Fe_2B} - 2C_0}$ known as the square of the normalized growth parameter for the (Fe₂B/Substrate) interface and it is dimensionless.

Lastly, the model that describes and simulates the parabolic growth of the Fe₂B boride layer thickness is attained as equation (40). However, it is not established until the diffusion coefficient's dependence on temperature $D_{Fe_2B}(T)$ is determined. This determination is explained in the simulation section.

$$v = 2\varepsilon\sqrt{4D_{Fe_2B}\left(t - t_0^{Fe_2B}\right)} \tag{40}$$

Moreover, both approaches were used to simulate the kinetics of Fe_2B layer formation on an A36 steel after powder pack boriding, with the presence of boride incubation time being nearly half an hour. The squared values of the boride layer thickness are given in Figure 80 with respect to time for different temperatures [138]. The slopes of each of the straight lines supply the values of the parabolic growth rate constants ($2k_{Fe_2B}$), Table 20.
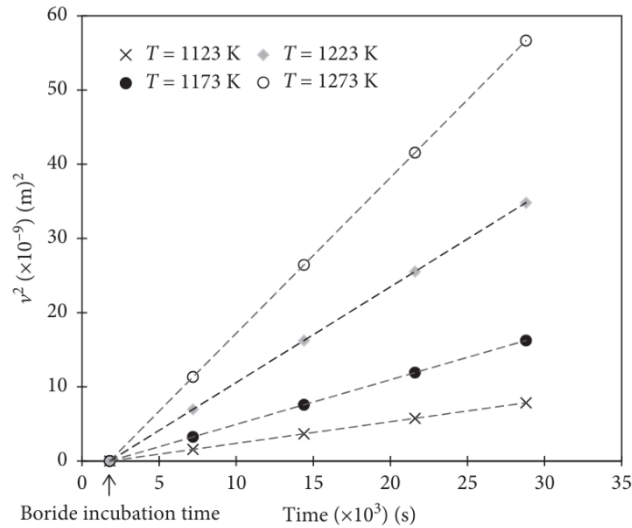
Figure 80. *Averaged squares of boride layer thicknesses with respect to time for different temperatures on a borided A36 steel* [138].

Using the parabolic growth rate constants, the boron diffusion coefficients are estimated at each of the four given temperatures by means of both approaches, steady and non-steady state diffusion approaches, equation (35) and (38). The estimated values are given in Table 20.

Table 20. *Estimated parabolic growth constant and diffusion coefficient values for each temperature* [138].

T [K]	$2\,k_{Fe_2B}$ $[10^{-1}\,m^2/s]$	Steady State D_{Fe_2B} $[10^{-11}\,m^2/s]$	Non-Steady State D_{Fe_2B} $[10^{-11}\,m^2/s]$
1123	2.810	4.28	4.28076
1173	6.120	9.32	9.3056
1223	12.80	19.50	19.467
1273	20.89	31.80	31.822

A final step in establishing the model of Fe_2B boride layer growth is needed to simulate its thickness v at any given temperature and time, equation (40). This step entails the determination of the activation energy Q and the pre-exponential factor D_0, found in the equation which follows the Arrhenius relationship, governing the boron diffusion coefficient as a function of temperature, equation (7). Doing so requires a linear fitting, Figure 81, based on the previously estimated values of the diffusion coefficients, Table 20. The plots demonstrate a diffusion-controlled process [149].
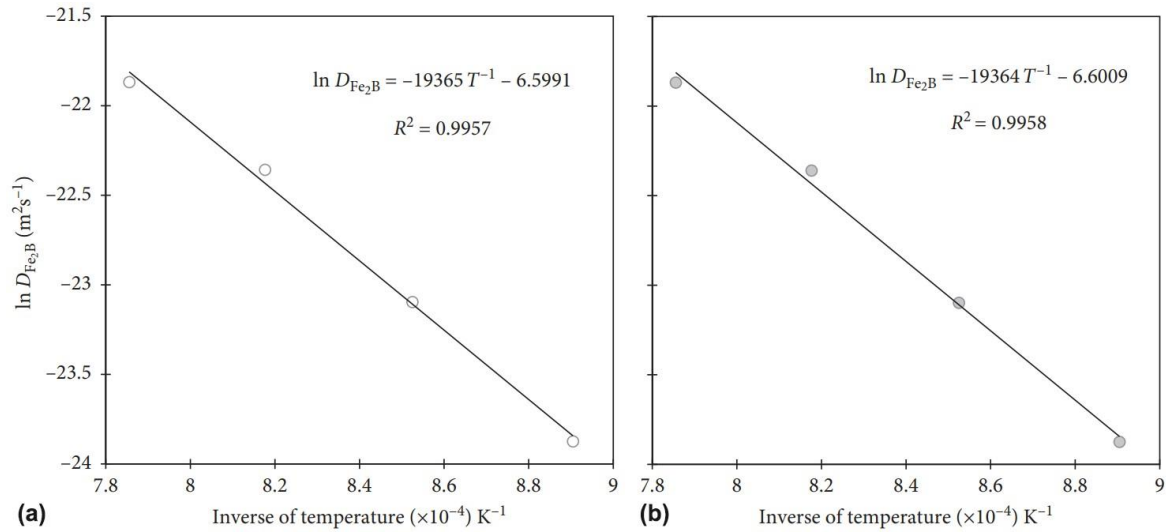
Figure 81. The logarithmic boron diffusion coefficient with respect to the inverse of temperature in (a) steady state diffusion and (b) non-steady state diffusion [138].

The values of the activation energies Q and pre-exponential factors D_0 calculated after the linear fittings from the slope and interception of the straight line are given in equations (41) and (42), representing both approaches, respectively [138].

$$D_{Fe_2B} = 1.361592 \ 10^{-3} \exp\left(-\frac{161.00061 \text{ kJ/mol}}{RT}\right) \ [\text{m}^2\text{s}^{-1}] \tag{41}$$

$$D_{Fe_2B} = 1.35914 \ 10^{-3} \exp\left(-\frac{160.9922 \text{ kJ/mol}}{RT}\right) \ [\text{m}^2\text{s}^{-1}] \tag{42}$$

Table 21. Parabolic growth model estimation of a boride layer thickness [138].

Boride layer thickness v [μm]	
Estimated	**Experimental**
2.5 h at 1123 K	
46.081	42.066±6.9947

An estimation of the model is compared to an experimental Fe₂B boride layer thickness, Table 21, and a good agreement is observed for the given boriding conditions. The results obtained by both equations (35) and (38), representing the two approaches, were pretty similar. Nonetheless, it was inferred that the results from the non-steady-state diffusion approach are superior to those of the steady-state diffusion one and should be preferred when modeling the kinetic growth of boride layer thicknesses. However, the models are equivalent in numerous cases [138].

IV.5.4. Integral model

The integral model is a mathematical model that incorporates a concentration-dependent diffusion coefficient. It offers a more accurate prediction for scenarios where boron concentrations significantly impact the diffusion behavior. The concentrations at the boundaries are used as, $C_{up}^{Fe_2B} = 9 \, wt.\%$ at $x = 0$ the beginning of the formation of the phase after the incubation period t_0, and $C_{low}^{Fe_2B} = 8.83 \, wt.\%$ at $x = u$ after a certain treatment time t. As for the boron concentration expression through the Fe$_2$B layer, the heat balance integral method HBIM of Goodman's method [154] is used, equation (43).

$$C_{Fe_2B}(x,t) = C_{low}^{Fe_2B} + a(t)(u(t) - x) + b(t)(u(t) - x)^2 \tag{43}$$

The HBIM method describes the distribution of boron concentration inside the Fe$_2$B layer with three time-dependent variables a(t), b(t) and u(t). The latter being the Fe$_2$B boride layer thickness, while the two others are positive parameters.

Using the boundary condition at the Fe$_2$B/Substrate interface, a first algebraic equation (44) is gotten.

$$a(t)u(t) + b(t)u(t)^2 = C_{up}^{Fe_2B} - C_{low}^{Fe_2B} \tag{44}$$

The equation (31) of the principle of mass conservation at the (Fe$_2$B/substrate) interface can be rewritten as equation (45).

$$W\left(-\frac{\frac{\partial C_{Fe_2B}(x)}{\partial t}}{\frac{\partial C_{Fe_2B}(x)}{\partial x}}\bigg|_{x=v}\right) = -D_{Fe_2B}\frac{\partial C_{Fe_2B}(x)}{\partial x}\bigg|_{x=v} \tag{45}$$

With $W = \dfrac{C_{up}^{Fe_2B} + C_{low}^{Fe_2B} - 2C_0}{2}$

After derivation and some developments in equation (45), a second algebraic equation (46) is obtained.

$$\left(C_{up}^{Fe_2B} + C_{low}^{Fe_2B}\right)b(t) = a(t)^2 \tag{46}$$

Lastly, integrating Fick's second law, equation (5), using the integral rule of Leibniz, equation (47), in the limits of the layer permits to obtain a first order differential algebraic equation (48).

$$\frac{d}{dx}\left(\int_{a(x)}^{b(x)} f(x,t)dt\right) = d(x,b(x))\frac{d}{dx}b(x) - d(x,a(x))\frac{d}{dx}a(x) + \int_{a(x)}^{b(x)}\frac{\partial}{\partial x}f(x,t)dt \tag{47}$$

$$\frac{u(t)^2}{2}\frac{da(t)}{dt} + \frac{u(t)^3}{3}\frac{db(t)}{dt} + [a(t)u(t) + b(t)u(t)^2]\frac{du(t)}{dt} = 2D_{Fe_2B}b(t)u(t) \tag{48}$$

The three resulting equations (44), (46) and (48) obtained, form a differential algebraic equation DAE system whose unknowns are the three time-dependent variables. That system can either be solved using Runge-Kutta methods and other numerical solvers [155], or analytically [156,157].

The analytical solution begins by solving the two algebraic equations (44) and (46), finding two possible solutions, equation (49) and (50).

$$a(t) = \frac{C_{up}^{Fe_2B} + C_{low}^{Fe_2B}}{2u} \left[-1 + \sqrt{1 + 4\frac{C_{up}^{Fe_2B} - C_{low}^{Fe_2B}}{C_{up}^{Fe_2B} + C_{low}^{Fe_2B}}} \right] \tag{49}$$

$$b(t) = \frac{(C_h + C_b)}{4u^2} \left[2 + 4\frac{C_{up}^{Fe_2B} - C_{low}^{Fe_2B}}{C_{up}^{Fe_2B} + C_{low}^{Fe_2B}} - 2\sqrt{1 + 4\frac{C_{up}^{Fe_2B} - C_{low}^{Fe_2B}}{C_{up}^{Fe_2B} + C_{low}^{Fe_2B}}} \right] \tag{50}$$

Using equation (16) and substituting the two found equations (49) and (50) into equation (48) of the differential algebraic equation DAE system, then deriving and developing it, provides the diffusion coefficient expression as a function of the parabolic growth rate constant k and boron concentrations, equation (51).

$$D = k^2 \left[\frac{1}{12} + \frac{1}{16} \frac{C_{up}^{Fe_2B} - C_{low}^{Fe_2B}}{C_{up}^{Fe_2B} - C_{low}^{Fe_2B}} \left(1 + \sqrt{1 + 4\frac{C_{up}^{Fe_2B} - C_{low}^{Fe_2B}}{C_{up}^{Fe_2B} - C_{low}^{Fe_2B}}} \right) \right] \tag{51}$$

Equation (51) is rewritten afterward for simplification as equation (52), introducing a parameter η that represents the influence of the boundary conditions regarding boron concentrations within the Fe$_2$B boride layer on the diffusion kinetics.

$$D_{Fe_2B} = \eta k^2 \tag{52}$$

Where: $\eta = \frac{1}{12} + \frac{1}{16} \frac{C_{up}^{Fe_2B} + C_{low}^{Fe_2B}}{C_{up}^{Fe_2B} - C_{low}^{Fe_2B}} \left(1 + \sqrt{1 + 4\frac{C_{up}^{Fe_2B} - C_{low}^{Fe_2B}}{C_{up}^{Fe_2B} + C_{low}^{Fe_2B}}} \right)$

After that, the estimation and the usage of the parabolic growth rate constant k is done similarly to the elaborated parabolic growth model by doing a linear fitting from the experimental data. With that, the activation energy Q is obtained along with the final expression of the Fe$_2$B boride layer thickness u, equation (53).

$$u = \sqrt{\frac{D_{Fe_2B}\left(t - t_0^{Fe_2B}\right)}{\eta}} \tag{53}$$

IV.5.5. Multiple phases models

Concerning diffusions that form multiple phased layers, numerous models can be envisaged, such as the Dybkov model, alternative diffusion, mean diffusion coefficient, along with the ones seen previously. Table 22 provides a comparison between specific models when it comes to the determination of the parameters of the diffusion coefficient on a bi-phased layer formed after boriding AISI 316L steel [158].

Table 22. Boron activation energies on borided AISI 316L steel determined by different models [158].

Model	D_0^{FeB} or k_0^{FeB} $[m^2/s]$	Q_{FeB} $[kJ/mol]$	$D_0^{Fe_2B}$ or $k_0^{Fe_2B}$ $[m^2/s]$	Q_{Fe_2B} $[kJ/mol^{-1}]$
Alternative diffusion	$9.35\ 10^{-4}$	187.95	$4.86\ 10^{-4}$	185.69
Integral diffusion	$8.58\ 10^{-5}$	167.27	$7.37\ 10^{-6}$	156.04
Mean diffusion coefficient	$1.12\ 10^{-4}$	167.04	$7.42\ 10^{-6}$	154.94
Bilayer growth	$1.15\ 10^{-4}$	167.21	$8.61\ 10^{-6}$	156.32
Dybkov	$2.29\ 10^{-6}$	166.67	$2.35\ 10^{-7}$	154.38

Taking, for example, the approach of the integral model, it can be extended to model bi-phased Fe$_2$B/FeB boride layers [159,160], equation (54) to (55), and even tri-phased Fe$_2$B/FeB/DZ layers [161].

$$u(t) = k'\sqrt{t - t_0} \tag{54}$$

$$v(t) = k\sqrt{t - t_0} \tag{55}$$

Where: u and v represent boride layer thicknesses, FeB and Fe$_2$B, while k' and k represent the parabolic growth rate constants in the FeB/Fe$_2$B and Fe$_2$B/Substrate interfaces.
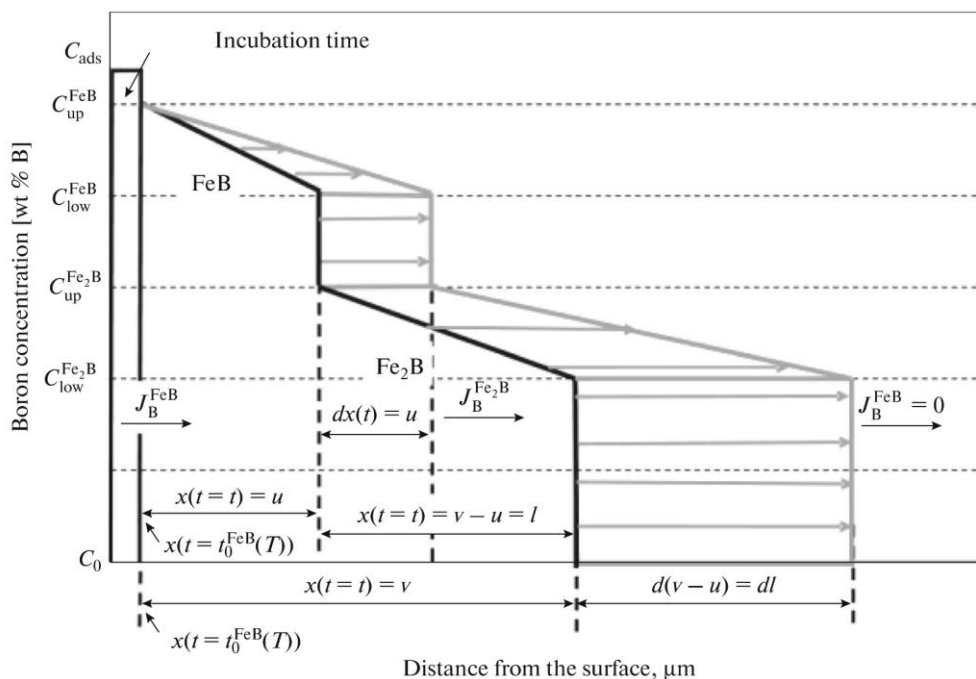
Figure 82. Boron concentration profile throughout a bi-phased FeB/Fe$_2$B boride layer [159].

The diffusion coefficient of the bi-phased FeB/Fe$_2$B is calculated using equation (56) and (57).

$$D_{FeB} = k'^2 \left(\frac{\alpha_1 + \beta_1}{8\beta_1} - \frac{1}{24} \right) \tag{56}$$

$$D_{Fe_2B} = \left(k^2 - k'^2 \right) \frac{(\alpha_2 + \beta_2)}{8\beta_2} - (k - k')^2 \frac{1}{24} \tag{57}$$

With:

$$\alpha_1 + \beta_1 = C_{up}^{FeB} - C_{low}^{FeB} \tag{58}$$

$$\alpha_2 + \beta_2 = C_{up}^{Fe_2B} - C_{low}^{Fe_2B} \tag{59}$$

$$(\alpha_1^2 - 2W_1\beta_1)(\alpha_2^2 - 2W_2\beta_2) = 2W_{12}\beta_1\alpha_2(2W_{12} + \beta_2) \tag{60}$$

Where: the boundary conditions are $\alpha_1 = a_1 u(t)$, $\beta_1 = b_1 u(t)^2$, $\alpha_2 = a_2\big(v(t) - u(t)\big)$, and $\beta_2 = b_2\big(v(t) - u(t)\big)^2$, while the initial conditions are $C_{up}^{FeB} = 16.40\ wt.\%$, $C_{low}^{FeB} = 16\ wt.\%$, $C_{up}^{Fe_2B} = 9\ wt.\%$, $C_{up}^{Fe_2B} = 8.83\ wt.\%$, and $C_0 = 35\ 10^{-4}\ wt.\%$, represented in Figure 82. Additionally, $W_1 = \frac{C_{up}^{FeB} + C_{low}^{FeB}}{2} - C_{up}^{Fe_2B}$, $W_2 = \frac{C_{up}^{Fe_2B} + C_{low}^{FeB}}{2} - C_0$, and $W_{12} = \frac{C_{up}^{Fe_2B} - C_{low}^{Fe_2B}}{2}$.

Nevertheless, the tri-phased FeB/Fe$_2$B/DZ layers have similar developments of the integral model as the bi-phased layers but with additional variables and conditions for the third phase, which is the diffusion zone DZ [161]. Figure 83 illustrates the similarities between it and the bi-phased layer regarding the concentration profile of boron within them, and Table 23 provides the diffusivity differences found in a tri-phased layer.
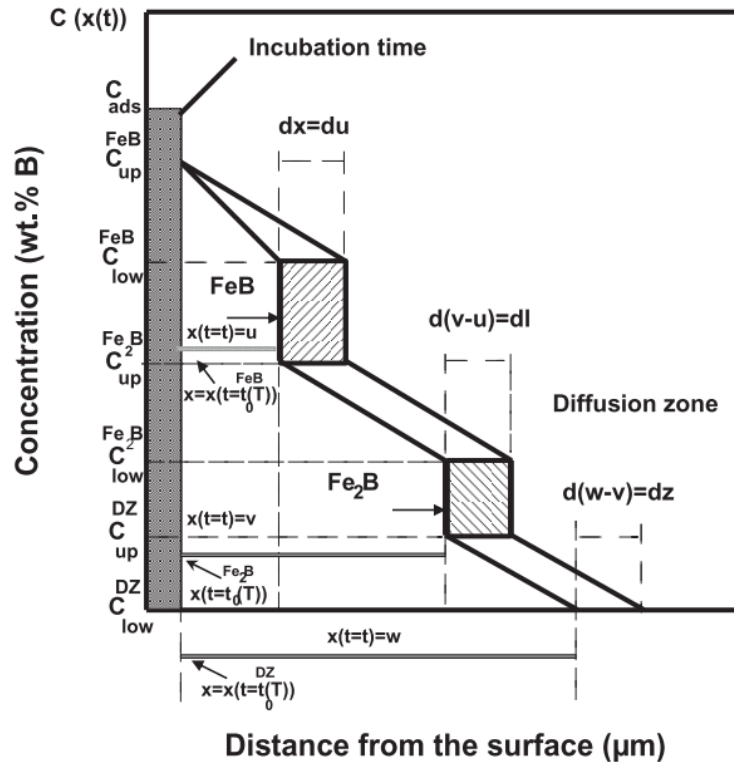
Figure 83. *Boron concentration profile throughout a tri-phased FeB/Fe$_2$B/DZ boride layer* [161].

Table 23. Boron diffusivity in a borided AISI 316 steel estimated with the integral model [161].

T [°C]	D_{FeB} [$10^{-13}\ m^2/s$]	D_{Fe_2B} [$10^{-13}\ m^2/s$]	D_{DZ} [$10^{-14}\ m^2/s$]
850	1.81	1.97	1.93
900	8.38	6.00	3.78
950	11.09	10.10	7.02
1000	31.09	25.00	11.23
Estimating activation energies Q equal to 210.26/193.80/140.55 for FeB/Fe$_2$B/DZ			

As of the unseen models, the Dybkov model for example, it is applied generally to the bi-phased layers [162–164] where a set of two ordinary differential equations ODE, equations (61) and (62), is used to model the Fe$_2$B/FeB boride layer thicknesses after solving the system using numerical solvers such as Runge-Kutta methods [155].

$$\frac{du(t)}{dt} = \frac{k_{FeB}}{u(t)} - \frac{rg}{p}\frac{k_{Fe_2B}}{u(t)} \tag{61}$$

$$\frac{dl(t)}{dt} = \frac{k_{Fe_2B}}{l(t)} - \frac{q}{sg}\frac{k_{FeB}}{u(t)} \tag{62}$$

With: $k_{FeB} = \frac{0.5k'}{p-\frac{rq}{s}}[(p-rg)k' + rgk]$ and $k_{Fe_2B} = \frac{0.5(k-k')}{1-\frac{rq}{sp}}\left[k + \left(\frac{q}{sg}-1\right)k'\right]$

The constant g = 0.60 denotes the molar volume ratio of the FeB and Fe$_2$B phases. The constants p, q, and r are equal to 1, while s is equal to 2, designated from the stoichiometric coefficients of the phases, FeB and Fe$_2$B.

Other than that, concerning the detailed theory behind boron diffusions that form multiple phased layers, other models than the integral model can be found. One case study used such modeling to investigate the kinetics of a tri-phased layer FeB/Fe$_2$B/DZ formed on a borided AISI 316 steel [165].

IV.6. SUMMARY

In brief, boriding, where boron atoms are diffused to the surface of machinable materials, from ferrous to nonferrous, is a surface hardening process that enhances wear resistance and hardness properties. The resulting boride layer formed on top of the material is the key factor underpinning such properties. Thus, investigating and grasping the modeling approaches regarding the kinetics of boride layers permits the optimization of the process and the achievement of the desirable surface characteristics for various applications.

While models translate the physical and chemical changes governing boron kinetics into a set of mathematical equations or computational simulations, exploring aspects that help understand diffusion processes such as point defects, solid-state diffusion, and Fick's Laws aided on comprehending the parameters that influence the diffusion mechanisms. These parameters are the main variables within the models, including temperature, time, concentration, and so on. Depending on the technique and conditions of the boriding process, the resulting boride layer differs in its thickness and composition, from mono to multi-phased.

In the process of modeling the boriding process, it was observed that the boride layer thickness is mainly sensitive to temperature and time exposures. Furthermore, the activation energy, the key parameter within the models, is not affected by such variants but rather by the substrate's material and the diffusion technique, helping in comparing different experiments regarding the diffusivity of boron within machinable materials, Table 24.

Modeling and simulating that boride layer thickness helps in the improvement and adjustment of boriding processes by enabling precise selection of the technological parameters to accommodate and attain the characteristics that are tailored to the intended applications. All while providing valuable insights and reducing experimental testing costs, and the forthcoming last chapter will cover a comparison of certain simulations for optimization purposes.

Table 24. Different activation energies in boriding.

Substrate material	Boriding technique	Activation energy Q [kJ/mol]	Model used	Ref.
Armco iron	Gas	73.08/120.65 FeB/Fe_2B	Diffusion	[166]
AISI H13	Salt bath	244.37 FeB/Fe_2B	Empirical	[147]
AISI 304	Salt bath	253.35 FeB/Fe_2B	Empirical	[147]
AISI 316	Plasma-paste	118.12 FeB/Fe_2B	Empirical	[167]
AISI 316	Powder	204/198/116 $FeB/Fe_2B/DZ$	Multi-phase	[165]
AISI 316	Powder	210.26/193.80/140.55 $FeB/Fe_2B/DZ$	Integral	[161]
AISI 1518	Powder	160.45 Fe_2B	Integral	[62]
A286 superalloy	Powder	175.86/198.70/205.73 $FeB/Fe_2B/DZ$	Integral	[168]
Inconel 718	Powder	233.2/206.17/218.06 $Ni_4B_3/Ni_3B/Ni_2B$	Integral	[169]
Nickel 201 alloy	Powder	203.87 $Ni_4B_3/Ni_3B/Ni_2B/NiB$	Parabolic growth	[170]
Ni$_3$Al	Electrochemical	185.95 $Ni_4B_3/Ni_3B/Ni_2B/Ni_{20}AlB_{14}$	Parabolic growth	[133]
Ni$_3$Al	Powder	188.80 Ni_4B_3/Ni_3B	Parabolic growth	[171]
Ni-Mg·3	Powder	158.843 $Ni_3B/Ni_2B/NiB$	Parabolic growth	[172]
Ni-Mg·7	Powder	136.506 $Ni_3B/Ni_2B/NiB$	Parabolic growth	[172]

BLANK PAGE

CHAPTER V

SIMULATION FOR OPTIMIZATION PURPOSES

This concluding fifth chapter highlights additional self-contributions to the field regarding modeling and simulating boriding built on the foundational knowledge of prior chapters. The work leveraged both deterministic and nondeterministic models, providing optimization insights for prior experiments regarding boride layer growth kinetics.

V.1.   INCENTIVE

From the previous chapters, it was elucidated that boron, as a versatile element, when diffused through the surface hardening process of boriding, a boride layer is formed at the surface of a material. This process favors low alloy materials, primarily ferrous ones, where they have the ability to acquire either thin or thick boride layers, depending on the boriding conditions, technique, media, and so on, but most importantly, the boriding parameters, time and temperature.

Accordingly, the incentive was modeling and simulating boron diffusion, more precisely the formation of the boride layer thickness. In doing so, different models were investigated, and on different substrates, which were subjected to different boriding techniques. The models varied from empirical to physically governed ones, and two borided substrates were used from the literature, Armco iron [173], a known pure iron, and C38 steel [174], a low alloy medium carbon steel. These differences in variables helped investigate the simulations for optimization purposes.

The determination of the boride layer thickness through a proper selection of the technological boriding parameters helps provide the desired thickness that is tailored to the intended applications. Additionally, modeling and simulating its kinetic growth provides valuable insights with regard to boron diffusion.

The chapter begins by providing the experiments regarding the substrates, then elaborating on the self-works, which encompassed deterministic and non-deterministic models. Some of them were presented at conferences, while others were submitted for publication. Regarding the published works on the field, three were co-authored, [175–177], regarding modeling FeB/Fe$_2$B bi-phase layers, along with two as the principal author, [178,179], regarding modeling Fe$_2$B mono-phase layers. Only the last two will be elaborated below since the thesis relies on self-works regarding the principal author.

V.2.   USED EXPERIMENTS

Before providing the contributed works, the experiments used in them are provided and elaborated to comprehend the entire aspect of the boron diffusion regarding these experiments. Those experiments include two ferrous materials that are broadly utilized in machinable applications, Armco iron and C38 steel. The first treated with powder pack boriding [173], while the latter with liquid salt bath boriding [174].

V.2.1. Armco iron

The samples of Armco iron used in the first experiment [173] are of pure iron with negligible amounts of alloying elements. It has near-perfect purity, over 99.6 %, with a nominal chemical composition given in Table 25.

Table 25. Chemical composition of the Armco Iron [173].

Element	C	Mn	P	S	N	Cu
wt.%	0.02	0.20	0.015	0.015	0.007	0.06

A.   Powder boriding process

Prior to the boriding process, the bulk is sectioned into cubic samples with dimensions of 10x10x10 mm^3, polished, rinsed ultrasonically for 15 min at room temperature in an alcohol solution and deionized water, then dried and kept in clean conditions.

Proceeding with the process, the samples were embedded in a closed cylindrical case made of AISI 304L, Figure 84, containing a Durboride fresh powder mixture with particles sizes of about 50 μm, englobing the sample. The Durboride agent contained boron carbide B_4C as a boron source, silicon carbide SiC as an inert filler, and Potassium Fluoroborate KBF_4 as an activator.
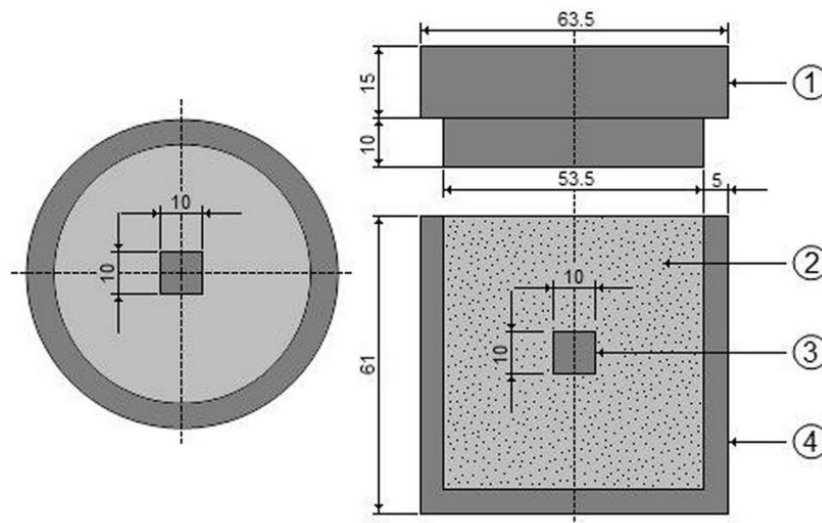
Figure 84. Schematization of the AISI 304L stainless steel container used in the powder boriding treatment, 1 lid, 2 powder medium, 3 sample, 4 container [173].

The container was placed in a conventional furnace under a pure argon atmosphere with temperatures ranging from 850 to 1000 by 50 degrees Celsius for different times, 2 to 8 by 2 hours. With the boriding completed, the container is removed and slowly cooled to room temperature.

B.   Layer characterization

By the end of the treatment, the treated samples were cross sectioned using a LECO VC-50 cutting precision machine, and the surface layers were observed by optical microscopy OM using GX51 Olympus instrument, Figure 85. The Fe_2B boride needles are visible and different in length, exhibiting a saw-tooth morphology at the Fe_2B/substrate interface.
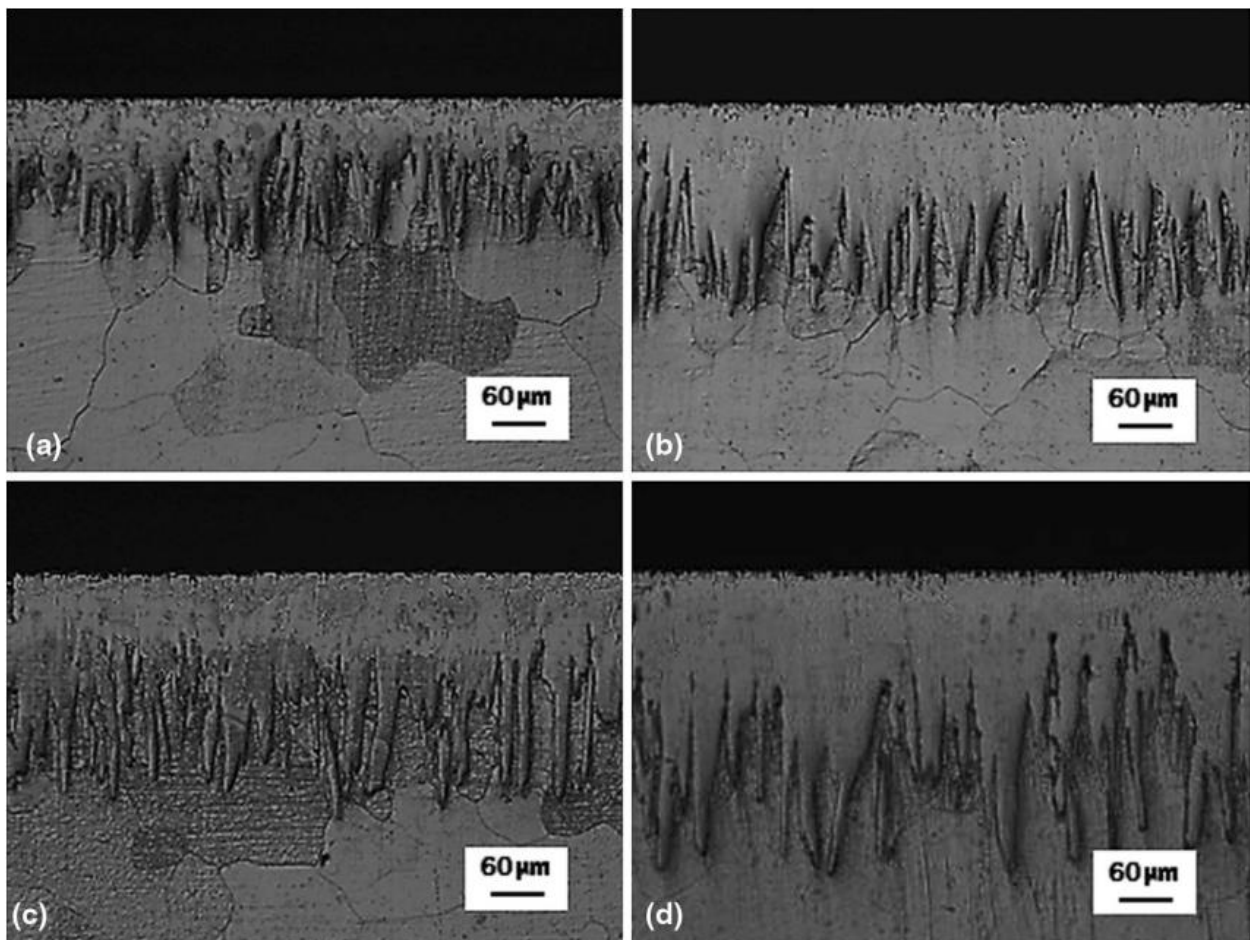
Figure 85. *Cross sections optical micrography OM of the Armco iron samples after powder boriding at 1000 °C for 2, 4, 6, and 8 h (a-d)* [173].

The obtained optical images were analyzed with MSQ PLUS software, which helped measure the thickness of the formed boride layer. All thickness measurements were collected from a fixed reference on the surface of the borided Armco iron, and the roughness effect at the interface was minimized by taking the average value of the long boride teeth. Fifty measurements were collected in different sections of the borided samples to estimate the thickness of the Fe_2B boride layers. The boride layer thickness obtained at 1000 °C reached a value of 244.02 ± 16.35 μm for 8 h of treatment, while it was only 109.47 ± 14.15 μm for 2 h.

The presence of the Fe_2B diiron boride formed at the borided sample's surface was identified by means of x-ray diffraction XRD using an Equinox 2000 with $CoK\alpha$ radiation at $\lambda = 0.179$ nm. The diffraction peaks of the Fe_2B phase exhibited a difference in intensities, Figure 86. The morphology of the Fe_2B boride layer was observed by scanning electron microscopy SEM with JEOL JSM 6300, Figure 86, and its growth had a highly anisotropic nature.
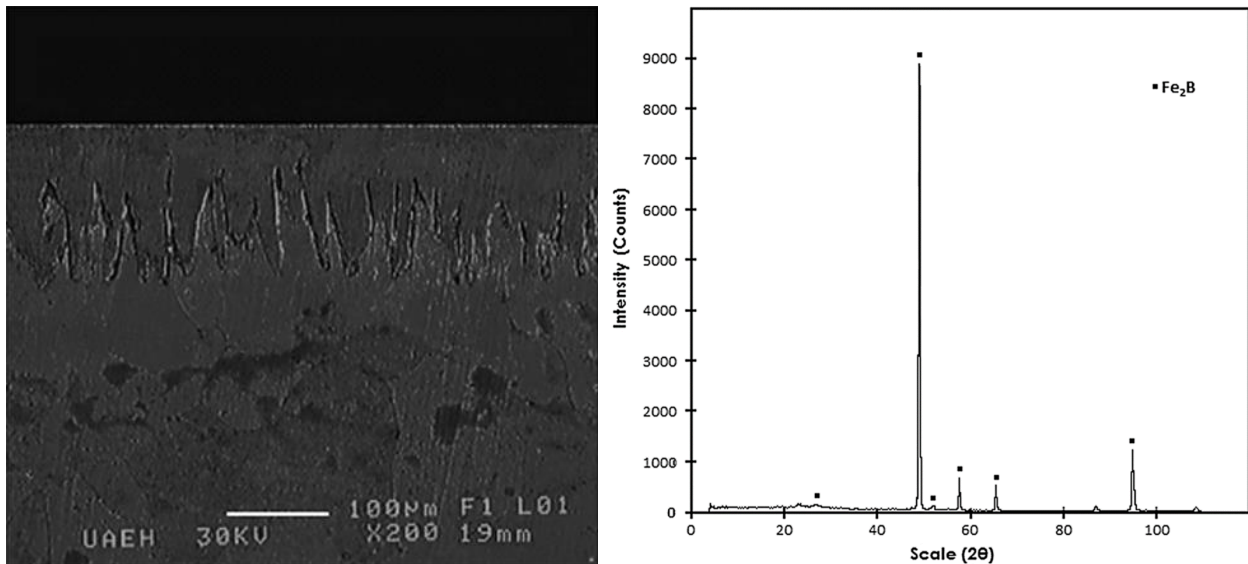
Figure 86. Borided Armco iron samples characterized with (a) SEM micrograph of a cross section after 2 h at 1000 °C, and (b) XRD patterns at the surface after 8h at 1000°C [173].

C.   Layer simulation

Using a diffusion model, the boron activation energy for the Fe_2B boride layer was estimated as equal to 157.5 kJ/mol on Armco iron [173]. The reported activation energies of Armco iron listed in Table 26 agree in the literature as far as solid boriding is concerned, but differ when it comes to gas boriding. The disagreement insinuates that the rate-determining steps in solid boriding deviate from that of gas boriding and may also be the case for dissimilar techniques.

Table 26. Estimated boron activation energies on Armco iron.

Boriding technique	Temperatures [°C]	Phase formed	Activation energy Q [kJ/mol]	Ref.
Powder	750-1000	FeB/Fe_2B	175/157	[149]
Powder	850-1000	Fe_2B	157.6	[173]
Paste	950-1050	Fe_2B	157	[180]
Paste	950-1050	Fe_2B	151	[181]
Gas	800-1000	FeB/Fe_2B	87.867/117.508	[75]
Gas	800-1000	FeB/Fe_2B	78.03/120.65	[166]

Furthermore, an additional experiment was carried out for 5 hours at 980 degrees Celsius, Figure 87, and was used for validating the simulation of the diffusion model [173]. The model estimated a thickness of 181.6 μm, which was comparable to the 175.25 ±12.15 μm experimental value.
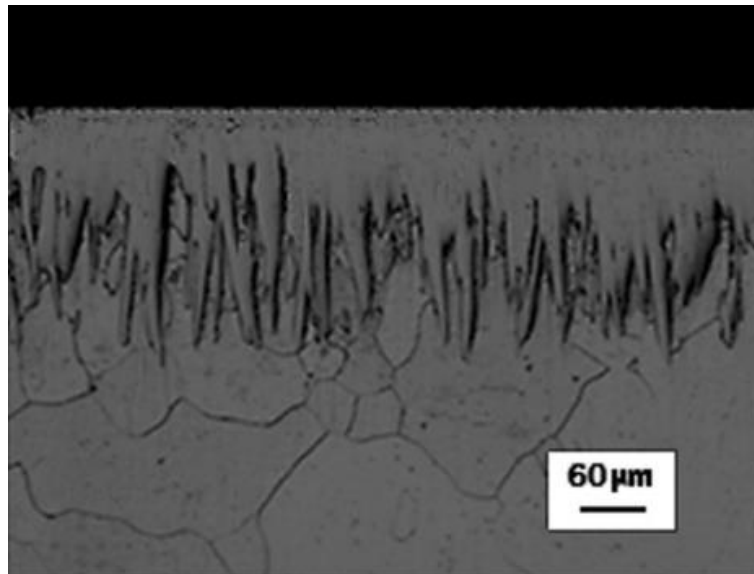
Figure 87. *Cross section optical micrography of the Armco iron after powder boriding*
for 5 h at 980 °C [173].

This powder boriding of the same Armco iron was also analyzed by different models [173,182–184], and the integral model was observed to have great accuracy in its predictions, Table 27. Especially regarding the additional validating experiment, boriding for 5 h at 1000 °C, Figure 87, as observed in and Table 28.

Table 27. *Experimental values of Fe_2B boride layer thickness along with predicted ones*
according to the integral model [173,182].

Temperature [K]	1123 K		1273 K	
Time [h]	Predicted	Experimental	Predicted	Experimental
2	41.39	40.34 ±6.7	112.10	109.47 ±8.6
4	63.09	61.48 ±5.6	170.88	166.84 ±4.1
6	79.04	77.02 ±3.8	214.08	209.03 ±5.3
8	92.27	89.92 ±4.6	249.93	244.02 ±5.1

Table 28. *Simulated Fe_2B layer thickness formed after boriding Armco iron for 5 h at 1000 °C*
with different models.

Boriding Armco iron for 5h at 1000 [°C]			
Experimental [173]		175.25	±12.15
Simulated	Diffusion model [173]	181.60	+6.35
	Integral model [182]	171.95	-3.30
	Diffusion model [183]	172.79	-2.46
	Mean diffusion coefficient model [184]	179.00	+3.75

V.2.2. C38 steel

The C38 steel used in the second experiment [174] is considered a medium carbon steel with small amounts of alloying elements. Its chemical composition is given in Table 29, determined by spectroscopical analysis at the refinery of Arzew NAFTEC, Algeria.

Table 29. Chemical composition of the C38 steel [174].

Element	C	Mn	Si	Co	Cr	Cu	Ni
wt.%	0.38	0.67	0.34	0.17	<0.1	<0.05	0.045

A.   Liquid boriding process

Before proceeding with the experiments, bulks of hexagonal bars having thicknesses about 25 to 30 mm are sectioned to samples having 5 to 8 mm. These samples were afterward annealed at 850 °C for 1 hour within a furnace which is then turned off until the samples are slowly cooled, providing a controlled temperature descent for stress relief.

Following the annealing, the samples are cleaned from extra contaminants. The cleaning was done by polishing with silicon carbide SiC papers having 420 grits/cm^2. With the samples being prepared, they are borided through immersion in an electroless liquid bath medium set in an electric furnace with open-air conditions, Figure 88.
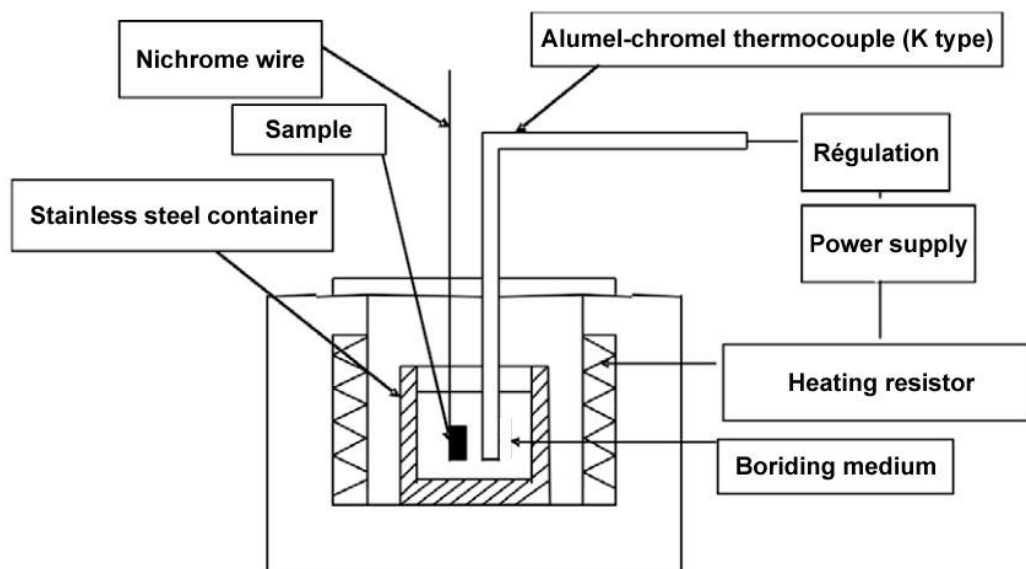
Figure 88. Schematization of the salt bath liquid boriding technique carried on the C38 steel [174]*.*

The chemical composition of the salt bath had 70 % of borax $Na_2B_4O_7$ and 30 % of silicon carbide SiC. The silicon carbide grains influence on the boron diffusion kinetics was investigated, and it was found that the more the grains were refined, the better and faster the boron diffusion becomes [174].

The boriding conditions varied in terms of temperatures and time treatments. The first was of 850, 950 and 1000 degrees Celsius while the latter ranged from 2 to 8 by 2 hours. After the treating is completed, the samples were cooled down in open air then cleaned from the salts that adhere to the surface. The cleaning was through immersion in boiled water for 30 to 60 minutes, applying a progressive dissolution of residuals. A gentle brushing followed, completing the cleaning.

The salt bath's repeated usage was observed to influence the ease of cleaning of the samples after multiple treatments. Over 15 hours of treatments with the same bath renders it sensibly viscous, and after 25 hours, the cleaning of the borided samples becomes problematic. Additionally, the bath should be replaced after a relative usage of 36 hours at 950 °C.

B.   Layer characterization

In order to identify the formed boride layer, optical microscopy OM and Scanning Electron Microscopy SEM were utilized. With a negligible FeB phase, the boride layer was determined as having a Fe_2B mono-phased. The layer had a saw-toothed morphology at the Fe_2B/substrate interface, allowing good anchoring to the substrate.
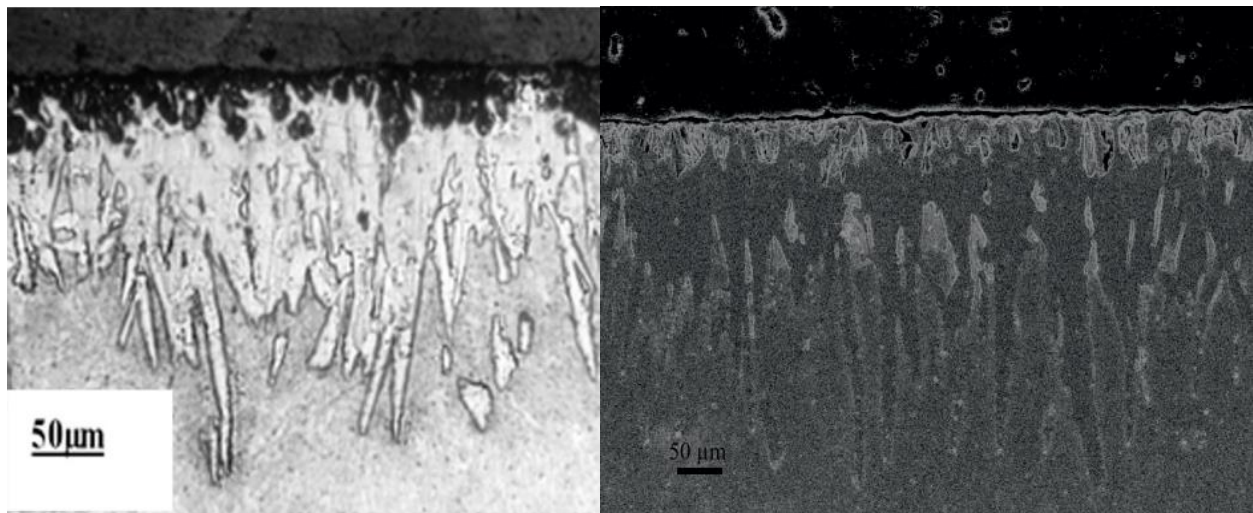
Figure 89. Cross section optical micrography OM and scanning electron microscopy SEM of the C38 steel samples after salt bath liquid boriding for 8 h at 1000 °C [174].

The boriding process was observed to affect the roughness of the substrate after using a portable profilometer, Surftest 201. After measuring the samples' roughness before and after boriding, Figure 89, it was observed that the roughness deteriorated slightly. Thus, it was concluded that the surface roughness of the formed boride layer is correlated with the prior roughness of the substrate.
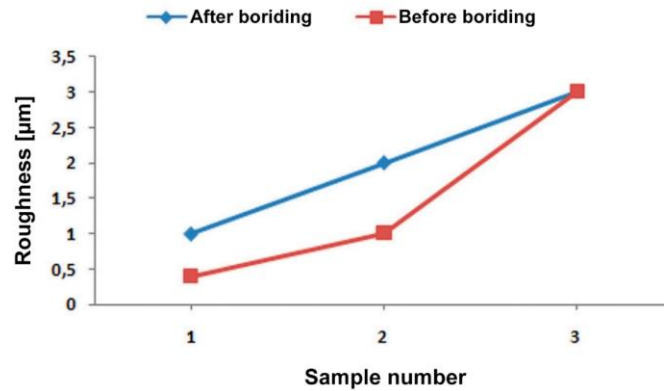
Figure 90. Boriding effect on the sample's roughness [174].

Other than that, the sample that was borided for 8 h at 1000 °C was characterized in terms of hardness. Before the boriding treatment, it was about 275 ±21 HV. With the treatment applied, the boride layer adds an extreme hardness nearing 1694 ±46 HV, decreasing from the surface to the substrate, as provided in Figure 91.
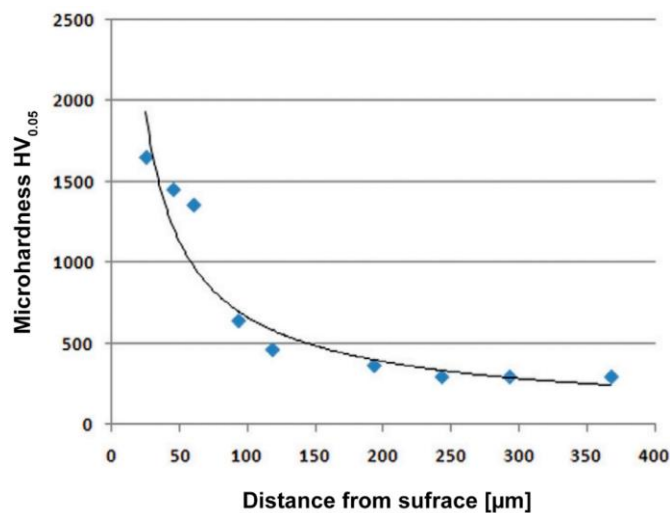
Figure 91. Microhardness profile along the boride layer formed on C38 steel [174].

When it comes to the boride layer thickness, two measurement methods were utilized, optical microscopy OM and weighing method. The first method was by taking two lengths of both the two deepest and shallowest peaks, then averaging them, Figure 69, while the second was by weighing the samples before and after boriding. A discrepancy between the two methods was observed, and it was suggested that the formation of porosities took place in the first stages of the formation of the layer, hindering the calculations regarding the weighing. Thus making the first method more reliable accuracy-wise [174].

That is what makes the Optical microscopy OM more dominant in the literature when it comes to the measurement of boride layer thicknesses. Additionally, the weighing method is unsuitable for analyzing multi-phase layer formations.

Furthermore, annealing helped in refining the grains within the austenite found in the sample by heating in a neutral salt bath of Barium chloride $BaCl_2$ for an hour. This refinement diminished the grain sizes from 125 to 40 μm, and this impacted the boron diffusion process, promoting a better diffusion and a thicker boride layer, 60 instead of 30 μm for the same conditions [174]. That was in concordance with the principles seen in the previous chapters, where it was postulated that prior treatments influence the growth kinetics in subsequent treatments.

Lastly, the effect of boriding on the wear resistance of the C38 steel was investigated through cyclical rotational bending, and it was concluded that the treatment in question helped provide about 20 to 25 % fatigue resistance [174].

C.   Layer simulation

Modeling and simulating the experiment was investigated in another paper [185], where the effect of boride incubation time was considered and examined through a mathematical diffusion model. The approach attempted to provide an introduced equation modeling the effect of the incubation time, which differs with respect to temperature, equation (63).

$$B(T) = 0.0012\text{T} - 0.2 \tag{63}$$

The boron activation energy was estimated as 207.8 kJ/mol through the Arrhenius relationship between the experimental boride layer thicknesses [174] and the reciprocal temperature regarding 2 h of treatment. Accordingly, the diffusivity of boron deduced is given in equation (64), and the obtained growth rate constants are given in Table 30.

$$D_B^{Fe_2B} = 1.388\ 10^{-4} \exp\left(-\frac{207.8\ kJ/mol}{RT}\right) \tag{64}$$

Table 30. Obtained growth rate constants of C38 steel after salt bath boriding [185].

Temperature [°C]	750	800	850	900	950	1000	1050
k [μm/s$^{0.5}$]	0.1481	0.2275	0.3365	0.480	0.6672	0.9037	1.1960

After modeling the boride incubation time, the boride layer formed after liquid salt bath boriding the C38 steel was simulated, Table 31. Figure 92 includes simulations of that boride layer thickness, sim 1 represented a simulation that does not consider the incubation time, where it was assumed that the Fe_2B layer formed instantly, immediately covering the steel. While sim 2 represented the results of the proposed approach, which was based on the modeled incubation time effect.

Table 31. *Simulated boride layer thickness formed on C38 steel after salt bath boriding* [185].

t [h]	2	4	6
T [°C]	Fe_2B boride layer thickness [μm]		
850	23.41	33.11	40.55
950	53.22	75.26	92.17
1000	76.68	108.4	132.8
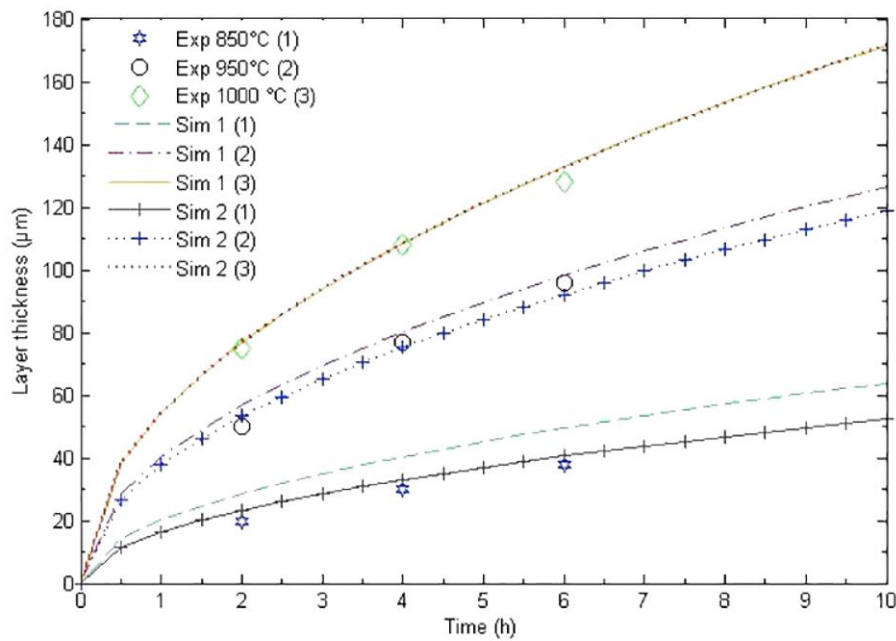
Figure 92. *C38 steel boride layer thickness simulation comparison* [185].

All and all, it was concluded that the proposed approach, sim2, gives better results compared to sim 1, justifying the effect and relevance of the incubation time in providing better predictions with a mean error of 2.8 μm [185]. This relevance was more observed in lower temperatures due to the fact that high temperatures decrease the boron incubation time, lessening its effect and explaining the similitude of sim1 and sim2 the higher the temperature gets.

V.3.   SIMULATIONS

Putting forward the self-works regarding the theme of the thesis, modeling and simulating boron diffusion, the goal was predicting the boride layer thickness and comparing between models accordingly for optimization purposes.

V.3.1. Initiated works

Focusing on Fe$_2$B mono-phase boride layer thicknesses, three works were presented at conferences. Two of them investigated deterministic models and the last was about a non-deterministic one. As some of these works are either under review or not yet submitted, only the underlying concepts will be presented about them.

A.   Simulating boride layer thicknesses using an empirical linear regression model

The first work, a simple and straightforward deterministic regression model was used, elaborated in the previous chapter. The utilization of a linear regression, equation (65), to predict boride layer thicknesses of the first used experiment, powder boriding Armco iron [173]. The simulated results are given in Figure 93 as u_L, representing the linear boride layer predictions, and by it being a regression, it accordingly gave good fittings with a mean error of 3.8 μm to the experiments, represented as u_E.

$$u_L \approx -228.4195 + 0.2985\,T - 71.6751\,t + 9.3737\,10^{-2}\,Tt \qquad (65)$$

Where time is given in hours and temperature in degrees Celsius.
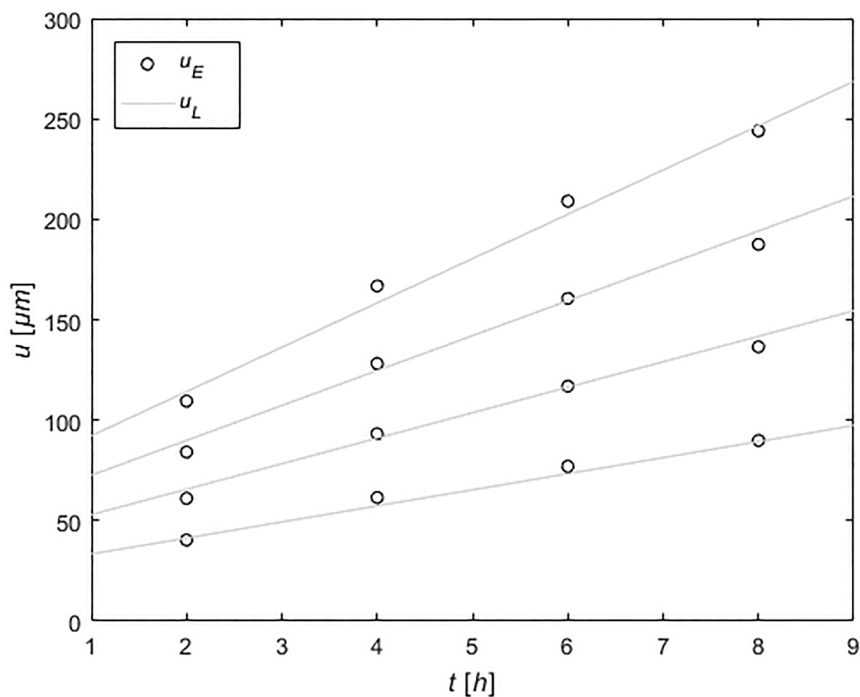
Figure 93. *Borided Armco iron boride layer thickness simulation using an empirical linear model.*

To test the validity of the linear model, it was used to predict another point not introduced in the regression, regarding the same experiment given above in Figure 87, boriding Armco iron for 5 h at 980 °C. The predicted boride layer thickness was equal to about 165.1 μm, which is not that far from the experimental value, 175 μm, and within the range given experimentally, ±12 μm. In comparison with the other models' predictions that were given in Table 28, it is less accurate because it does not consider factors that influence the kinetics nonlinearly.

B.   Simulating boride layer thicknesses using an empirical nonlinear regression model

In the second work, a nonlinear quadratic model was investigated regarding boride layer thickness predictions. After applying the regression, equation (66), on the second provided experiment, liquid boriding C38 steel [174]. The simulation is given in Figure 94 as u_Q where instead of providing the actual predictions, the mean error found, 1.18 μm, was added and minimized from it, providing a plot of a range.

$$u_Q \approx 539.0556 - 1.3929\, T + 8.8889\ 10^{-4}\, T^2 - 39.0417\, t - 0.9792\, t^2 + 0.0607\, Tt \qquad (66)$$

Where time is given in hours and temperature in degrees Celsius.
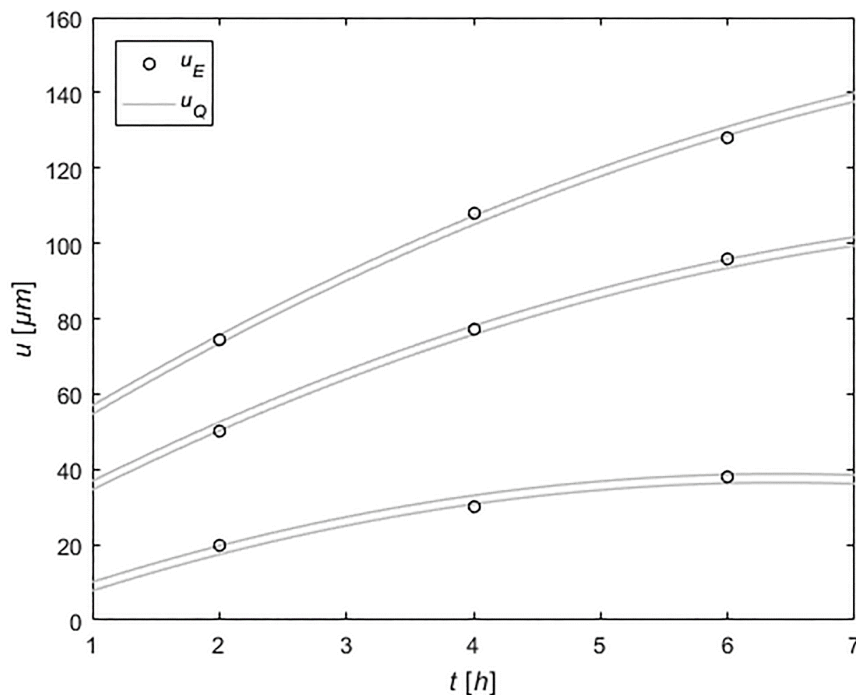
Figure 94. *Borided C38 steel boride layer thickness simulation using an empirical nonlinear model.*

As a regression, the model disregarded physical laws predicting for 6 to 7 hours of treatments at 850 °C, the bottom simulation, a diminishing boride layer thickness, which is physically impossible. However, when it comes to the experimental points, it had impeccable predictions with a correlation R^2 equal to 0.9985, making the predictions between them relatively accurate.

C.   Simulating boride layer thicknesses using an artificial neural network model

As for the third work, it involved a non-deterministic model that uses an artificial neural network ANN approach, elaborated in the previous chapter.

A note about this work is that after presenting it at a conference, it was restructured and further developed then submitted for publication elsewhere. Subsequently, it was accepted but at the current time in which this thesis is being written, it has not been published yet.

Starting with the ANN model, three layers constructed the model:

- **The first being the input layer,** specified as two variables, temperature T and treatment time t of the boriding process conditions.
- **A hidden layer as the second,** where a set neuron configuration that uses training and validating data to regulate itself by extracting patterns for optimal predictions.
- **A third output layer,** which provides the final prediction of the boride layer thickness u.

The artificial neural network architecture type was the feed-forward back-propagation network. Feed-forward for having no connections between neurons in the same layer and no connections with opposite directions. Back-propagation refers to a type of computation that determines the minimal error when trying to extract the patterns of the data [140,141,186].

While different training optimization algorithms can be used, the Levenberg-Marquardt algorithm was the most suited, and it used the Jacobian for calculations, with the mean squared error MSE. The transfer functions used in the last two layers were the Sigmoid function, equation (67), and the Linear function, equation (68). As for the neuron configuration in the hidden layer, different sets of neurons give different predictions, this can only be fixed with trial and error, and the optimal number of neurons found was nine.

$$f_1(x) = \frac{1}{1+e^{-x}} \tag{67}$$

$$f_2(x) = x \tag{68}$$

After structuring the artificial neural network, the boriding data is provided for the training phase. The data provided were those of the liquid boriding of C38 steel, the second used experiment. The process had nine experimentations, 2, 4, and 6 h of treatment times t, at temperatures T 850, 950, and 1000 °C [174], presented individually.

The three treatment times of the first and last temperature, 850 and 1000 °C, were taken as training data while the middle ones, three treatment times at 950 °C, were taken as validating data, Figure 95. In addition to those nine observations, others were also added as training data regarding the beginning of the process where no matter the temperature, the boride layer is undoubtedly not formed yet.
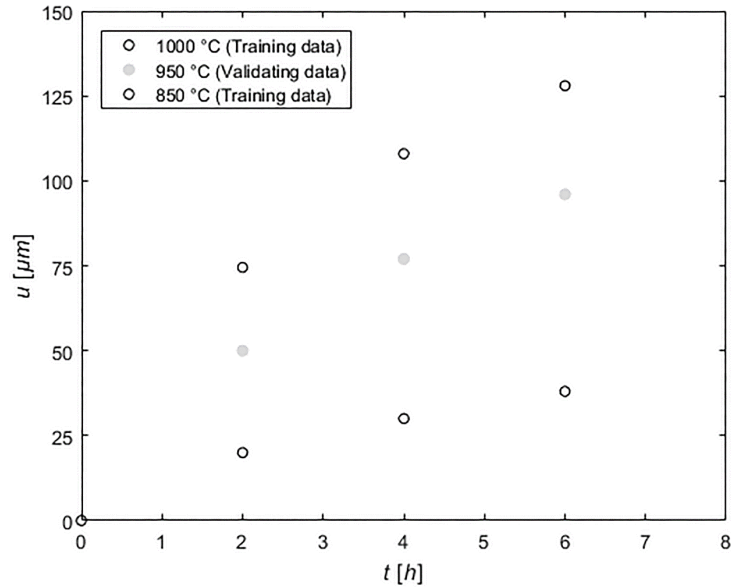
Figure 95. *ANN Data usage regarding the boriding of C38 steel with respect to temperature and time.*

Moving on with the training phase, the ANN extracts patterns of the training data and then regulates itself by trying to find the optimal mean squared error on the validating data after a number of training cycles. In this case, the model found the best mean squared error MSE to be 3.2359 at the 56th training cycle, as given in Figure 96.
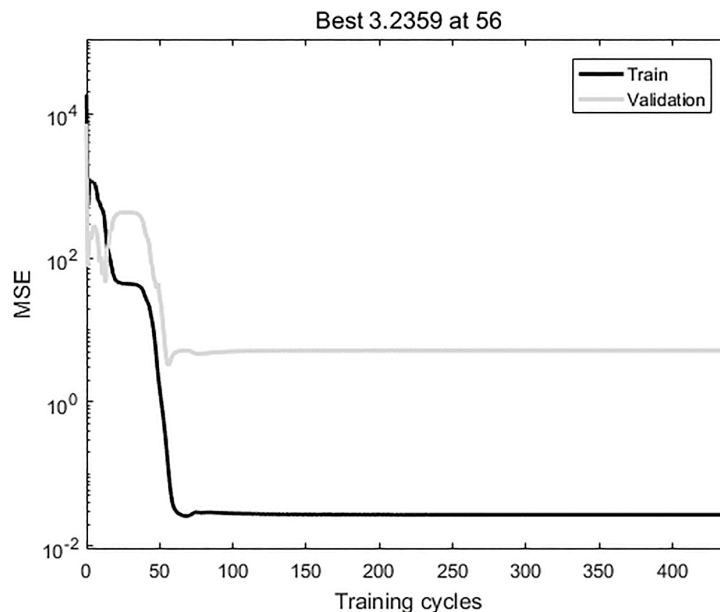
Figure 96. *Simulation of the boride layer thickness over time at different temperatures,*
from 850 to 1000 by 25 °C.

With the training phase finished, the model becomes able to predict accordingly, and the simulation is plotted in Figure 97, with 7 lines representing the change of the boride layer thickness over time, each at different temperatures, from 850 to 1000 with increments of 25 °C.
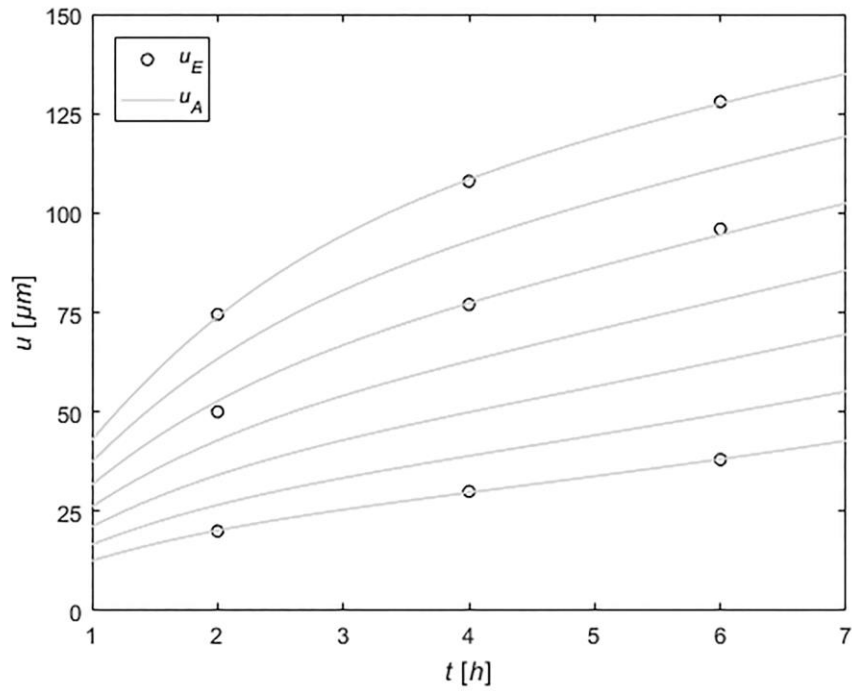
Figure 97. *Simulation of the boride layer thickness formed on C38 steel by the presented artificial neural network and the diffusion model.*

After finishing the simulation, it was compared to the diffusion model [185], provided previously. Figure 98 demonstrates that the ANN model u_A is clearly superior to the diffusion model u_D, with a mean error of 0.8 over 2.8 μm. Hence, it can be said that ANN models have great potential regarding the kinetics of boride layer thicknesses.
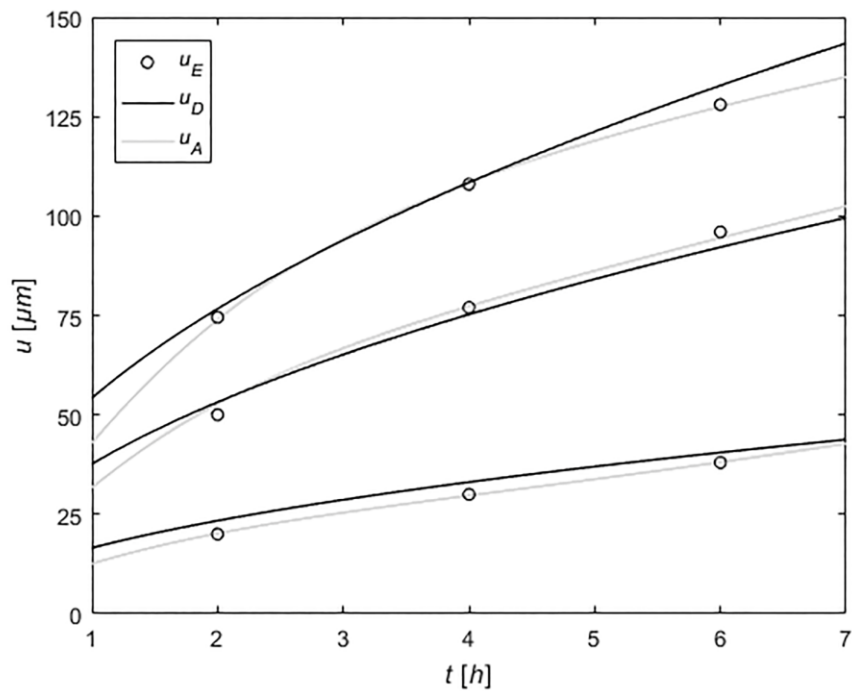
Figure 98. *Simulation of the boride layer thickness formed on C38 steel by the presented artificial neural network and the diffusion model.*

V.3.2. Established works

Finishing off, regarding the published works on the field, this thesis was built correspondingly upon the findings of four published papers. Two co-authored, [176] and [175], regarding modeling FeB/Fe₂B bi-phase layers, along with two others as the principal author, [179] and [178], regarding modeling Fe₂B mono-phase layers. Only the last two papers will be presented.

A.   Confronting linear and nonlinear models

As a parallel work to the first presentation, in this paper, the empirical linear model was applied to the liquid boriding of the C38 steel experiment [174], and compared to the diffusion model [185]. Doing so allowed a thorough confrontation between a linear and a nonlinear model [179]. This comparison helps in investigating if using lesser variables, only temperature T and time t, rather than others, such as incubation time t_0, boron concentrations C, growth rate constants k, and diffusion coefficients D, can be accurate and conceivable in predicting boride layer thicknesses.

Primarily, the paper begins by elaborating on the theories behind both the nonlinear model [185] and the linear model, which is based on a type of regression referred to either as multilinear regression or multiple linear regression MLR [145,187]. Subsequently, both models are simulated and compared by assessing their errors. The purpose was to ascertain if using engineering lenses via an empirical linear model rather than a theoretical one, which is based on physical laws and more variables, can be of use in the studies of Fe₂B boride layer kinetics.

a)   Simulation

The linear model used an equation of similar form to equation (65) with different values of the coefficients, given in Table 32. Both models, the linear u_L and the nonlinear u_D, are simulated in Figure 99, representing the predicted Fe₂B boride layer thicknesses u_{pre} formed on the C38 steel after salt bath boriding with respect to time for three temperatures, 850, 950, and 1000 °C.

Table 32. Coefficients of the linear model [179].

Coefficient	c_0	c_1	c_2	c_3
$[10^{-3}]$	- 199000	245.2381	- 46875	60.7143
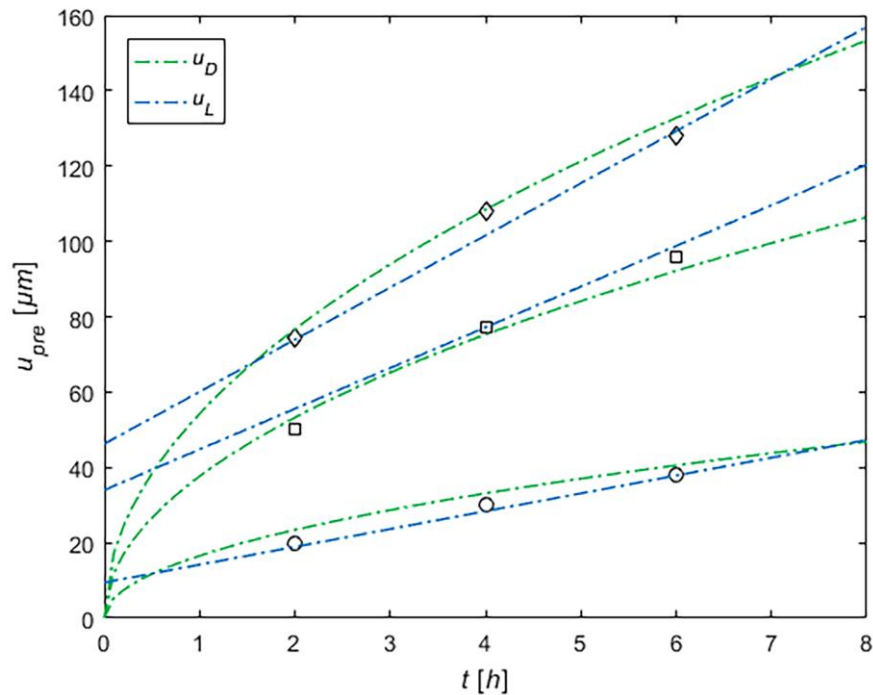
Figure 99. *Simulation of the boride layer thickness formed on C38 steel*
by the linear and nonlinear models [179].

From Figure 99, it can be observed that the linear model before 2 and after 6 hours of treatment times provides questionable predictions, especially at the beginning of the experiment, predicting the presence of a boride layer without even proceeding with the boriding treatment. Thus, the linear model should only be considered within the scope of the studied interval, which was from 2 to 6 hours of treatment time. The predictions of both models regarding the experimental points are given in Table 33 along with their residuals, also plotted in Figure 100 for better discernibility.

Table 33. *Values of the boride layer thicknesses formed on C38 steel*
by the linear and nonlinear models [179].

u_{pre} [μm]	T [$^\circ C$]	t [h] 2	4	6	Residuals		
	850	23.41	33.11	40.55	3.41	3.11	2.55
u_D	950	53.22	75.26	92.17	3.22	-1.74	-3.83
	1000	76.68	108.44	132.82	2.18	0.44	4.82
	850	18.92	28.38	37.85	-1.08	-1.62	-0.15
u_L	950	55.58	77.19	98.80	5.58	0.19	2.80
	1000	73.92	101.60	129.27	-0.58	-6.40	1.27
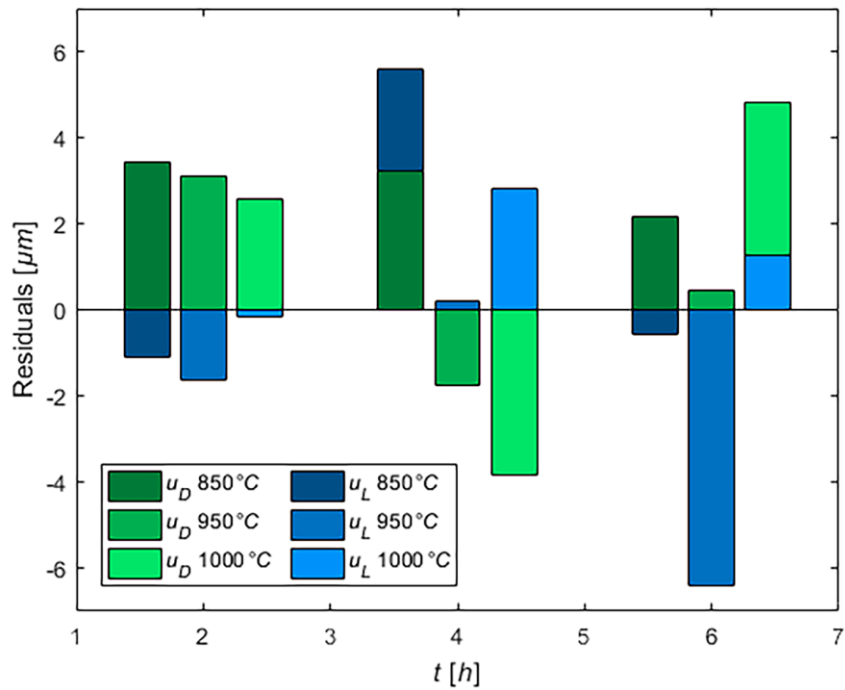
Figure 100. *Both the linear and nonlinear models' residuals* [179].

b)   Errors assessment

From Table 33 and Figure 100, even though the predictions of the linear model differ from those of the nonlinear model, the linear model had two poor predictions while the nonlinear had only one. As a whole, the linear model was more accurate in seven out of the nine predictions.

Furthermore, the linear model was observed to have more negative residuals than the nonlinear one. For certain use cases, having more negative residuals is better than positive ones because predicting a layer thickness less than its actual value is more preferred. Accordingly, the nonlinear model having only two negative residuals may be detrimental in those specific use cases.

Moreover, other than the minimal and maximal errors, two statistical metrics were used for further comparison in Table 34, the mean absolute error MAE, equation (69), and the standard error of the estimate SEE, equation (70).

$$MAE = \frac{1}{n}\sum_{i=1}^{n}| u_i - \bar{u} | \tag{69}$$

$$SEE = \sqrt{\frac{\sum_{i=1}^{n}(u_i - \bar{u})^2}{n - 2}} \tag{70}$$

Where: u_i denotes the predicted value, $\bar{u}$ actual value, and n number of predictions.

Table 34. *Both the linear and nonlinear models' overall errors* [179].

Model	MAE	SEE
u_D	2.81	3.46
u_L	2.19	3.50

The results of the two statistical metrics, Table 34, show an insignificant difference of 0.04 between the models in the standard error of the estimate SEE and a favorable mean absolute error MAE for the linear model over the nonlinear one by 0.62. Besides, each model's actual predictions had the mean absolute error added and minimized to it, providing a range of acceptable errors, Figure 101. From that, it was observed that the nonlinear model had five out of nine predictions out of the scope but nearing it, while the linear model had only three, with two being quite far, indicating that the nonlinear model is slightly more reliable when it comes to the mean absolute error. Still, considering that the linear model uses lesser variables, it can be said that it is still relatively acceptable.
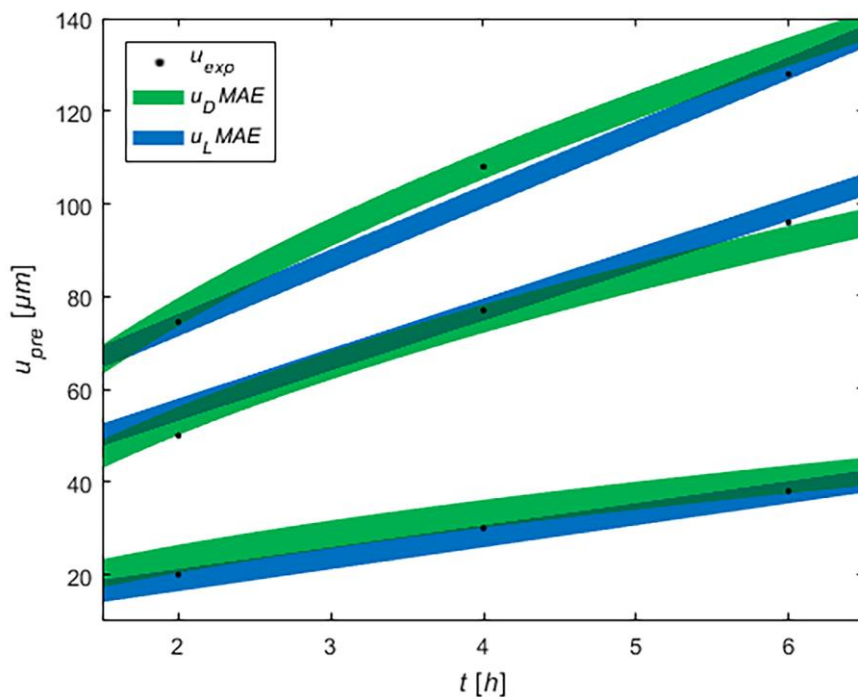
Figure 101. *Scope of the mean absolute error MAE along each predicted point for both the linear and nonlinear models* [179].

c)   Iso-thickness diagram

Plotting the formation of the boride layer three-dimensionally with respect to temperature and time displays a surface plot, Figure 102, which allows to see that the influence of temperature is more significant than that of time in the growth of the boride layer thickness. Correspondingly, it can also be visioned as a two-dimensional plot contour recognized as the iso-thickness diagram, Figure 103.

Other predictions of the boride layer thickness were estimated at 2, 3, and 5 h with a temperature of 850, 850, and 1000 °C, respectively. The results are encircled in the iso-thickness diagram within Figure 103 and given in Table 35.
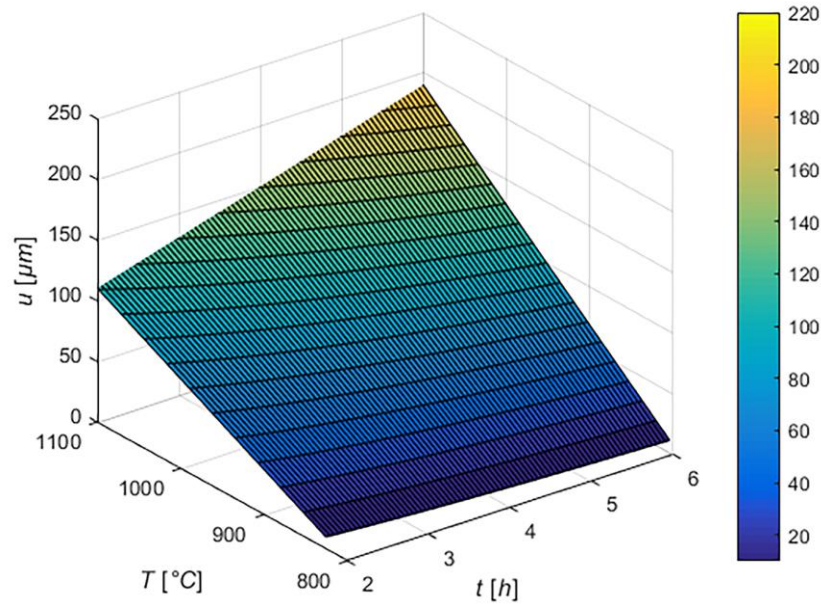
Figure 102. *Three-dimensional simulation of the boride layer thickness with respect to temperature and time* [179].
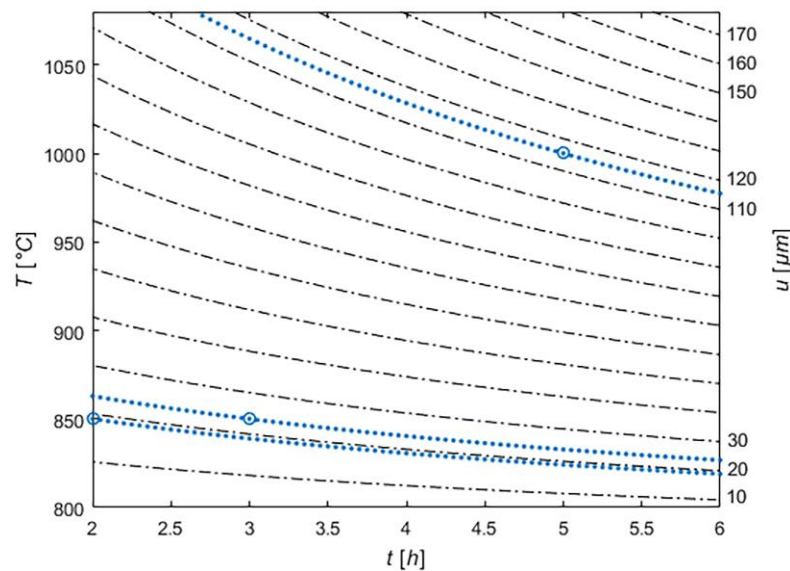
Figure 103. *Iso-thickness diagram of the borided C38 steel by means of the linear model* [179].

The boride layer thickness can be taken instantly graphically by means of the iso-thickness diagram. According to it, Boriding for 3 h at 850 °C forms a boride layer of nearly 24 μm, which is found if calculated using the coefficients given in Table 32 as 23.65 μm. The same thing is seen for other identified instances, Table 35.

Table 35. Iso-thickness diagram's graphical and calculated predictions [179].

Temperature [°C]	850	850	1000
Time [h]	2	3	5
Calculated u_L [μm]	18.92	23.65	115.43
Graphical u_L [μm]	19	24	115

d)   **Discussions and interpretations**

Through an engineer's lens, empirical models such as the one thoroughly examined, the linear model, give decent estimations regarding the simulation of boride layer thicknesses even though it uses only two variables from experimental data, temperature and time. However, extrapolating its predictions beyond the studied scope may lead to detrimental results.

An advantage of the linear model over the nonlinear one is that it often gives predictions that are nearer or inferior to the actual value, i.e. negative residuals, and that is favorable when it comes to predicting a layer thickness since expecting less and getting more is beneficial in the end, contrary to predicting a certain thickness and ending up with less which was more the case of the nonlinear model.

the iso-thickness diagram is a valuable engineering tool that helps determine graphically the temperature T and the treatment time t required for any desired boride layer thickness u, with minor reading errors as seen in Table 35.

While the results are representative of this specific Fe_2B boride layer formed on C38 steel after liquid boriding, it can be said that the approach is valid for other substrates and boriding techniques. Even for the FeB/Fe_2B dual-phase boride layers.

B.   **Impact of diffusion coefficient deduction**

The second paper addressed the impact of the diffusion coefficient deduction on the simulation of boride layer thicknesses [178]. This deduction is done through an estimate of the pre-exponential constant, also referred as the frequency factor, and the activation energy from each temperature's growth rate constants. Additionally, the influence of the incubation time on the simulation was also investigated in the end.

Both the previously given used experiments, powder boriding of Armco iron [173] and liquid boriding of C38 steel [174], Figure 104, were modeled using an approach that is based on the integral model. Initially, the incubation time was disregarded to simplify things. Then, it was investigated if disregarding it hinders the simulations.
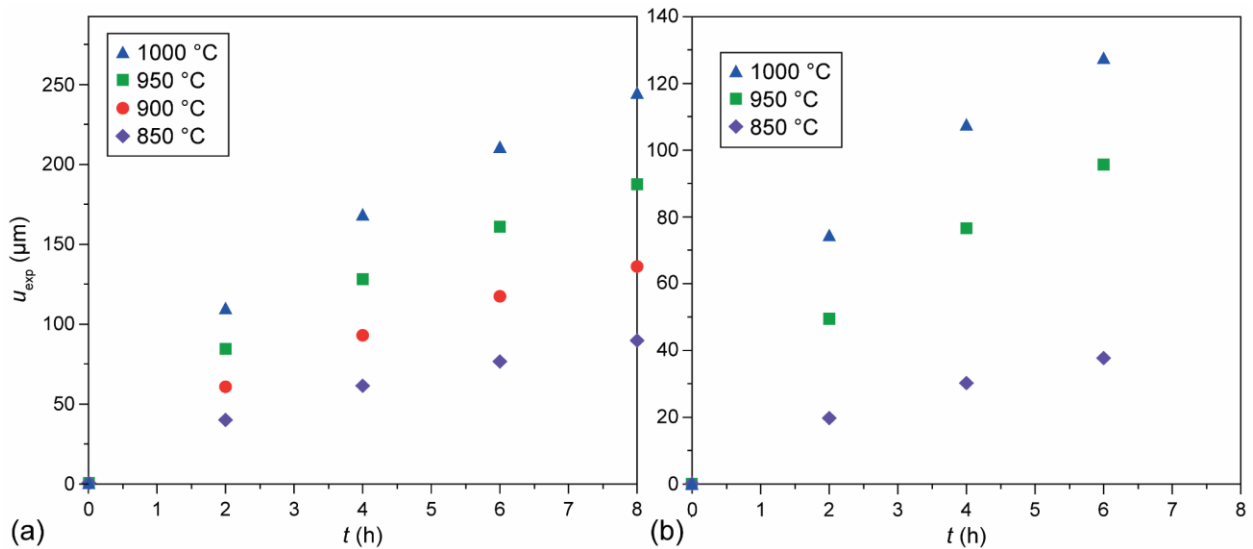
Figure 104. Experimental boride layer thicknesses over treatment times at different boriding temperatures for both the borided (a) Armco Iron [173] and (b) C38 Steel [174] substrates [178].

a)   Diffusion coefficient deduction

Calculation steps are explained through the first experiment, the borided Armco iron substrate, while the results of both experiments, Borided Armco iron and C38 steel, are given and interpreted separately.

The calculations start by extracting the growth rate constants at each point of the experiment using equation (71), which represents the experimental boride layer thicknesses as a function of the growth constant k and time t. The calculated growth rate constants are arranged in Table 36.

$$u_{exp} = k\sqrt{t} \tag{71}$$

Table 36. The set of growth rate constants [178].

$T\,[°C]$	k_T^{2h}	k_T^{4h}	k_T^{6h}	k_T^{8h}	k_T^{mean}
850	0.4754	0.5123	0.5241	0.5299	0.5104
900	0.7198	0.7772	0.7953	0.8043	0.7742
950	0.9911	1.0683	1.0927	1.1047	1.0642
1000	1.2901	1.3903	1.4223	1.4379	1.3852

Generally, researchers take the changes in the growth rate constant based on the temperature k_T for a fixed treatment time, either $2h$, $4h$, or else. This approach proposes the usage of the mean of the changes found in each treatment time through equation (72), and its results are given in Table 36.

$$k_T^{mean} = \frac{\left(\sum_{i=t}^{n} k_T^i\right)}{n} \tag{72}$$

Where: k_T^{mean} is the mean of each temperature's growth rates, and $i = 2h, 4h, 6h$ ... depending on the experiment.

The diffusion coefficient can be calculated using equation (73), obtained from the integral method. However, different diffusion coefficients can be deduced from the changes in growth rates constants k_T at each fixed treatment time. Hence why, the title of the study, impact of the diffusion coefficient calculation on predicting Fe$_2$B boride layer thickness [178].

$$D_T = \eta k^2 \tag{73}$$

Where: η is a constant that is based on boron concentrations found in the boride layer, as given in the previous chapter within the integral model.

Taking, for example, the changes in the growth rate constant for a treatment time of 2 hours, the calculated diffusion coefficient constants for each temperature in 2 hours of treatment D_T^{2h} are given in Table 37.

Table 37. *Diffusion coefficients calculated from the set of growth rate constants obtained from two hours of treatment time at different temperatures* [178].

T [°C]	850	900	950	1000
k_T^{2h} [$\mu m/s^{0.5}$]	0.4754	0.7198	0.9911	1.2901
D_T^{2h} [$\mu m^2/s$]	3.0100	6.9006	13.0822	22.1656

Subsequently, a diffusion coefficient function can be deduced by the Arrhenius relationship, equation (74), after plotting the natural logarithm of the calculated diffusion coefficient constants, Table 37, with respect to the reciprocal of temperature, Figure 105.

$$D_T = D_0 \exp\left(-\frac{Q}{RT}\right) \tag{74}$$

Where: D_0 is the frequency factor, and Q the activation energy, both as parameters of the diffusion coefficient D_T.
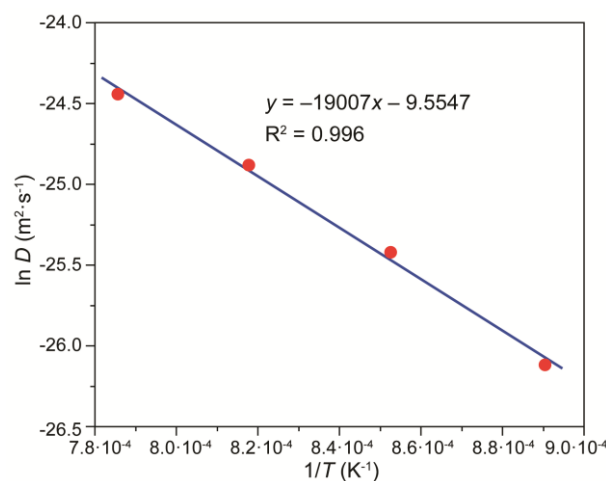
Figure 105. *Natural logarithm of the diffusion coefficient with respect to the reciprocal of temperature for a treatment time of 2 hours* [178].

From a linear fitting applied in Figure 105, a diffusion coefficient function D_T^{2h} is deduced, equation (75), based on the approach that uses the growth rate constants of 2 h of treatment time k_T^{2h}. The same calculations are repeated for the other treatment times, each representing an approach, and the parameters of each deduced diffusion coefficient are given in Table 38.

$$D_T^{2h} = 7{,}0870 \ 10^{-5} \ exp \left(- \frac{158{,}0266 \ kJ/mol}{RT} \right)$$

(75)

Table 38. *Activation energies and frequency factors of the different deduced diffusion coefficients* [178].

Substrate	D_T^i		D_T^{2h}	D_T^{4h}	D_T^{6h}	D_T^{8h}	D_T^{mean}
Armco iron	$D_0 \ 10^{-5}$		7.0870	8.1806	8.5565	8.7262	8.1246
	Q		158.0266	157.9562	157.9500	157.9263	157.9632
C38 steel	$D_0 \ 10^{-3}$		3.719	2.950	1.171	-	2.327
	Q		208.549	205.091	195.736	-	203.053

b)   Boride layer thickness simulation

After the deduction of each diffusion coefficient, D_T^{2h}, D_T^{4h}, D_T^{6h}, D_T^{8h} and that of the proposed approach D_T^{mean}, their use in equation (76) provides different simulations of the Fe₂B boride layer thickness, illustrated in Figure 106.

$$u = \sqrt{\frac{D_T^i \ t}{\eta}}$$

(76)

Where: D_T^i represents the deduced diffusion coefficient for each approach $i = 2h, 4h \ ...$
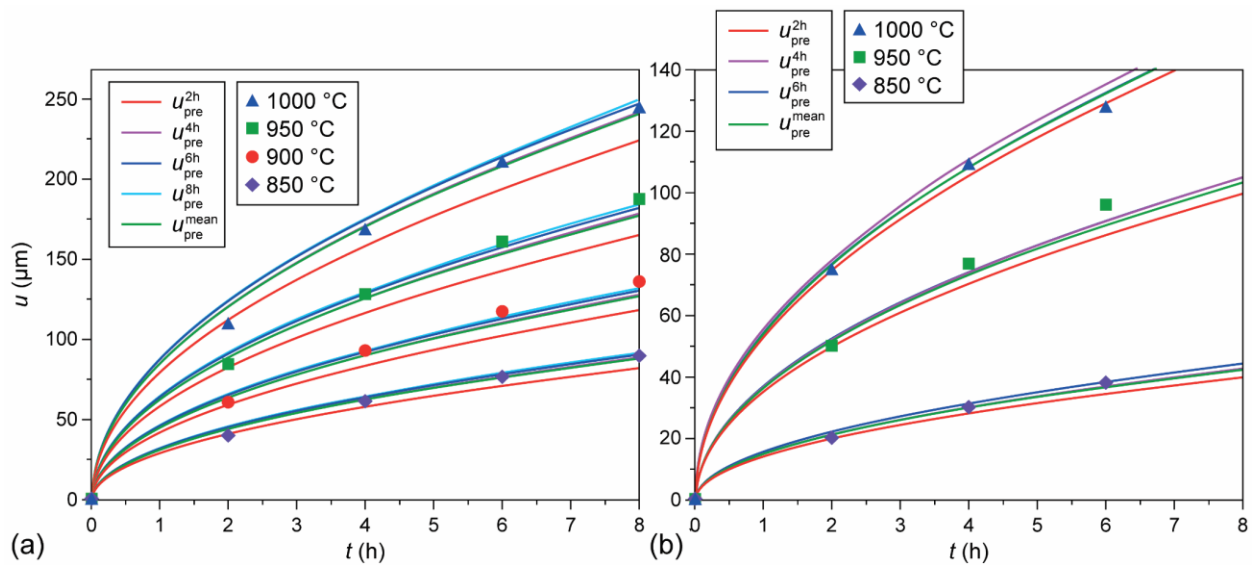
Figure 106. *Simulations of the boride layer thickness formed on (a) Armco iron and (b) C38 steel* [178].

153

c)   Errors assessment

To assess the impact of the differed diffusion coefficients deduced, their generated errors regarding the predictions $Errors_{pre}^i$ are assessed using the standard error of the estimate SEE, equation (70), the mean absolute error MAE, equation (69), and the minimal and maximal errors, Table 39. Along with diagrams, Figure 107, representing the standard error of the estimate SEE for each approach and at each treatment time $SEEt$.

Table 39. *SEE, MAE and min-max errors of each approach's predictions on Armco iron and C38 steel substrates* [178].

Substrate	Armco iron					C38 steel			
Approach	u_{pre}^{2h}	u_{pre}^{4h}	u_{pre}^{6h}	u_{pre}^{8h}	u_{pre}^{mean}	u_{pre}^{2h}	u_{pre}^{4h}	u_{pre}^{6h}	u_{pre}^{mean}
SEE	12.93	5.72	5.91	6.62	5.87	4.71	4.07	3.27	3.53
MAE	9.91	4.26	4.49	4.97	4.41	2.78	2.93	2.46	2.37
Min Err	1.00	0.19	0.62	0.27	0.09	0.01	0.31	0.45	0.05
Max Err	22.32	11.32	14.10	15.46	10.87	9.60	7.44	4.99	6.46
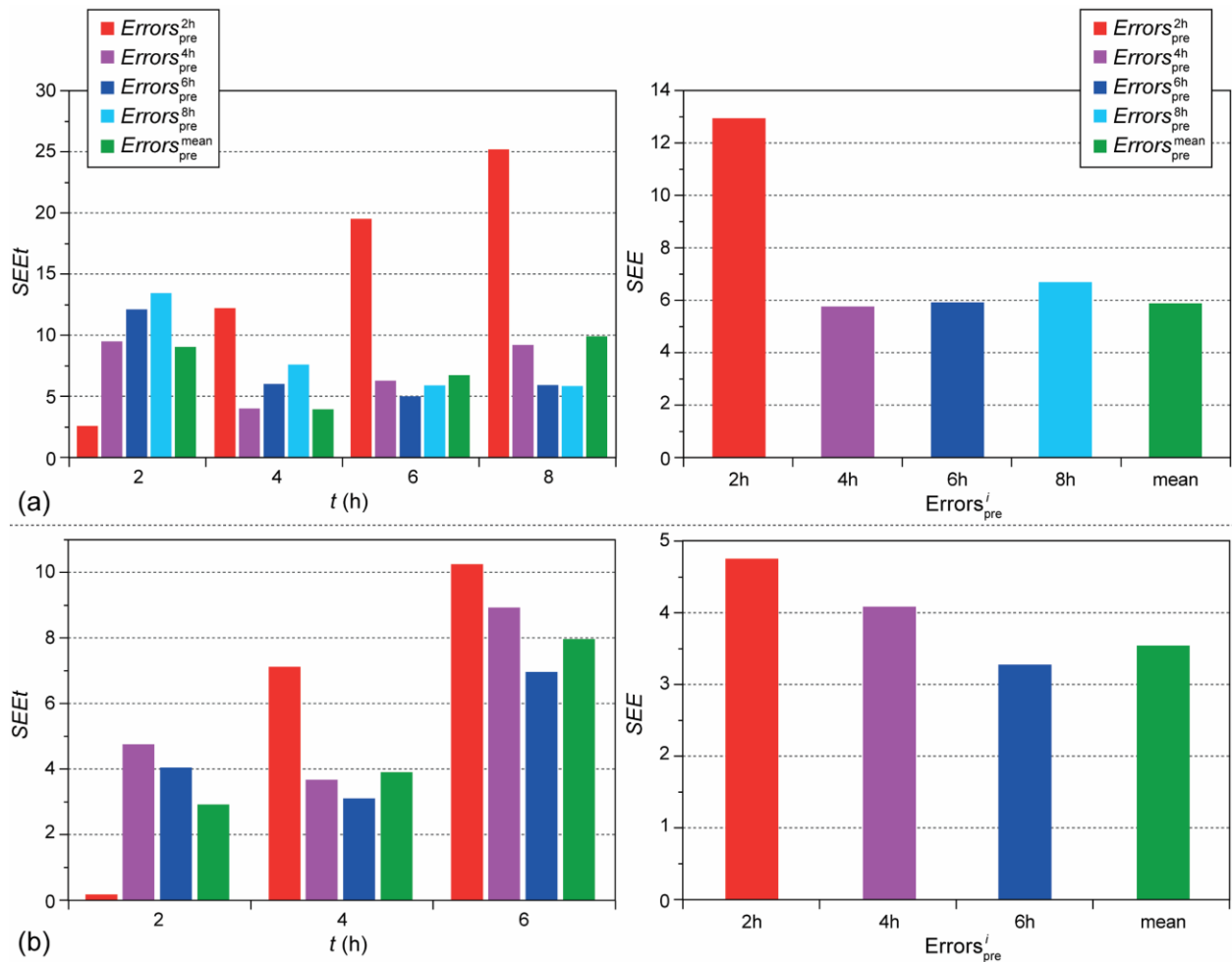
Figure 107. *Diagrams of the standard error of the estimate found within each treatment time SEEt and for each approach SEE when predicting boride layer thicknesses formed on (a) Armco iron and (b) C38 steel* [178].

The first diagram in Figure 107 illustrate the inaccuracies of each approach regarding the Armco iron predictions, where when focusing on the red ones, which refer to deducing the diffusion coefficient based on 2 hours of treatment time D_T^{2h} impacts the prediction of the boride layer thickness u_{pre}^{2h} by concentrating mainly on the predictions of 2 hours, leading to inaccurate results regarding the others and an overall standard error of the estimate of more than 12. This is explained in the standard error of the estimate at each treatment time, where it is lower than 2.5 for 2 h compared to more than 10, near 20, and more than 25 for 4, 6, and 8 hours, respectively. The same is observed regarding the other deduced diffusion coefficients D_T, and for the C38 steel substrate.

Moreover, in agreement with both Figure 107 and Table 39, the finest results in the borided Armco iron were those deduced from 4 h of treatment time u_{pre}^{4h}, while in the borided C38 steel, it was those deduced from 6 h of treatment time u_{pre}^{6h}. Hence why, a generalized mean approach u_{pre}^{mean} was proposed [178] to get decent and fine results without deducing the boron diffusion coefficient according to an arbitrary treatment time, which can end up with less accurate predictions, unknowingly.

d)   Incubation time influence

To see the impact of disregarding the incubation time, the proposed results u_{pre}^{mean}, which predict the boride layer thickness without considering the incubation time [178], are compared to models that did $u_{pre}^{incubation}$, the integral model with incubation time regarding Armco iron [182], and the diffusion model with incubation time regarding C38 steel [185]. The simulations of these models are given in Figure 108 and their errors are provided in Table 40.
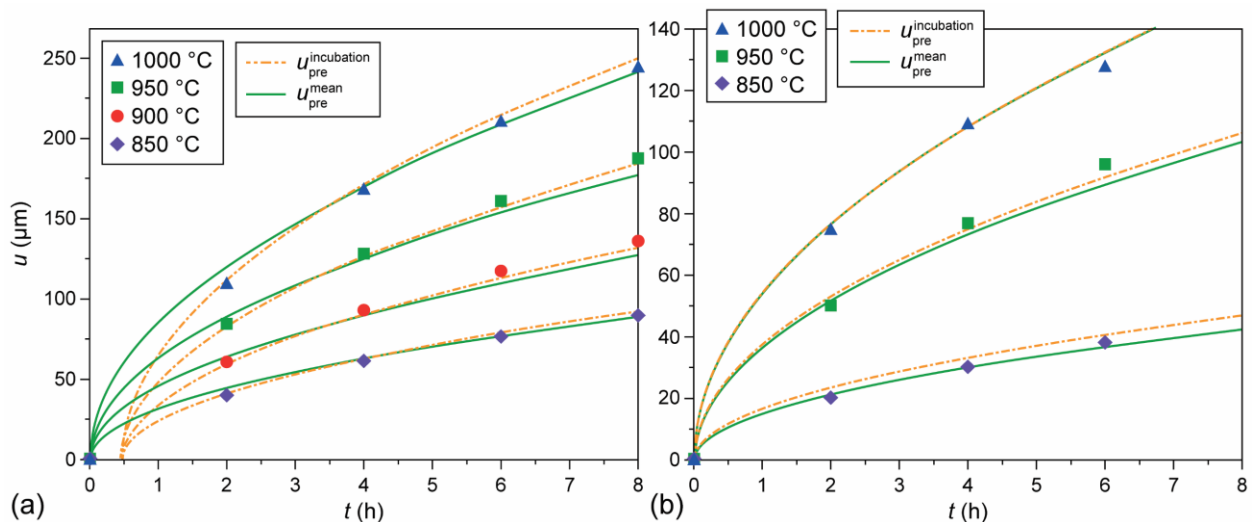
Figure 108. *Simulation of boride layer thicknesses by a model that considers the incubation time and another proposed which does not for (a) Armco iron and (b) C38 steel* [178].

Table 40. Errors of a model that considers the incubation time and another proposed which does not when predicting boride layer thicknesses of Armco iron and C38 steel substrates [178].

Substrate	Armco iron		C38 steel	
Approach	u_{pre}^{mean}	$u_{pre}^{incubation}$	u_{pre}^{mean}	$u_{pre}^{incubation}$
SEE	5.87	3.44	3.53	3.46
MAE	4.41	2.94	2.37	2.81
Min Err	0.09	1.06	0.05	0.44
Max Err	10.87	5.91	6.46	4.82

From both Figure 108 and Table 40, it can be said that even though the incubation time was disregarded in the proposed approach, taking all data into account using the mean of the growth rate constants k_T^{mean}, helped provide predictions that are balanced, decent, and even comparable to the models that considered the incubation time.

e)   Discussions and interpretations

The diffusion coefficient is the main factor impacting the predictions' accuracies when studying the kinetics growth of Fe₂B boride layers' thicknesses. Its deduction is influenced by the choice of the set of growth rate constants. As elucidated in the first impact.

The proposed approach disregarded the incubation time and was based on using the proposed mean set of growth rate constants, equation (72), of all the available experimental data to deduce the mean diffusion coefficient that helps simulate accurate boride layer thicknesses, avoiding choosing an arbitrary set of growth rate constants of a specific treatment time and ending up with less accurate overall predictions, unknowingly.

Additionally, for the last point in the first experiment, where after powder boriding the Armco iron for 5 h at 980 °C, the proposed model predicts that the formed boride layer would be 168.91 μm. That prediction had an error of -6,34 compared to the given experimental thickness, 175.25 μm, and that is not far from the given tolerance ± 12.15 μm [173]. Additionally, even though the model did not consider the incubation time in its calculations, the accuracy was comparable to other models that did regarding this new point, Table 28, and even other points, as seen in Figure 108 and confirmed in Table 40.

All and all, the use of two different boriding techniques, liquid and powder, along with two different substrates, Armco iron and XC38 steel, helped in confirming and validating the proposed approach by observing consistent and similar conclusions on both of them regarding the simulation of the Fe₂B boride layer kinetics. The approach can also be applied to FeB/Fe₂B dual-phase boride layers.

V.4.   OBSERVATIONS

The observations regarding the machinable materials were, as observed for other examples in the previous chapters, low alloying means better boron diffusion and, therefore, thicker boride layers. Compared to C38 steel, the Armco iron is a purer ferrous material. Hence why, the thicker layers simulated on the Armco iron. Additionally, if the C38 steel had not been annealed before boriding, lesser boride layer thicknesses would have been observed because the annealing helped reduce the substrate's grain size for better boron diffusion.

Modeling the kinetics of boride layers through multiple models helped in viewing the possibilities regarding the accuracy of each one. Empirical models based on regression provide good accuracies if they are linear and better ones if they are nonlinear, and from an engineering perspective, that is good enough. Models that are based on physical governing laws, like the parabolic growth model or the integral model, hold the middle ground, with great accuracies that can be interpreted and explained from a scientific point of view, affirming the boron diffusion as a controlled process. As for the artificial neural network models, they have the upper hand due to their effective and excellent ability to learn and adapt to the data with numerous factors.

However, if the predictions of the simulations were to be extrapolated outside the scope of the studied intervals, empirical models tend to fall flat, especially the linear models, due to their lack of physical sense. The nonlinear ones depend on the chosen formula; certain ones may go beyond the scope by a certain margin. Artificial neural networks need more investigations, as they may and may not give bad predictions outside the scope. One work on the matter was not conclusive enough to imply factual observations. Regardless of that, they have great potential for simulating boride layers.

On the other hand, regarding the approach that was based on the integral model, which studied the impact of the diffusion coefficient deduction, it was put forward that certain studies used to base their modeling on a portion of the data, for example, extracting growth rate constants from only 2 hours of treatment time and deducing the diffusion coefficient accordingly, and with the residuals' assessment given in the work, it was interpreted to result in not wholly inaccurate predictions, but rather inferior ones. To avoid that, and for optimal predictions, it was proposed to use the mean set of growth rate constants through equation (72).

Optimizing the modeling of boride layer growth provides better, accurate, and therefore accurate selection of the technological boriding parameters that give the proper desired thickness, tailored to the intended applications, abrasive wear, adhesive wear, and so on.

General Conclusion

I n conclusion, this exploration has shed light on the fascinating world of boron diffusion. Starting from the versatility of boron compounds, other than their usage in numerous application fields, their specific usage as boron sources for the diffusion process. Whether as nonmetallic, such as boron carbide B_4C, the third hardest existing compound, borax $Na_2B_4O_7$ or boric acids $B(OH)_3$, abundant natural borates, diborane B_2O_3, a toxic gas, all different boron sources.

The mechanical and chemical properties of borided materials depend mainly on:

- The technique of boriding, traditional or modern, with solid, liquid, gas, plasma, ions, or else.
- The composition of the substrate material, including its alloying elements.
- The borides formed within the layer and their morphology.
- The layer thickness.

The boriding techniques split mainly in two groups, traditional and modern. Traditional ones can be with solid compounds in the form of powder or paste, liquid with different approaches, or gas with two main different gas types. As of the modern ones, they are through plasma, ion implantation, and other mixed approaches. Traditional techniques are often performed at high temperatures, promoting deeper diffusions and thicker boride layers. However, doing so can lead to more significant distortion and residual stresses. On the other hand, modern techniques offer better control over the process parameters, enabling thinner and more uniform layers with less distortion, but with the downside of being complicated and expensive.

Focusing on the boron source, higher content means higher flux, therefore the formation of a more brittle boron rich boride layer, which can be problematic. For example, in ferrous materials, lowering boron content in the source was observed to reduce the flux, resulting in a more controlled diffusion and a formation of a single phase Fe_2B boride layer, which is ideal. Contrary to the augmentation, which results in the formation of a second phase FeB on top of the Fe_2B phase, hence a bi-layer. FeB is richer in boron than Fe_2B, making it more brittle, and when the substrate is soft. The difference of gradient between the layers, both in hardness and residual stresses, was observed to promote crack formations during cooling, or to spalling after some mechanical strain.

This problem can be resolved through additional treatments like annealing to reduce the brittle boron rich phase FeB and promote more boron diffusion towards the substrate, homogenizing and thickening the more desirable Fe_2B phase, as it has a good balance of toughness and hardness.

Moreover, annealing the boron source before boriding was observed to promote better boride layer morphology. Annealing refines the grains of the mixture containing boron, and finer grains are more uniformly distributed during diffusion, offering superior properties compared to coarse ones.

Investigating the different machinable materials to be borided, they are mostly ferrous, with some other metals like nickel and hard metals like titanium, with the exception of some. And with all of them, it was observed that before boriding, the type and amount of alloying elements within the substrate material significantly influence the diffusion process.

Regarding the amount, the lower the alloying, the better the diffusion. However, low alloyed materials tend to be softer, so careful processing should be required so as not to end up with the gradient problem highlighted before. As for the type of elements alloyed, certain ones like chromium or nickel don't pose a problem and can even enhance the formation of desirable borides within the primary phase or phases, but others like carbon and aluminum can hinder the diffusion and limit the formation of beneficial borides or promote the formation of less desirable phases with lower performance.

As of the boride layer thickness, the key aspect affecting boride layer properties, thicker layers typically offer greater wear resistance but may also lead to increased brittleness and potential for spallation if not properly controlled, while thinner layers provide a balance of improved wear resistance without compromising the substrate's toughness.

From that, encompassing the structured and gathered knowledge presented in the previous chapters, along with most of the plausible models and simulations regarding the kinetics of boride layers, be they deterministic or non-deterministic models, helped in providing a holistic understanding and representation of the boron diffusion.

The boron diffusion, as modeled and simulated in the last two chapters, is mainly affected by two critical parameters, the treatment time and the temperature exposure, with the temperature having a greater impact. The selection of these technological parameters provides the desired thickness that is demanded from the intended application.

The last observations regarding the machinable materials confirmed that low alloying promotes better boron diffusion and thicker boride layers, as seen in the simulations, where boriding Armco iron, a pure ferrous material, resulted in thicker layers compared to C38 steel, a medium alloy ferrous material.

Lastly, as a last induced observation regarding the models' simulations concerning the boron diffusion, the empirical models had acceptable predictions, the integral model that uses a physically governed law had more adequate predictions that are justified scientifically, while the artificial neural network model had the best predictions due to its learning capability making it an interesting choice in future works on establishing optimized and accurate simulations of the boride layer thicknesses.

References

[**1**]   J. T. Kloprogge, C. P. Ponce, and T. A. Loomis, *The Periodic Table: Nature's Building Blocks An Introduction to the Naturally Occurring Elements, Their Origins and Their Uses*. 2020. DOI: 10.1016/C2019-0-03114-7

[**2**]   Y. Zhu, *Fundamentals and Applications of Boron Chemistry*. Elsevier, 2022. DOI: 10.1016/C2019-0-00779-0

[**3**]   W. M. Haynes, *CRC Handbook of Chemistry and Physics (95th ed.)*. CRC Press, 2014. DOI: 10.1201/b17118

[**4**]   W. H. Jin, C. Seldon, M. Butkus, W. Sauerwein, and H. B. Giap, *A Review of Boron Neutron Capture Therapy: Its History and Current Challenges*, International Journal of Particle Therapy, vol. 9, no. 1, pp. 71–82, 2022, DOI: 10.14338/ijpt-22-00002.1

[**5**]   A. K. Khanra, *Production of boron carbide powder by carbothermal synthesis of gel material*, Bulletin of Materials Science, vol. 30, no. 2, pp. 93–96, 2007, DOI: 10.1007/s12034-007-0016-7

[**6**]   J. R. Davis, *Surface Hardening of Steels: Understanding the Basics*. ASM International, 2002. DOI: 10.1361/shos2002p001

[**7**]   E. J. Mittemeijer and M. A. J. Somers, Eds., *Thermochemical Surface Engineering of Steels: Improving Materials Performance*. Woodhead Publishing, 2015. ISBN: 9780857096524

[**8**]   Q. J. Wang, *Encyclopedia of Tribology*. Boston, MA: Springer US, 2013. DOI: 10.1007/978-0-387-92897-5

[**9**]   M. G. Krukovich, B. A. Prusakov, and I. G. Sizov, *Plasticity of Boronized Layers*, vol. 237. in Springer Series in Materials Science, vol. 237. Cham: Springer International Publishing, 2016. DOI: 10.1007/978-3-319-40012-9

[**10**] M. Kulka, *Current Trends in Boriding*. in Engineering Materials. Cham: Springer International Publishing, 2019. DOI: 10.1007/978-3-030-06782-3

[**11**] C. Martini, G. Palombarini, and M. Carbucicchio, *Mechanism of thermochemical growth of iron borides on iron*, Journal of Materials Science, vol. 39, no. 3, pp. 933–937, 2004, DOI: 10.1023/B:JMSC.0000012924.74578.87

[**12**] J. L. Dossett and G. E. Totten, Eds., *ASM Handbook: Steel Heat Treating Fundamentals and Processes*. ASM International, 2013. DOI: 10.31399/asm.hb.v04a.9781627081658

[**13**] W. Fichtl, *Boronizing and its practical applications*, Materials and Design, vol. 2, no. 6, pp. 276–286, 1981, DOI: 10.1016/0261-3069(81)90034-0

[**14**] P. A. Dearnley and T. Bell, *Engineering the Surface with Boron Based Materials*, Surface Engineering, vol. 1, no. 3, pp. 203–217, 1985, DOI: 10.1179/sur.1985.1.3.203

[**15**] J. X. Prochaska, J. C. Howk, and A. M. Wolfe, *The elemental abundance pattern in a galaxy at z = 2.626*, Nature, vol. 423, no. 6935, pp. 57–59, 2003, DOI: 10.1038/nature01524

[**16**] W. M. White, Ed., *Encyclopedia of Geochemistry*. in Encyclopedia of Earth Sciences Series. Cham: Springer Cham, 2020. DOI: 10.1007/978-3-319-39193-9

[**17**] W. G. Woods, *An introduction to boron: History, sources, uses, and chemistry*, Environmental Health Perspectives, vol. 102, no. 7, pp. 5–11, 1994, DOI: 10.1289/ehp.94102s75

[**18**] M. P. Crosland, *Louis Joseph Gay-Lussac*, Encyclopedia Britannica, 2023. Accessed: 12/01/2023. URL: britannica.com/biography/Joseph-Louis-Gay-Lussac

[**19**] Britannica Editors, *Louis-Jacques Thenard*, Encyclopedia Britannica, 2023. Accessed: 12/01/2023. URL: britannica.com/biography/Louis-Jacques-Thenard

[20] F. W. Gibbs, *Sir Humphry Davy*, Encyclopedia Britannica, 2023. Accessed: 12/01/2023. URL: britannica.com/biography/Sir-Humphry-Davy-Baronet

[21] W. Haynes, *Portrait of Ezekiel Weintraub*, Portrait Collection Box 16, Science History Institute, Philadelphia., 1958. Accessed: 12/01/2023. URL: digital.sciencehistory.org/works/zg64tk959

[22] E. Weintraub, *On the properties and preparation of the element boron*, Industrial and Engineering Chemistry, vol. 3, no. 5, pp. 299–301, 1911, DOI: 10.1021/ie50029a007

[23] J. Emsley, *Nature's Building Blocks: An A-Z Guide to the Elements (2nd ed.)*. Oxford University Press, 2011. ISBN: 9780199605637

[24] F. Bortz, *The Periodic Table of Elements and Dmitry Mendeleyev*. Rosen Young Adult, 2014. ISBN: 9781477718070

[25] E. Boldyreva and P. Dera, Eds., *High-Pressure Crystallography*. in NATO Science for Peace and Security Series B: Physics and Biophysics. Dordrecht: Springer Netherlands, 2010. DOI: 10.1007/978-90-481-9258-8

[26] R. Feather, C. W. McLaughlin, M. Thompson, and D. Zike, *Physical Science with Earth Science*. Glencoe and McGraw Hill, 2008. ISBN: 9780078802485

[27] B. Hönisch and J. Hall, *Paleoceanography, physical and chemical proxies | Carbon cycle proxies*, Encyclopedia of Quaternary Science, pp. 1699–1710, 2007, DOI: 10.1016/B0-44-452747-8/00312-4

[28] D. R. Metcalf, *Nuclear Reactor Theory*, Nuclear Technology, vol. 12, no. 4, pp. 415–416, 1971, DOI: 10.13182/nt71-a30994

[29] P. C. Hewlett, *Lea's Chemistry of Cement and Concrete*. Elsevier, 2003. DOI: 10.1016/B978-0-7506-6256-7.X5007-3

[30] M. F. Hernández, P. V. López, M. S. Conconi, and N. M. Rendtorff, *Effect of boron sources in the thermal behavior of a clay-based ceramics*, Open Ceramics, vol. 9, no. December 2021, 2022, DOI: 10.1016/j.oceram.2022.100227

[31] L. K. Nanver, L. Qi, X. Liu, and T. Knežević, *Nanolayer boron-semiconductor interfaces and their device applications*, Solid-State Electronics, vol. 186, no. May, pp. 4–7, 2021, DOI: 10.1016/j.sse.2021.108041

[32] A. R. Oganov *et al.*, *Ionic high-pressure form of elemental boron*, Nature, vol. 457, no. 7231, pp. 863–867, 2009, DOI: 10.1038/nature07736

[33] W. Hayami, T. Hiroto, K. Soga, T. Ogitsu, and K. Kimura, *Thermodynamic stability of elemental boron allotropes with varying numbers of interstitial atoms*, Journal of Solid State Chemistry, vol. 329, no. September 2023, p. 124407, 2024, DOI: 10.1016/j.jssc.2023.124407

[34] B. E. Douglas and S.-M. Ho, *Structure and Chemistry of Crystalline Solids*, vol. 44, no. 07. New York, NY: Springer New York, 2006. DOI: 10.1007/0-387-36687-3

[35] A. J. Mannix *et al.*, *Synthesis of borophenes: Anisotropic, two-dimensional boron polymorphs*, Science, vol. 350, no. 6267, pp. 1513–1516, 2015, DOI: 10.1126/science.aad1080

[36] X. Sun *et al.*, *Two-Dimensional Boron Crystals: Structural Stability, Tunable Properties, Fabrications and Applications*, Advanced Functional Materials, vol. 27, no. 19, 2016, DOI: 10.1002/adfm.201603300

[37] K. P. Hilleke, T. Ogitsu, S. Zhang, and E. Zurek, *Structural motifs and bonding in two families of boron structures predicted at megabar pressures*, Physical Review Materials, vol. 5, no. 5, p. 053605, 2021, DOI: 10.1103/PhysRevMaterials.5.053605

[38] B. F. Decker and J. S. Kasper, *The crystal structure of a simple rhombohedral form of boron*, Acta Crystallographica, vol. 12, no. 7, pp. 503–506, 1959, DOI: 10.1107/S0365110X59001529

[39] V. L. Solozhenko, O. O. Kurakevych, and A. R. Oganov, *On the hardness of a new boron phase, orthorhombic γ-B28*, Journal of Superhard Materials, vol. 30, no. 6, pp. 428–429, 2008, DOI: 10.3103/s1063457608060117

[40] R. G. Delaplane, U. Dahlborg, W. S. Howells, and T. Lundström, *A neutron diffraction study of amorphous boron using a pulsed source*, Journal of Non-Crystalline Solids, vol. 106, no. 1–3, pp. 66–69, 1988, DOI: 10.1016/0022-3093(88)90229-3

[41] N. Kostoglou, K. Polychronopoulou, and C. Rebholz, *Thermal and chemical stability of hexagonal boron nitride (h-BN) nanoplatelets*, Vacuum, vol. 112, pp. 42–45, 2015, DOI: 10.1016/j.vacuum.2014.11.009

[42] Y. Kimura, T. Wakabayashi, K. Okada, T. Wada, and H. Nishikawa, *Boron nitride as a lubricant additive*, Wear, vol. 232, no. 2, pp. 199–206, 1999, DOI: 10.1016/S0043-1648(99)00146-5

[43] G. V. Samsonov and V. K. Kazakov, *Refractory materials made from boron nitride-silicon nitride and boron nitride-silicon carbide*, Refractories, vol. 6, no. 7–8, pp. 347–352, 1965, DOI: 10.1007/BF01279412

[44] J. ran Xu, C. guang Yan, and C. guang Zhu, *Combustion of B4C/KNO3 binary pyrotechnic system*, Defence Technology, vol. 17, no. 2, pp. 692–702, 2021, DOI: 10.1016/j.dt.2020.10.003

[45] Nathan M, *Electronegativity of the Elements*, 2021. Accessed: 12/01/2023. URL: breakingatom.com/learn-the-periodic-table/electronegativity-of-the-elements

[46] T. Gray, *The Elements: A Visual Exploration of Every Known Atom in the Universe*. Black Dog & Leventhal, 2009. ISBN: 9781579128142

[47] A. Brunning, *The Mohs Mineral Hardness Scale*, Compound Interest, 2022. Accessed: 12/29/2023. URL: compoundchem.com/2022/11/28/mohs-hardness-scale

[48] L. Pizzorno, *Nothing boring about boron*, Integrative Medicine (Boulder), vol. 14, no. 4, pp. 35–48, 2015, URL: ncbi.nlm.nih.gov/pmc/articles/PMC4712861

[49] E. O. Ajayi *et al.*, *The Toxicity of Environmental Pollutants*, vol. 11, no. tourism. IntechOpen, 2022. DOI: 10.5772/intechopen.98127

[50] C. Bindal and A. H. Ucisik, *Characterization of boriding of 0.3% C, 0.02% P plain carbon steel*, Vacuum, vol. 82, no. 1, pp. 90–94, 2007, DOI: 10.1016/j.vacuum.2007.04.039

[51] E. Uhlmann, J. Polte, M. Polte, and T. Hocke, *Boron-doped monocrystalline diamond as cutting tool for temperature measurement in the cutting zone*, Procedia CIRP, vol. 101, no. March, pp. 258–261, 2021, DOI: 10.1016/j.procir.2021.02.026

[52] J. C. LaSalvia, Ed., *Advances in Ceramic Armor XI*. in Ceramic Engineering and Science Proceedings. Wiley, 2015. DOI: 10.1002/9781119211549

[53] P. Kumar *et al.*, *Influence of different grades of CBN inserts on cutting force and surface roughness of AISI H13 die tool steel during hard turning operation*, Materials, vol. 12, no. 1, 2019, DOI: 10.3390/ma12010177

[54] A. O. Maselugbo, H. B. Harrison, and J. R. Alston, *Boron nitride nanotubes: A review of recent progress on purification methods and techniques*, Journal of Materials Research, vol. 37, no. 24, pp. 4438–4458, 2022, DOI: 10.1557/s43578-022-00672-5

[55] W. Liu, P. Feng, X. Ren, and L. Zhu, *Preparation of silicon boride SiB x (x = 3, 4, 5, 6) powders by chemical oven self-propagating combustion synthesis*, International Journal of Materials Research, vol. 111, no. 10, pp. 792–798, 2020, DOI: 10.3139/146.111949

[56] A. W. Weimer, Ed., *Carbide, Nitride and Boride Materials Synthesis and Processing*. Dordrecht: Springer Netherlands, 1997. DOI: 10.1007/978-94-009-0071-4

[57] A. T. Lech, C. L. Turner, J. Lei, R. Mohammadi, S. H. Tolbert, and R. B. Kaner, *Superhard Rhenium/Tungsten Diboride Solid Solutions*, Journal of the American Chemical Society, vol. 138, no. 43, pp. 14398–14408, 2016, DOI: 10.1021/jacs.6b08616

[58] O. Gómez-Vagas *et al.*, *TiN and Boride Layers Obtained by Dehydrated Paste-Pack Boriding and PVD Treatments Formed on AISI M2 Steel*, Microscopy and Microanalysis, vol. 25, no. S2, pp. 770–771, 2019, DOI: 10.1017/s1431927619004586

[59] J. Lin, D. Balint, and M. Pietrzyk, *Microstructure evolution in metal forming processes*. 2012. DOI: 10.1533/9780857096340

[60] B. Parveez, M. I. Kittur, I. A. Badruddin, S. Kamangar, M. Hussien, and M. A. Umarfarooq, *Scientific Advancements in Composite Materials for Aircraft Applications: A Review*, Polymers, vol. 14, no. 22, 2022, DOI: 10.3390/polym14225007

[61] B. McMahon, *Boron in Sports Equipement*, Industry Sectors, 2021. Accessed: 12/01/2023. URL: borates.today/boron-sports-equipment

[**62**] M. Elias-Espinosa *et al.*, ***Investigation of Growth Kinetics of Fe2B Layers on AISI 1518 Steel by the Integral Method***, High Temperature Materials and Processes, vol. 38, no. 2019, pp. 219–228, 2019, DOI: 10.1515/htmp-2017-0166

[**63**] W. B. Rowe, ***Principles of Modern Grinding Technology***. Elsevier, 2014. DOI: 10.1016/C2013-0-06952-6

[**64**] I. Gunes, I. Taktak, C. Bindal, Y. Yalcin, S. Ulker, and Y. Kayali, ***Investigation of diffusion kinetics of plasma paste borided AISI 8620 steel using a mixture of B2O3 paste and B4C/SiC***, Sadhana - Academy Proceedings in Engineering Sciences, vol. 38, no. 3, pp. 513–526, 2013, DOI: 10.1007/s12046-013-0136-2

[**65**] W. E. Bryson, ***Heat Treatment***. München: Carl Hanser Verlag GmbH & Co. KG, 2015. DOI: 10.3139/9781569904862

[**66**] J. L. Dossett and G. E. Totten, Eds., ***Steel Heat Treatment Handbook - 2 Volume Set***. CRC Press, 2006. DOI: 10.1201/9781482293029

[**67**] G. Roberts, G. Krauss, and R. Kennedy, ***Tool Steels, 5th Edition***. ASM International, 1998. ISBN: 978-871705990

[**68**] F. Czerwinski, Ed., ***Heat Treatment - Conventional and Novel Applications***. InTech, 2012. DOI: 10.5772/2798

[**69**] C. Liu, J. bin Shen, C. hua Lin, J. fei Wang, and J. xin Wang, ***Experimental investigation on the subsurface stress distributions in specimens with different strengths after ultrasonic impact treatment***, Journal of Mechanical Science and Technology, vol. 35, no. 5, pp. 2123–2129, 2021, DOI: 10.1007/s12206-021-0428-0

[**70**] A. Çiçek, F. Kara, T. Kıvak, E. Ekici, and İ. Uygur, ***Effects of Deep Cryogenic Treatment on the Wear Resistance and Mechanical Properties of AISI H13 Hot-Work Tool Steel***, Journal of Materials Engineering and Performance, vol. 24, no. 11, pp. 4431–4439, 2015, DOI: 10.1007/s11665-015-1712-x

[**71**] Y. Sun and T. Bell, ***Combined plasma nitriding and PVD treatments***, Transactions of the Institute of Metal Finishing, vol. 70, no. pt 1, pp. 38–44, 1992, DOI: 10.1080/00202967.1992.11870939

[**72**] M. Kulka, N. Makuch, A. Pertek, and A. Piasecki, ***Microstructure and properties of borocarburized and laser-modified 17CrNi6-6 steel***, Optics & Laser Technology, vol. 44, no. 4, pp. 872–881, 2012, DOI: 10.1016/j.optlastec.2011.11.016

[**73**] N. Makuch, P. Dziarski, and M. Kulka, ***Gas Technique of Simultaneous Borocarburizing of Armco Iron Using Trimethyl Borate***, Coatings, vol. 10, no. 6, p. 564, 2020, DOI: 10.3390/coatings10060564

[**74**] S. Zuo *et al.*, ***Tribological Study of Borocarburizing/Sulfurizing Composite Coatings on 2Cr13 Stainless Steel***, Journal of Materials Engineering and Performance, vol. 30, no. 1, pp. 685–695, 2021, DOI: 10.1007/s11665-020-05364-x

[**75**] M. Kulka, N. Makuch, A. Pertek, and L. Małdziński, ***Simulation of the growth kinetics of boride layers formed on Fe during gas boriding in H2-BCl3 atmosphere***, Journal of Solid State Chemistry, vol. 199, pp. 196–203, 2013, DOI: 10.1016/j.jssc.2012.12.029

[**76**] G. E. Totten and R. Colas, Eds., ***Encyclopedia of Iron, Steel, and Their Alloys***. CRC Press, 2016. DOI: 10.1081/E-EISA

[**77**] F. Yan *et al.*, ***A Novel Decarburizing-Nitriding Treatment of Carburized/through-Hardened Bearing Steel towards Enhanced Nitriding Kinetics and Microstructure Refinement***, Coatings, vol. 11, no. 2, p. 112, 2021, DOI: 10.3390/coatings11020112

[**78**] O. Bican, S. U. Bayca, S. Ocak-Araz, B. Yamanel, and N. A. Tanis, ***Effects of the boriding process and of quenching and tempering after boriding on the microstructure, hardness and wear of aisi 5140 steel***, Surface Review and Letters, vol. 27, no. 6, pp. 1–9, 2020, DOI: 10.1142/S0218625X19501579

[**79**] A. G. Morachevskii, ***Henri Moissan (To 150th Anniversary of His Birthday)***, Russian Journal of Applied Chemistry, vol. 75, no. 10, pp. 1720–1722, 2002, DOI: 10.1023/A:1022268927198

[80] R. A. García-León, J. Martínez-Trinidad, and I. Campos-Silva, *Historical Review on the Boriding Process using Bibliometric Analysis*, Transactions of the Indian Institute of Metals, vol. 74, no. 3, pp. 541–557, 2021, DOI: 10.1007/s12666-020-02174-6

[81] E. H. Kottcamp and E. L. Langer, Eds., *ASM handbook volume 3: Alloy phase diagrams*. ASM International, 1992. ISBN: 9780871703811

[82] A. Calik, N. Ucar, M. S. Karakas, and H. Tanis, *Pack-Boriding of Pure Iron with Powder Mixtures Containing ZrB 2*, High Temperature Materials and Processes, vol. 38, no. 2019, pp. 342–346, 2019, DOI: 10.1515/htmp-2017-0081

[83] J. Zuno-Silva *et al.*, *The Powder-pack Boriding Process: A Microstructure Comparison of Boride Layers Formed on AISI 4150 and M2 Steels*, Microscopy and Microanalysis, vol. 24, no. S1, pp. 1064–1065, 2018, DOI: 10.1017/s1431927618005809

[84] I. Campos-Silva *et al.*, *Pulsed-DC powder-pack boriding: Growth kinetics of boride layers on an AISI 316 L stainless steel and Inconel 718 superalloy*, Surface and Coatings Technology, vol. 421, no. May, 2021, DOI: 10.1016/j.surfcoat.2021.127404

[85] I. Campos, G. Ramírez, U. Figueroa, and C. V. Velázquez, *Paste bonding process: Evaluation of boron mobility on borided steels*, Surface Engineering, vol. 23, no. 3, pp. 216–222, 2007, DOI: 10.1179/174329407X174416

[86] M. I. Bayazitov, V. A. Volkov, and A. A. Aliev, *Boronizing from paste with furnace heating*, Metal Science and Heat Treatment, vol. 18, no. 5, pp. 457–458, 1976, DOI: 10.1007/BF00775214

[87] H. YOKOTA and T. SUZUKI, *Improvement in the Oxidation of TiAl by Molten Salt Boronizing*, Tetsu-to-Hagane, vol. 91, no. 1, pp. 217–223, 2005, DOI: 10.2355/tetsutohagane1955.91.1_217

[88] O. Allaoui, N. Bouaouadja, and G. Saindernan, *Characterization of boronized layers on a XC38 steel*, Surface and Coatings Technology, vol. 201, no. 6, pp. 3475–3482, 2006, DOI: 10.1016/j.surfcoat.2006.07.238

[89] G. I. Yukin, *The mechanism of electroplating with boron*, Metal Science and Heat Treatment, vol. 13, no. 8, pp. 662–664, 1971, DOI: 10.1007/BF00651786

[90] G. Kartal and S. Timur, *Growth kinetics of titanium borides produced by CRTD-Bor method*, Surface and Coatings Technology, vol. 215, pp. 440–446, 2013, DOI: 10.1016/j.surfcoat.2012.08.076

[91] K. Matiašovský, M. Chrenková-Paučírová, P. Fellner, and M. Makyta, *Electrochemical and thermochemical boriding in molten salts*, Surface and Coatings Technology, vol. 35, no. 1–2, pp. 133–149, 1988, DOI: 10.1016/0257-8972(88)90064-3

[92] K. Matiasovsky, P. Fellner, M. Chrenkovapaucirova, Z. Lubyova, and A. Silny, *Electrolytic Metal-Coating in Molten-Salts*, Chemical Papers-Chemicke Zvesti, vol. 41, no. 4, pp. 527–565, 1987, ISBN: 0366-6352

[93] G. Kartal, S. Timur, V. Sista, O. L. Eryilmaz, and A. Erdemir, *The growth of single Fe2B phase on low carbon steel via phase homogenization in electrochemical boriding (PHEB)*, Surface and Coatings Technology, vol. 206, no. 7, pp. 2005–2011, 2011, DOI: 10.1016/j.surfcoat.2011.08.049

[94] M. Arslan-Kaba, M. Karimzadehkhoei, M. Keddam, S. Timur, and G. Kartal Sireli, *An experimental and modelling study on pulse current integrated CRTD-Bor process*, Materials Chemistry and Physics, vol. 302, no. March, p. 127735, 2023, DOI: 10.1016/j.matchemphys.2023.127735

[95] K. G. Anthymidis, G. Stergioudis, and D. N. Tsipas, *Boride coatings on non-ferrous materials in a fluidized bed reactor and their properties*, Science and Technology of Advanced Materials, vol. 3, no. 4, pp. 303–311, 2002, DOI: 10.1016/S1468-6996(02)00038-4

[96] P. A. Dearnley, T. Farrell, and T. Bell, *Developments in plasma boronizing*, Journal of Materials for Energy Systems, vol. 8, no. 2, pp. 128–131, 1986, DOI: 10.1007/BF02833337

[97] I. Gunes, S. Ulker, and S. Taktak, *Kinetics of plasma paste boronized AISI 8620 steel in borax paste mixtures*, Protection of Metals and Physical Chemistry of Surfaces, vol. 49, no. 5, pp. 567–573, 2013, DOI: 10.1134/S2070205113050122

[98] L. G. Yu, K. A. Khor, and G. Sundararajan, *Boriding of mild steel using the spark plasma sintering (SPS) technique*, Surface and Coatings Technology, vol. 157, no. 2–3, pp. 226–230, 2002, DOI: 10.1016/S0257-8972(02)00134-2

[99] L. Qin, K. Yang, C. Liu, and B. Tang, *Enhanced plasma boriding with molybdenum using double glow plasma surface alloying technique*, Materials Letters, vol. 82, pp. 127–129, 2012, DOI: 10.1016/j.matlet.2012.05.069

[100] B. El-Kareh, *Fundamentals of Semiconductor Processing Technology*, vol. 5, no. 1. Boston, MA: Springer US, 1995. DOI: 10.1007/978-1-4615-2209-6

[101] W. Ensinger, *Plasma immersion ion implantation for metallurgical and semiconductor research and development*, Nuclear Instruments and Methods in Physics Research, Section B: Beam Interactions with Materials and Atoms, vol. 120, no. 1–4, pp. 270–281, 1996, DOI: 10.1016/S0168-583X(96)00526-5

[102] X. Zong, R. Xia, Y. Zhang, Y. Zhang, and Q. Zhu, *Boriding kinetics and mechanical properties of X65Cr14 martensitic stainless steel by pack method*, Journal of Physics: Conference Series, vol. 2368, no. 1, 2022, DOI: 10.1088/1742-6596/2368/1/012008

[103] J. A. Kohn, W. F. Nye, and G. K. Gaulé, Eds., *Boron Synthesis, Structure, and Properties*. Boston, MA: Springer US, 1960. DOI: 10.1007/978-1-4899-6572-1

[104] N. Makuch, M. Kulka, M. Keddam, and A. Piasecki, *Growth Kinetics, Microstructure Evolution, and Some Mechanical Properties of Boride Layers Produced on X165CrV12 Tool Steel*, Materials, vol. 16, no. 1, 2023, DOI: 10.3390/ma16010026

[105] L. Silvestroi, H. J. Kleebe, S. Lauterbach, M. Müllet, and D. Sciti, *Transmission electron microscopy on Zr- and Hf-borldes with MoSI 2 addition: Denslfkatlon mechanisms*, Journal of Materials Research, vol. 25, no. 5, pp. 828–834, 2010, DOI: 10.1557/jmr.2010.0126

[106] C. T. Sezgin and F. Hayat, *The effects of boriding process on tribological properties and corrosive behavior of a novel high manganese steel*, Journal of Materials Processing Technology, vol. 300, no. October 2021, p. 117421, 2022, DOI: 10.1016/j.jmatprotec.2021.117421

[107] M. A. Doñu Ruiz *et al.*, *Growth kinetics of boride coatings formed at the surface AISI M2 during dehydrated paste pack boriding*, Thin Solid Films, vol. 596, pp. 147–154, 2015, DOI: 10.1016/j.tsf.2015.07.086

[108] T. Burakowski and T. Wierzchon, *Surface Engineering of Metals*. CRC Press, 1998. DOI: 10.1201/9780367802325

[109] H. Qvarnström, *Technical Note: A mathematical formula for transformation between the steel hardness scales of Rockwell C and Vickers*, Journal of Heat Treating, vol. 7, no. 1, pp. 65–67, 1989, DOI: 10.1007/BF02833189

[110] A. S. Pomel'nikova, M. N. Shipko, and M. A. Stepovich, *Features of structural changes due to the formation of the boride crystal structure in steels*, Journal of Surface Investigation. X-ray, Synchrotron and Neutron Techniques, vol. 5, no. 2, pp. 298–304, 2011, DOI: 10.1134/S1027451011030165

[111] L. G. Voroshnin, L. S. Lyakhovich, and Y. N. Funshtein, *Boronizing with powdered mixtures*, Metal Science and Heat Treatment, vol. 8, no. 12, pp. 1035–1037, 1966, DOI: 10.1007/BF00653013

[112] G. Kartal Sireli, A. S. Bora, and S. Timur, *Evaluating the mechanical behavior of electrochemically borided low-carbon steel*, Surface and Coatings Technology, vol. 381, p. 125177, 2020, DOI: 10.1016/j.surfcoat.2019.125177

[113] L. S. Lyakhovich, L. N. Kosachevskii, A. Y. Kulik, V. V. Surkov, and Y. V. Turov, *Possibility of predetermining the distribution of residual stresses in borided steels*, Soviet Materials Science, vol. 9, no. 3, pp. 272–275, 1975, DOI: 10.1007/BF00722544

[114] G. Rodríguez-Castro, I. Campos-Silva, E. Chávez-Gutiérrez, J. Martínez-Trinidad, E. Hernández-Sánchez, and A. Torres-Hernández, *Mechanical properties of FeB and Fe2B layers estimated by Berkovich nanoindentation on tool borided steel*, Surface and Coatings Technology, vol. 215, pp. 291–299, 2013, DOI: 10.1016/j.surfcoat.2012.05.145

[115] T. Arai, G. M. Baker, and et al., *ASM Handbook Volume 04: Heat Treating*. ASM International, 1991. ISBN: 9780871703798

[116] I. Campos-Silva, M. Flores-Jiménez, G. Rodríguez-Castro, E. Hernández-Sánchez, J. Martínez-Trinidad, and R. Tadeo-Rosas, *Improved fracture toughness of boride coating developed with a diffusion annealing process*, Surface and Coatings Technology, vol. 237, pp. 429–439, 2013, DOI: 10.1016/j.surfcoat.2013.05.050

[117] W. Bunk, J. Hansen, and M. Geyer, Eds., *Tribologie: Reibung Verschleiß Schmierung (Friction Wear Lubrication)*. Berlin, Heidelberg: Springer Berlin Heidelberg, 1982. DOI: 10.1007/978-3-642-52224-6

[118] Z. Salyi *et al.*, *Boride Coatings on Steel Protecting it Against Corrosion by a Liquid Lead-Free Solder Alloy*, Metallurgical and Materials Transactions B: Process Metallurgy and Materials Processing Science, vol. 53, no. 2, pp. 730–743, 2022, DOI: 10.1007/s11663-021-02412-2

[119] E. V. Sidorov, *Equilibrium phase diagram of the iron-carbon system*, Steel in Translation, vol. 38, no. 11, pp. 889–891, 2008, DOI: 10.3103/S0967091208110016

[120] O. Ozdemir, M. Usta, C. Bindal, and A. H. Ucisik, *Hard iron boride (Fe2B) on 99.97 wt% pure iron*, Vacuum, vol. 80, no. 11–12, pp. 1391–1395, 2006, DOI: 10.1016/j.vacuum.2006.01.022

[121] K. Sotoodeh, *Cryogenic Valves for Liquefied Natural Gas Plants*. Elsevier, 2022. DOI: 10.1016/C2021-0-02496-2

[122] J. Jiang, Y. Wang, Q. Zhong, Q. Zhou, and L. Zhang, *Preparation of Fe2B boride coating on low-carbon steel surfaces and its evaluation of hardness and corrosion resistance*, Surface and Coatings Technology, vol. 206, no. 2–3, pp. 473–478, 2011, DOI: 10.1016/j.surfcoat.2011.07.053

[123] G. Kartal, O. L. Eryilmaz, G. Krumdick, A. Erdemir, and S. Timur, *Kinetics of electrochemical boriding of low carbon steel*, Applied Surface Science, vol. 257, no. 15, pp. 6928–6934, 2011, DOI: 10.1016/j.apsusc.2011.03.034

[124] A. Pertek and M. Kulka, *Two-step treatment carburizing followed by boriding on medium-carbon steel*, Surface and Coatings Technology, vol. 173, no. 2–3, pp. 309–314, 2003, DOI: 10.1016/S0257-8972(03)00522-X

[125] A. Milinović, V. Marušić, P. Konjatić, and N. Berić, *Effect of Carbon Content and Boronizing Parameters on Growth Kinetics of Boride Layers Obtained on Carbon Steels*, Materials, vol. 15, no. 5, 2022, DOI: 10.3390/ma15051858

[126] A. Miliinovic, D. Krumes, and M. Radojke, *An Investigation of Boride Layers' Growth Kinetics on Carbon Steels*, Tech. Gaz., pp. 19,27-31, 2012.

[127] C. M. Allen and B. Boardman, *Properties and Selection: Irons, Steels, and High-Performance Alloys*, Properties and Selection: Irons, Steels, and High-Performance Alloys, 1990, DOI: 10.31399/asm.hb.v01.9781627081610

[128] S. Sahin and C. Meric, *Investigation of the effect of boronizing on cast irons*, Materials Research Bulletin, vol. 37, no. 5, pp. 971–979, 2002, DOI: 10.1016/S0025-5408(02)00697-9

[129] N. Makuch, M. Kulka, M. Keddam, S. Taktak, V. Ataibis, and P. Dziarski, *Growth kinetics and some mechanical properties of two-phase boride layers produced on commercially pure titanium during plasma paste boriding*, Thin Solid Films, vol. 626, pp. 25–37, 2017, DOI: 10.1016/j.tsf.2017.02.033

[130] N. T. Taazim, I. Jauhari, Y. Miyashita, and M. F. M. Sabri, *Development and Kinetics of TiB2 Layers on the Surface of Titanium Alloy by Superplastic Boronizing*, Metallurgical and Materials Transactions A: Physical Metallurgy and Materials Science, vol. 47, no. 5, pp. 2217–2222, 2016, DOI: 10.1007/s11661-016-3359-0

[131] K. G. Anthymidis, G. Stergioudis, D. Roussos, P. Zinoviadis, and D. N. Tsipas, *Boriding of ferrous and non-ferrous metals and alloys in fluidised bed reactor*, Surface Engineering, vol. 18, no. 4, pp. 255–259, 2002, DOI: 10.1179/026708401225005296

[132] N. Ueda, T. Mizukoshi, K. Demizu, T. Sone, A. Ikenaga, and M. Kawamoto, *Boriding of nickel by the powder-pack method*, Surface and Coatings Technology, vol. 126, no. 1, pp. 25–30, 2000, DOI: 10.1016/S0257-8972(00)00517-X

[133] O. Kahvecioglu, V. Sista, O. L. Eryilmaz, A. Erdemir, and S. Timur, *Ultra-fast boriding of nickel aluminide*, Thin Solid Films, vol. 520, no. 5, pp. 1575–1581, 2011, DOI: 10.1016/j.tsf.2011.08.077

[134] I. Yildiz, *Surface Characterization and Boriding of Nickel and Cobalt Alloys*, Protection of Metals and Physical Chemistry of Surfaces, vol. 58, no. 4, pp. 772–778, 2022, DOI: 10.1134/S2070205122040244

[135] J. F. Shackelford, *Introduction to Materials Science for Engineers*. Pearson, 2014. ISBN: 9780133826654

[136] M. Ortiz-Domínguez, O. A. Gómez-Vargas, M. Bárcenas-Castañeda, and V. A. Castellanos-Escamilla, *Comparison and Analysis of Diffusion Models: Growth Kinetics of Diiron Boride Layers on ASTM A283 Steel*, Materials, vol. 15, no. 23, p. 8420, 2022, DOI: 10.3390/ma15238420

[137] M. G. Albayrak, E. Evin, O. Yiğit, M. Toğaçar, and B. Ergen, *Experimental and artificial intelligence approaches to measuring the wear behavior of DIN St28 steel boronized by the box boronizing method using a mechanically alloyed powder source*, Engineering Applications of Artificial Intelligence, vol. 120, no. December 2022, 2023, DOI: 10.1016/j.engappai.2023.105910

[138] M. Ortiz-Domínguez *et al.*, *Modeling of the Growth Kinetics of Boride Layers in Powder-Pack Borided ASTM A36 Steel Based on Two Different Approaches*, Advances in Materials Science and Engineering, vol. 2019, 2019, DOI: 10.1155/2019/5985617

[139] K. Genel, I. Ozbek, A. Kurt, and C. Bindal, *Boriding response of AISI W1 steel and use of artificial neural network for prediction of borided layer properties*, Surface and Coatings Technology, vol. 160, no. 1, pp. 38–43, 2002, DOI: 10.1016/S0257-8972(02)00400-0

[140] M. T. Hagan, H. B. Demuth, M. H. Beale, and O. De Jesús, *Neural Network Design (2nd Edition)*. Martin Hagan, 2014. ISBN: 9780971732117

[141] N. Buduma, *Fundamentals of Deep Learning*. O'Reilly Media, Inc., 2017. ISBN: 9781491925614

[142] B. Mebarek and M. Keddam, *Prediction model for studying the growth kinetics of Fe2B boride layers during boronizing*, Ingenierie des Systemes d'Information, vol. 24, no. 2, pp. 201–205, 2019, DOI: 10.18280/isi.240212

[143] G. K. Uyanık and N. Güler, *A Study on Multiple Linear Regression Analysis*, Procedia - Social and Behavioral Sciences, vol. 106, pp. 234–240, 2013, DOI: 10.1016/j.sbspro.2013.12.027

[144] J. W. Osborne and E. Waters, *Four Assumptions of Multiple Regression That Researchers Should Always Test. - Practical Assessment, Research & Evaluation*, Practical Assessment, Research and Evaluation, vol. 8, no. 2, pp. 1–5, 2019, DOI: 10.7275/r222-hv23

[145] P. Roback and J. Legler, *Beyond Multiple Linear Regression: Applied Generalized Linear Models And Multilevel Models in R*. Chapman and Hall/CRC, 2021. DOI: 10.1201/9780429066665

[146] O. Azouani, M. Keddam, O. Allaoui, and A. Sehisseh, *Characterization of boride coatings on a ductile cast iron*, Protection of Metals and Physical Chemistry of Surfaces, vol. 53, no. 2, pp. 306–311, 2017, DOI: 10.1134/S207020511702006X

[147] S. Taktak, *A study on the diffusion kinetics of borides on boronized Cr-based steels*, Journal of Materials Science, vol. 41, no. 22, pp. 7590–7596, 2006, DOI: 10.1007/s10853-006-0847-4

[148] P. A. Ruiz-trabolsi *et al.*, *Kinetics of the boride layers obtained on aisi 1018 steel by considering the amount of matter involved*, Coatings, vol. 11, no. 2, pp. 1–17, 2021, DOI: 10.3390/coatings11020259

[149] C. M. Brakman, A. W. J. Gommers, and E. J. Mittemeijer, *Bonding of Fe and Fe-C, Fe-Cr, and Fe-Ni alloys; Boride-layer growth kinetics*, Journal of Materials Research, vol. 4, no. 6, pp. 1354–1370, 1989, DOI: 10.1557/JMR.1989.1354

[150] M. A. Flores-Rentería *et al.*, *A Simple Kinetic Model for the Growth of Fe2B Layers on AISI 1026 Steel during the Powder-pack Boriding*, High Temperature Materials and Processes, vol. 34, no. 1, pp. 1–11, 2015, DOI: 10.1515/htmp-2014-0004

[151] M. Keddam, M. Ortiz-Domínguez, I. Campos-Silva, and J. Martínez-Trinidad, *A simple model for the growth kinetics of Fe2B iron boride on pure iron substrate*, Applied Surface Science, vol. 256, no. 10, pp. 3128–3132, 2010, DOI: 10.1016/j.apsusc.2009.11.085

[152] J. Zuno-Silva *et al.*, *Boriding kinetics of Fe2B layers formed on aisi 1045 steel*, Journal of Mining and Metallurgy, Section B: Metallurgy, vol. 50, no. 2, pp. 101–107, 2014, DOI: 10.2298/JMMB140323019Z

[153] M. Ortiz-Domínguez *et al.*, *Simulation of growth kinetics of Fe2B layers formed on gray cast iron during the powder-pack boriding*, Materiali in Tehnologije, vol. 48, no. 6, pp. 905–916, 2014, URL: uaeh.edu.mx/investigacion/productos/6375

[154] T. R. Goodman, *Application of Integral Methods to Transient Nonlinear Heat Transfer*, Advances in Heat Transfer, vol. 1, no. C, pp. 51–122, 1964, DOI: 10.1016/S0065-2717(08)70097-2

[155] W. H. Press, S. A. Teukolsky, W. T. Vetterling, and B. P. Flannery, *Numerical Recipes The Art of Scientific Computing Third Edition*. Cambridge University Press, 2007. ISBN: 9785984520973

[156] M. Keddam, M. Ortiz-Domínguez, I. Simón-Marmolejo, J. Zuno-Silva, and M. Elias-Espinosa, *Pack-boriding of AISI P20 steel: Estimation of boron diffusion coefficients in the Fe2B layers and tribological behaviour*, International Journal of Surface Science and Engineering, vol. 11, no. 6, pp. 563–585, 2017, DOI: 10.1504/IJSURFSE.2017.088997

[157] J. Zuno-Silva *et al.*, *Kinetics of formation of Fe2B layers on AISI S1 steel*, Materials Research, vol. 21, no. 5, pp. 1–10, 2018, DOI: 10.1590/1980-5373-MR-2018-0173

[158] S. Mansour, M. Keddam, and B. Boumaali, *Prediction models for the kinetics of iron boride layers on AISI 316L steel*, Koroze a Ochrana Materialu, vol. 66, no. 1, pp. 40–49, 2022, DOI: 10.2478/kom-2022-0007

[159] M. Keddam and M. Kulka, *Simulation of the Growth Kinetics of FeB and Fe2B Layers on AISI D2 Steel by the Integral Method*, Physics of Metals and Metallography, vol. 119, no. 9, pp. 842–851, 2018, DOI: 10.1134/S0031918X18090065

[160] C. Zouzou and M. Keddam, *Boriding Kinetics of FeB and Fe2B Layers on AISI M2 Steel by the Integral Diffusion Model*, Annales de Chimie - Science des Matériaux, vol. 43, no. 3, pp. 159–164, 2019, DOI: 10.18280/acsm.430304

[161] C. Zouzou and M. Keddam, *Application of integral method for investigating the boriding kinetics of AISI 316 steel*, Metallurgical Research and Technology, vol. 117, no. 2, 2020, DOI: 10.1051/metal/2020011

[162] V. I. Dybkov, *Reaction diffusion and solid state chemical kinetics*. Kyiv, Ukraine: IPMS Publications, 2002. ISBN: 9660225431

[163] V. I. Dybkov, *Diffusional Growth Kinetics of Boride Layers at the 13% Cr Steel Interface with Amorphous Boron*, Defect and Diffusion Forum, vol. 263, pp. 183–188, 2007, DOI: 10.4028/www.scientific.net/ddf.263.183

[164] V. I. Dybkov, L. V. Goncharuk, V. G. Khoruzha, K. A. Meleshevich, A. V. Samelyuk, and V. R. Sidorko, *Diffusional growth kinetics of boride layers on iron-chromium alloys*, Solid State Phenomena, vol. 138, pp. 181–188, 2008, DOI: 10.4028/www.scientific.net/SSP.138.181

[165] I. Campos-Silva *et al.*, *Formation and kinetics of FeB/Fe2B layers and diffusion zone at the surface of AISI 316 borided steels*, Surface and Coatings Technology, vol. 205, no. 2, pp. 403–412, 2010, DOI: 10.1016/j.surfcoat.2010.06.068

[166] M. Keddam, M. Kulka, N. Makuch, A. Pertek, and L. Małdziński, *A kinetic model for estimating the boron activation energies in the FeB and Fe 2 B layers during the gas-boriding of Armco iron: Effect of boride incubation times*, Applied Surface Science, vol. 298, pp. 155–163, 2014, DOI: 10.1016/j.apsusc.2014.01.151

[167] M. Keddam *et al.*, *Characterization, Tribological and Mechanical Properties of Plasma Paste Borided AISI 316 Steel*, Transactions of the Indian Institute of Metals, vol. 71, no. 1, pp. 79–90, 2018, DOI: 10.1007/s12666-017-1142-6

[168] A. Günen, M. Keddam, S. Alkan, A. Erdoğan, and M. Çetin, *Microstructural characterization, boriding kinetics and tribo-wear behavior of borided Fe-based A286 superalloy*, Materials Characterization, vol. 186, no. February, 2022, DOI: 10.1016/j.matchar.2022.111778

[169] A. D. Contla-Pacheco, M. Keddam, L. Lartundo-Rojas, M. Ortega-Avilés, I. Mejía-Caballero, and I. Campos-Silva, *Application of the Heat Balance Integral Method to the growth kinetics of nickel boride layers on an Inconel 718 superalloy*, Surface and Coatings Technology, vol. 420, no. March, 2021, DOI: 10.1016/j.surfcoat.2021.127355

[170] I. Gunes, M. Keddam, R. Chegroune, and M. Ozcatal, *Growth kinetics of boride layers formed on 99.0% purity nickel*, Bulletin of Materials Science, vol. 38, no. 4, pp. 1113–1118, 2015, DOI: 10.1007/s12034-015-0931-y

[171] O. Torun, *Boriding of nickel aluminide*, Surface and Coatings Technology, vol. 202, no. 15, pp. 3549–3554, 2008, DOI: 10.1016/j.surfcoat.2007.12.034

[172] Ismail Yildiz, A. G. Çelik, and I. Gunes, *Characterization and Diffusion Kinetics of borided Ni–Mg Alloys*, Protection of Metals and Physical Chemistry of Surfaces, vol. 56, no. 5, pp. 1015–1022, 2020, DOI: 10.1134/S2070205120050287

[173] M. Elias-Espinosa *et al.*, *Growth kinetics of the Fe2B layers and adhesion on Armco iron substrate*, Journal of Materials Engineering and Performance, vol. 23, no. 8, pp. 2943–2952, 2014, DOI: 10.1007/s11665-014-1052-2

[174] S. A. Bouaziz, N. Boudaoud, and A. Zanoun, *Boruration thermochimique d'un acier C38 dans un bain de sels borax-SiC*, Materiaux et Techniques, vol. 97, no. 4, pp. 253–259, 2009, DOI: 10.1051/mattech/2009036

[175] O. Belguendouz, B. Mebarek, M. Keddam, and Y. El Guerri, *Diffusion Model for Simulating the Kinetics of Boronizing Process in the Case of FeB/Fe2B Bilayer Configuration*, Annales de Chimie - Science des Matériaux, vol. 44, no. 3, pp. 191–197, 2020, DOI: 10.18280/acsm.440306

[176] O. Belguendouz, B. Mebarek, Y. El Guerri, M. Keddam, N. Hadjadj, and Y. Djafri, *Simple model and integral method for simulating the growth of the borided layer FeB/Fe2B on the AISI H13 steel*, Zastita materijala, vol. 64, no. 4, pp. 491–502, 2023, DOI: 10.5937/zasmat2304491B

[177] N. Hadjadj, B. Mebarek, Y. El Guerri, and M. Keddam, *Dybkov model for the estimation of boron diffusion in the FeB/Fe2B bilayer on AISI 316 steel*, Zastita Materijala, vol. 65, no. 2, pp. 220–235, 2024, DOI: 10.62638/ZasMat1125

[178] Y. El Guerri, B. Mebarek, and M. Keddam, *Impact of the diffusion coefficient calculation on predicting Fe2B boride layer thickness*, Koroze a ochrana materialu, vol. 66, no. 1, pp. 25–35, 2022, DOI: 10.2478/kom-2022-0005

[179] Y. El Guerri, B. Mebarek, and M. Keddam, *Confrontation of linear versus nonlinear approach in Fe2B boridelayer thickness predictions*, Zastita Materijala, vol. 65, no. 1, pp. 97–109, 2024, DOI: 10.62638/ZasMat1016

[180] I. Campos-Silva *et al.*, *Diffusion model for growth of Fe2B layer in pure iron*, Surface Engineering, vol. 27, no. 3, pp. 189–195, 2011, DOI: 10.1179/026708410X12550773057820

[181] I. Campos, J. Oseguera, U. Figueroa, J. A. García, O. Bautista, and G. Kelemenis, *Kinetic study of boron diffusion in the paste-boriding process*, Materials Science and Engineering: A, vol. 352, no. 1–2, pp. 261–265, 2003, DOI: 10.1016/S0921-5093(02)00910-3

[182] M. Keddam and M. Kulka, *Analysis of the growth kinetics of Fe2B layers by the integral method*, Journal of Mining and Metallurgy, Section B: Metallurgy, vol. 54, no. 3, pp. 361–367, 2018, DOI: 10.2298/JMMB180405026K

[183] M. Elias-Espinosa *et al.*, *Boriding kinetics and mechanical behaviour of AISI O1 steel*, Surface Engineering, vol. 31, no. 8, pp. 588–597, 2015, DOI: 10.1179/1743294415Y.0000000065

[184] M. Keddam and M. Kulka, *Mean Diffusion Coefficient Method in Studying Armco Iron Boriding Kinetics*, Metal Science and Heat Treatment, vol. 62, no. 5–6, pp. 326–330, 2020, DOI: 10.1007/s11041-020-00562-9

[185] B. Mebarek, A. Benguelloula, and A. Zanoun, *Effect of Boride Incubation Time During the Formation of Fe2B Phase*, Materials Research, vol. 21, no. 1, 2018, DOI: 10.1590/1980-5373-mr-2017-0647

[186] I. N. da Silva, D. Hernane Spatti, R. Andrade Flauzino, L. H. B. Liboni, and S. F. dos Reis Alves, *Artificial Neural Networks*. Cham: Springer International Publishing, 2017. DOI: 10.1007/978-3-319-43162-8

[187] K. M. Ramachandran and C. P. Tsokos, *Mathematical Statistics with Applications in R, Third Edition*. 2020. DOI: 10.1016/C2018-0-02285-9

BLANK PAGE

ملخص

تستكشف الأطروحة كيفية تعزيز خواص البورون للمواد القابلة للتشغيل الآلي من خلال عمليات تصليب السطح. فهي تدرس مركبات البورون ذات الصلة وتحلل مختلف عمليات التصليب السطحي، بما في ذلك العمليات المدمجة، مثل البوروكربنة، والعمليات المتعارضة، مثل التبريد بعد التصليب بالبورون.

بعد تحليل شامل لتقنيات تصليب السطح، يتم التركيز على البورايدينغ، بقول آخر، البوردة أو التصليب بالبورون، وهو عملية حراروكيميائية، أي حرارية كيميائية، لنشر البورون، مصنفة على أنها تقليدية أو حديثة، اعتمادًا على مدى تعقيد أو حداثة التقنية، وعلى الوسائط المستخدمة؛ صلبة، سائلة، غازية، بلازما، أيونات، أو غير ذلك.

تتم العملية أساسيا على معظم المواد المعدنية القابلة للتشغيل الآلي، مثل الحديد، التيتانيوم والنيكل، مع وجود حدود لبعض منها، مثل الألومنيوم والنحاس، في حين أنها غير متوافقة مع معظم المواد الغير معدنية. إضافة على ذلك، يفضل البورايدينج معادن غير مسبوكة، ويميل إلى أن يكون صعبًا، كلما ارتفعت نسبة السبائك.

طبقات البورايد، إحدى أصلب المركبات وأكثرها مقاومة للتآكل، مُصنّعة وموضوعة كطبقة على سطح المواد. إن وقت المعالجة والتعرض لدرجات الحرارة من العوامل الرئيسية التي تؤثر على سمك طبقة البورايد الناتج، وهو السمة الحاسمة التي تؤثر على خصائص طبقة البورايد وتوافقها مع التطبيق المطلوب.

وفقًا لذلك، يستكشف البحث نماذج مختلفة، تجريبية، رياضية، ذات النمو القطعي المكافئ، وحتى الشبكات العصبية الاصطناعية، لمحاكاة سماكة طبقة البورايد، ثم تقديم بعض المقارنات بينها لأغراض التحسين فيما يتعلق بدقة وفعالية تنبؤاتها.

الكلمات المفتاحية: انتشار البورون، التصليب بالبورون، طبقة البورايد، المواد القابلة للتشغيل الآلي، النمذجة والمحاكاة.

Abstract

The thesis explores how boron's properties enhance machinable materials through surface hardening processes. It examines relevant boron compounds and analyzes various surface hardening processes, including combined ones, such as borocarburizing, and conflicting ones, like quenching after boriding.

Following a comprehensive analysis of surface hardening techniques, the focus narrows to boriding, a thermochemical boron diffusion process categorized as traditional or modern, depending on the complexity and newness of the technique, and the media used, solid, liquid, gas, plasma, ions, and so on.

The process is carried out mainly on most metallic machinable materials, such as iron, titanium, and nickel, with limitations to some, like aluminum and copper, while incompatible with nonmetallic ones. Additionally, boriding prefers unalloyed metals and tends to be difficult the higher the alloying becomes.

Boride layers, one of the hardest and wear resistant compounds, are synthesized through boron diffusion and layered on the surface of materials. The boriding treatment time and temperatures exposures are the key factors affecting the resulting boride layer thickness, the critical feature affecting the boride layer properties and their compatibility to the demanded application.

Accordingly, the research explores different models, empirical, mathematical, of parabolic growth, and even artificial neural networks, to simulate boride layer thicknesses, then provides some comparisons between them for optimization purposes regarding the accuracy and effectiveness of their predictions.

Keywords: boron diffusion, boriding, boride layer, machinable materials, modeling and simulating.

•